Analysis of functional morphology in carnassial dentitions (Carnivora, Dasyuromorphia, Hyaenodonta)

Dissertation

zur

Erlangung des Doktorgrades (Dr. rer. nat.)

der

Mathematisch-Naturwissenschaftlichen Fakultät

der

Rheinischen Friedrich-Wilhelms-Universität Bonn

vorgelegt von

Andreas Lang

aus

Köln

Bonn 2023

Parts of this thesis have been published in:

Lang, A. J., Engler, T., & Martin, T. (2021). Dental topographic and three-dimensional geometric morphometric analysis of carnassialization in different clades of carnivorous mammals (Dasyuromorphia, Carnivora, Hyaenodonta). *Journal of Morphology*, 283(1), 91 – 108. https://doi.org/10.1002/jmor.21429

Summary of the publication with emphasis on own contributions

The publication encompasses the quantification of carnassial crown curvature by ariaDNE, the landmark based geometric morphometric analysis, the subsequent ancestral state reconstruction and the UPGMA cluster analysis. An introduction is given about the various clades of mammals which evolved carnivorous adaptations and the convergent evolution of carnassial dentitions in the Dasyuromorphia, Carnivora and Hyaenodonta. The three groups differ in their dental adaptations, as there are three carnassials per tooth row in the dasyuromorphs and the hyaenodonts, while there is only one in the carnivorans. The teeth were divided in two functional groups. In the "basal" carnassial functional group, all tribosphenic cusps are still present, while in the "derived" functional group, at least one cusp is reduced. For the study, a total of 110 individual lower carnassial teeth were used. Of these teeth, 106 were used for the ariaDNE calculation and 109 were used for the geometric morphometric analysis. The acquisition of the material was conducted by me and 49 of the 72 included specimens were CT-scanned by me. The preparation of 3D surface models for the analyses using Avizo and PolyWorks, including segmentation, cutting at the cervix line, downsampling of vertices, smoothing and landmark placement were done by me. T. Engler contributed by conceptualization and scripting for the ariaDNE batch processing in matlab and the calculation of ariaDNE values. The scripting and processing of the geometric morphometric analysis in R was done by myself. Further, I assembled a phylogenetic tree of the included taxa based on published phylogenetic data. The results show that crown curvature calculated by ariaDNE is sensitive to the degree of carnassialization, as the curvature decreases with increasing carnassialization. A procrustes ANOVA, conducted by myself in R, shows that the division between basal carnassialized and derived carnassialized teeth using ariaDNE is significant. A PCA of the geometric morphometric analysis, conducted by myself using R, shows that the largest proportion of variance (41.4%) is explained by a convergent shape shift of carnassial teeth in the dimension of PC1, which is connected to an enlargement of the carnassial cutting blade and a reduction of the talonid crushing basin. Additionally, a shape shift occurs in the cervix line, indicating a mesial and a distal flexure in basal carnassialized

teeth, and an enlarged mesial flexure in derived carnassialized teeth, while the distal flexure is reduced. The distribution of the various carnassial tooth positions of dasyuromorphs and hyaenodonts in the PC1 dimension indicates that the most distal carnassial of the lower tooth row is the most carnassialized in these taxa. In four out of seven taxa with multiple carnassials per tooth row, there is a successive shift of values in the PC1 dimension from mesial to distal, indicating a successively increasing carnassialization from the mesial to the distal tooth position. PC2 (explaining 13.9% of variance) is connected to a mesio-distal elongation of the carnassial tooth, which is only occurring in carnivoran taxa. An ancestral state reconstruction using R was conducted by myself. It is indicated that both the ariaDNE and the PC1 quantification describe a convergent signal, as the calculated ancestral condition for the Dasyuromorphia, Carnivora and Hyaenodonta is similar. The mesio-distally elongated carnassial shape as quantified by PC2 may be the plesiomorphic condition of the Carnivora, which show an ancestral condition different to the Dasyuromorphia and Hyaenodonta. An UPGMA cluster analysis, conducted by myself, is in congruence with this observation, as the basal carnassialized carnivoran m1 is separated from the basal carnassialized dasyuromorph and hyaenodont teeth. A detailed discussion is given about the significance of the differences in carnassial shape between the carnivorans and the dasyuromorphs and hyaenodonts. A mesio-distally elongated carnassial shape may enabe the co-occurrence of a mesio-distally oriented carnassial blade, effective for cutting, and a fully developed talonid basin, effective for crushing. Thus, the unique evolution of this carnassial morphotype within the Carnivora may have given them an adaptive advantage in comparison to the Dasyuromorphia and the Hyaenodonta, which did not evolve mesio-distally elongated carnassials. Functional constraints play a key role in the evolution of carnassial teeth, as functional versatility is generally reduced in carnassials. Compared to the Carnivora, the Hyaenodonta may have been affected by this constraint more severely, which may be one explanation for their eventual extinction. The original draft of the manuscript was written by me, with my co-authors reviewing and editing the text.

Table of Contents

1. Summary

Functional and structural changes in the evolution of carnassial teeth in the Carnivora, Dasyuromorphia and Hyaenodonta are analyzed by a combination of Occlusal Fingerprint Analysis, Dental Topographic Analysis (quantification of crown curvature by Dirichlet Normal Energy) and 3D geometric morphometrics. Carnassialization can be described as an increasing simplification of tooth structure and function. The documented tooth wear and virtual simulation of the power stroke indicate a functional shift from weakly to higher carnassialized teeth, where the cutting function is emphasized and the crushing function is reduced. In some taxa, a trenchant talonid with a hypoflexid groove evolves, performing a similar shearing and guiding function as the hypoflexid in pretribosphenic teeth, such as in dryolestids. This observation is consistent with the hypothesis that carnassialization is a simplification and structural reverse of the tooth crown to an ancestral pretribosphenic condition. The Dental Topographic Analysis of lower carnassials shows low crown curvature values in higher carnassialized teeth. The decrease of crown curvature with increasing carnassialization can be explained with the reduction of cusps and crests, which results in a simplified crown relief. The geometric morphometric analysis of lower carnassials indicates a convergent simplification of the crown relief connected to carnassial blade enlargement and talonid reduction. Along the lower tooth row of dasyuromorphs (m2 - m4) and hyaenodonts (m1 - m3) the most distal carnassial is the most carnassialized (principal carnassial), and in most taxa with overall higher carnassialized teeth, carnassialization successively increases from the mesial to the distal tooth position. Additionally, a shape difference connected to the phylogeny, showing a mesio-distal elongation of the carnassial unique to carnivorans with weakly carnassialized teeth, is indicated. The mesio-distal tooth elongation, present only in caniforms and unspecialized feliforms (viverrids and herpestids), enables the presence of a functional crushing talonid basin and a longitudinally oriented carnassial blade, performing an efficient carnassial cutting. As indicated by an ancestral state reconstruction, this condition may be plesiomorphic for the Carnivora and may have provided them with an advantage in terms adaptive versatility, as it did not evolve in dasyuromorphs or hyaenodonts.

2. Introduction

2.1 Carnivorous adaptations in mammals

Section 2.1 has been modified and published in: Lang, A. J., Engler, T., & Martin, T. (2021). Dental topographic and three-dimensional geometric morphometric analysis of carnassialization in different clades of carnivorous mammals (Dasyuromorphia, Carnivora, Hyaenodonta). *Journal of Morphology*, 283(1), 91 – 108.

Mammals evolved carnivory, as defined by a diet comprised of vertebrate meat, multiple times which resulted in similar adaptations that convergently evolved within different clades (Muizon & Lange-Badré, 1997). Among mammals, the earliest direct evidence for carnivory is known from the Early Cretaceous eutriconodontan *Repenomamus*, which fed on small dinosaurs (Hu, Meng, Wang, & Li, 2005). Molars that emphasized the shearing function, which is a typical adaptation to a carnivorous diet, also evolved in the Late Cretaceous metatherian groups Deltatheroidea and Stagodontidae (Muizon & Lange-Badré, 1997). When the non-avian dinosaurs went extinct at the end of the Cretaceous, the niches of meat-eaters became largely vacant. Thus, in the earliest Cenozoic a number of therian lineages began to evolve into predators and/or scavengers. The Mesonychia, a group of early ungulates, were among the first carnivorous mammals of the Paleocene, although their teeth evolved a greater emphasis on piercing and bone-cracking instead of precise shearing (Szalay & Gould, 1966). The degree of morphological convergence with a much higher emphasis on precise shearing increased by the end of the Paleocene, when clades which possessed true carnassials evolved. The first representatives of Oxyaenodonta (Gingerich, 1980), Hyaenodonta (Meng et al., 1998; Gheerbrant et al., 2006) and Carnivoramorpha (Flynn & Wesley-Hunt, 2005) comprise these more specialized taxa that appear in the Paleocene. The carnivorous niche in South America was occupied by the Sparassodonta, a metatherian clade with similar adaptations for precise shearing, until their extinction in the Early Pliocene (Prevosti & Forasiepi, 2018). The eutherian Carnivora, which are comprised of a great number of species and which are highly ecomorphologically diverse, became the dominant group of carnivorous mammals in the cenozoic (Van Valkenburgh & Wayne, 2010).

Among extant mammals, adaptations to carnivory are also present in various clades of marsupials. The South American didelphid *Lutreolina crassicaudata* shows such proclivities (Goin et al., 2016). Further, species that are particularly highly specialized to carnivory and survived into present time evolved within the australidelphian Dasyuromorphia (Hutchins et al., 2003). Another group of highly specialized Australian carnivorous marsupials were the diprotodontan Thylacoleonidae, which appeared in the Late Oligocene and were probably the

top carnivorous mammals in Australia in the later Cenozoic until they went extinct in the Pleistocene (Gillespie et al., 2019).

The Hyaenodonta are of special interest to this study as they coexisted with the Carnivora up to their extinction in the Miocene, but their dental adaptations more closely resembled the conditions found in extant Australian carnivorous marsupials.

2.2 Carnivora

The eutherian Carnivora are the crown group of the more inclusive group Carnivoramorpha (Wesley-Hunt & Flynn 2005). The Carnivoramorpha are included in the Ferae, together with the Pholidota and possibly also the extinct Hyaenodonta (O 'Leary et al., 2013; see 3.9). The Carnivora comprise the extant doglike (Caniformia) and catlike (Feliformia) carnivorans as well as several extinct lineages within these groups (Flynn et al., 2010). Some phylogenetic studies also include the extinct Nimravidae in the Carnivora, either at the base of the group (Solé et al., 2014) or as a clade within the Feliformia (Wesley-Hunt & Flynn 2005). The oldest carnivoramorphs are known from the Early Paleocene and are members of the Viverravidae, a group that existed until the Late Eocene (Spaulding & Flynn, 2012). The sister group of the Viverravidae comprises the Carnivoraformes, the clade that includes the Carnivora and their ancestors (Flynn et al., 2010). Based on the current fossil evidence, the Carnivoraformes are hypothesized to having originated from Asia with subsequent dispersal to Europe and North America before the Paleocene-Eocene boundary, indicated by European and North American carnivoraform fossils from the Late Paleocene (Solé et al., 2016). A key adaptation of the Carnivoramorpha is the adaptation of the upper distal premolar (P4) and the lower mesial molar (m1) to perform a specialized shearing function (Flynn & Wesley-Hunt, 2005). This indicates an early affinity to a carnivorous diet. Subsequent diversification of carnivoraforms in the Eocene was higher in North America than it was in Europe, possibly due to the competition with hyaenodonts (Solé et al., 2016).

The Caniformia originated in North America, where the earliest Amphicyonidae ("bear dogs") (Tomiya & Tseng, 2016) and the earliest Canidae (extant dogs and relatives) (Benton & Donoghue, 2007) appeared in the Middle Eocene. The Amphicyonidae subsequently spread to Europe, Asia and Africa and competed with other carnivorans, with some taxa even becoming specialized hypercarnivores, until the group went extinct around 8 Ma ago (Wang & Tedford, 2008). The exact phylogenetic position of the Amphicyonidae is unclear, although affinities with the Canidae and Ursidae (bears) are present (Tomiya & Tseng, 2016). The Caniformia exhibit highly diverse ecomorphological adaptations. They are subdivided into the Arctoidea, which include the Ursidae, Musteloidea (martens and relatives) and the Pinnipedia (seals and relatives), and into the Canidae, which include dogs and relatives (Flynn et al., 2010). The most extreme divergent adaptations can be found in the Pinnipedia,

which appear first in the Late Oligocene in the Pacific and became aquatic (Berta et al., 2018). Further, the Ursidae evolved carnivorous, omnivorous and herbivorous adaptations (Sacco & Van Valkenburgh, 2004). The oldest representative of the Ursidae, *Parictis*, appears in the Late Eocene of North America, but the major ursid radiation took place in the Miocene and later (Rose, 2006).

Further, the Musteloidea, including the Mustelidae (martens and relatives), Mephitidae (skunks), Procyonidae (racoons) and Ailuridae (red panda clade), are comprised of taxa with quite diverse adaptations as well (Law et al., 2018). The musteloid clade is known since the Late Eocene and Early Oligocene of North America (Rose, 2006). These earliest taxa are generally assumed to be stem representatives of the Mustelidae, a clade of probable Eurasian origin, based on younger and more plesiomorphic fossils from Europe (Paterson et al., 2020; Ferrusquía-Villafranca & Wang, 2021). The extant Musteloidea include many generalized species, but during the North American "cat-gap" between 25 and 17 Ma some mustelids also evolved more specialized carnivorous adaptations (Van Valkenburgh, 2007). Extant mustelid taxa are naturally distributed almost worldwide, except beyond the Wallace Line (Hutchins et al., 2003). These taxa mostly exhibit the primitive generalized carnivoran morphology but some also show aquatic adaptations with durophagous dentitions (Van Valkenburgh, 2007).

The Procyonidae appear first in the Late Oligocene to Larly Miocene in Europe, but are confined to North and South America nowadays (Wang et al., 2005a). All extant species of the Procyonidae are omnivorous, with the diet varying depending on food availability and season (Hutchins et al., 2003).

The European genus *Amphictis*, known form the Late Oligocene to Early Miocene, is the oldest known possible representative of the Ailuridae and shows generalized carnivorous adaptations (Salesa et al., 2011). This is in contrast to the only surviving extant member of the family, *Ailurus fulgens*, which is a highly derived folivore from Asia (Tanaka & Ogura, 2017). This herbivorous adaptation appears first in taxa known from the Miocene and Pliocene, which were probably close relatives of the extant *A. fulgens*, while a second lineage, the Simocyoninae, maintained the more primitive carnivorous condition (Salesa et al., 2011).

The oldest known representative of the Mephitidae is *Palaeomephitis steinheimensis* from the Middle Miocene of Europe (Wolsan, 1999). Younger European taxa such as *Mesomephitis* from the Late Miocene may represent forms that are ancestral to the New World mephitids which invaded North America (Wang et al., 2005b).

In the Early Oligocene, the Canidae began to diversify into the Hesperocyoninae, Borophaginae and Caninae (Wang & Tedford, 2008). The Borophaginae subsequently evolved taxa specialized in bone-cracking, but also some that were more generalized and lesser specialized in processing meat (Van Valkenburgh, 2007). They were confined to North America and went extinct only 2 Ma ago (Wang & Tedford, 2008). The Hesperocyoninae were

also confined to North America, where they diversified into many different species and went extinct in the Middle Miocene (Wang, 1994). Within the Hesperocyoninae, some taxa specialized in meat-eating while others adapted to a more omnivorous diet, thus this group of canids also evolved quite diverse adaptations (Wang & Tedford, 2008). The oldest known canine is *Leptocyon*, which lived from the Early Oligocene up to the Late Miocene in North America and remained small and much less diverse than the contemporary borophagine and hesperocyonine taxa it competed with (Wang & Tedford, 2007). *Leptocyon* was adapted for capturing small active prey but had a mixed diet also including fruit (Wang & Tedford, 2008). The Vulpini (true fox clade) appear in the Late Miocene, when fox-sized niches became vacant after the small borophagines went extinct, which resulted in the subsequent diversification of the clade and its eventual spreading to Eurasia in the Pliocene (Wang & Tedford, 2007). Extant foxes live in North America, Eurasia and Africa (Hutchins et al., 2003). Among the extant foxes, the generalized carnivoran morphology is common, indicating no high specialization to carnivory (Van Valkenburgh, 2007). One species (*Otocyon megalotis*) became a specialized insectivore (Hutchins et al., 2003). The Canini ("true dogs") appear first in the Middle Miocene of North America and subsequently dispersed eastwards to Asia and Europe (Wang & Tedford, 2007). The highly specialized carnivorous *Xenocyon* appears in the Middle Pleistocene of Eurasia and subsequently evolved into the extant dhole (*Cuon alpinus*) from Asia and the African hunting dog (*Lycaon pictus*), which are still highly carnivorous species (Wang & Tedford, 2008). Nowadays, the Canini inhabit North America, South America, Eurasia, Africa and Australia, although the latter occurrence (*Canis lupus dingo*) is most likely due to the anthropogenic introduction of their formerly domesticated ancestors (Hutchins et al., 2003). The South American Canini (Cerdocyonina) diversified in North America prior to the emergence of the Isthmus of Panama around 3 Ma ago (Wang & Tedford, 2008). Extant representatives include several fox-like species of *Lycalopex*, the crab-eating fox (*Cerdocyon thous*), the poorly known small-eared dog (*Atelocynus microtis*), the highly carnivorous bush dog (*Speothos venaticus*) (Fig. 1) and the maned wolf (*Chrysocyon brachyurus*), which stocks up its diet with a large proportion of vegetable material (Hutchins et al., 2003). The evolution of the "*Canis* clade" on the other hand is not as well understood, as it became part of a circum-arctic Pliocene and Pleistocene fauna that underwent expansions and contractions depending on climate changes (Wang & Tedford, 2007).

Researching the relationships and evolutionary history of the Feliformia, especially the generalized taxa found within the Viverridae, Nandiniidae, Prionodontidae and Eupleridae, is problematic, as these animals differ only slightly in morphology and have a rather poor fossil record (Barycka, 2007). Thus, the feliform phylogeny is mostly resolved through genomic data. There is, however, also some fossil evidence to back up proposed hypotheses. The oldest feliforms appear in probable Late Eocene deposits of Mongolia and early possible

representatives of the Felidae and the Viverridae appear in Early Oligocene deposits of Europe, indicating an Asian origin of these clades before the "Grande Coupure" (Rose, 2006). Molecular data estimates the split between the Feloidea (Felidae and Prionodontidae) and the Viverroidea (Viverridae, Herpestidae, Hyaenidae and Eupleridae) clades around 39 Ma ago (Zhou et al., 2017; Hassanin et al., 2021).

The extant most plesiomorphic feliform taxon is *Nandinia binotata*, with an ancestral lineage that split from the rest of the Feliformia around 43 Ma ago (Zhou et al., 2017).

Nimravids appear first in the Middle Eocene of Asia, which indicates an early Asian diversification, and a later dispersed to North America and Europe (Averianov et al., 2016). The Nimravidae exhibit a highly carnivorous adaptation, as shown by the presence of elongated "saber-tooth" canines (Van Valkenburgh, 2007). Whether the nimravids are a clade within Feliformia is still highly debated though.

The oldest definitive taxa belonging to the Felidae first appear in Europe and Asia in the Late Oligocene (Hunt, 1998). These early felids remained undiversified due to competition with the more specialized carnivorous nimravids up until the Middle Miocene (Barycka, 2007). Nonetheless, these early felid taxa already show well developed shearing blades on their carnassials, indicating an inclination towards a meat-based diet (Rose, 2006). An early divergence occurred around 32 Ma ago between the Felidae and the Prionodontidae, the clade that includes the extant Asiatic linsang (*Prionodon*) (Zhou et al., 2017). The radiation of the Felidae that started in the Late Miocene resulted in the evolution of highly specialized carnivorous taxa within the Machairodontinae, which include saber-toothed forms, and within the extant conical-toothed felid lineages (Barycka, 2007). The saber-toothed cats inhabited Eurasia, Africa, North America and South America and until they went extinct in the Late Pleistocene; they seem to have outnumbered the conical-toothed cats for the majority of their evolutionary history (Christiansen, 2013). The conical-toothed felids nowadays inhabit all continents except for Australia, the polar regions and some oceanic islands (Hutchins et al., 2003). They are subdivided into the Felinae, which comprise the genera of "small" cats with *Puma* and *Acionyx* being the largest among them, and the Pantherinae, which include the "big" cats within the genus *Panthera* and the clouded leopard (*Neofelis*) (Fig. 1) (Kitchener et al., 2017).

The extant Viverridae inhabit the southern latitudes of Eurasia as well as Africa (Hutchins et al., 2003). They mostly show generalized dietary adaptations, as seen in *Viverra zibetha* (Fig 1.1), with the binturong (*Arctictis binturong*) being more adapted towards frugivory (Van Valkenburgh, 2007; Lambert, et al., 2014). In the Plio-Pleistocene faunas of Asia and Africa, large viverrids also occupied the niches of large, specialized predators (Hunt, 1996).

The Hyaenidae appear first in the Middle Miocene in western Europe (Barycka, 2007). They split off from the herpestid/eulperid clade around 30 Ma (Zhou et al., 2017). The earliest

representatives of the Hyaenidae were small carnivores lacking the specializations of their extant relatives (Barycka, 2007). Extant hyaenid taxa inhabit Africa and most of western and central Asia (Hutchins et al., 2003). The cave hyaena was a subspecies of the extant *Crocuta crocuta* and lived in northern Eurasia in the Middle and Late Pleistocene (Bon et al., 2012). Extant hyaenids are mostly specialized carnivores, utilizing their enlarged premolars to crack bones; the aardwolf (*Proteles cristata*), however, is specialized on insects (Van Valkenburgh, 2007). Around 27 Ma the Eupleridae (malagasy carnivorans) split from the Herpestidae (mongooses) (Zhou, Wang, & Ma, 2017). Euplerids generally exhibit a mostly viverrid-like morphology and dispersed to Madagascar probably in the Late Oligocene or Early Miocene (Barycka, 2007). An exception is the fossa (*Cryptoprocta ferox*), which is a highly specialized predator with feline characteristics, such as retractile claws (Van Valkenburgh, 2007). The evolutionary history of the Herpestidae is especially poorly understood. Herpestid fossils that predate the Pliocene are rare (Hunt, 1996) and for most of those remains the taxonomic status remains problematic. For a long time, the fossil genus *Leptoplesictis*, known form the Early Miocene of Africa and the Middle Miocene of Europe, was believed to be the oldest true herpestid (Barycka, 2007). The remains formerly attributed to this genus however have recently been reassigned to the Viverridae, which shows how problematic the resolution of the early viverrid/herpestid evolution is (Morales & Pickford, 2021). The extant genus *Herpestes* appears first in the Late Miocene of Asia (Barry et al., 1980). The best documentation of herpestid fossils can be found in Plio-Pleistocene deposits from eastern and southern Africa, where a majority of the extant genera first appear (Hunt, 1996). The exhibition of rather subtle dietary and habitational adaptations throughout the Herpestidae may have been a result of the competition with more specialized carnivorans in Africa and Asia throughout their evolution and thus the extant taxa are generalized, opportunistic predators feeding on small vertebrates, invertebrates and in some cases fruits and tubers (Hutchins et al., 2003). The extant herpestid taxa are found almost exclusively in Africa, with only *Herpestes* also occurring in south Asia (Hunt, 1996).
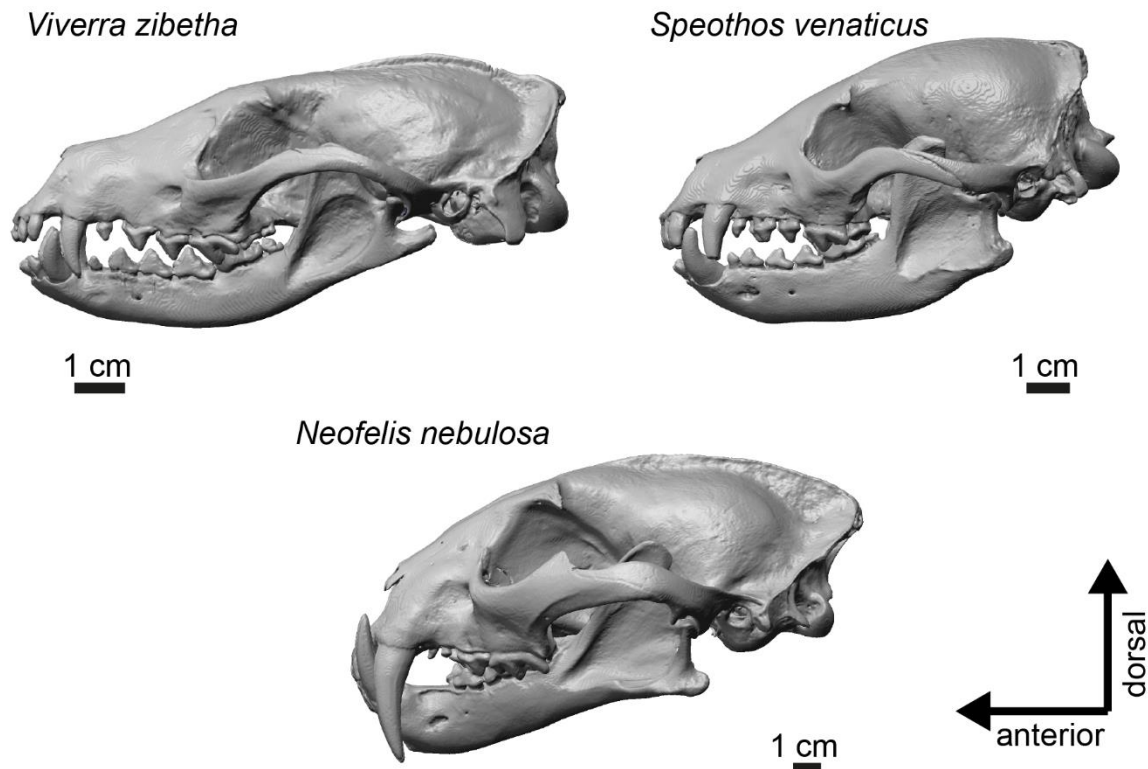
Fig. 1: A selection of skulls of carnivoran taxa included in this study, exemplified by *Viverra zibetha* (ZFMK MAM 1968.0085), *Speothos venaticus* (ZFMK MAM 1954-0154) and *Neofelis nebulosa* (ZFMK MAM 1984.0337). Rendering of µCT data.

2.3 Hyaenodonta

Section 2.3 has been modified and published in: Lang, A. J., Engler, T., & Martin, T. (2021). Dental topographic and three-dimensional geometric morphometric analysis of carnassialization in different clades of carnivorous mammals (Dasyuromorphia, Carnivora, Hyaenodonta). *Journal of Morphology*, 283(1), 91 – 108.

Although the fossil record of the Hyaenodonta remains fragmentary, new findings during the last decade have significantly improved our knowledge on the evolutionary history of this enigmatic group. The Hyaenodonta are generally classified as eutherian mammals within the clade Ferae (O 'Leary et al., 2013). The earliest unequivocal hyaenodont fossils are known from the Middle Paleocene of Africa, however they are not the most plesiomorphic, which makes it hard to reconstruct the geographic origin of the group (Solé et al., 2009). Further, the Late Cretaceous taxon *Altacreodus magnus* from North America is considered to be related to the Hyaenodonta (Fox, 2015). As shown by recent phylogenetic studies, it represents the stem group of the Hyaenodonta together with the Paleocene *Tinerhodon disputatum* (Borths & Stevens, 2019; Solé et al., 2020; Solé et al. 2021). This indicates that the split of the Carnivora and the Hyaenodonta, if both are sister clades within the Ferae, dates back into the

Cretaceous. Unfortunately, the lack of further fossil evidence in both groups doesn't allow yet to solve the enigma of their exact relationship. It is hypothesized that the Hyaenodonta sensu stricto have a European origin in the Early Paleocene, then dispersed into North America, Asia and Africa, forming endemic Northern American, Afro-Arabian and European clades during the Eocene (Borths & Stevens, 2019). Throughout the Eocene, hyaenodonts were present in Europe, where they filled the niches of top predators, and were also present in North America, where they competed with early carnivorans and oxyaenodonts (Morlo, 1999). In North America, there is a drastic decline of hyaenodont diversity at the end of the Eocene, which coincided with the radiation of early Canidae, while the decline of hyaenodont taxa in Europe was less abrupt and in steady progress throughout the Oligocene (Pires et al., 2015). Additionally, the fossil record shows a significant isolated radiation of the hyaenodont Hyainailouroidea in Afro-Arabia during the Paleogene and Neogene and points to a decline of African hyainailouroid diversity only after carnivoran taxa dispersed into Africa around the Oligocene-Miocene boundary (Borths & Stevens, 2017a). Miocene hyainailouroid taxa include some of the largest mammalian land predators and some of them might have been as heavy as a rhinoceros (Borths & Stevens, 2019). Only a few remaining hyaenodont lineages kept coexisting with the Carnivora up until the extinction of the Hyaenodonta in the Late Miocene (Barry, 1988; Wang et al., 2005c). In contrast to this, carnivoran diversity increased during the Oligocene and Miocene (Pires et al., 2015). This pattern is in congruence with the idea that hyaenodonts evolved specialized carnivorous morphotypes first and were later replaced by carnivorans with similar adaptations (Van Valkenburgh, 1988; Wesley-Hunt, 2005). The Hyaenodonta overall were confined to a carnivorous adaptation, with varying degrees of specialization to the consumption of vertebrate meat. Extreme carnivorous adaptations can be found in several taxa, such as the genus *Hyaenodon* (Fig. 2) (Mellett 1969) or the large hyainailouroids *Megistotherium*, *Hyainailouros,* and *Simbakubwa* (Borths & Stevens, 2019). Some taxa, like *Quercytherium*, show additional bone-cracking adaptations in the premolars (Savage 1977). The only known example of an extreme diverging adaptation can be found in the Late Eocene *Apterodon* from North Africa, which has been interpreted to exhibit a semi-aquatic lifestyle with a diet of mostly invertebrates (Grohé et al., 2012). The iterative evolution of convergent carnivorous morphotypes in different mammalian lineages throughout the Paleogene and Neogene, sometimes in direct competition, has been described as "dynastic replacement" by Van Valkenburgh (1999). According to current knowledge, in comparison to other Paleogene carnivorous mammals, the Carnivora and Hyaenodonta were evolutionarily the most successful in terms of diversity and dispersal in Eurasia, North America and Africa, and competed for the longest time of their existence for the same dietary resource, namely vertebrate meat.

Hyaenodon horridus

Fig. 2: Example of a hyaenodont skull (*Hyaenodon horridus* from North America, SMNK-PAL 8511).

2.4 Dasyuromorphia

In contrast to the Carnivora and the Hyaenodonta, the meat eating Dasyuromorpha from Australia belong to the Metatheria (May-Collado et al., 2015). Thus, they have been evolutionary separated from the extant eutherian carnivorous taxa since at least 160 Ma (Fig. 4), based on the discovery of the oldest putative eutherian *Juramaia sinensis* (Luo et al., 2011). Together with the South American Microbiotheria, the Australian marsupials form the clade Australidelphia, based on morphological and molecular data (Asher et al., 2004; May-Collado et al., 2015). The extant Australian mammal faunal composition is linked to the Australian continent, which was once part of the southern supercontinent Gondwana, uniting Australia, Antarctica and South America up until 55 Ma, when the Australian and New Guinean landmasses began to move north (Strahan, 2000). Until the Paleocene, South American marsupial taxa were still dispersing into Australia, which got separated from the other continents between 46 and 35 Ma (Dickman & Russel, 2006). From this point on, the Australian marsupial fauna was mostly isolated from the rest of the world. The oldest known Australian marsupial is the Early Eocene australidelphid *Djarthia murgonensis*, which shows generalized faunivorous adaptations (Godthelp et al., 1999; Beck et al., 2008).

The radiation of the Australidelphia throughout the Paleogene is only poorly documented in the fossil record, especially in regards to the lineages which evolved carnivorous adaptations. The oldest representatives of the Dasyuromorphia appear in the Late Oligocene as mouse sized, most likely insectivorous taxa, with the exact placement of most of these taxa within the

group being unclear (Long et al., 2003). The Late Oligocene *Badjcinus turnublli* was an unspecialized faunivore and is the earliest known representative of the Thylacinidae (Rovinsky et al., 2019). The oldest taxon tentatively assigned to the Dasyuridae is *Barinya*, with two species appearing in the Early and Middle Miocene (Binfield et al., 2016). The extant Dasyuridae include a large variety of small insectivorous species, of which some may occasionally consume vertebrate meat, as well as the exclusively carnivorous Tasmanian devil (*Sarcophilus harrisii*) (Fig 3) and the quolls (*Dasyurus* spp.) (Fig 3), including at least one species (*D. maculatus*) which relies exclusively on vertebrate meat (Hutchins et al., 2003). Throughout the evolution of the Dasyuromorphia, adaptations to carnivory were a recurring trend in several lineages. The earliest known dasyuromorph with a hypercarnivorous adaptation is the dasyurid *Whollydooleya tomnpatrichorum*, which probably lived in the Middle or Late Miocene and might have weighed twice as much as the extant *S. harrisii*, exhibiting a trend towards gigantism (Archer et al., 2016). The Late Miocene *Ganbulanyi djadjinguli*, tentatively referred to the Dasyuridae, exhibits adaptations to a bone-cracking diet (Wroe, 1998). Further, the Pliocene dasyurid *Glaucodon ballaratensis* is adapted to a carnivorous diet, forming a structural intermediate between *D. maculatus* and *S. harrisii* (Gerdtz & Archbold, 2003).

During the Oligocene and most of the Miocene, most of the known thylacinid taxa were small-bodied and showed a progression towards carnivory and increase in body mass throughout their evolution until their recent extinction (Ravinsky et al., 2019). The last member, the Tasmanian tiger (*Thylacinus cynocephalus*) (Fig 3), which went extinct in 1936, was a specialized carnivorous dasyuromorph, probably relying predominantly on small vertebrate prey (Jones & Stoddart, 1998; Rovinsky et al., 2021).

The Middle Miocene Climate Transition seems to mark an important shift in the evolution of Australian carnivorous marsupials, as the subsequent loss in generic diversity within the Thylacinidae seems to have favored the occupation of vacant niches by carnivorous dasyurids (Rovinsky et al., 2019).

Dasyurus hallucatus
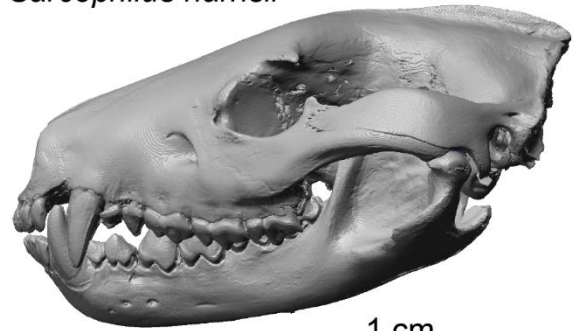
Sarcophilus harrisii

Thylacinus cynocephalus

1 cm

1 cm

1 cm

dorsal

anterior
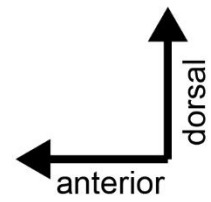
Fig. 3: A selection of skulls of dasyuromorph taxa included in this study, exemplified by *Dasyurus hallucatus* (TMM M-6921), *Sarcophilus harrisii* (ZMB_Mam_001733) and *Thylacinus cynocephalus* (ZMB_Mam_036877). Rendering of µCT data.
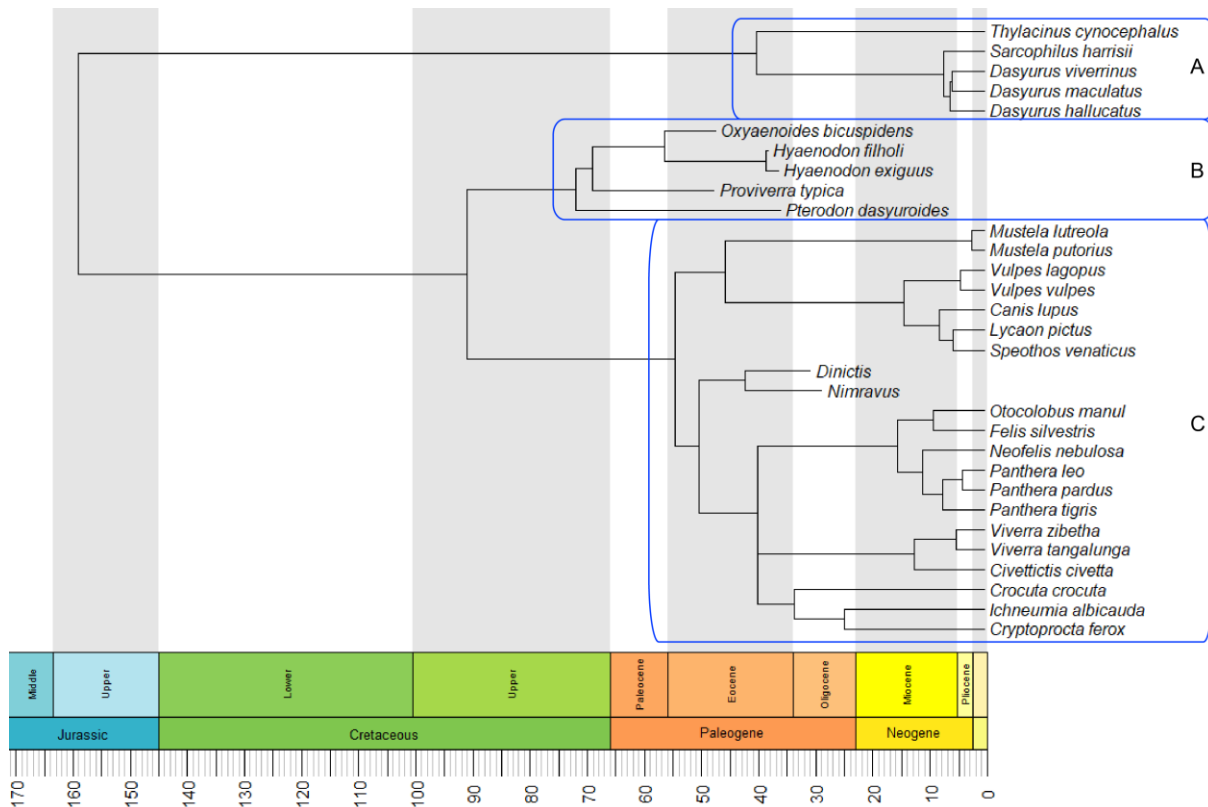
Fig. 4: Phylogeny of the species included in this study. A = Dasyuromorphia; B = Hyaenodonta; C = Carnivora. After: Kumar et al., 2017; Martín-Serra et al., 2014; Wesley-Hunt & Flynn, 2005; Solé & Mennecart, 2019; Bastl et al., 2014; Solé et al. 2018. For details on the phylogenetic data see Methods 3.9.

2.5 Carnassial adaptations

Section 2.5 has been modified and published in: Lang, A. J., Engler, T., & Martin, T. (2021). Dental topographic and three-dimensional geometric morphometric analysis of carnassialization in different clades of carnivorous mammals (Dasyuromorphia, Carnivora, Hyaenodonta). *Journal of Morphology*, 283(1), 91 – 108.

The convergent evolution of morphological characters in carnivorous mammals becomes apparent when looking at their dentitions, especially the cheek teeth. The premolars and molars become specialized for the processing of meat, which in fact may pose a key factor to our understanding of the evolutionary history of carnivorous mammals. The tribosphenic origin of the molars provided them with a set of tools (cutting crests and a crushing protocone/talonid), which were convergently modified for a carnivorous diet in multiple lineages. These modifications resulted in enlarged distal upper (metacrista) and mesial lower (paracristid) cutting blades and the reduction of subordinate cutting structures (prevallum/postvallid shearing) as well as the reduction of the crushing protocone-talonid functional complex (Muizon & Lange-Badré, 1997). Cheek teeth which evolved the

aforementioned characters are typically referred to as "carnassials". Modification and reduction of crown features, especially of the talonid cusps, has been demonstrated to follow a patterning cascade mode of successively (most likely genetically) blocked cusp development (Solé & Ladevèze, 2017). The carnassial blades are formed by two main cusps. Typically, at least one carnassial antagonist forms a V-shaped crest with a central notch to improve the concentration of forces when the teeth occlude, while the other antagonist may form a continuous cutting edge (Evans & Sanson, 2006).

2.6 On the terminology and definition of "carnassialization"

There are two aspects which hamper the understanding ofthe literature on specialized cutting teeth of meat-eating mammals. The first aspect is the terminology itself, as "specialized cutting teeth" have not been described by the same terms by different authors, and sometimes not even by the same authors, throughout the history of research in this field. The second aspect is more technical in nature, as there is no strict definition on when a tooth falls within the spectrum of "cutting specialization".

The term "carnassial" dates back to Frédéric Cuviers "Des dents des mammifères considérées comme caractères zoologiques" (1825), where "false", "true" and "carnassial" molars among mammal taxa are distinguished. As pointed out later by Owen (1840), this primary division of teeth was evidently based on form, size and (relative) position rather than describing same tooth types in a developmental sense, as in the case of carnivoran upper (P4) and lower (m1) carnassials, originally termed "molars". Owen introduces the term "dens sectorius" or "sectorial", referring to the scissor-like function, and proposes its usage for describing the secondary differentiation of premolars or molars (Owen 1840). Thus, the term "sectorial" eventually became frequently used alongside "carnassial" in the literature. Especially, it is used to differentiate teeth with an emphasis on a cutting function, exhibiting cutting crests, from "tubercular" teeth with more blunted cusps. Most influential on this usage of terms is probably "The evolution of mammalian molars to and from the tritubercular type" by Osborn (1888). However, Owen (1868) himself points out that the term "carnassial" is applicable for all lower molars of *Hyaenodon*. Likewise, Cope (1884) describes these same molars as sectorial. It seems that by the end of the 19th century, both terms were simply referring to the same thing, but a debate was about to emerge about exactly what that thing is.

An early link in the chain of the confusing usage of terms can be found in Wortman (1899), who distinguishes the Hyaenodonta (described as "Hyaenodontidae") from two families of Oxyaenodonta ("Oxyaenidae" and "Palaeonictidae") by differences of the position of the most enlarged lower molar (referred to as "sectorial") in each group. An article was published in the same year by Wortman and Matthew (1899), where the terms "carnassial" and "sectorial" are used seemingly interchangeable, the only difference being that both are used as a noun but

the former is never used as an adjective to describe differences in morphology. Matthew (1901) expands upon Wortmans (1899) differentiation of taxa but returns to the exclusive usage of the term "carnassial" for the complementary pair of teeth which chiefly perform the cutting function, and by the position of these teeth distinguishes the Carnivora (in his study extinct groups of Carnivora are described as "adaptive Creodonta") from the Hyaenodonta (in his study included in the "inadaptive Creodonta"), in which the cutting function is chiefly performed by a pair of more distally positioned carnassials (M2 and m3). The same year this definition of carnassials, restricted to a single pair of teeth in each respective clade, is criticized by Wortman (1901), who points out it would have been more accurate to describe which tooth positions overall are specialized for cutting instead of focusing on the "most specialized", as a consequence describing the hyaenodont tooth positions P4-M2 and m1-m3 as carnassials. Specifically, it is proposed that the characterization of a carnassial would be better expressed by stating "which teeth are sectorial" (Wortman 1901, p. 284). In retrospective this seems like a reiteration of Owens (1840) original introduction of the term "sectorial". Nonetheless, in a subsequent and very influential study Matthew (1909) points out the significant difference of the positions of the molar pairs performing the "chief shearing function" between the Carnivora and the Creodonta (including the Hyaenodonta), describing only these "principle shearing teeth" as carnassials, although pointing out that in some taxa the rest of the molars perform a subordinate cutting function This definition is to this day still frequently cited, especially in secondary literature (e.g. Thenius 1989; Rose 2006). At this point, the different usage of nomenclature is mixing with differences in the interpretation of tooth morphology. The restriction of the term "carnassial" to a single pair of complementary teeth in the Creodonta was deemed "not useful" by Butler (1946), who proposed to use the term carnassial for the same teeth as Wortman (1901) did, the most distal pair forming the "principal carnassials". Likewise, he described all molar positions except for the most distal upper one of carnivorous metatherians (Dasyuromorphia and Borhyaenidae) as carnassial teeth, although the degree of specialization decreases from distal to mesial molars (Butler 1946). Butler (1946) used the asymmetry of upper cheek teeth of Carnivora, Hyaenodonta, Oxyaenodonta, Mesonychia and Arctocyonia, quantified as the "posterior edge/anterior edge" ratio, as an indicator for carnassial specialization. This adaptive trend was later coined "carnassialization" by Simpson (1959). Later again, "carnassialization" was specified to refer to the evolution of metacrista/paracristid shear and subsequently has been used as a character in marsupial phylogenetics (Reig & Simpson 1972; Voss & Jansa 2003). In which way a molar position of a specific marsupial taxon is adapted to a carnassial condition thus becomes dependent on specific crown features, resulting in a fluent morphological spectrum of "more" or "less" carnassialized teeth. Molars which perform a prominent shearing function have also been described as "carnassiform" teeth (Werdelin 1987), a term originally introduced by Matthew

(1909) to simply distinguish between carnassial and non-carnassial teeth. The problem is that this original description was purely of qualitative nature. The quantitative based research which became more common throughout the second half of the 20th century used this formerly introduced terminology somewhat more loosely, typically describing relative morphological differences between taxa as indicated by the results of morphometric methods. For example, the molars of Didelphinae are described as "carnassiform" by Szalay (1993), which surely differs from the originally intended usage of the term as introduced by Matthew (1909). Referring to an emphasis on the cutting function, teeth of dilambdodont taxa such as *Chacodelphys* have even been described as "highly carnassialized" (Voss et al., 2004). In contrast, Muizon & Lange-Badré (1997) state that only Carnivora and Creodonta have well-defined carnassials, while the Dasyuromorphia and Borhyaenidae don't. More recent studies emphasize the fact that the Carnivora differ from the Hyaenodonta and the Dasyuromorphia in restricting the cutting function to a single pair of teeth (Van Valkenburgh 2007, Van Valkenburgh & Wayne 2010, Solé & Ladevèze 2017). Additional carnassial teeth have also been called "accessory carnassials"

(Muizon & Lange-Badré 1997). However, given the diverse adaptive patterns of the tooth positions of individual species, inconsistencies can still be found on whether a tooth is interpreted to be a carnassial or not, for example whether the Hyaenodonta have three pairs of carnassials, as interpreted by Van Valkenburgh & Wayne (2010), or two, as indicated by Solé & Ladevèze (2017). Within the spectrum of teeth which are adapted to a more or less carnivorous diet, a strict definition of when exactly a tooth is to be interpreted as a carnassial cannot be identified, and may be impossible due to the subjective nature of the term. Since teeth specialized for carnivorous diets evolved independently in different phyletic lineages, the presence of specific characters like talonid cusps, hypertrophy of the metacone or metastyle, fusion of paracone and metacone or reduction of the metaconid differs between taxa (see Muizon & Lange-Badré 1997, Solé & Ladevèze 2017).

Thus, to a certain degree, the term "carnassial" doesn't even refer to a state of homologous characters, depending on which taxa are included. In the broadest sense, what is described is functional analogy, and only depending on the selection of taxa it may also structural homology. The decision where to draw the line between "carnassial" and "non-carnassial" teeth is arbitrary. Any tooth performing some kind of cutting function may be interpreted to be part of the carnassial adaptive spectrum, including even plesiomorphic tribosphenic dentitions.

The most extreme end of the adaptive spectrum of cutting teeth is undoubtedly interpreted to represent a "carnassial" crown structure. Which structural changes lead to this condition is irrelevant, so it is not inherently describing anatomical homology. The most derived condition is present in Carnivora (e.g., *Felis*), Hyaenodonta (e.g., *Hyaenodon*) and Dasyuromorphia (e.g., *Thylacinus*). In this work, the term "carnassialized" is used for any tooth within this

spectrum, including basal, less-specialized conditions as well as higher specialized teeth which evolved into "true" carnassials (e.g., purely cutting teeth) as defined above. An evolutionary trend towards a more specialized carnassial condition is termed "carnassialization". The term "principal carnassial" is used to describe the most carnassialized tooth of the tooth row.

2.7 Carnassial adaptations in the Carnivora

The carnivoran carnassial condition is characterized by the shearing blades, formed by the P4 and the m1 (Fig. 5), and the posterior post-carnassial molars (Van Valkenburgh, 2007). In older literature, it was postulated that on the upper carnassial of carnivorans, the paracone and the metacone got fused, and the distal part of the carnassial blade is formed by the metastyle (Biknevicius & Van Valkenburgh, 1996). More recent literature, however, acknowledges that this fusion did not happen in carnivoran carnassials and instead the shearing blade of the upper carnassial is formed by the crest connecting the paracone and the metacone (Solé & Ladevèze, 2017). The protocone of the P4 is either absent or, depending on the taxon, situated lingual, anterior or posterior to the paracone and it is always reduced in size compared to the general tribosphenic condition (Muizon & Lange-Badré, 1997).

In the early carnivoramorphs, the posterior molars successively decrease in size from mesial to distal (Thenius, 1989). The main shearing locus is between the P4 distal trigon and m1 mesial trigonid blade, with the paracone of the M1 projecting far lingually and forming the embrasure for the trigonid blade (Flynn & Wesley-Hunt, 2005). Extant carnivorans are characterized by a high variability of molar reduction and development of the carnassial complex (Ungar, 2010). A typical character of extant carnivoran dentitions is the loss of the M3 (Flynn & Wesley-Hunt, 2005). The more generalized species like *Ichneumia albicauda, Viverra tangalunga, Viverra zibetha, Vulpes lagopus,* and *Vulpes vulpes* tend to be more conservative in their tooth formula, with only one or two post-carnassial molar positions being lost (Fig. 5A1 5A2). These taxa also have a lower m1 with a tricuspid talonid and with all trigonid cusps present (Fig. 5 A4). In the caniform species *Canis lupus*, *Lycaon pictus,* and *Speothos venaticus*, both the post-carnassial reduction as well as talonid cusp reduction are more advanced (Fig. 5B1–B4). In *L. pictus* and *S. venaticus*, the talonid basin is restructured into a unicuspid cutting "trenchant heel" with only the hypoconid being present (Fig. 5 B4) (Van Valkenburgh, 1991). Additionally, the metaconid is reduced. A cutting talonid on the lower carnassial is also present in the Nimravidae, with the metaconid either being integrated in the talonid blade or absent and the post-carnassial teeth apart from a vestigial M1 missing entirely (Barrett 2015). The most carnassialized carnivoran teeth are found among feliforms. In the Hyaenidae (excluding the insectivorous *Proteles*), the post-carnassial dentition is absent and the carnassials exhibit enlarged carnassial blades, forming from the parastyle along the paracone to the metacone, with mesiad displacement of the small protocone (Thenius 1989).

The talonid of the m1 is vestigial. The carnassials of felids exhibit an even more pronounced simplification. The carnassial blade on the P4 is formed by the parastyle, paracone and metacone, whereas the protocone is vestigial (Fig. 5C3). The talonid on the m1 and the post-carnassial dentition apart from a vestigial M1 are absent. The carnivoran post-carnassial molars (M1, M2, M3, m2, m3), if present, are not carnassialized. They are characterized by a reduced trigonid with blunted cusps and an overall flat, bunodont crown relief. In some taxa with weakly carnassialized teeth such as *Viverra zibetha* and with more carnassialized teeth such as *Speothos venaticus*, a prominent paracingulum extends from the praeprotocrista along the base of the paracone on the M1. In contrast to the Hyaenodonta and the Dasyuromorphia, which have multiple carnassialized "homodont" cheek teeth, the cheek dentition of carnivorans can be described as "heterodont" in taxa where the post-carnassial teeth are not reduced.
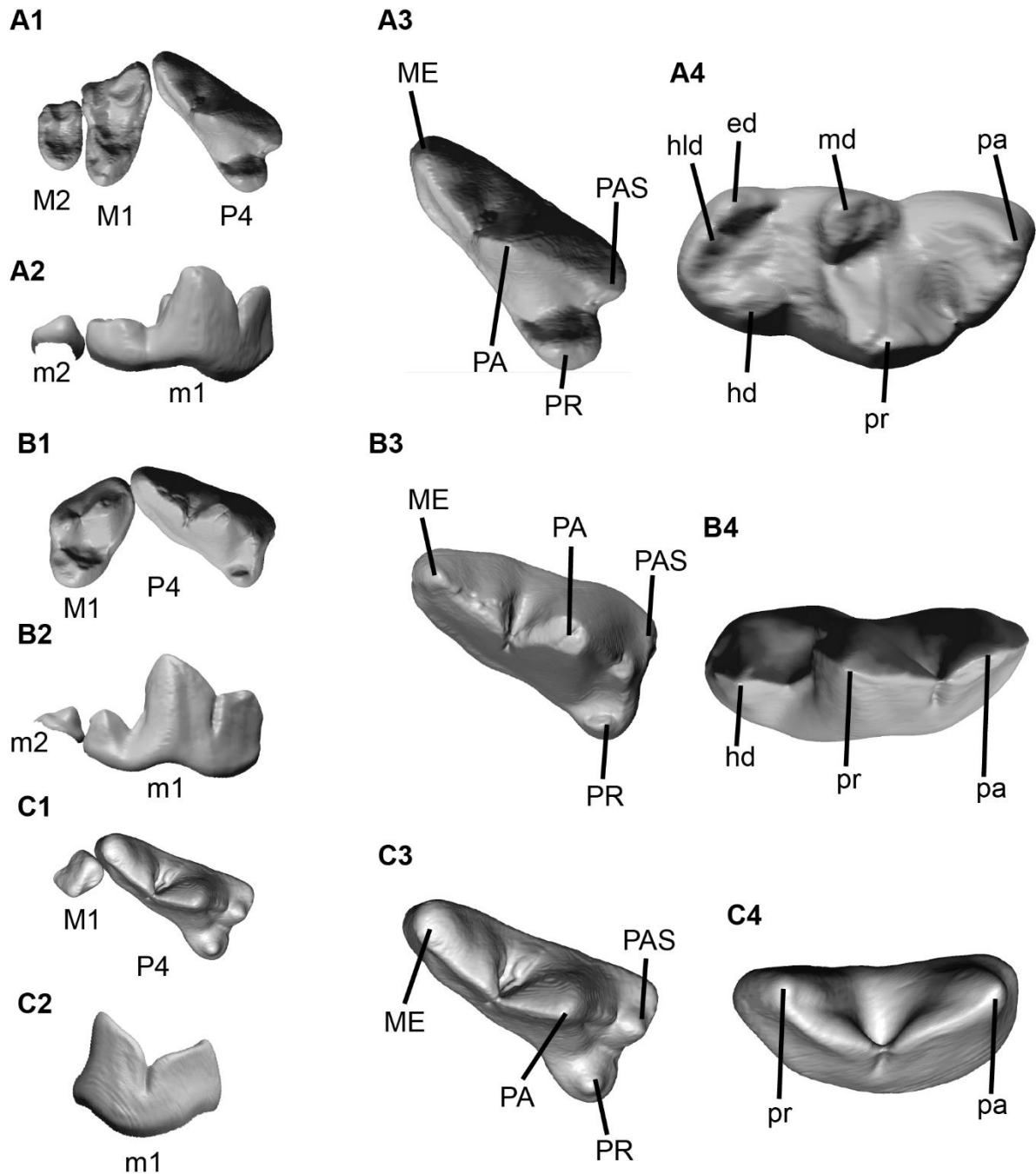
Fig. 5: Cheek dentitions of *Viverra zibetha* (A1 – A4), *Speothos venaticus* (b1 – b4) and *Felis silvestris* (C1 – C4) in detail. Depicted are the upper right tooth row from P4 to M2 (M2 reduced in *S. venaticus* and *F. silvestris*) in occlusal view (A1, B1, C1), the lower right tooth row from m1 to m2 (m2 reduced in *F. silvestris*) in buccal view (A2, B2, C2) as well as the right P4 (A3, B3, C3) and the right m1 (A4, B4, C4) in detail in occlusal view. Anterior is to the right. The depicted teeth are not to scale. Rendering of μCT data .

2.8 Carnassial adaptations in the Hyaenodonta

The upper carnassials of hyaenodonts are formed by the P4, M1 and the M2. The crest extending distally from the metacone connecting to the metastyle forms the carnassial blade (Fig. 6). In the primitive condition (e.g., *Proviverra*), the paracone and metacone are well separated and the mesial and distal portion of the molars are equal in size (Fig. 6 A3) (Thenius, 1989). The metacone and the paracone may become paired or completely fused in higher specialized taxa, with the metacone absorbing the paracone (Fig. 6 B3) in the Hyaenodontidae (Fig. 6 C3) or the paracone absorbing the metacone in the Hyainailouridae (Muizon & Lange-Badré, 1997). In cases of complete absorption, the remaining cusp has been referred to as "pseudamphicone" (Lange-Badré & Dashzeveg, 1989) or in more recent literature as "amphicone" (Solé et al, 2015). The M3 is either reduced in size with a simplified morphology or in some taxa (e.g., *Hyaenodon*) it is completely absent (Fig. 6 C1). The carnassial blade of the P4 is only weakly pronounced, whereas it is more emphasized in the M1 and M2 and not present in the M3 (see Figs. 6A1, 6B1 6C1). The protocone is generally reduced in size and either located well separated (*Proviverra*) or close in mesio-lingual position to the paracone (*Pterodon*) or it is located at the base of the paracone (*Hyaenodon*). The lower carnassials are formed by the m1, m2, and m3 (Figs. 6A2, 6B2, 6C2). In general, the lower molar morphology tends to be more conservative and the pattern of carnassial specialization is very similar to the Carnivora. The carnassial blade is formed by the crest connecting the protoconid and the paraconid and is well pronounced on all molar positions, whereas the metaconid is lost in several taxa (e.g., *Oxyaenoides*, *Pterodon*, *Hyaenodon*). The talonid with a hypoconid, entoconid and hypoconulid is present in "primitive" hyaenodont taxa like *Proviverra* (Fig. 6A4), in others it is largely reduced with only the hypoconid present (*Oxyaenoides*, *Pterodon*) (Fig. 6B4) and in the m3 of *Hyaenodon* it is completely reduced (Fig. 6C4). As noted by Butler (1946), the M2 and m3 are the principal carnassial teeth, which are the largest in size and possess the largest carnassial blades. Emphasizing this locus of the dentition is in expense of the most distal (M3) and mesial (P3 - P2 and p4 - p2) tooth positions, which get reduced (Butler, 1946).
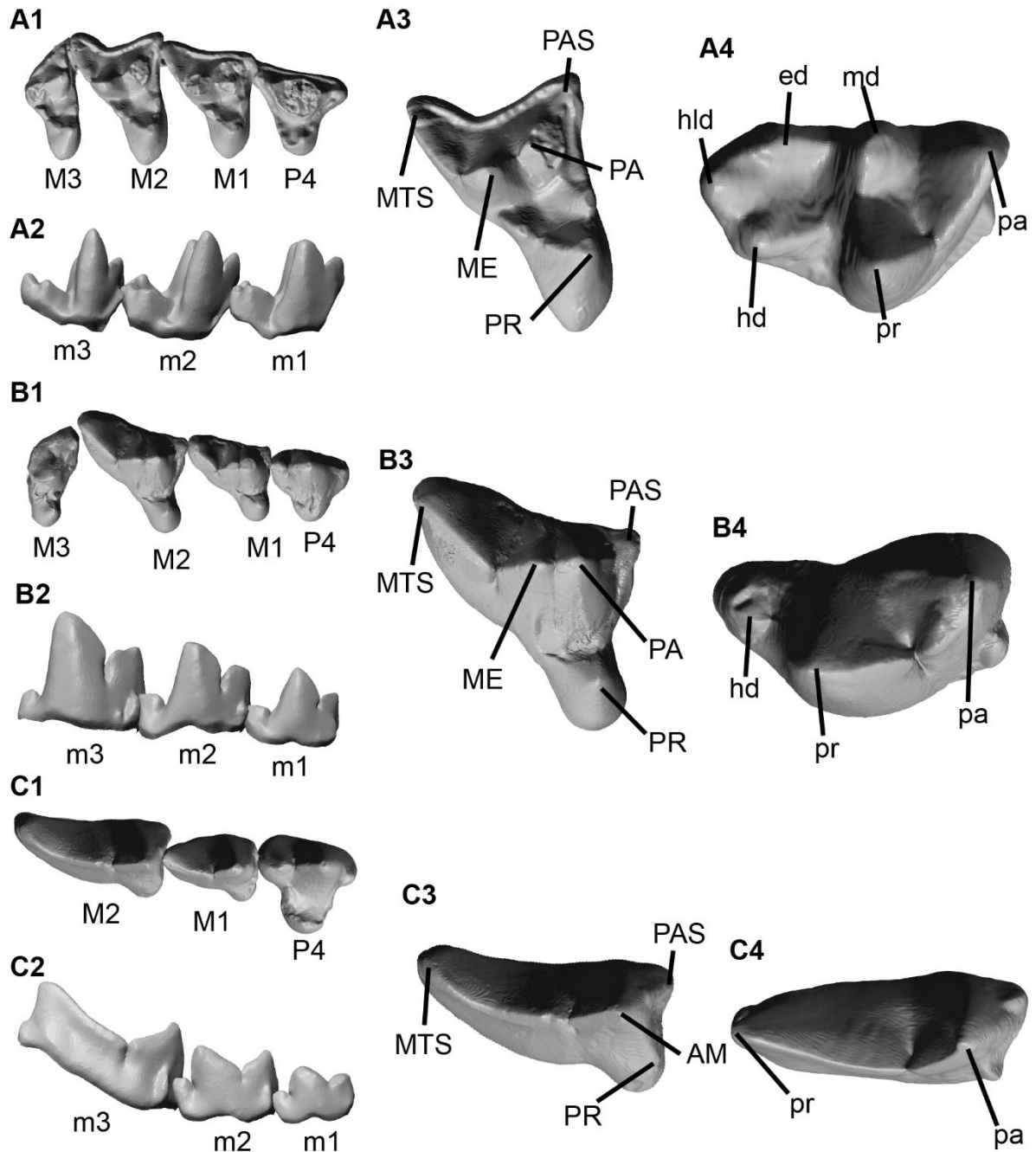
Fig. 6: Cheek dentitions of *Proviverra typica* (A1 – A4), *Pterodon dasyuroides* (B1 – B4) and *Hyaenodon exiguus* (C1 – C4) in detail. Depicted are the upper right tooth row from P4 to M3 (M3 reduced in *H. exiguus*) in occlusal view (A1, B1, C1), the lower right tooth row from m1 to m3 in buccal view (A2, B2, C2) as well as the right M2 (A3, B3, C3) and the right m3 (A4, B4, C4) in detail in occlusal view. Anterior is to the right. The depicted teeth are not to scale. Rendering of µCT data.

2.9 Carnassial adaptations in the Dasyuromorphia

In dasyuromorphs, the carnassials are formed by the upper M1, M2 and M3 and the lower m2, m3 and m4 molar positions (Fig. 7) (Solé & Ladevèze, 2017). The upper molars, of which the M4 is typically reduced in size, have three main cusps (paracone, metacone and protocone) and additional stylar cusps, with an enlarged metacone (Thenius, 1989). The paracone is reduced in size and may become connate to the metacone

(Muizon & Lange-Badré, 1997). The metacone is connected to the distobuccally positioned metastyle via a well-developed postmetacrista (Archer, 1976). This elongated postmetacrista forms the upper carnassial blade in dasyuromorphs and the edge is not forming a carnassial notch (Muizon & Lange-Badré, 1997). In *Sarcophilus*, there is a tendency of the metacone to get fused with stylar cusp D (Thenius, 1989). The protocone is well developed in *Dasyurus* (Fig. 7A3), but is reduced in size in *Sarcophilus* (Fig. 7B3) and *Thylacinus* (Fig. 7C3). The M4 has a simplified morphology and lacks the presence of a carnassial blade. The lower first molar has a weakly developed paraconid and thus does not have a carnassial blade. On the m2, m3 and m4, the carnassial blade is well developed between the paraconid and the protoconid and forms a V-shaped crest. The metaconid is well developed in the molars of *Dasyurus* (Fig. 7A4). (Thenius, 1989). In *Sarcophilus*, the metaconid is displaced distally (on the m2 and m3) and the bicuspid talonid is located posterobuccally, with the entoconid being absent (Archer et al., 2016 earliest carnivorous daysurid). In *Thylacinus*, the metaconid is completely reduced (Fig. 7A4) (Thenius, 1989). The talonid typically has a hypoconid, hypoconulid and an entoconid, with the hypoconulid projecting posteriad and locking into the hypoconulid notch of the anterior cingulid of the distal molar in *Dasyurus* (Archer et al., 2016). In *Thylacinus*, the entoconid and hypoconulid are reduced in size, with the hypoconid forming a trenchant heel (Solé & Ladevèze, 2017). Like in the Hyaenodonta, the carnassial condition increases along the tooth row from mesial to distal, with the M3 and the m4 showing the most extreme specializations, as in the loss of the metaconid on the m4 in *Sarcophilus* (Fig. 7B3), whereas it is present on the mesial molars (Butler, 1946).
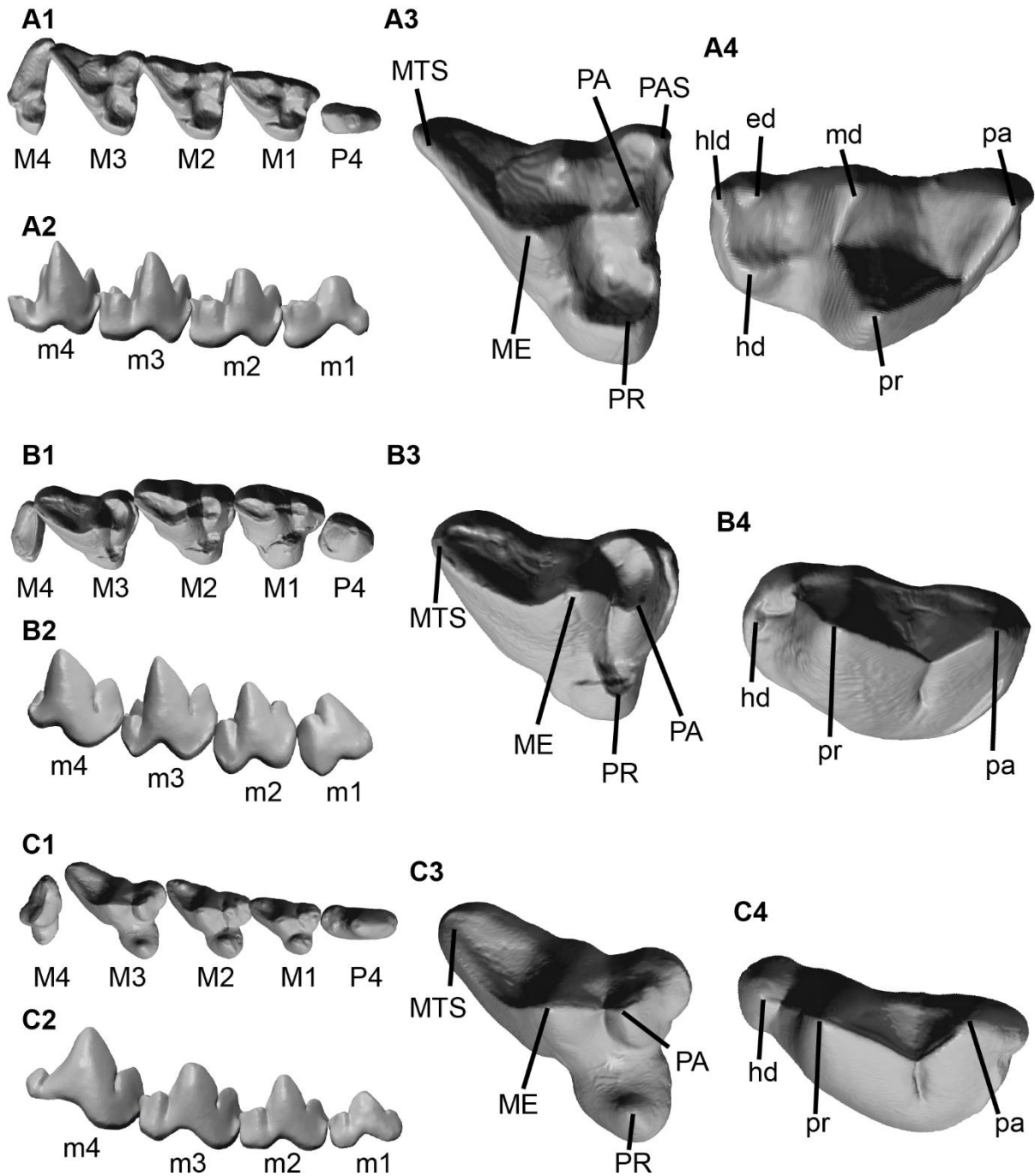
Fig. 7: Cheek dentitions of *Dasyurus viverrinus* (A1 – A4), *Sarcophilus harrissii* (B1 – B4) and *Thylacinus cynocephalus* (C1 – C4) in detail. Depicted are the upper right tooth row from P4 to M4 in occlusal view (A1, B1, B1), the lower right tooth row from m1 to m4 in buccal view (A2, B2, C2) as well as the right M3 (A3, B3, C3) and the right m4 (A4, B4, C4) in detail in occlusal view. Anterior is to the right. The depicted teeth are not to scale. Rendering of µCT data.

3. Materials and Methods

3.1 Investigated taxa

Section 3.1 has been modified and published in: Lang, A. J., Engler, T., & Martin, T. (2021). Dental topographic and three-dimensional geometric morphometric analysis of carnassialization in different clades of carnivorous mammals (Dasyuromorphia, Carnivora, Hyaenodonta). *Journal of Morphology*, 283(1), 91 – 108.

A total of 12 dasyuromorph, 47 carnivoran and 12 hyaenodont specimens were included in this study, resulting in 110 individual teeth of 31 species within 23 different genera that were quantified (Tab. 1). Since in the Carnivora the bunodont post-carnassials are not part of the convergent adaptive spectrum of carnassialization (see 2.7), only the carnivoran m1 was included in this study, while the complete lower molar series of hyaenodonts (m1-m3) and the three distal molars of the dasyuromorphs (m2-m4) were included. Because the dasyuromorph m1 lacks a complete trigonid and mesial cutting blade with associated attritional shearing wear and further there is no antagonistic shearing blade on the P4, it was excluded from this study as it is not regarded as "carnassialized".

Taxon	Order	Carnassial type	Specimens	n MCP	n ICP	n PCP
Canis lupus (Linnaeus, 1758)	Carni-vora	derived	ZFMK MAM 1978.0268, ZFMK MAM 1988.0151, SMF 15 699, SMF 36 408	-	-	4
Civettictis civetta (Schreber, 1776)	Carni-vora	basal	ZFMK MAM 1958.0012†, ZFMK MAM 1993.0705, ZFMK MAM 1958.0015	-	-	DTA: 3 GMA: 2
Crocuta crocuta (Erxleben, 1777)	Carni-vora	derived	IGPB M 5997, IGPB M 418, IGPB M 427	-	-	3
Cryptoprocta ferox (Bennett, 1833)	Carni-vora	derived	ZFMK MAM 1987.0584	-	-	1

Dinictis sp. (Leidy, 1854)	Carni-vora	derived	SMNK-PAL 35101, SMNK-PAL 35102†, SMNK-PAL 9090§	-	-	DTA: 2 GMA: 1
Felis silvestris (Schreber, 1777)	Carni-vora	derived	ZFMK MAM 2018.0100, ZFMK MAM 2018.0102, ZFMK MAM 2018.0106	-	-	3
Otocolobus manul (Pallas, 1776)	Carni-vora	derived	ZFMK MAM 1965.0510	-	-	1
Ichneumia albicauda (Cuvier, 1829)	Carni-vora	basal	ZFMK MAM 1931.0056†, ZFMK MAM 1976.0125, SMF 16 553, SMF 32 735, SMF 32733‡	-	-	4
Lycaon pictus (Temminck, 1820)	Carni-vora	derived	ZFMK MAM 1956.0888, ZFMK MAM 1981.0527, ZFMK MAM 2001.0275	-	-	3
Mustela lutreola (Linnaeus, 1761)	Carni-vora	derived	IGPB M 2151a, IGPB M 2151b, IGPB M 2151c	-	-	3
Mustela putorius (Linnaeus, 1758)	Carni-vora	derived	IGPB M 335	-	-	1
Neofelis nebulosa (Griffith, 1821)	Carni-vora	derived	ZFMK MAM 1984.0337	-	-	1
Nimravus sp. (Cope, 1879)	Carni-vora	derived	IGPB M 6134	-	-	1

Panthera leo (Linnaeus, 1758)	Carni-vora	derived	ZFMK MAM 2006.0031	-	-	1
Panthera pardus (Linnaeus, 1758)	Carni-vora	derived	ZFMK MAM 1997.0547	-	-	1
Panthera tigris (Linnaeus, 1758)	Carni-vora	derived	ZFMK MAM 1986.0118	-	-	1
Speothos venaticus (Lund, 1842)	Carni-vora	derived	ZFMK MAM 1992.0565, ZFMK MAM 1954.0154, ZFMK MAM 1987.0386	-	-	3
Viverra tangalunga (Gray, 1832)	Carni-vora	basal	SMF 20 928, SMF 697	-	-	2
Viverra zibetha (Linnaeus, 1758)	Carni-vora	basal	ZFMK MAM 1968.0085, SMF 16 516	-	-	2
Vulpes laogpus (Linnaeus, 1758)	Carni-vora	basal	IGPB M 553, IGPB M 4005, IGPB M 4007	-	-	3
Vulpes vulpes (Frisch, 1775)	Carni-vora	basal	IGPB M 6182, IGPB M 6238, IGPB M 6258	-	-	3
Dasyurus viverrinus (Shaw, 1800)	Dasyuro-morphia	basal	SMF 378†, SMF 1480, SMF 1485, SMF 15505	DTA: 4 GMA: 3	4	4

Dasyurus hallucatus (Gould, 1842)	Dasyuro-morphia	basal	TMM M-6921	1	1	1
Dasyurus maculatus (Kerr, 1792)	Dasyuro-morphia	basal	UMZC A6.10/3	1	1	1
Sarcophilus harrisii (Boitard, 1841)	Dasyuro-morphia	derived	ZMB_Mam_001733, ZMB_Mam_002343, ZMB_MAM_089499§, NMB 2521§, NMB 10548§, NMB 10550§, NMB 10596§	2	2	2
Thylacinus cynocephalus (Harris, 1808)	Dasyuro-morphia	derived	ZMB_MAN_002986§, ZMB_Mam_047902, ZMB_Mam_036877, HLMD-M-1250, NMB 2526	4	4	4
Hyaenodon sp. (Laizer & Parieu, 1838)	Hyaeno-donta	derived	MNHN.F.Qu 8471, MNHN.F.Qu 8467	2	2	2
Hyaenodon exiguus (Gervais, 1872)	Hyaeno-donta	derived	NMB Q.B.603, NMB Q.C.221, NMB Q.C.2526§, NMB Q.C.938§, NMB Q.B.860§, NMB Q.C.977§	2	2	2
Hyaenodon filholi (Schlosser, 1877)	Hyaeno-donta	derived	NMB Q.B.771, MNHN.F.Qu 8421	2	2	2
Oxyaenoides bicuspidens (Matthes, 1967)	Hyaeno-donta	derived	GMH XIV-2909-1954, GMH XIV-2910-1954§	1	1	1

Proviverra typica (Rütimeyer, 1862)	Hyaeno-donta	basal	NMB En.130, NMB En.176, NMB En.179, NMB Ek.30§, NMB Ek.178§, NMB En.252§, MNB En.198§, NMB En.160§, NMB En.191§	1	1	1
Pterodon dasyuroides (Blainville, 1839)	Hyaeno-donta	derived	NMB Q.B.606, NMB Q.C. 413, MNB Q.C.854§, MNB Q.C.972§, NMB Q.B.569§, MNHN.F.Qu 8669§, MNHN.F.Qu 8734§, MNHN.F.Qu 8787§, MNHN.F.Qu 8736§, MNHN.F.LDB 49§	1	1	1

Tab. 1: List of taxa with specimen collection number of which lower carnassials were used for this study. Abbreviations: GMH = Geiseltal Collection, Halle an der Saale, Germany; HLMD = Hessisches Landesmuseum Darmstadt, Germany; IGPB = Institute of Geosciences, Paleontology, Rheinische Friedrich-Wilhelms-Universität Bonn, Germany; MNHN = Muséum national d'Histoire naturelle, Paris, France; NMB = Naturhistorisches Museum Basel, Switzerland; SMF = Senckenberg Naturmuseum Frankfurt, Senckenberg Gesellschaft für Naturforschung, Germany; SMNK = Staatliches Museum für Naturkunde Karlsruhe, Germany; TMM = Texas Memorial Museum, University of Texas, Austin, USA; UMCZ = University Museum of Zoology, University of Cambridge, United Kingdom; ZFMK = Zoologisches Forschungsmuseum Alexander Koenig, Bonn, Germany; ZMB = Museum für Naturkunde, Humboldt-Universität zu Berlin, Germany. The numbers specify the count of lower carnassials used in the DTA and/or GMA. † = Teeth of this specimen were omitted in the GMA. ‡ = Teeth of this specimen were omitted in the DTA. § = Specimen was not used in DTA and GMA.

3.2 Function and wear of teeth

The mapping of tooth wear, especially by attrition, is an important tool in odontology to characterize the function of teeth. Attrition occurs when antagonistic teeth come into contact, which produces flattened, polished wear facets on the enamel surface, typically with parallel striations which indicate the relative tooth movement (Butler, 1972). These facets indicate which structures of the crown relief are part of occlusal interaction, based on where they are located, and further indicate the alignment of the lower jaw during mastication (Butler, 1952). In contrast to attrition, abrasion results in a successive removal of the enamel cover. This

results in areas with exposed dentine, with enamel ridges forming at the margin that may be used for the processing of highly abrasive food, especially in herbivores (Janis & Fortelius, 1988). Like the molars of all extant mammals, carnassial molars are derived from a plesiomorphic tribosphenic molar condition (Solé & Ladevèze, 2017). Thus, to understand the occlusal relationships of carnassial teeth, the function of tribosphenic teeth must be discussed first. Mills (1955, 1966) recognizes that the chewing stroke in tribosphenic dentitions can be divided in multiple phases in which occlusal contact is occurring. He distinguishes a "buccal phase" during which the jaw is closing, the terminal "centric" point of jaw closure and the final "lingual phase" when the jaw is opening again.

Crompton and Hiimae (1969) subdivide the chewing stroke of *Didelphis* as a representative with a "primitive" tribosphenic condition into a "preparatory stroke", a "power stroke" and a "recovery stroke", whereby the occlusal contact occurs during the power stroke. Since most mammals exhibit an anisognathic condition in which the mandibular rami are narrower than those of the maxilla, the mandibular teeth must first be moved in direction of the antagonists via lateral movement of the lower jaw. Thus, the chewing stroke in tribosphenic dentitions is performed only by the "active side", while the teeth of the "balancing side" do not come into contact.

Based on these observations, Crompton and Hiimae (1970) note, that the point of "centric occlusion", in which the protocone of the upper molar is firmly locked in the talonid basin of the lower antagonist, occurs only in one side of the jaw (unilateral) during the power stroke of tribosphenic teeth. This point is also described as "maximum intercuspation" and should not be confused with the "centric position" of the jaw in symmetrical position about the midline, during which no occlusal contact occurs.

In their study on the function of different primate molars, Kay and Hiimae (1974) describe the power stroke in more detail. In the tribosphenic dentition, it is divided into two phases. At the beginning of phase I the lower molar is positioned buccally to the upper antagonist. It moves upwards in mesio-distal direction until it reaches the point of centric occlusion. This point is followed by phase II, where the lower molar is moving downwards and the protocone is moving out of the talonid basin until the mesio-lingual movement results in the loss of occlusal contact. Jaw movement remains continuous, there is no interruption between both phases. This terminology replaces the former introduced terms of "buccal phase" and "lingual phase".

Crompton (1971) mapped the attritional facets of tribosphenic and more plesiomorphic pretribosphenic molars and introduced a unified facet terminology. The facet naming scheme of Crompton homologizes the facets of different taxa and makes it possible to determine

similarities and differences in the presence of specific facets or occlusal relationships of complementary crown structures in tribosphenic and pretribosphenic molars.

For the tribosphenic molar, Crompton (1971) describes six characteristic facets. The halfmoon shaped facet 1 is located along the edge of the vertical oriented shearing surface on the mesial side of the praeparacrista that connects the paracone with the stylocone. On the lower molar, the distal trigonid blade forms the antagonistic occlusal structure on which facet 1 forms. The margin of this surface is the protocristid. During the power stroke, the lower molar is moving upwards in lingual direction, thus facet 1 on the lower molar runs from the apex of the metaconid to the point of juncture between the distal trigonid blade and the oblique cristid. Facet 2 runs along the distal edge of the postmetacrista, which connects the metacone with the metastyle. During the power stroke, this surface occludes with the mesial trigonid blade, where facet 2 extends from the paracristid. While the shearing surfaces of facet 1 stay in contact for the complete power stroke, the surfaces of facet 2 may lose occlusal contact during tooth movement. On the upper molar, facet 3 is found on the shearing surface that extends distally from the postparacrista. The antagonistic shearing surface is located mesially along the oblique cristid on the lower molar. The shearing surface of facet 4 runs mesially along the praemetacrista of the upper molar. On the lower molar, facet 4 can be found on the distal shearing surface that extends from the hypocristid. The surfaces of facet 3 and 4 are inclined lingually, parallel to the jaw movement during the power stroke. The shearing surfaces of facet 5 occlude at the end of the power stroke. On the upper molar, facet 5 extends mesial to the praeprotocrista, connecting the protocone with the metacone. Since facet 5 is bordering facet 1 on the upper molar, the same is true for the lower molar, where facet 5 is bordering facet 1 lingually on the distal trigonid blade. Facet 6 is formed on the shearing surface distally bordering the postprotocrista. During the power stroke it occludes with the surface bordering the entocristid, which connects the entoconid with the buccal base of the distal trigonid blade. The subordinate facets 1b, 2b and 3b can be found on tribosphenic molars with a paraconulus or a metaconulus present, where they duplicate the function of the main facets (Crompton, 1971). This terminology has been extended by Kay & Hiimae (1974), who describe additional facets that form during phase II of the power stroke or when an additional hypocone is present. For some carnassial dentitions, facet 9 is of interest, since it forms during phase II, when the protocone is in occlusion with the talonid basin. Facet 9 forms on the buccal flank of the protocone, bordering the praeprotocrista and the postprotocrista. The antagonistic facet forms on the lower molar, on the lingual flank of the hypoconid, bordering the precristid and the hypocristid lingually. The presence of facet 9 can be correlated with a grinding function during phase II of the power stroke (Kay & Hiimae, 1974).

As an alternative to the facet nomenclature of Crompton (1971) and Kay & Hiimae (1974), a modular facet nomenclature was proposed by Schultz et al. (2017). This nomenclature, based on the topographic position of facets, is comprised of two modules (Fig. 8). The first module describes the crown structure on which a facet is located, whereas the second module describes the incident angle of the facet (Schultz et al., 2017, Schultz et al., 2020). Thus, the exact location and orientation of a facet is stated using this nomenclature and this makes it easier to use in a morphologically diverse sample like in this study, as differences concerning facet formation are emphasized in the naming scheme.
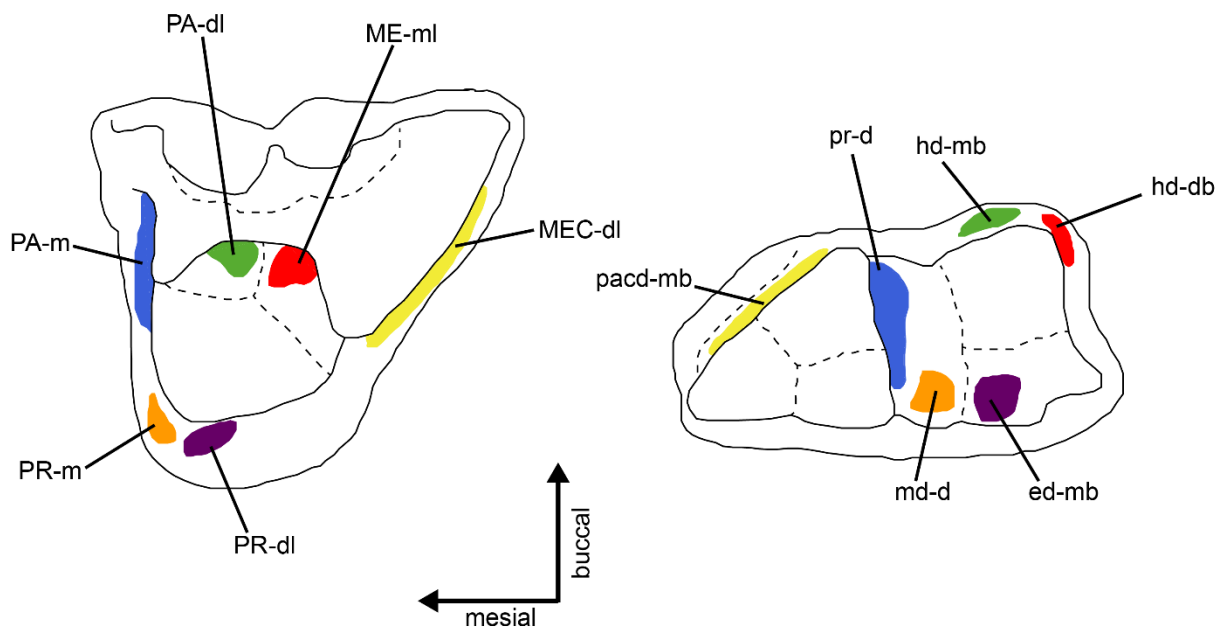

Fig. 8: Schematic drawings of an upper (left) and lower (right) tribosphenic molar with the corresponding wear facets. Drawings, position of facets and naming scheme after the molars of *Didelphis* as figured in Schultz et al. (2017).

3.3 Documentation of tooth wear

Tooth wear was documented using the digital microscope AXIO Zoom V16 (Zeiss). Pictures were generated from image stacks of 20 to 30 focal planes, using the augmented focus depth function of the ZEN pro software (Zeiss). The wear was documented either on the original specimen or on epoxy resin tooth casts. The Provil ® novo Light regular set (Heraeus Kulzer) was used to create molds of the teeth. This silicone is used in dentistry and due to its high casting accuracy of < 0.1 mm can be used to document microwear on the tooth surface. Casts were made using the RenLam ® M-1 (Huntsman Advanced Materials) epoxy resin and the Ren ® HY 956 (Huntsman Advanced Materials) hardener. For coloration of the casts, the Araldite ® DW 0137 Colouring Paste (Huntsman Advanced Materials) was used.

3.4 OFA Analysis

The Occlusal Fingerprint Analyser (OFA), developed as part of the DFG Research Unit 771, enables a virtual reconstruction of the chewing stroke. For the reconstruction, 3D-surface models of antagonistic molars are imported into the software, which are then brought into occlusion via movement in virtual space (Benazzi et al., 2011; Kullmer et al. 2020). In this study, the 3D-models constructed from µCT-data were used for the simulation of occlusion. For the selected taxa, the carnassial tooth rows were used for OFA analysis. In carnivoran taxa, post-carnassials, if present, were also included in the analysis to check the difference in the occlusal pattern in contrast to dentitions with multiple carnassial teeth and no post-carnassials. The model for each single tooth was reduced to a maximum of 50,000 triangles before the analysis to reduce the required processing power using the mesh optimization tool of PolyWorks 2015 IR 13 (InnovMetric Software Inc.). The antagonistic tooth rows were positioned in centric occlusion using the manual alignment tools of PolyWorks. Then, a new coordinate system was generated, in which the xy-axis spans the occlusal plane and the z-axis is oriented in occlusal direction. The oriented tooth rows were then imported in the OFA software and a Scene Path Point was placed for the lower teeth in centric occlusion. A second Scene Path Point was then placed at the starting point of the chewing stroke, with the jaw opened. If a second phase is present, an additional Scene Path Point was placed with the lower teeth in location of the end of Phase II. Then, points were placed for the lower teeth which are passed during the movement of chewing. Only the power stroke can reliably be reconstructed using the OFA, as it is the phase in which occlusal contacts occur which can be backed up with qualitative evidence from facets present on the teeth. The directions of the preliminary stroke and the recovery stroke are inferred from the movements of the teeth in phase I and phase II. If no phase II is present, a simple orthal opening of the jaw is inferred. The OFA software detects collision areas between antagonistic structures during the power stroke. Based on these contact areas, the movement of the teeth from one Scene Path Point to another may be altered. During movement of the lower tooth row points are placed in regular intervals which mark the trajectory path.

The OFA software enables the simulation of a chewing stroke with a characterization of movement, inclination, number of phases and occlusal contacts that approximates the information obtained from observations of the morphology and wear patterns of teeth. A hypothesis regarding movement and interaction of teeth can thus be verified. Further, the temporal and spatial occurrence of occlusal contacts, calculated as contact areas, can be inferred. The area of occlusal contacts occurring per timestep were exported and used to construct diagrams for a graphical depiction of occlusal area during the power stroke in six different taxa.

3.5 Quantification of tooth morphology by DTA and GMA

Section 3.5 has been modified and published in: Lang, A. J., Engler, T., & Martin, T. (2021). Dental topographic and three-dimensional geometric morphometric analysis of carnassialization in different clades of carnivorous mammals (Dasyuromorphia, Carnivora, Hyaenodonta). *Journal of Morphology*, 283(1), 91 – 108.

Quantification of the total Dirichlet Normal Energy (DNE), first introduced by Bunn et al. (2011), was used as a method of DTA (Dental Topographic Analysis). The DNE method measures curvature (undulation) of a surface as the deviation from a planar surface (Bunn et al., 2011). In the context of dental topography, DNE is interpreted to quantify the change in height and curvature of cusps and crests (Evans, 2013). DNE is a strong indicator for dietary adaptations (e.g., Bunn et al., 2011; Winchester et al., 2014) and further has been shown to be correlated with other factors such as precipitation seasonality and annuality (Fulwood, 2020). DNE is independent of homologue orientation, which makes it especially suitable for a database as phylogenetically diverse as ours.

For calculation of DNE, the implementation of the ariaDNE ("A Robustly Implemented Algorithm for Dirichlet Normal Energy") script for Matlab 9.10.0.1710957 R2021a (The MathWorks Inc.), developed and provided by Shan, Kovalsky, Winchester, Boyer, and Daubechies (2019), was used. The ariaDNE algorithm has the advantage of reducing surface noise, making it less susceptible to the method of surface mesh preparation than earlier algorithms for the calculation of DNE, which results in less scattered values. Further, by implementation of the ϵ parameter, it is possible to selectively increase the weight of small surface fluctuations (low ϵ) or large surface features, potentially ridges, cusps and crests (high ϵ), on the ariaDNE calculation (see Shan et al. 2019 for detailed explanation). For visualization of local ariaDNE values on the carnassial surface, the script provided by Shan Shan via github.com/sshanshans/ariaDNE_code was used.

While DTA has been referred to as a "shape descriptor", capturing molar morphology in a landmark-free abstraction, GMA (geometric morphometric analysis) is a "shape specifier", representing the shape via the positions of specific landmarks (Evans, 2013). As both methods capture quite different aspects of morphology, with DTA being useful for measuring a more functional signal and GMA being useful for observing the positions of landmarks within morphospace, they can be used to complement each other (Selig et al., 2020).

The surface meshes used in this study are mostly based on CT-scans conducted with the v|tome|x s 240, situated at the Institute of Geosciences (Rheinische Friedrich-Wilhelms-Universität Bonn). Scan voxel sizes vary between 0.018 mm and 0.246 mm. Additional scan data was acquired from the digimorph.org (scan of TMM M-6921) and morphosource.org (scan of UMZC A6.10/3) digital databases. Specimen NMB 2526 was scanned at the

Naturhistorisches Museum Basel. All carnassials used in this study showed as minimal wear as possible. Some teeth still were slightly more worn than others and while they are not problematic for DTA, they were excluded from the GMA (Selig et al., 2020). Teeth with all landmarks present but other parts of the crown being damaged were used in the GMA but not in the DTA. Thus, the sample size differs between both analyses. The mesh preparation protocol used in this study is based on to the workflow of previous studies which used DNE (a summary of DNE workflow protocols can be found in Pampush et al., 2016). Individual molars were cropped from segmented scan data at the cervix line, down-sampled to 10,000 faces (or left unchanged if initial face number was lower) using the PolyWorks mesh optimization tool and subsequently smoothed using the smooth surface tool in Avizo 8.1 (FEI *Visualization Sciences Group*) with 100 iterations and a lambda of 0.6. Individual tooth models were exported as Stanford Triangle Format (.PLY) files. The ϵ parameter was set to 0.08. The placing of landmarks for the GMA was conducted on the same down-sampled and smoothed meshes, which has been shown to work in previous studies (Selig, et al., 2019a; Selig et al., 2020). The lower left teeth were used for the analysis, if available and in better condition than the right teeth. Otherwise right teeth were used and mirrored using PolyWorks.
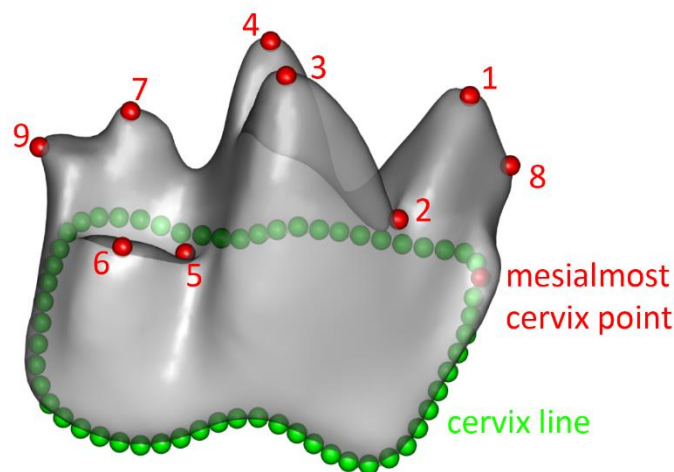

Fig. 9: 3D model of a lower carnassial (m3 of *Dasyurus viverrinus*) showing the placement of fixed landmarks (red) and semilandmarks (green). The model is in buccal view, mesial is to the right. Rendering of µCT data. This figure is published in Lang et al. (2021).

The landmark configuration for the GMA is based largely on the workflow applied by Tarquini et al. (2020), using the paraconid (landmark 1), carnassial notch (landmark 2), protoconid (landmark 3), metaconid (landmark 4), distal trigonid edge (landmark 5), hypoconid (landmark 6), entoconid (landmark 7), mesial trigonid edge (landmark 8) and distal talonid edge (landmark 9) as fixed landmarks. The positions of landmarks 5, 8 and 9 were determined in occlusal view.

In case of metaconid, hypoconid or entoconid reduction, the missing landmarks were placed as described by Tarquini et al. (2020). To capture the base of the crown in detail, 60 semi-landmarks along the cervix line were used (Fig. 9). Landmarks and semi-landmarks were placed using the point placing tool of PolyWorks. For each molar, at least 60 semi-landmark points were placed, starting at the most mesial point. In cases where more than 60 points were placed, these were down-sampled to 60 points and before performing the GMA the semi-landmarks were made equidistant using the equidistantCurve function of the R library Morpho (Schlager et al., 2020) for the software R (R Core Team, 2020; version 4.0.5). The Procrustes alignment and a Procrustes ANOVA of the aligned shape data were carried out with the R library geomorph (Adams et al., 2021).

Topographic height models were created with MorphoTester (Winchester, 2016).

All lower carnassial teeth included in this study were assigned to a "basal" and a "derived" functional group. The criteria used for a priori grouping are presence of a complete talonid (hypoconid, hypoconulid and entoconid) and presence of the metaconid. The absence of one of the aforementioned cusps was interpreted as a deviation relative to the basal condition to a more derived carnassialized condition.

In taxa with multiple carnassials, the individual carnassial teeth based on their respective positions in the tooth row were grouped. The most mesial carnassials of dasyuromorphs (m2) and hyaenodonts (m1) are referred to as the "mesial carnassial position" (MCP), the intermediate carnassials of dasyuromorphs (m3) and hyaenodonts (m2) are referred to as the "intermediate carnassial position" (ICP) and the distal carnassial of dasyuromorphs (m4) and hyaenodonts (m3) as well as the carnivoran m1 are referred to as the "principal carnassial position" (PCP).

Due to both the study design and the underlying biological circumstances, testing the results of the DTA and GMA values for a phylogenetic signal is not trivial. First of all, this study analyses the morphology of a trait in taxa where it is present multiple times (dasyuromorphs and hyaenodonts with multiple carnassials per tooth row) and compares it with taxa where it is present only once (carnivorans with a single carnassial per tooth row). Thus, in some cases multiple traits are being analyzed both on the individual as well as the species and genus levels. This is further complicated by the fact that the analyzed traits do for the most part not represent homologous anatomical features. While presence of homologous traits (carnassialization of molar positions) on homologous anatomical features can be dependent on phylogenetic history within the respective taxonomic orders, the analyzed anatomical features in the Carnivora (m1), the Hyaenodonta (m1, m2, m3) and the Dasyuromorphia (m2, m3, m4) are mostly present on non-homologous tooth positions and testing them for phylogenetic significance would not yield meaningful results, as no analysis including a single molar position per group would include a homologous tooth position in all taxa.

The evolution of carnassialization was analyzed in a phylogenetic context by conducting an ancestral state reconstruction on calculated values of the DTA and GMA (PC values of PCA) for PCPs. The calculated signal is interpreted as a functional morphological trait of adaptation, not a homologous anatomical trait or feature. This makes it possible to compare the hypothetical ancestral states of the Carnivora, Hyaenodonta and Dasyuromorphia, although differences or similarities of lineages within these groups could potentially still depend on the respective phylogenetic intrataxon history.

3.6 Statistical analyses of ariaDNE values using ANOVA and LDA

For statistical analyses, the Shapiro-Wilk test, the Tukey's honest-significant-difference-test and the one-way ANOVA (analysis of variance) base functions of the software R were used. Additionally, the function for Welch's heteroscedastic F test from the "onewaytests" library (Dag et al., 2019), the function for Levene's test from the "car" library (Fox et al., 2020) and the LDA (linear discriminant analysis) function from the "MASS" library were used (Ripley et al., 2020). Further, the Games-Howell script provided by Schlegel (2016) and the script for bootstrap cross-validation of LDA provided by Maindonald (2008) were used.

Only the principal carnassial teeth (dasyuromorph m4, carnivoran m1, hyaenodont m3) were used in the evaluation of group difference, so that each specimen is represented by a single value. Differences of five groups were tested: basal Carnivora (n = 17), derived Carnivora (n = 29), basal Dasyuromorphia (n = 6), derived Dasyuromorphia (n = 6) and derived Hyaenodonta (n = 8). To test group differences for statistical significance, a one-way ANOVA and Welch's heteroscedastic F omnibus test were applied. The basal hyaenodont group was excluded from this analysis, since it is only represented by a single principal carnassial (m3 of Proviverra) tooth in the sample.

The predictive accuracy of ariaDNE to distinguish basal from derived carnassial morphotypes was tested with LDA. For the LDA, the ariaDNE values of both morphotypes were investigated regardless of phylogeny, as the ANOVA indicates a strong convergent signal (see 5.3). Thus, all principal carnassials were either assigned to a "basal" (n = 23) or a "derived" (n = 43) morphotype group. All principal carnassial teeth except for the basal hyaenodont were used as training data for the LDA. Prediction of group assignment and classification of the basal hyaenodont carnassial was calculated with the complete original data. Posterior probabilities for group assignment were calculated with cross validated LDA. A subsequent bootstrap leave-one-out cross-validation was conducted to estimate the average accuracy of classification, as proposed for small sample sizes by Fu et al. (2005). The same procedure was repeated with all basal (n = 35) and derived (n = 71) carnassials, regardless of tooth position and excluding the basal hyaenodont carnassials, for which group assignment was predicted subsequently.

3.7 Construction of the „carnassial blade angle"

Based on the landmarks used for the GMA, the "carnassial blade angle" was constructed for the principal carnassial teeth using PolyWorks. For this, a vector (protoconid-paraconid vector) was created which connects landmark 1 (apex of paraconid) to landmark 3 (apex of protoconid) (Fig. 10). Then, using the 60 semi-landmark points along the cervix line, the mean plane and the mean vector for the cervix line were created. The constructed cervical plane is used as reference for the occlusal plane and the mean vector is used as reference for the mesial vector (resp. the longitudinal vector of the tooth) that is included in the cervical plane. The protoconid-paraconid vector was then projected onto the cervical plane. The "carnassial blade angle" is the angle formed by the projected vector and the mesial vector (Fig. 10).

The distribution of the carnassial blade angle, using the means of species, was plotted on a rose diagram of the quadrant between 0° and 90°, with 0° corresponding to a shearing blade orientation in buccal direction and 90° corresponding to a shearing blade orientation in mesial direction, using the rose.diag function of the R library circular (Lund et al. 2022). The quadrant was partitioned in steps of 10°, resulting in nine sectors in which the proportional frequency of measured angles per group can be plotted as petals. Groups were subdivided by taxonomic order (Carnivora, Dasyuromorphia or Hyaenodonta) and type of carnassialization (basal or derived). The frequency of observations within the resulting six groups were plotted per group.
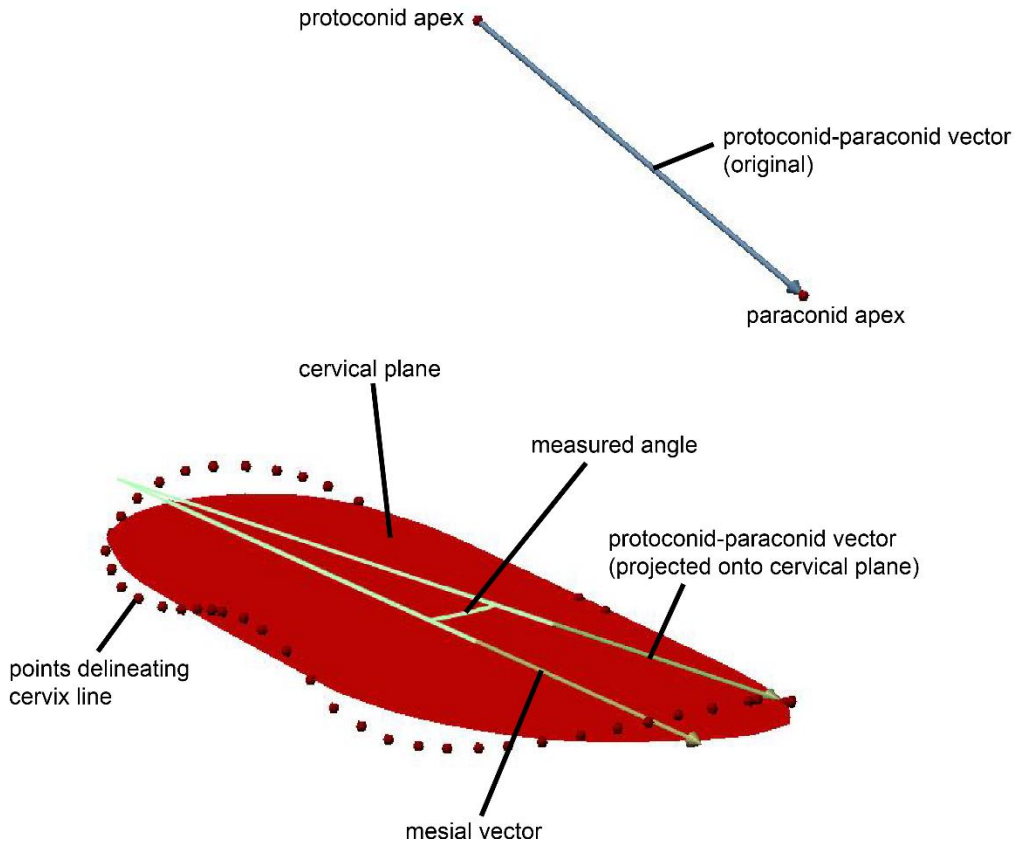
Fig. 10: Elements used for the construction of the carnassial shearing angle in 3D space in PolyWorks.

3.8 Shape comparison by Cloud-to-Cloud distance

In addition to landmark based morphometrics, the three-dimensional surfaces of anatomical structures such as bones and teeth can be compared measuring the distance of points on the surface. Examples are the study by Renaud & Ledevin (2017), comparing house mouse molar surfaces, the study by Cerio & Witmer (2019), comparing the inner ear labyrinths of wild turkeys or the study of Newton et al. (2021), comparing the skull shapes of dasyuromorphs and carnivorans. For the comparison of molar shapes, the non-downsampled surfaces of carnassials were used, cropped at the cervix line. The software CloudCompare version 2.12.alpha (www.cloudcompare.org) was used for calculation and visualization of the point distances. For each carnassial surface, a random point cloud of 10,000 points was generated. First, the surfaces of two teeth were roughly aligned using the "align (point pairs picking)" tool, placing five points on the same positions on both teeth (most distal point in occlusal view; tip of paraconid; carnassial notch; tip of protoconid; most distal point in occlusal view). This was followed by using the "fine registration" tool, which calculates a more precise automated alignment. For this alignment, "adjust scale" was selected, as the distance calculation is only supposed to consider differences in molar relief structure and not the size differences between the individual carnassials. Finally, using the aligned and scale-adjusted point clouds, the surface distances were calculated using the "Cloud/Cloud distance". To compare carnassials within the tooth row of a taxon, first the MCP was used as a reference with the ICP compared

to it, then the MCP was used as a reference with the PCP compared to it. Thus, both the MCP and the PCP of a tooth row were adjusted and compared to the same reference surface. Then, the procedure was repeated with the ICP used as a reference once with the MCP and then with the PCP compared to it. This way, every carnassial tooth within the tooth row is directly compared to each other carnassial. For all points the nearest neighbor distances, calculated as the Euclidean distances between the carnassial surfaces, were displayed on a color scale and mapped onto the tooth surface.

3.9 Phylogenetic data

Section 3.9 has been modified and published in: Lang, A. J., Engler, T., & Martin, T. (2021). Dental topographic and three-dimensional geometric morphometric analysis of carnassialization in different clades of carnivorous mammals (Dasyuromorphia, Carnivora, Hyaenodonta). *Journal of Morphology*, 283(1), 91 – 108.

A calibrated phylogenetic tree based on mitochondrial data for extant species (all dasyuromorphs and all carnivorans except nimravids) was downloaded from TimeTree.org (Kumar et al., 2017). The root of the tree is at 159 Ma (split of Eutheria and Metatheria), which is in congruence with *Juramaia sinensis* being interpreted as the earliest eutherian (Luo et al., 2011). However, it has to be noted that some authors have proposed to exclude *J. sinensis* from Eutheria, as discussed in Sweetman et al. (2017). Absolute ages for *Nimravus* (34 Ma) and *Dinictis* (37 Ma) were taken from the published composite tree of Martín-Serra et al. (2014). The placement of Nimravidae within Feliformia is followed according to Wesley-Hunt & Flynn (2005) and Tomiya (2011), with a split of Nimravidae from the non-nimravid feliforms at 50 Ma. The split of *Nimravus* and *Dinictis* was dated at 42 Ma, according to Wesley-Hunt & Flynn (2005). The phylogeny for the hyaenodont taxa in this study is based on the published calibrated tree of Solé & Mennecart (2019). *Hyaenodon filholi* was not included in the published hyaenodont phylogeny. In the tree, it is placed as a sister taxon to *Hyaenodon exiguus* with a split at the base of the *Hyaenodon* clade. This is based on the interpretation of the European *H. filholi* as an immigrant taxon from Asia with a split from the endemic European *H. exiguus* deep within the *Hyaenodon* clade (Bastl et al., 2014). Since an absolute age of this split was not calculated, the placement within the tree estimates the split between European and Asian *Hyaenodon* clades at the base of the genus. The absolute age for *H. filholi* is 30.9 Ma according to its oldest stratigraphic occurrence in European MP 23 faunas (Bastl et al., 2018). The oldest internal Hyaenodonta split in the tree of Solé & Mennecart (2019) (split between the *Tinerhodon*/*Altacreodus* clade and the rest of the Hyaenodonta) was used as the age for the split between the Carnivora and the Hyaenodonta. To our knowledge, there is no comprehensive dated phylogeny for the relationship between Hyaenodonta and Carnivora and

the timing of the split of both lineages. The general consensus of placing Hyaenodonta within Ferae is followed, e.g. as proposed by O 'Leary et al. (2013), with a split dating back well into the Late Cretaceous.

The two specimens of *Hyaenodon* sp. were excluded from the phylogenetic analysis because of unknown phylogenetic placement and range of stratigraphic age.

Ancestral states at individual nodes of the tree were calculated using the fastAnc function (fast estimation of maximum likelihood ancestral states) of the phytools library (Revell, 2020) for R and were further investigated by using the contMap function for a graphical depiction of trait change.

The difference of the distribution of values for PCPs of the Carnivora, Dasyuromorphia and Hyaenodonta is measured by calculating the deviation of the calculated base value of the respective group from the calculated value of the base (root) of the tree, expressed as percentage of the total range of values of the respective trait (ariaDNE, PC1 or PC2).

3.10 Traitgram analysis

Based on the calibrated phylogenetic tree, a traitgram was constructed based on the means of species of ariaDNE values, as well as the PC1 and PC2 scores of the GMA analysis calculated for the principal carnassials, with the "basal" and "derived" carnassial functional morphotype mapped onto the tips of the tree as a discrete character. For the calculation, the phylomorphospace function of the phytools library for R was used.

3.11 UPGMA Cluster analysis

Section 3.11 has been published in: Lang, A. J., Engler, T., & Martin, T. (2021). Dental topographic and three-dimensional geometric morphometric analysis of carnassialization in different clades of carnivorous mammals (Dasyuromorphia, Carnivora, Hyaenodonta). *Journal of Morphology*, 283(1), 91 – 108.

The mean values of the scores of the first five PCs (explaining more than 75% of total variation) for the MCPs, ICPs and PCPs of Carnivora, Dasyuromorphia and Hyaenodonta, using the a priori classification of "basal" and "derived" (Table 1) within each group, were included in an unweighted pair group method with arithmetic mean (UPGMA) cluster analysis using the linkage function of the mdendro library (Fernandez & Gomez, 2018) for R to examine shape similarities among the tooth positions.

3.12 List of abbreviations

Abbreviations for structures on mammalian molars (modified after Schultz et al. 2017)	
AM	Amphicone
ed	Entoconid
hd	Hypoconid
hld	Hypoconulid
MEC	Metacrista
ME	Metacone
md	Metaconid
MTS	Metastyle
PACL	Paracingulum
PA	Paracone
pa	Paraconid
PAS	Parastyle
PRMEC	Premetacrista
PR	Protocone
pr	Protoconid
Positions of facets (after Schultz et al. 2017)	
b	buccal
d	distal
l	lingual
m	mesial
Abbreviations for lower carnassial tooth positions	
ICP	Intermediate carnassial position
MCP	Mesial carnassial position
PCP	Principal carnassial position
Abbreviations of methods	
ariaDNE	A robustly implemented algorithm for Dirichlet Energy of the Normal (after Shan et al. 2019)
DTA	Dental Topographic Analysis
GMA	Geometric Morphometric Analysis
OFA	Occlusal Fingerprint Analysis
UPGMA	Unweighted Pair Group Method with Arithmetic Mean
Institutional abbreviations	
GMH	Geiseltal collection, Halle an der Saale, Germany
HLMD	Hessisches Landesmuseum Darmstadt, Germany
IGPB	Institute of Geosciences, Rheinische Friedrich-Wilhelms-Universität Bonn, Germany
MNHN	Muséum national d'Histoire naturelle, Paris, France
NMB	Naturhistorisches Museum Basel, Switzerland
SMF	Senckenberg Naturmuseum Frankfurt, Germany
SMNK	Staatliches Museum für Naturkunde Karlsruhe, Germany
TMM	Texas memorial museum, University of Texas, Austin, USA
UMCZ	University Museum of Zoology, University of Cambridge, United Kingdom
ZFMK	Zoologisches Forschungsmuseum Alexander Koenig, Bonn, Germany
ZMB	Museum für naturkunde, Humboldt-Universität zu Berlin, Germany

4. Results

4.1 Analysis of carnassial functionality

4.1.1 Grouping of taxa

For the analysis of carnassial functionality, the included taxa were grouped into two categories based on the presence of tooth morphotypes in the cheek dentition. The first category includes hyaenodont and dasyuromorph taxa, as these possess a "homodont" cheek dentition with multiple carnassial teeth. The second category includes the carnivoran taxa, which possess carnassial teeth as well as post-carnassial teeth. From both of these categories, wear patterns were analyzed and the power stroke was subsequently reconstructed for taxa with "basal" carnassials and for taxa with "derived" carnassials.

4.1.2 Wear patterns on basal homodont carnassial dentitions

Facets pacd-mb and MEC-dl

All lower carnassial teeth have a prominent mesial trigonid cutting blade with a well-developed, V-shaped crest with a carnassial notch, formed by the paracristid. From the paracristid, facet pact-mb forms along the cutting edge, connecting the paraconid and the protoconid. It may cover the entire trigonid flank depending on the ontogenetic stage of the specimen. This facet is found on all lower carnassials of *Dasyurus* (m2, m3, m4) and of *Proviverra* (m1, m2, m3). The striations found on this facet are steeply inclined, oriented in a slightly transverse angle towards buccal from apical (Figs. 11A, 19). In *Dasyurus*, the mesialmost lower carnassial is the m2 with the upper M1 functioning as its antagonist. In *Proviverra,* it is the lower m1 with the upper P4 serving as its antagonist, implying the inclusion of the distal metastylar P4 cutting blade in carnassial cutting in the basal hyaenodont condition.

On the upper carnassial teeth, the most prominent cutting blade is formed between the metacone and the metastyle. It serves as the antagonistic structure to the lower mesial trigonid blade along the paracristid. In *Dasyurus*, facet MEC-dl forms along the cutting edge of the metacrista, extending from the metacone to the metastyle (Figs. 11B, 18). It forms on the mesial (M1), intermediate (M2) and distal (M3) carnassials. While a prominent V-shaped crest is formed by the metacrista of the upper carnassial teeth in *Proviverra*, it is lacking in *Dasyurus*. Although this facet could not be documented in the fossil material of *Proviverra* used in this study, the wear on the antagonistic lower carnassials indicates its formation also along the metacristae of the upper carnassials, despite the different structure of the cutting edge. Thus, cutting between the paracristid and the metacrista is performed by all carnassials of *Dasyurus* and *Proviverra*. The striations on this facet are steeply inclined running from apical towards lingual.
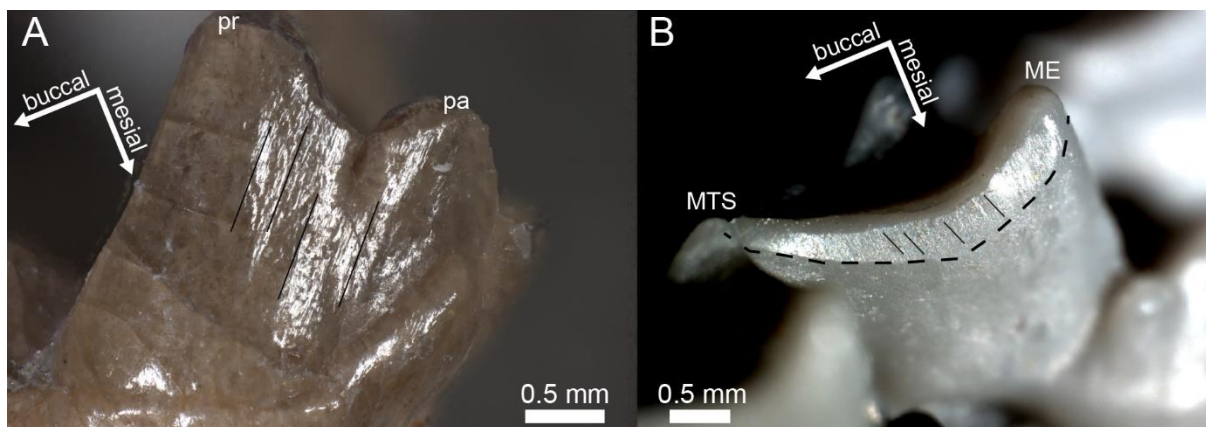
Fig. 11: A, facet pacd-mb on the m1 of *Proviverra typica* (NMB En.191) and B, facet MEC-dl on the M3 of *Dasyurus viverrinus* (SMF 1480, epoxy cast). The dashed line marks the visible edge of the facet. Solid lines indicate the inclination of striations.

Facets pr-d and PA-m

The distal flank of the trigonid on the lower carnassial teeth forms a cutting blade along the metacristid, with the metacristid forming a V-shaped crest between the paraconid and the protoconid. Along the buccal half of this crest, facet pr-d extends along the edge from the apex of the paraconid (Figs. 12A, 19). In lingual direction, it may connect with facet md-d to form one continuous facet, which may cover the entire distal trigonid flank depending on the progression of wear. The facet is present on all lower carnassials of *Dasyurus* and *Proviverra*. This indicates occlusal contact of the lower carnassials, respectively with the upper intermediate and distal carnassials, as well as the vestigial most distal molar position (m4 in *Dasyurus* and m3 in *Proviverra*).

The striations on this facet are running in a steep inclination from apical to buccal.

The antagonistic structure on the upper carnassials is the praeparacrista. Along the praeparacrista, facet PA-m forms, covering the mesial flank of the paracone (Figs. 12B, 18). On all the upper carnassials of *Dasyurus*, the paracone is relatively small in size and well separated from the protocone. In contrast to this, the paracone is a bit more enlarged on the upper carnassials of *Proviverra*. Thus, the potential surface area to occlude with the lower distal trigonid flank is a bit larger. On this facet, the striations run in a steep inclination from apical to lingual.
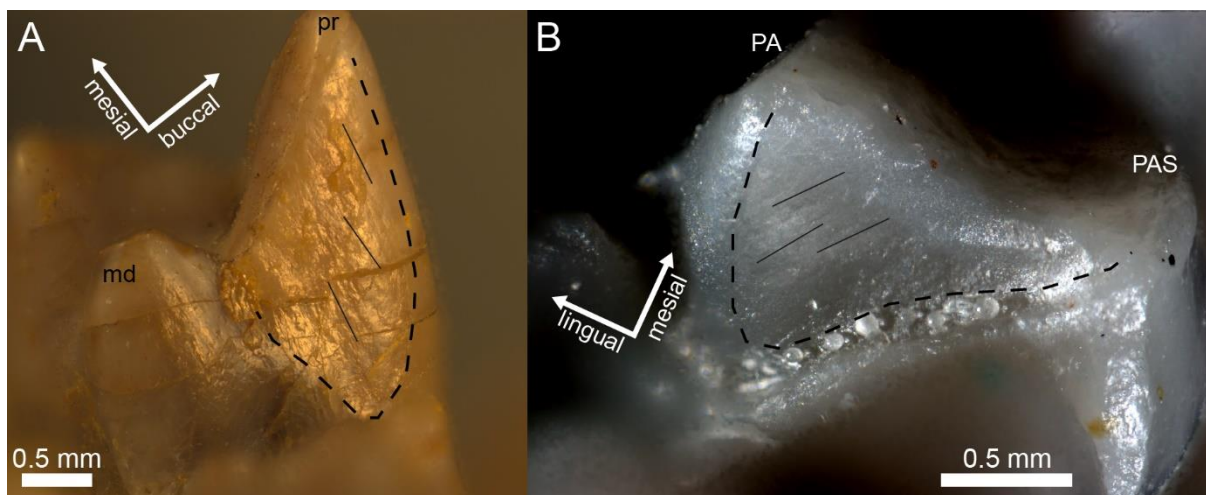
Fig. 12: A, facet pr-d on the m3 of *Proviverra typica* (NMB En.178) and B, facet PA-m on the M2 of *Dasyurus viverrinus* (SMF 378, epoxy cast). The dashed line marks the visible edge of the facets. Solid lines indicate the inclination of striations.

Facets md-d and PR-m

As mentioned above, facet md-d forms on the lingual side of the distal trigonid blade, extending from the tip of the metaconid along the metacristid (Figs. 13A, 19). In some specimens, this facet and facet pr-d on the buccal part of the metacristid respectively cover a small, punctiform area. In specimens with more progressed wear, both areas are fused into one big facet running along the metacristid, eventually covering the entire distal flank of the trigonid. Like facet pr-d, facet md-d forms on all lower carnassials of *Dasyurus* and *Proviverra*. The striations on facet md-d have the same orientation as on facet pr-d, running steeply from apical to buccal. The antagonistic structure to occlude with the lingual part of the distal trigonid flank is the mesial flank of the protocone, extending from the praeprotocrista. The upper carnassials of *Dasyurus* and *Proviverra* possess prominent protocones, with facet PR-m forming along the praeprotocrista (Figs. 13B, 18). In the upper carnassials of *Proviverra*, a paraconule is present along the praeprotocrista, forming a small additional V-shaped crest. The praeprotocrista in the molars of *Proviverra* is a bit more elongated than in the molars of *Dasyurus*, extending below the base of the paracone, which indicates that protocone-cutting is a bit more emphasized. On the most distal upper molars of *Dasyurus* (M4), facet PR-m is also present on the mesial protocone flank, indicating that the reduced distal molar position contributes to the cutting function. Although the wear on the most distal upper molar of *Proviverra* (M3) could not be documented due to the bad preservation of the fossil material, the presence of extensive wear on the distal trigonid flank of the lower m3 indicates that the protocone of the M3 may have performed a similar function as in the M4 of *Dasyurus*. On facet PR-m, the striations have a similar orientation as on facet Pa-m.
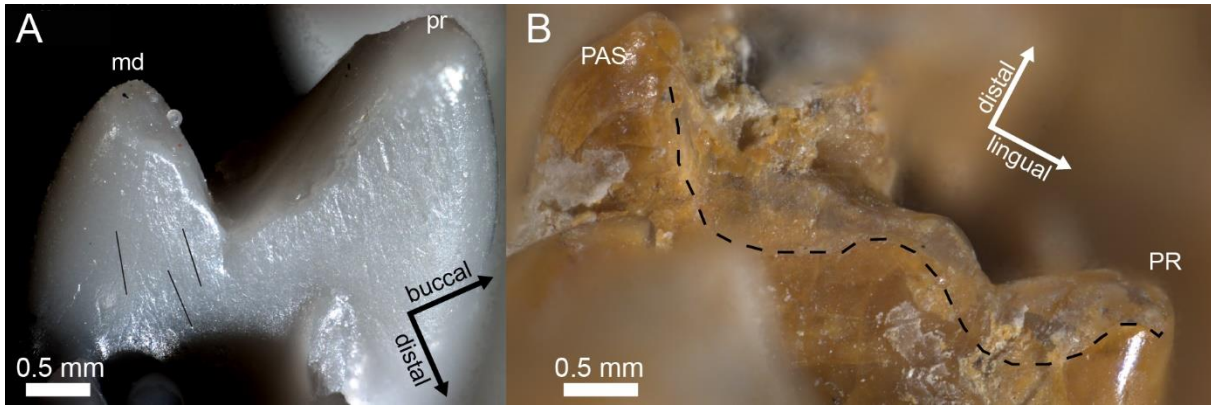
Fig. 13: A, facet md-d on the m3 of *Dasyurus viverrinus* (SMF 378, epoxy cast) and B, facet PR-m on the M1 of *Proviverra typica* (NMB Ek.30). The dashed line marks the visible edge of the facets. Solid lines indicate the inclination of striations.

Facets hd-mb and PA-dl

Facet hd-mb forms on the mesial flank of the talonid on the lower carnassials of *Dasyurus* and *Proviverra*. It extends from the praehypocristid and may cover the entire mesial flank of the talonid (Figs. 14A, 19). It is present on all lower carnassial teeth, with striations running in a steep inclination from apical to buccal. The antagonistic structure to occlude with the praehypocristid is the postparacrista of the upper molars. Along the postparacrista, facet PA-dl forms on the distal flank of the paracone in *Dasyurus* (Figs. 14B, 18). Its most likely the same structure to occlude with the mesial talonid flank in the dentition of *Proviverra*, although no distinctive wear on the upper molars could be documented with the available material. The striations on facet PA-dl in *Dasyurus* are steeply inclined from apical to buccal. On the distalmost lower molars of *Dasyurus* (m4) and *Proviverra* (m3), facet hd-mb is also present, indicating occlusion with the distalmost upper molar.
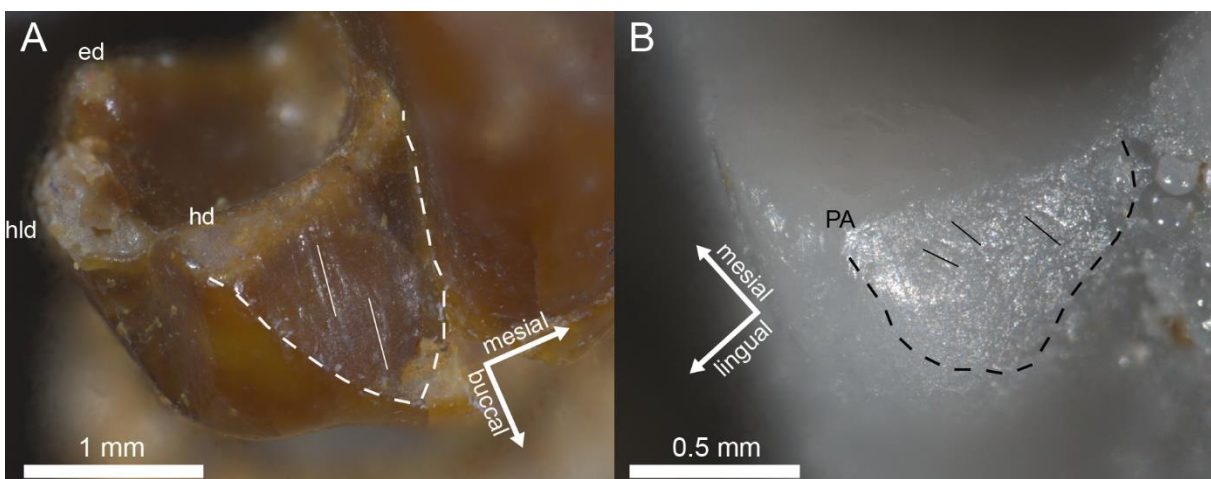

Fig. 14: A, facet hd-mb on the m1 of *Proviverra typica* (NMB En.176) and B, facet PA-dl on the M3 of *Dasyurus viverrinus* (SMF 378, epoxy cast). The dashed line marks the visible edge of the facets. Solid lines indicate the inclination of striations.

Facets hd-db and ME-ml

Facet hd-db forms on the distal flank of the talonid on the lower carnassials of *Dasyurus* and *Proviverra*, with the exception of the distalmost lower teeth (m4 in *Dasyurus* and m3 in *Proviverra*) (Figs. 15A, 19). It starts forming along the posthypocristid and with progressive wear extends on the entire distal talonid flank. The striations on the facet run in a steep inclination from apical to buccal. The posthypocristid occludes with the praemetacrista of the upper molars. In *Dasyurus*, facet ME-ml forms on the mesial flank of the metacone on the M2 and the M3 (Figs. 15B, 18). Although the metacone on the molars of *Dasyurus* is more enlarged than on the molars of *Proviverra*, the crown structure indicates that facet hd-db forms by the same occlusal interaction in both taxa. On the distalmost upper molars of *Dasyurus* (M4) and *Proviverra* (M3), the metacone is reduced to a vestigial conule. It is thus unlikely that these molars perform a cutting function with the cristae of the metacone. The striations on facet ME-ml are oriented from apical in a steep inclination towards lingual.
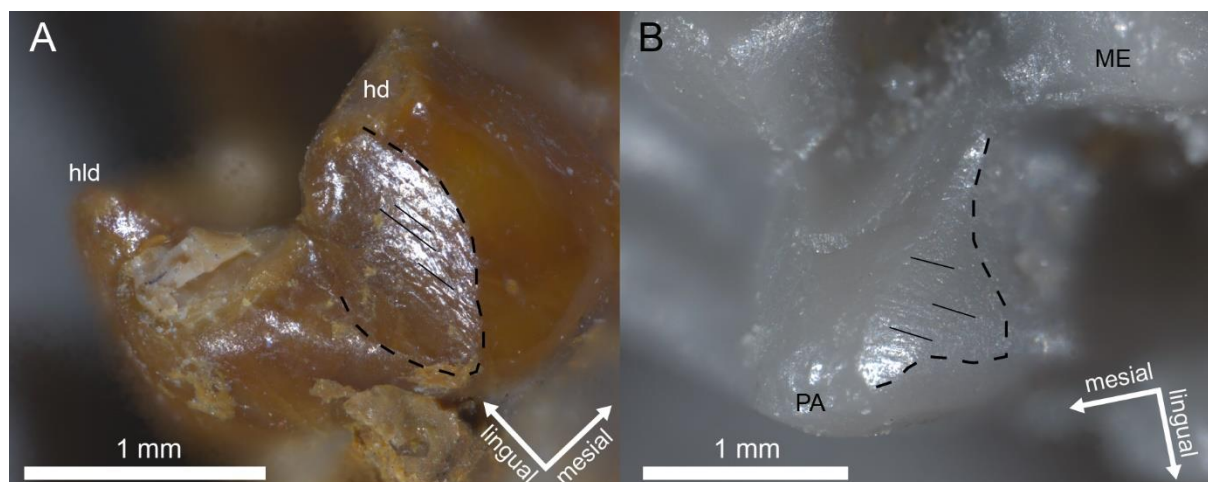

Fig. 15: A, facet hd-db on the m1 of *Proviverra typica* (NMB En.176) and B, facet ME-ml on the M2 of *Dasyurus viverrinus* (SMF 378, epoxy cast). The dashed line marks the visible edge of the facets. Solid lines indicate the inclination of striations.

Facets ed-mb, hld-mb and PR-dl

Facets ed-mb and hld-mb respectively can be found on the mesial flanks of the entoconid and the hypoconulid, where they start to form in proximity to the apices (Figs. 16B, 19). With progressing wear, these facets fuse along the cristid connecting the entoconid with the hypoconulid and form a uniform facet running along the inner disto-lingual margin of the talonid basin. The antagonistic structure that occludes with the entoconid and the hypoconulid is the distal flank of the protocone. Along the postprotocrista, facet PR-dl can be found (Figs. 16A, 18). Unidirectional striations are present on facet PR-dl, which are oriented in a steep inclination, running from apical to lingual. The area covered by facets ed-mb and hld-mb on

the lower molars and facet PR-dl on the upper molars remains relatively small and the faceted areas are restricted to the proximity of the respective cutting crests.
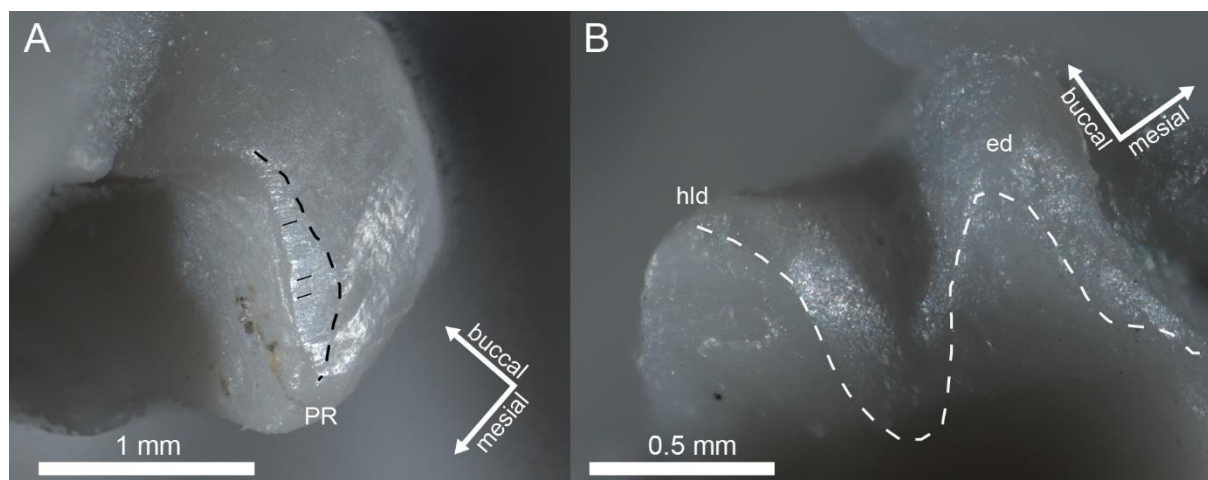

Fig. 16: A, facet PR-dl on the M3 of *Dasyurus viverrinus* (SMF 1480) and B, facet ed-mb and hld-mb on the m3 of the same specimen (epoxy casts). The dashed line marks the visible edge of the facets. Solid lines indicate the inclination of striations.

Wear in the talonid basin and on the protocone

The structure of the protocone and the talonid basin in the basal carnassial teeth of *Dasyurus* and *Proviverra* indicates that a crushing and grinding function similar as in the tribosphenic condition can be performed. On the molars of *Dasyurus*, wear on the buccal protocone flank and the lingual hypoconid flank is present in some specimens. Occlusion between both structures is mostly indicated by the presence of striations, running from the apex of the hypoconid to lingual and from the apex of the protocone to buccal (Fig. 17). The small punctiform facet PR-b, forming on the apex of the protocone, could be found on one upper molar of *Proviverra*. The forming of facet hd-l on the lingual flank of the hypoconid, bordering the praehypocristid and the posthypocristid, could only be documented on a few teeth (Figs. 17A, 19). This shows that interaction of the protocone and the talonid basin still plays a prominent role in the mastication process of basal carnassial teeth, with no indications for functional differences among the multiple carnassial teeth of the tooth row. Phase I of the power stroke is followed by a second phase during which crushing is predominant and grinding may be performed, as indicated by the striations.
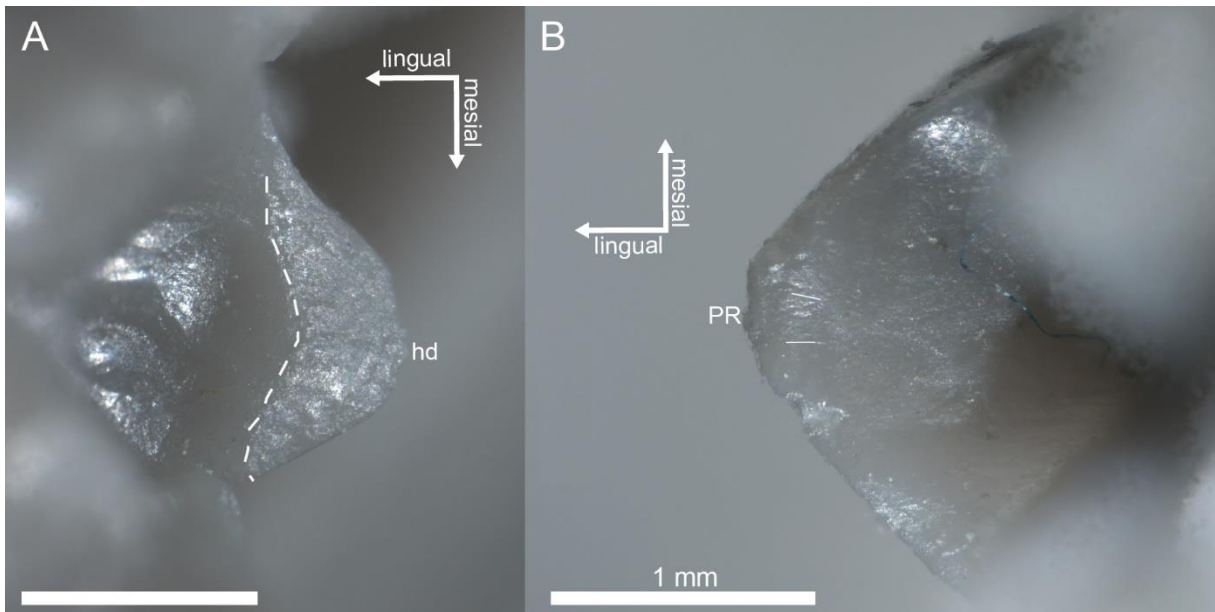
Fig. 17: A, facet hd-l on the m2 of *Dasyurus viverrinus* (SMF 378) and B, facet PR-b on the M2 of the same taxon (SMF 1480) (both epoxy casts). The dashed line marks the visible edge of the facets. Solid lines indicate the inclination of striations.
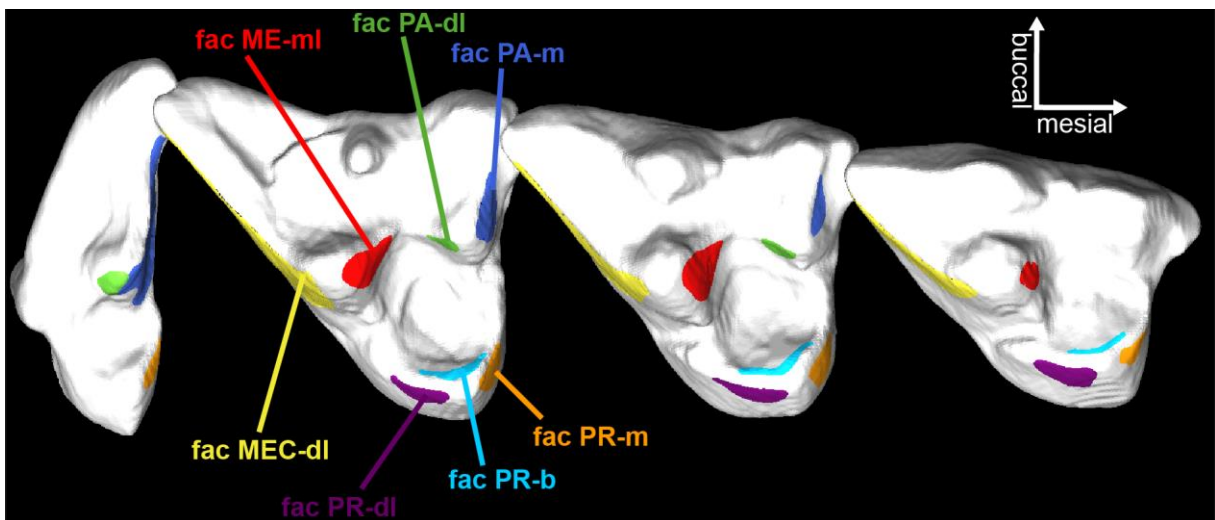

Fig. 18: Facets on the upper distal cheek dentition of a taxon with multiple basal carnassial teeth, as exemplified by the distal cheek dentition (M1 – M4) of *Dasyurus viverrinus*. Rendering of µCT data.
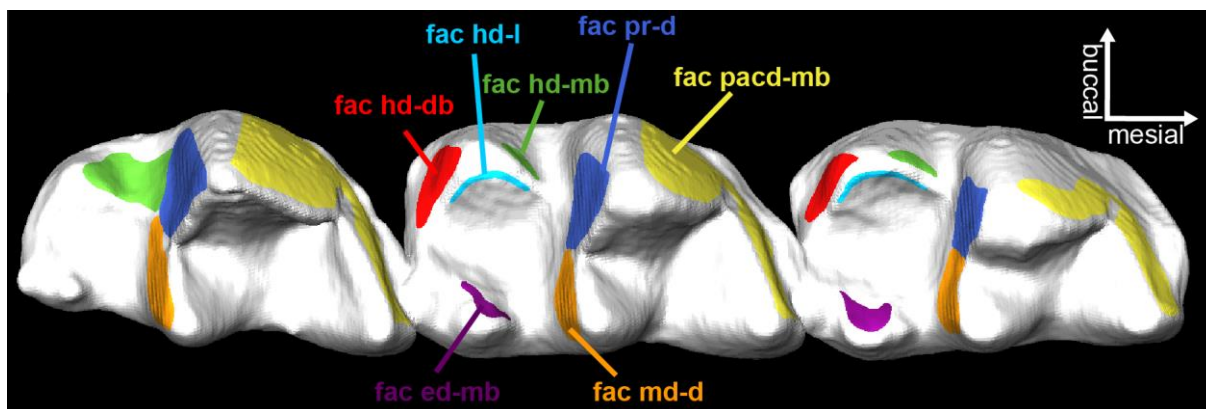
Fig. 19: Facets on the lower distal cheek dentition of a taxon with multiple basal carnassial teeth, as exemplified by the distal cheek dentition (m2 – m4) of *Dasyurus viverrinus*. Rendering of µCT data.

4.1.3 Wear patterns on derived homodont carnassial dentitions

Facets pacd-mb and MEC-dl

The most well pronounced facet on the lower derived carnassial teeth of hyaenodonts and dasyuromorphs is facet pacd-mb, forming along the paracristid (Figs. 20A, 25). Depending on the progression of the tooth wear, it may extend over the entire mesial trigonid flank. The paracristid forms a V-shaped crest between the protoconid and the paraconid, which is used as the cutting edge. This cutting crest is present on all lower carnassials in hyaenodonts (m1, m2, m3) and dasyuromorphs (m2, m3, m4). The associated facet pacd-mb is also found on all lower carnassial tooth positions. The striations found on facet pacd-mb show a steep inclination from apical to buccal. The corresponding antagonistic structure that occludes with the paracristid is the metacrista of the upper molars. The presence of facet pacd-mb on the mesial-most lower carnassials indicates the inclusion of the upper P4 in hyaenodonts and the upper M1 of dasyuromorphs in carnassial cutting, respectively functioning as antagonists to the lower carnassials. Facet MEC-dl forms along the metacrista of the upper carnassial teeth (Figs. 20B, 24). In hyaenodonts, the metacrista forms a V-shaped cutting edge with a carnassial notch. The associated facet MEC-dl extends along the cutting edge and also encompasses the carnassial notch. In contrast to this, the metacrista in dasyuromorphs (*Sarcophilus* and *Thylacinus*) is continuous and lacks a carnassial notch. In these taxa, facet MEC-dl starts to form in a U-shaped outline along the edge of the metacrista. The extension of facet MEC-dl with progressing wear may additionally encompass the distal flank of the protocone (see below). The distalmost upper molars, if not absent like in *Hyaenodon*, possess a vestigial metacone that does not show wear on the distal side, as no antagonistic structure for occlusion is present on the lower teeth.
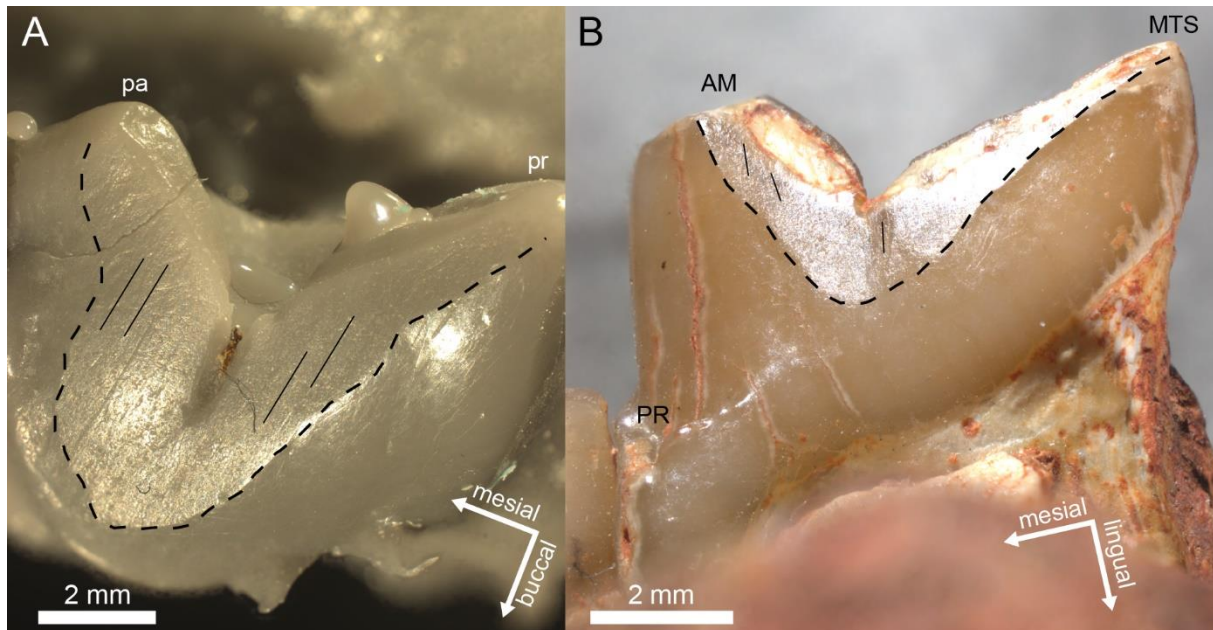
Fig. 20: A, facet pacd-mb on the m4 of *Thylacinus cynocephalus* (NMB 2526, epoxy cast) and B, facet MEC-dl on the M1 of *Hyaenodon exiguus* (NMB Q.C.977). The dashed line marks the visible edge of the facets. Solid lines indicate the inclination of striations.

Facet PR-dl

A distinctive functional shift can be observed in the protocone, which is typically reduced in size on derived carnassials. Since the entoconid is either vestigial or absent on the talonid of the derived lower carnassials, the antagonistic structure that occludes with the distal protocone flank is absent, in contrast to basal carnassials, such as in *Dasyurus*. The protocone does not perform a crushing function with the talonid and in *Hyaenodon* and *Thylacinus*, there is no trace of wear that indicates occlusion of the praeprotocrista or postprotocrista with an antagonistic structure. In some specimens of *Sarcophilus*, MEC-dl is forming on the apical part of the distal carnassial blade, and in the cervical part of the same blade a second facet forms, which extends onto the distal protocone flank (Fig. 21A). On specimens with more progressed wear, these two facets are connected (Fig. 21B). This indicates functional integration of the protocone into carnassial cutting, at least in some taxa with derived carnassials like *Sarcophilus*. In all specimens, the striations that are present on the distal protocone flank have the same direction as on facet MEC-dl, indicating a unidirectional, continuous tooth movement.
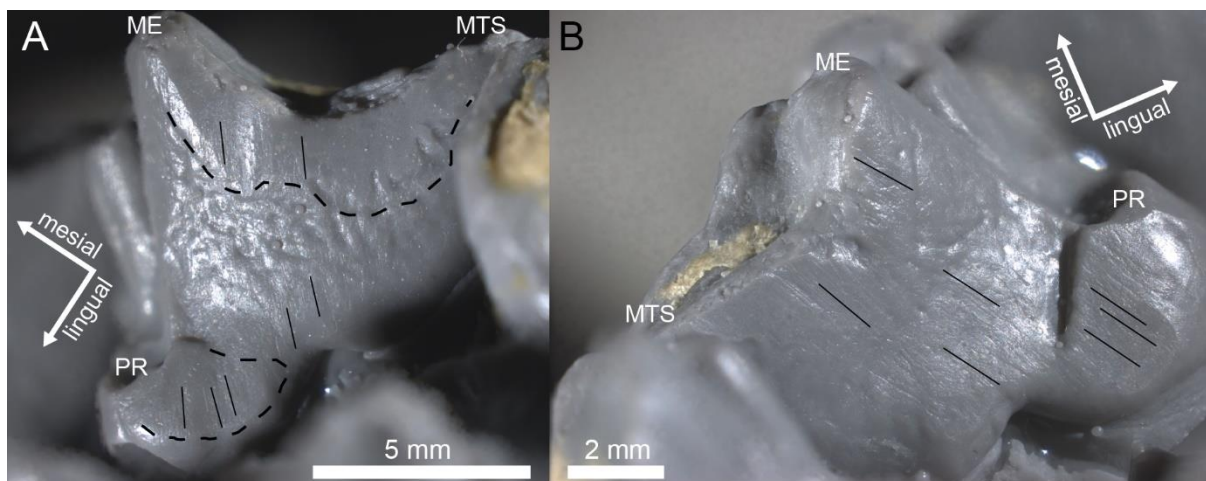
Fig. 21: A, isolated facet pr-dl on the M3 of *Sarcophilus harrisii* (NMB 10550) and B, the same facet connected to facet MEC-dl on the M2 of the same specimen (epoxy casts). The dashed line marks the visible edge of the facets. Solid lines indicate the inclination of striations.

Facets pr-d and PA-m

Facet pr-d forms on the distal flank of the trigonid. It occurs on all lower carnassials of hyaenodonts and dasyuromorphs (except for the m3 of *Hyaenodon*, which lacks an antagonist). The facet begins to form below the apex of the protoconid and with progressing wear increasingly extends over the surface of the distal protoconid flank in cervical direction. The striations are oriented in a steep angle from apical to buccal. The mesial flank of the upper molar paracone is the antagonistic structure that occludes with the distal protoconid flank. On derived carnassials, the paracone is reduced in size and thus the facet on the mesial paracone flank is either bordering the small praeparacrista, as in *Sarcophilus*, or is present as a small, punctiform area, as in *Thylacinus*. On some molars, a distinctive facet is missing, but unidirectional striations still indicate that attrition may have occurred. The striations on facet PA-m run from apical to lingual, in a steep angle. On the upper molars of *Hyaenodon*, paracone reduction is more pronounced than in any other taxa and facet PA-m could not be documented. It can be inferred that functional reduction of paracone/protoconid occlusion is progressed further in *Hyaenodon*, and also the resulting facet pr-d on the lower molars most likely remains rather small and facet PA-m only forming in specimens with more progressed wear. Another possibility is that instead of the mesial paracone flank, the reduced protocone of the upper molar may occlude with the distal trigonid of the lower carnassial. In some specimens of *Hyaenodon*, a dent can be found located distobuccally from the protoconid apex of the m1 and the m2. It is possible, that this dent is formed by occlusion with the upper mesial protocone flank, which is also indicated by the OFA analysis (see OFA of *Hyaenodon* 4.1.8).

The reduced crown structure of the upper M4 in dasyuromorphs results in a functional difference. The paracone is the most prominent cusp on the M4, with the protocone being

reduced in size in *Thylacinus* and absent in *Sarcophilus*. Facet PA-m on the M4 covers the entire mesial flank of the paracone in these species, indicating that a cutting function during occlusion with the lower distal trigonid flank is present (Figs. 22B, D). This is confirmed by the presence of facet pr-d on the m4, which cervically extends from the tip of the protoconid to the distal base of the trigonid, in some more extensively worn specimens extending into the hypoflexid (Figs. 22A, C).

With progressing wear, the facet PA-m on the M4 extends lingually and wraps around the paracone. This is the result of the buccal talonid flank moving along the paracone during occlusion. On the m4, this results in the formation of a distinctive polished groove on the buccal talonid flank, with striations formed by attrition in the hypoflexid.
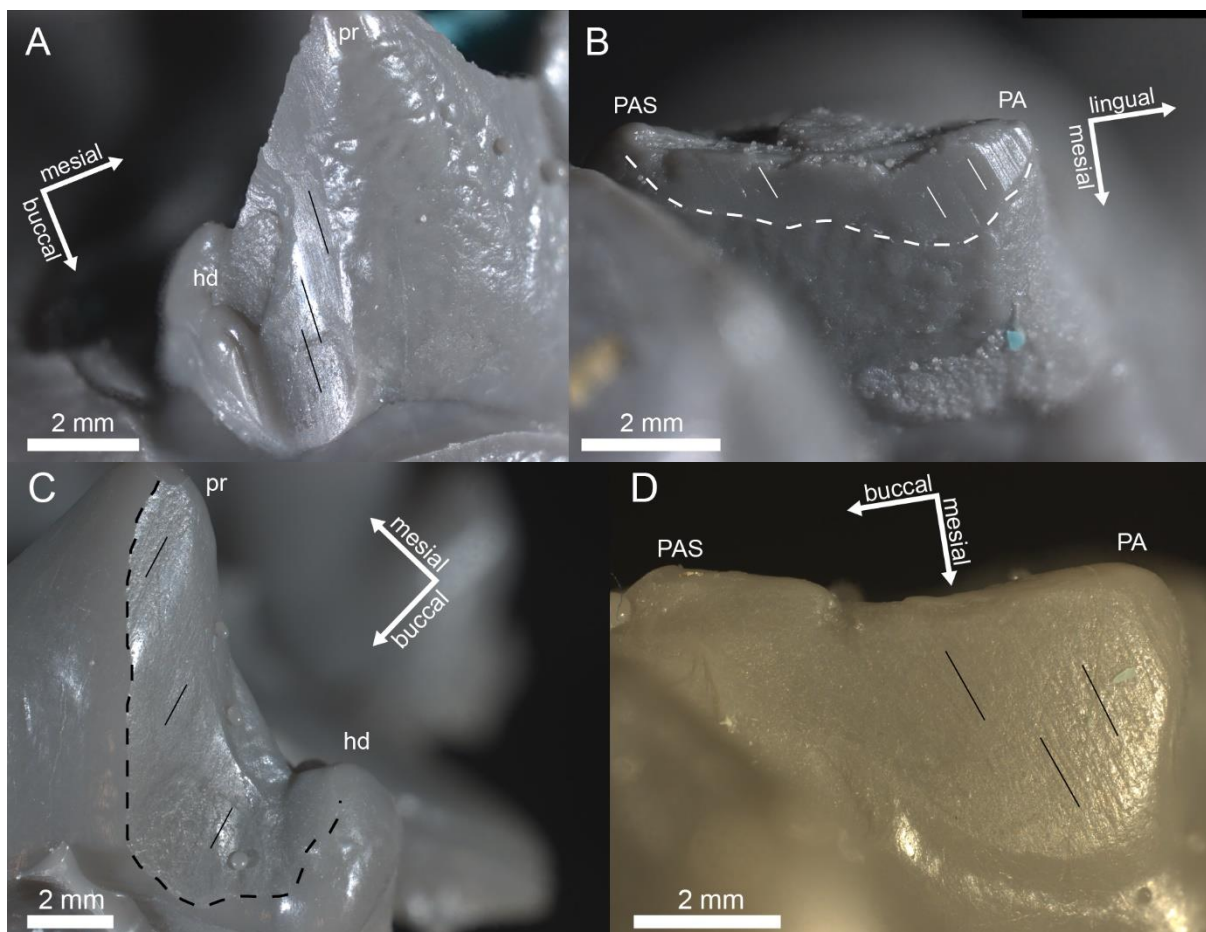
Fig. 22: A, facet pr-d extending into the hypoflexid groove on the m4 of *Sarcophilus harrisii* (NMB 10548) and B, facet PA-m on the M4 of the same specimen. A similar wear pattern can be observed on C, the m4 of *Thylacinus cynocephalus* (NMB 2526) and on D, the M4 of the same specimen. The dashed line marks the visible edge of the facets. Solid lines indicate the inclination of striations. All pictures taken from epoxy casts.

Facets on the "trenchant heel"

Although facets indicating occlusion of the lingual hypoconid flank with the buccal protocone flank are absent in the investigated taxa with derived carnassials, facets are present that indicate occlusion of the buccal talonid rim with the paracone and the metacone. Here, a cutting function is performed between the mesio-buccal and distobuccal talonid flanks ("trenchant heel") and the distal paracone and mesial metacone flanks. In *Thylacinus*, the rather large metacone occludes with the distal talonid flank, resulting in the formation of facets hd-db (Figs. 23C, 25) on the lower molar and ME-ml (Figs. 23D, 24) on the upper molar. These facets form between the M2/m2 and the M3/m3 but are absent in the M4/m4. The smaller paracone occludes with the mesial talonid flank, forming facets hd-mb (Figs. 23A, 25) on the lower molar and and PA-dl (Figs. 23B, 24) on the upper molar. Striations show a steep inclination pointing to a mostly orthal tooth movement. In *Sarcophilus* and *Thylacinus*, the hypoflexid of the lower molars are integrated in the occlusion, where facet hd-mb tends to connect with facet pr-d with

progressing wear. This fusion of facets could be seen in one specimen of *Sarcophilus* and one specimen of *Thylacinus* on the m3 hypoflexid, and is better pronounced as well as occurring more frequently in the m4 hypoflexid (see above). Facet PA-dl on the upper molar tends to wrap around the lingual paracone flank with progressing wear. In the hyaenodonta, tooth morphology results in a wear pattern that is distinct from that observed in the Dasyuromophia. On the paired paracone and metacone of *Oxyaenoides*, a continuous facet running from the paracone along the postparacrista and the praemetacrista to the metacone can be found, covering the distal paracone flank and the mesial metacone flank (Fig. 23 E). The antagonistic structures are the praehypocristid and the posthypocristid of the lower molar, along which a facet can be found covering the mesial and distal hypoconid flanks, extending into the hypoflexid (Fig. 23 F). The striations on these facets show a steep inclination from cervical to apical. On the m3, occlusion of the trenchant heel is restricted to the mesial hypoconid flank and the distal amphicone flank.
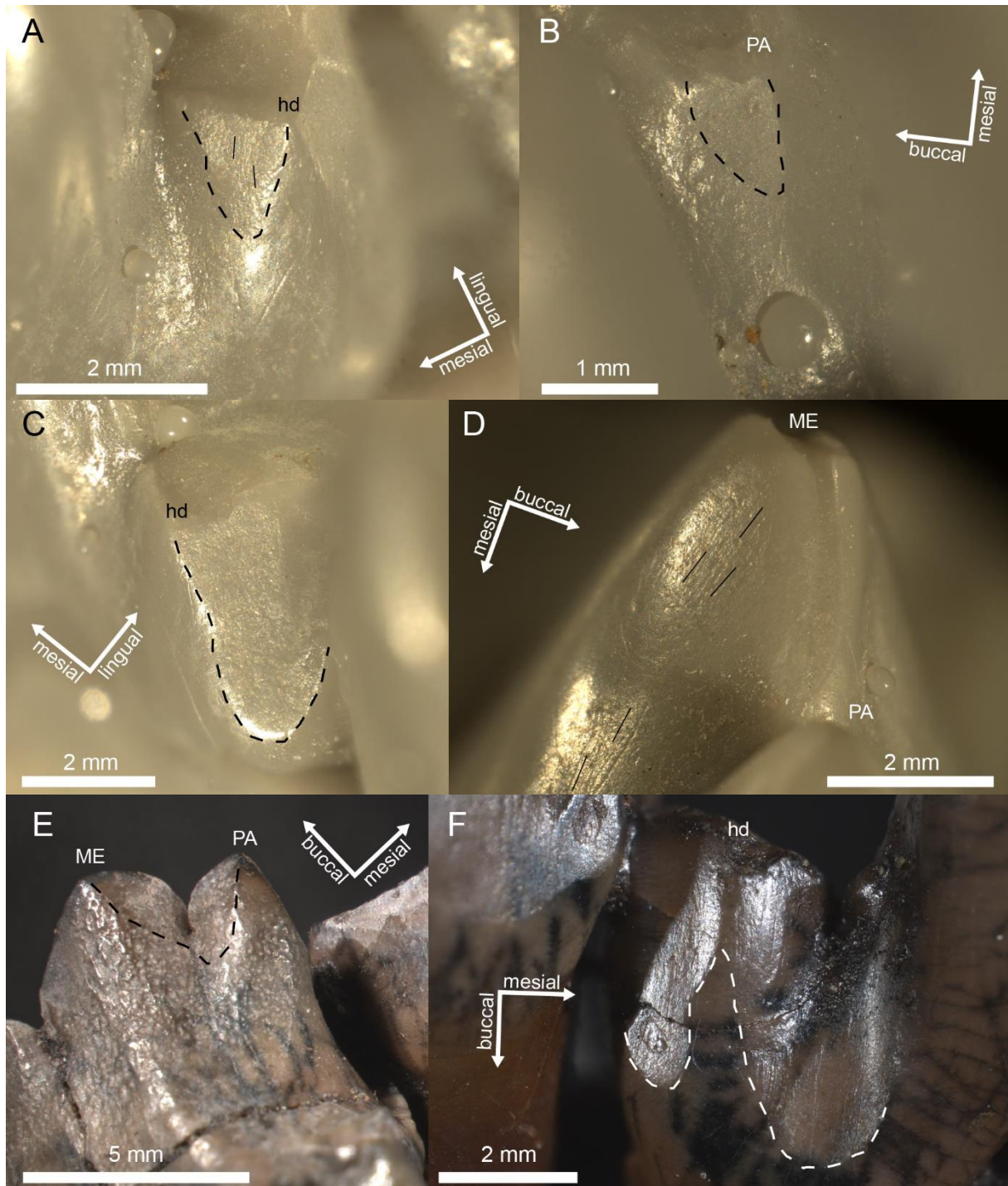
Fig. 23: A, Facet hd-mb on the m4 of *Thylacinus cynocephalus* (NMB 2526, epoxy cast) and B, facet PA-dl on the M2 of the same specimen (epoxy casts). In comparison, as seen in C, facets hd-db on the m2 and D, facet ME-ml on the M3 are larger (both epoxy casts). E shows the M2 of *Oxyaenoides bisucpidens* (GMH XIV 2910-1954), where facets PD-dl and ME-dl are connected, as are the facets hd-mb and hd-dl on the m1 of the same taxon (GMH XIV 2909-1954), shown in F. The dashed line marks the visible edge of the facets. Solid lines indicate the inclination of striations.
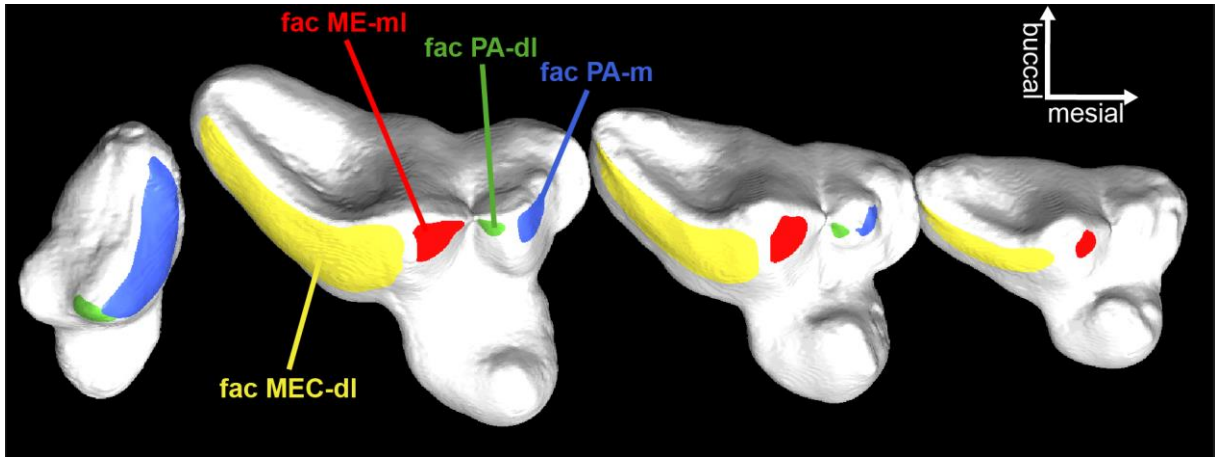
Fig. 24: Facets on the upper distal cheek dentition of a taxon with multiple derived carnassial teeth, as exemplified by the distal cheek dentition (M1 – M4) of *Thylacinus cynocephalus*.
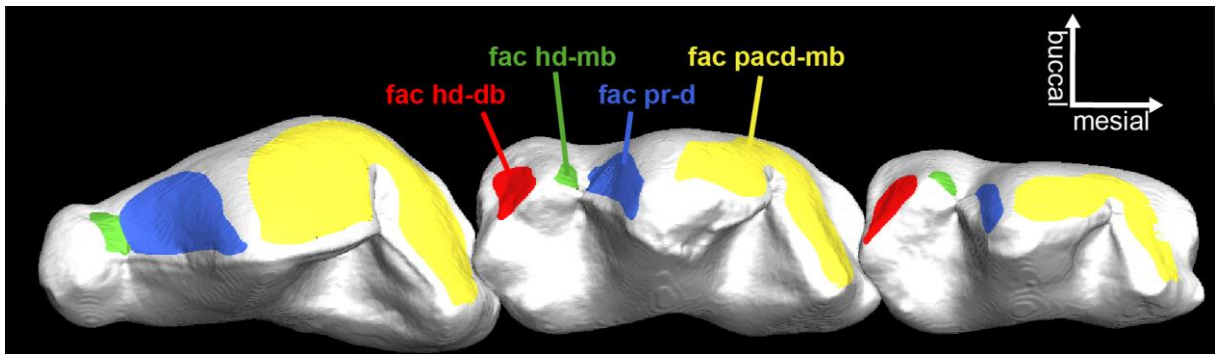
Fig. 25: Facets on the lower distal cheek dentition of a taxon with multiple derived carnassial teeth, as exemplified by the distal cheek dentition (m2 – m4) of *Thylacinus cynocephalus*. Rendering of µCT.

4.1.4 Wear patterns on basal heterodont carnassial dentitions

Facets pacd-mb and PRMEC-dl

Carnassial cutting in basal carnivoran carnassial dentitions, as documented in the closely related viverrid species *Viverra tangalunga* and *Viverra zibetha* and the herpestid species *Ichneumia albicauda*, is performed by the paracristid of the lower m1 and the praemetacrista of the upper P4. Occlusion of these two structures produces facet pacd-md along the m1 paracristid (Figs. 26A, 33) and facet PRMEC-dl along the P4 praemetacrista (Figs. 26B, 32). Despite the carnassial morphology being basal and showing all features of a tribosphenic condition (complete trigonids and talonids), the carnassial blades of *V. tangalunga* and *V. zibetha* are elongated and in addition to the carnassial notches roughly located midway along the cutting blades exhibit a small secondary carnassial notch respectively along the paracristid and along the praemetacrista. The facets wrap around the carnassial notches and the secondary carnassial notches, indicating that these structures are incorporated in the cutting function. Striations on these facets are only weakly pronounced in *Viverra* and more clearly

identifiable in *Ichneumia*, where they show a steep, mostly orthal inclination towards buccal on the upper tooth and towards lingual on the lower tooth.
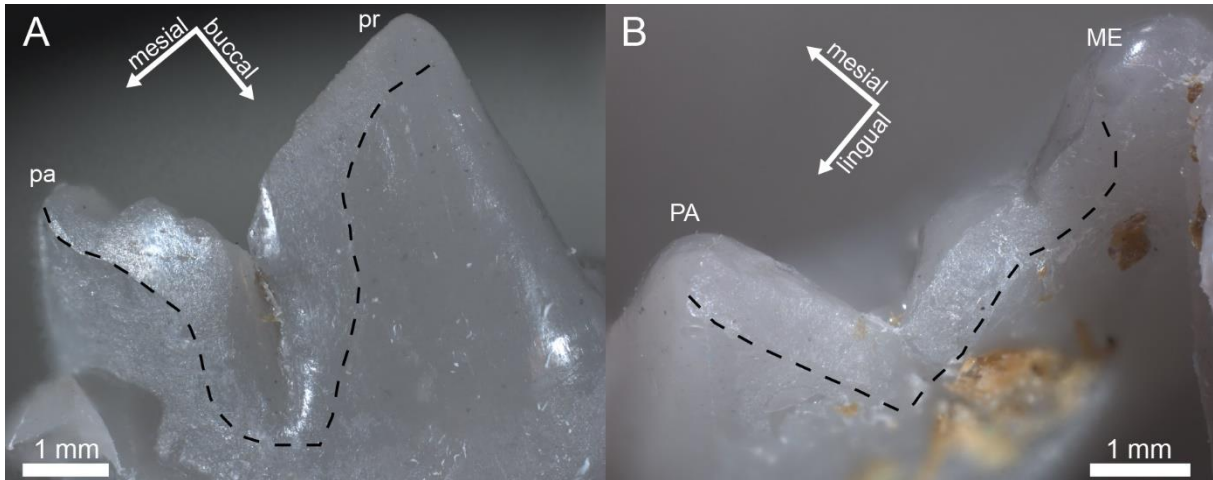

Fig. 26: A, facet pacd-mb on the m1 of *Viverra tangalunga* (SMF 20928) and B, facet PRMEC-dl on the P4 of the same specimen (epoxy casts). The dashed line marks the visible edge of the facets. Solid lines indicate the inclination of striations.

Facets pr-d and PA-m

Facet pr-d forms on the lingual side of the distal m1 trigonid flank. The facet is small and covers only a punctiform area on the specimens of *Viverra* that were included in this study, with no striations being present. In *Ichneumia*, facet pr-d extends from the apex of the protoconid along the postprotocristid to the notch of the distal trigonid blade (Figs. 27A, 33). Striations running from apical to cervical indicate a steep inclination. The antagonistic facet PA-m forms on the mesial paracone flank of the upper M1 (Figs. 27B, 32). It covers the lingual side of the paracone flank along the praeparacrista. A few isolated striations are present *Viverra*, while in *Ichneumia* the striations are unidirectional and oriented in a steep angle from cervical to apical.
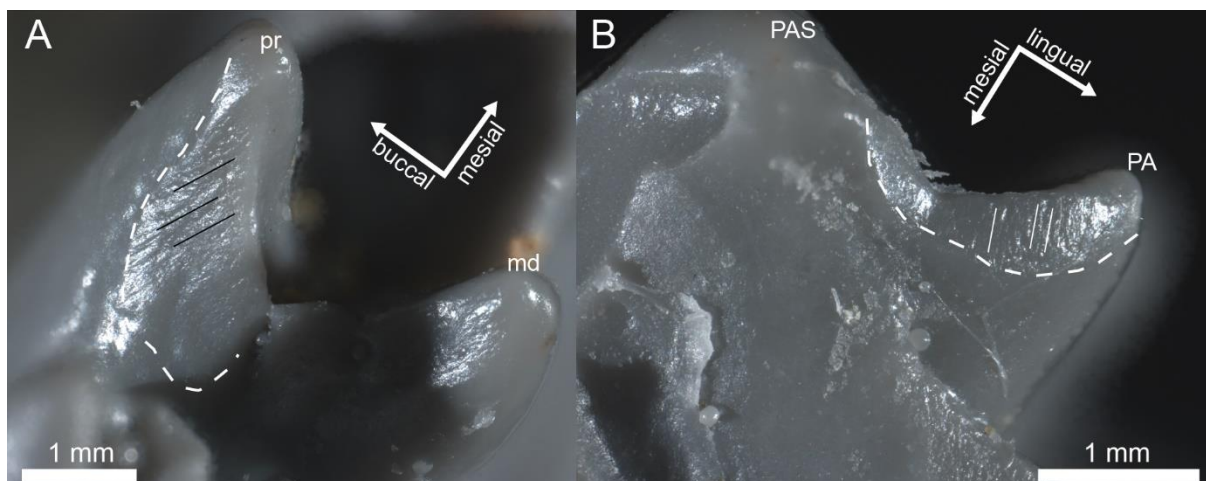
Fig. 27: A, facet pr-d on the m1 of *Ichneumia albicauda* (ZMFK MAM 1976.0125) and B, facet PA-m on the M1 of the same specimen (epoxy casts). The dashed line marks the visible edge of the facets. Solid lines indicate the inclination of striations.

Facets md-d and PR-m and PACL-m

Occlusion of the buccal side of the distal m1 trigonid flank with the mesial M1 protocone flank is indicated by the presence of facets md-d and PR-m. In both *Ichneumia* and *Viverra*, the mesial protocone flank is extended to the base of the paracone, exhibiting an elongated praeprotocrista that forms a cingulum-like structure. In some specimens, facet PACL-m extends in buccal direction from facet PR-m along the praeprotocrista to the base of the paracone along the paracingulum (Figs. 28A, 32). Facet md-d forms on the distal metaconid flank, running from the apex of the metaconid along the postprotocristid to the notch of the distal trigonid flank. Striations are absent in *Viverra*, but are well pronounced in *Ichneumia* and run in a steep inclination from the apex of the metaconid to cervical (Figs. 28B, 33).
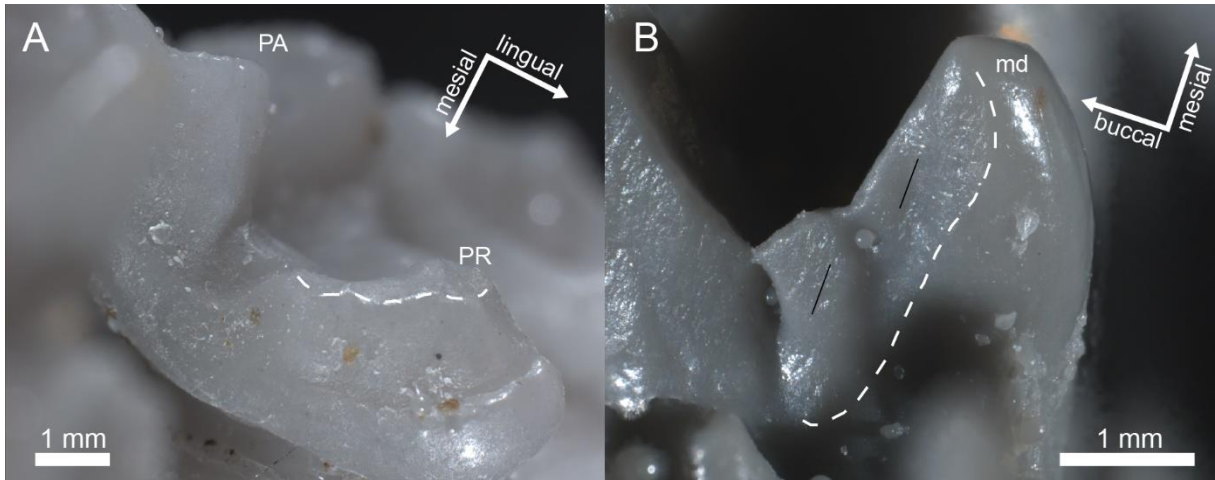
Fig. 28: A, facet PR-m on the M1 of *Viverra zibetha* (SMF 16516) and B, facet MEC-dl on the m1 of *Ichneumia albicauda* (ZMFK MAM 1976.0125) (both epoxy casts). The dashed line marks the visible edge of the facets. Solid lines indicate the inclination of striations.

Facets hd-mb and PA-dl

Facet hd-mb forms on the mesial flank of the m1 talonid, where it extends along the praehypocristid (Figs. 29B, 33). In some specimens, striations are present on the facet which have an almost vertical orientation with a slight inclination from buccal on the cervical part to buccal on the apical part of the facet. The antagonistic structure that occludes with the praehypocristid is the postparacrista of the P4 paracone, where facet PA-dl is present (Figs. 29A, 32). In some specimens, this facet covers the entire distal paracone flank. The striations show a mostly orthal orientation with a slight inclination from cervical to lingual.

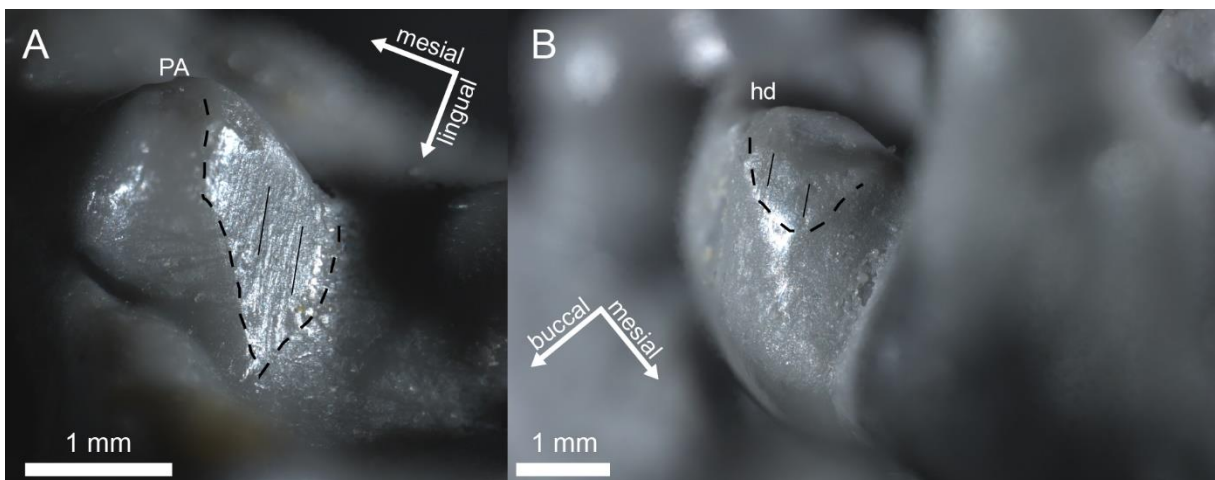**Fig. 29**: A, facet PA-dl on the M1 of *Ichneumia albicauda* (ZMFK MAM 1931.0056) and B, facet hd-mb on the m1 of *Viverra zibetha* (ZMFK MAM 1968.0085) (both epoxy casts). The dashed line marks the visible edge of the facets. Solid lines indicate the inclination of striations.

Facets hd-db and ME-ml

The distal m1 talonid flank forms a U-shaped crest between the hypoconid and the hypoconulid in *Viverra* and a V-shaped crest with a small notch in *Ichneumia*. Along this crest, formed by the posthypocristid, facet hd-db can be found, which also forms a U-shaped outline in *Viverra*. A few isolated, weakly pronounced striations show a vertical orientation, running from cervical to apical. In *Ichneumia*, facet hd-db remains small, restricted to the vicinity of the hypoconid apex, with striations running from cervical to apical being more abundant (Fig. 30A). The structure that occludes with the distal talonid flank is the mesial metacone flank of the M1. Along the praemetacrista, facet ME-ml can be found, which covers the entire mesial metacone flank in some specimens of *Viverra* (Fig. 30B). The facet shows a smooth surface *Viverra*, striations indicating a steep orthal inclination are found in some specimens of *Ichneumia*.
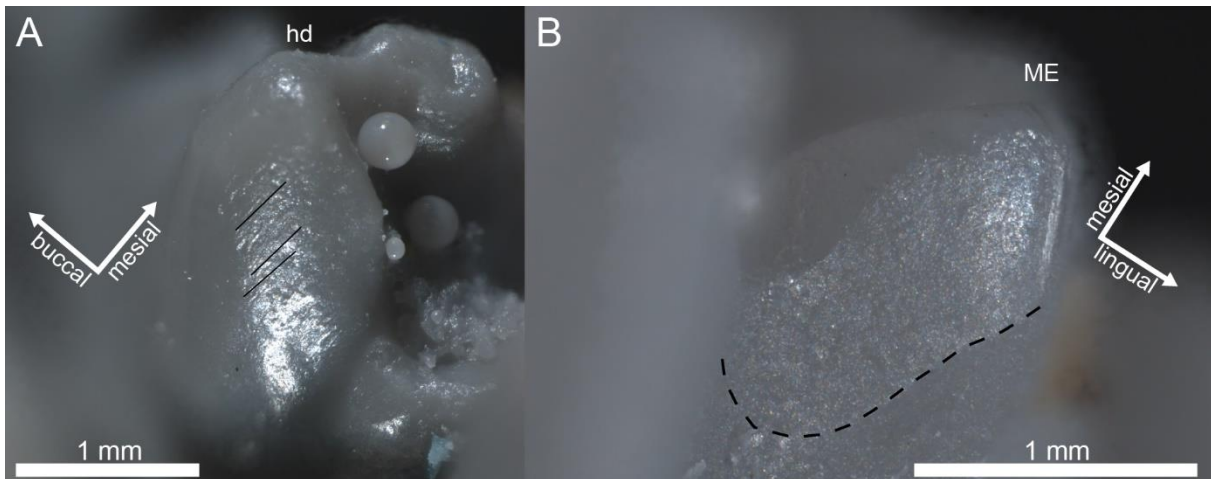
Fig. 30: A, facet hd-db on the m1 of *Ichneumia albicauda* (ZMFK MAM 1976.0125) and B, facet ME-ml on the M1 of *Viverra zibetha* (SMF 16516) (both epoxy casts). The dashed line marks the visible edge of the facets. Solid lines indicate the inclination of striations.

Facets ed-mb, hld-mb and PR-dl

Occlusion of the distal protocone flank of the M1 with the mesial flanks of the entoconid and the hypoconulid of the m1 is indicated by the presence of facets ed-mb, hld-mb and PR-dl. The mesial flanks of the entoconid and the hypoconulid appear polished in the specimens of *Viverra*, indicating attritive wear (Fig. 31A). Striations running from the apices to cervical are only faintly recognizable. In *Ichneumia*, facets are not as pronounced, however striations showing a similar inclination as in *Viverra* are more clearly pronounced. The antagonistic facet PR-dl covers the entire distal protocone flank in some specimens of *Viverra*, however, striations are ebsent (Fig. 31B).
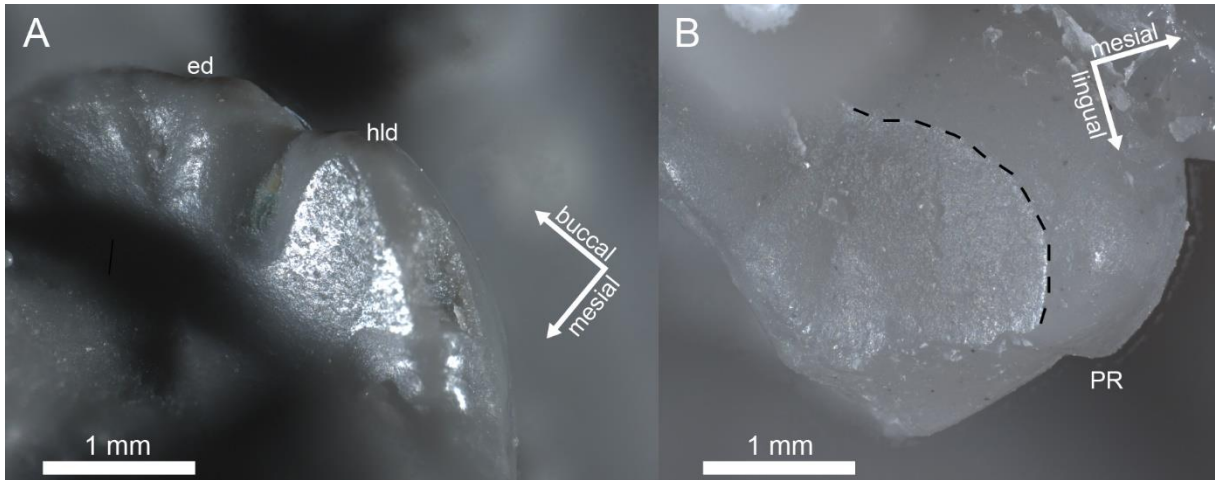
Fig. 31: A, facets ed-mb and hld-mb on the m1 of *Viverra zibetha* (ZMFK MAM 1968.0085) and B, facet PR-dl on the M1 of *Viverra zibetha* (SMF 16516) (both epoxy casts). The dashed line marks the visible edge of the facet. Solid lines indicate the inclination of striations.

Wear in the talonid basin and on the protocone

The postcarnassial occlusal surface in *Ichneumia* and *Viverra*, including the m1 talonid and the M1 protocone, is characterized by apical wear, with no evidence for attrition present. With progressing wear, the apices of the individual cusps appear blunted. Striations are only sparsely present and appear mostly in random orientations. They can be found in the trigon basin of the upper M1, where no uniform direction can be identified, and along the rim of the m2, where the orientation is mostly from apical to cervical.
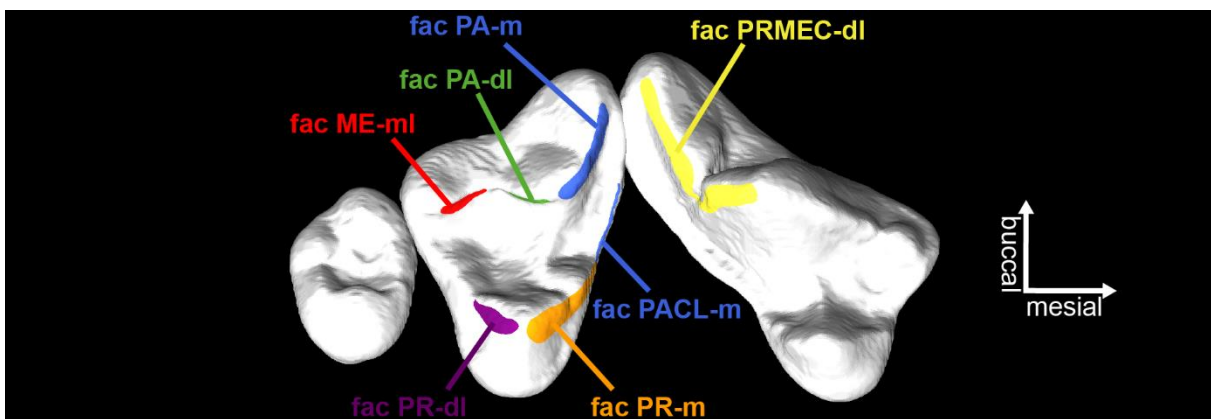
Fig. 32: Facets on the upper distal cheek dentition of a taxon with one basal carnassial and post-carnassial teeth, as exemplified by the distal cheek dentition (P4 – M2) of *Viverra tangalunga*. Rendering of μCT data.
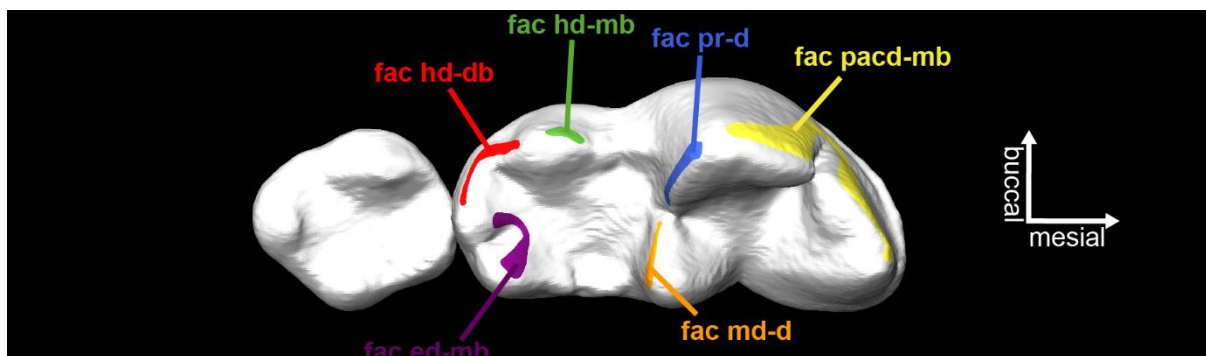
Fig. 33: Facets on the upper distal cheek dentition of a taxon with one basal carnassial and a post-carnassial tooth, as exemplified by the distal cheek dentition (m1 – m2) of *Viverra tangalunga*. Rendering of µCT data.

4.1.5 Wear patterns on derived heterodont carnassial dentitions

For the documentation of tooth wear in the heterodont cheeck dentitions of carnivorans, the canid *Speothos venaticus* and felid *Felis silvestris* were chosen for the derived carnassial condition. In *S. venaticus*, the talonid is lacking a basin structure, as the entoconid and the hypoconulid, marking the lingual and distal margin of the talonid basin in more basal carnassial teeth (e.g., of viverrids and herpestids), are absent. Thus, also facets associated with these structures are absent. In *S. silvestris*, the talonid is missing entirely, and the carnassials of this taxon exemplify the most derived carnassialized condition that can be found among carnivorans.

Facets pacd-mb, PRMEC-dl, pacd-m and PR-d

As in the basal carnivoran carnassials, the main carnassial cutting function is performed by the occlusion of the paracristid of the m1 with the praemetacrista of the P4. On the m1, facet pacd-mb forms on the mesial trigonid flank, extending from the protoconid to the paraconid and wrapping along the carnassial notch (Figs. 34A, 38). Striations on this facet show an orthal orientation from cervical to apical. Facet PRMEC-dl extends from the metastyle to the metacone of the P4, wrapping around the carnassial notch (Figs. 34C, 37). The striations on this facet also show an orthal orientation. On the m1 of *F. silvestris*, the additional facet pacd-m can be found bordering facet pacd-mb on the mesial side (Fig. 34B). It is situated in cervical direction from the apex of paraconid. This facet is formed by occlusion with the distal protocone flank of the P4. The antagonistic facet PR-d forms along the postprotocrista (Fig. 34D). Striations on these two facets show a similar orthal orientation as on the facets pacd-mb and PRMEC-dl.
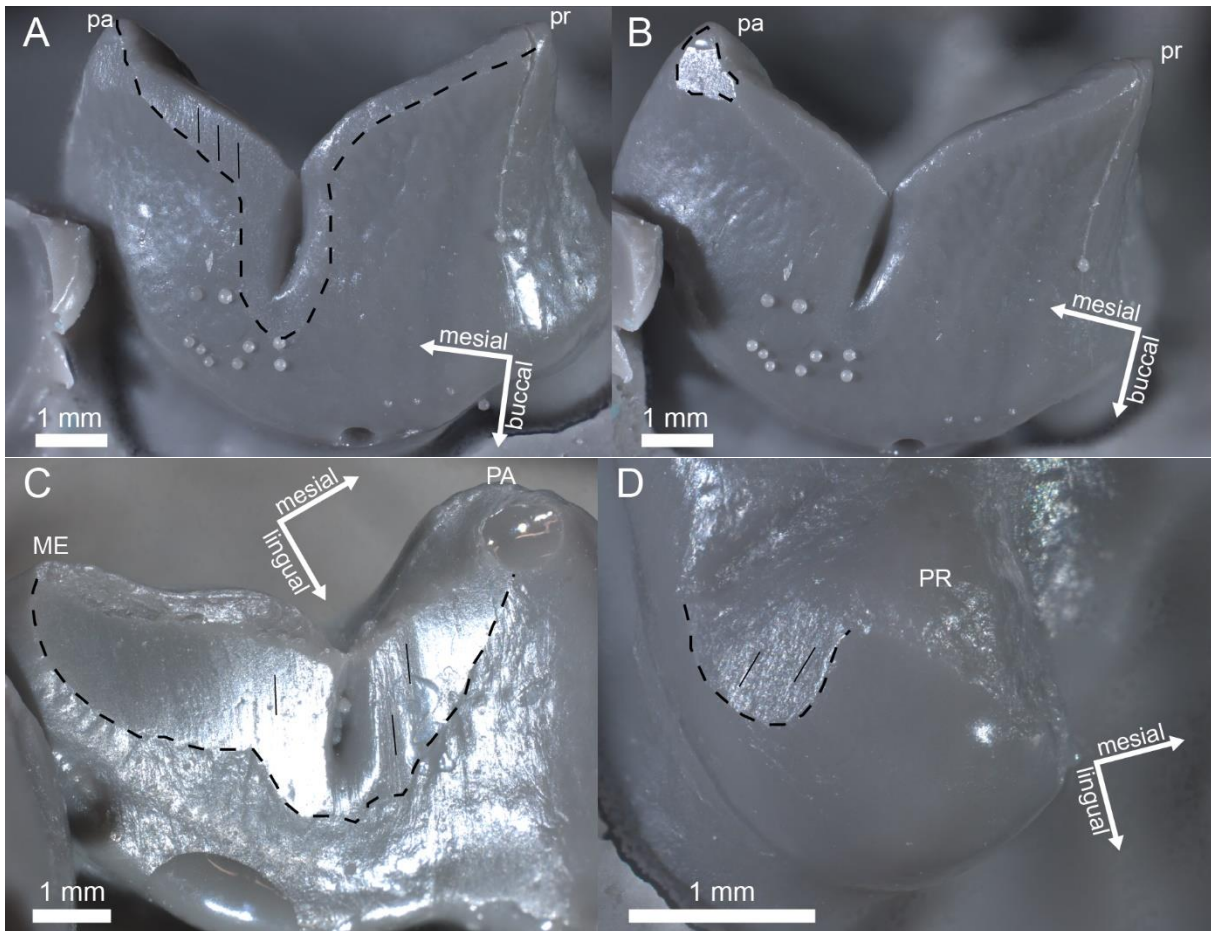
Fig. 34: A, facet pacd-mb on the m1 of *Felis silvestris* (ZMFK MAM 2018.0106) and B, facet pacd-m on the same tooth, bordering facet pacd-mb on the mesial side. The antagonistic facets form on the P4, as seen in facet PRMEC-dl on the P4 of *Speothos venaticus* (ZMFK MAM 1992.0565), shown in C, and facet PR-d on the P4 of *F. silvestris* (ZMFK MAM 2018.0106), shown in D. Facets pacd-m and PR-d are missing in the weaker carnassialized m1 and P4 of *S. speothos*. The dashed line marks the visible edge of the facet. Solid lines indicate the inclination of striations. All pictures taken from epoxy casts.

Facets pr-d, PA-m and PACL-m

Facet pr-d forms on the distal trigonid flank of the m1. It covers the entire distal trigonid flank in *S. venaticus* and striations on this facet show a mostly orthal orientation with a slight buccal inclination (Fig. 35A). The striations extend cervically into the hypoflexid and in some specimens connect with facet hd-md. The antagonistic structure that occludes with the distal trigonid is the paracingulum of the M1, where facet PACL-m forms (Fig. 35B). The striations on this facet show a steep orientation with a slight inclination towards lingual. Additional striations can be found on the mesial paracone flank, where in specimens with further progressed wear, facet PA-m forms (Fig. 35B). This points to the paracringulum as the main antagonistic structure to occlude with the distal trigonid flank. In *F. silvestris*, facet pr-d occurs as a small punctiform polished area right below the apex of the paraconid (Fig. 35C). The antagonistic structure that occludes with the distal trigonid in *F. silvestris* is the mesial flank of

what is presumed to be a vestigial paracone of the M1, generally exhibiting a reduced crown morphology (Fig. 35D).
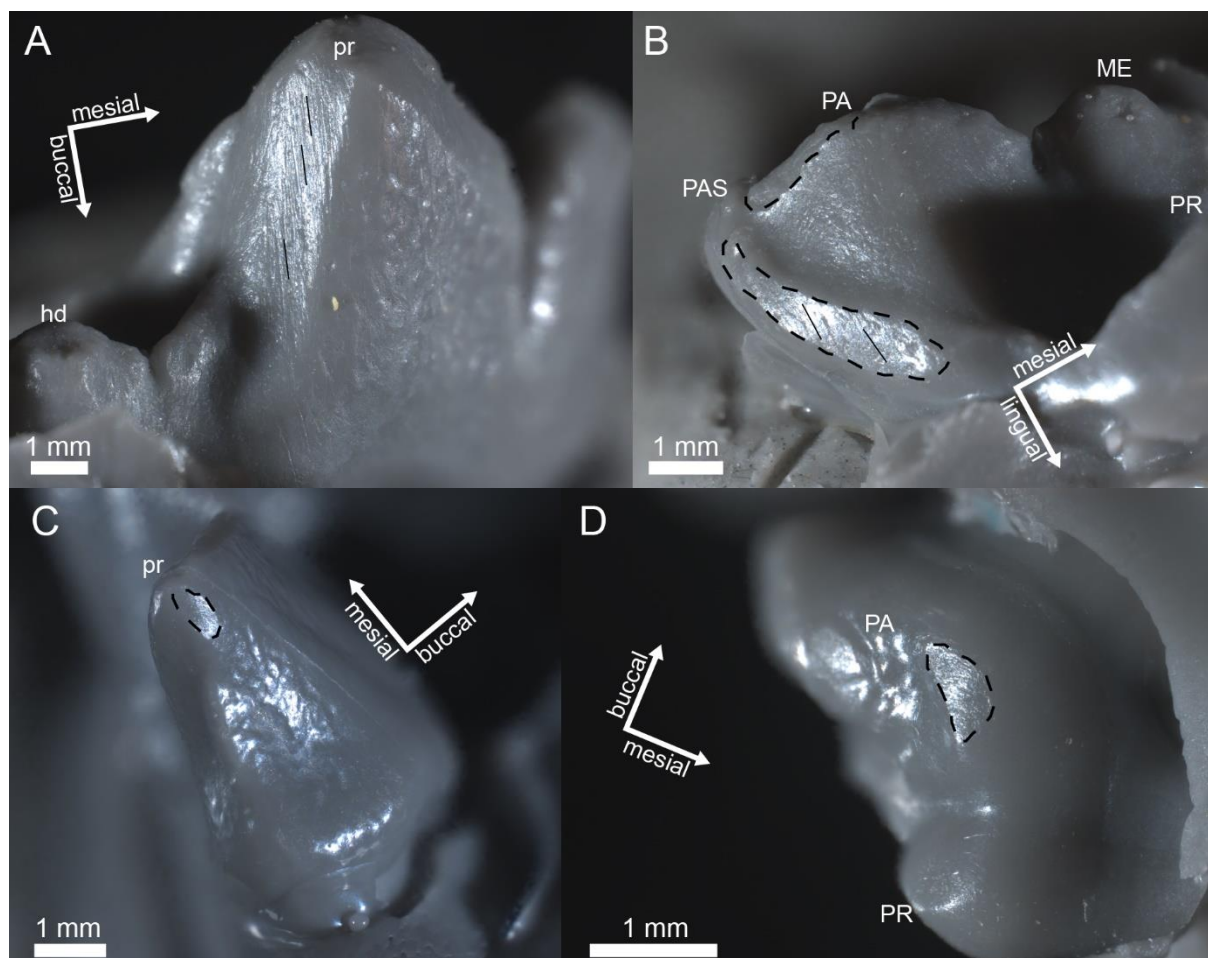
Fig. 35: A, facet pr-d on the m1 of *Speothos venaticus* (ZMFK MAM 1992.0565) and B, facets PA-m and PACL-m on the M1 of the same taxon (ZMFK MAM 1954.0154). In *Felis silvestris*, facet pr-d on the m1 (ZMFK MAM 2018.0106), as shown in C, and PA-m on the P4 of the same specimen shown in D are smaller, as the teeth are more carnassialized. The dashed line marks the visible edge of the facet. Solid lines indicate the inclination of striations. All pictures taken from epoxy casts.

Facets on the "trenchant heel"

When a unicuspid trenchant heel is present, the mesial hypoconid flank of the m1 occludes with the distal paracone flank of the M1. This results in the formation of the facets hd-md (Fig. 36A) and PA-dl (Fig. 36B). Striations show a steep orientation, running with a slight inclination towards buccal on the mesial hypoconid flank and towards lingual on the distal paracone flank. In specimens with further progressed wear, facet hd-mb covers the hypoflexid and connects with facet pr-d on the lower molar and facet PA-dl wraps around the lingual paracone flank, connecting with facet PA-m on the upper molar. The inclination of the striations is parallel to the buccal hypoflexid groove in *S. venaticus*. A similar wear pattern can be found on the m1 of

Dinictis sp., where facet hd-ml extends into the hypoflexid and the striations on the distal trigonid flank are oriented parallel to the inclination of the hypoflexid groove (Fig. 36C), while the antagonistic facet PA-dl wraps around the lingual paracone flank (Fig. 36D). In *F. silvestris*, the talonid is reduced to a small knob on the distal flank of the trigonid. Traces of wear are missing and point to a complete loss of function of the talonid.
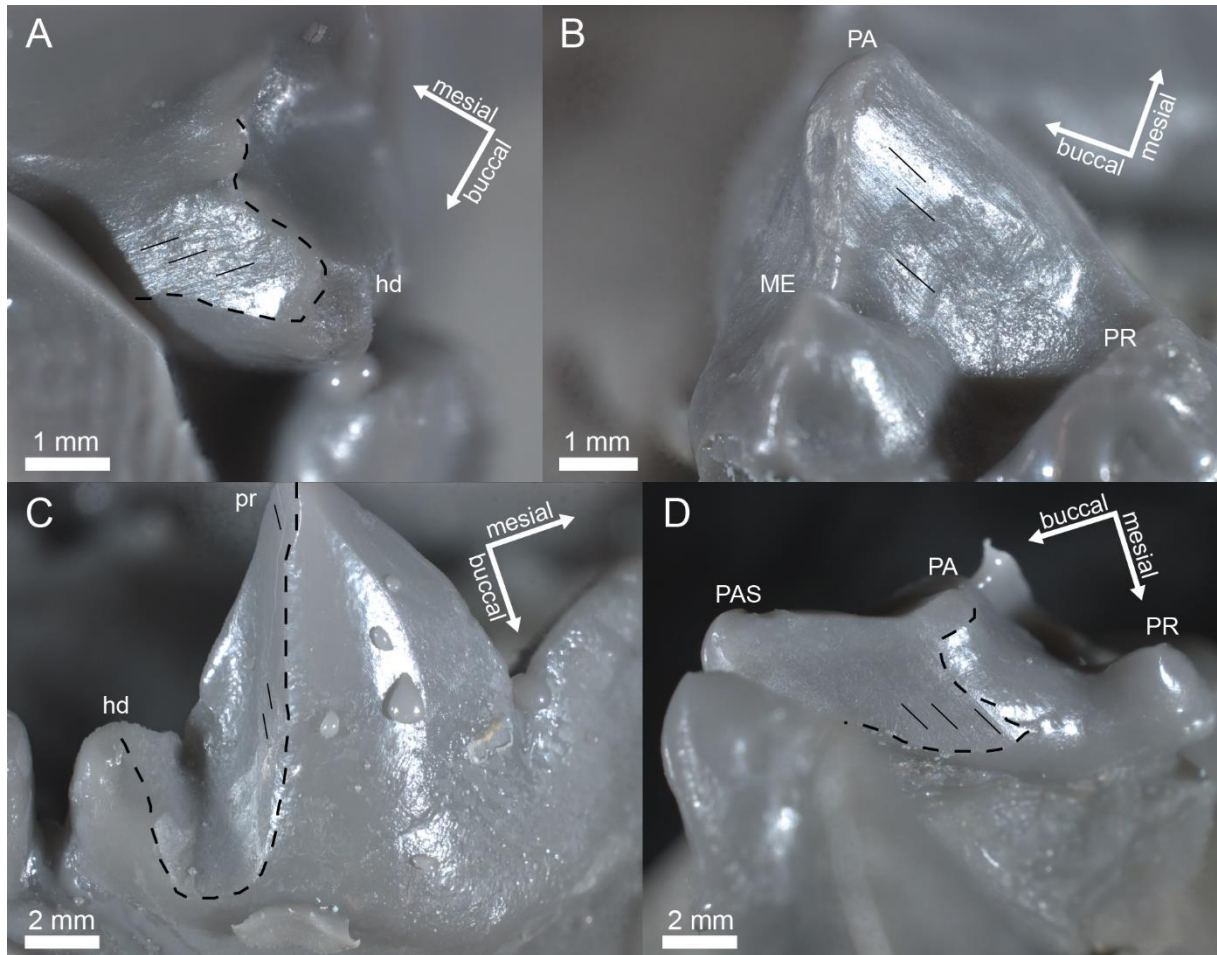
Fig. 36: A, facet hd-mb, extending into the hypoflexid and connecting with facet pr-d on the m1 of *Speothos venaticus* (ZMFK MAM 1992.0565). The antagonistic facet PA-dl forms on the M1 and wraps around the lingual paracone flank (same specimen), shown in B. In *Dinictis* sp., facet hd-md extends into the hypoflexid groove of the m1 and connects with facet pr-d (SMNK-PAL 9090), hsown in C. Similar to *S. venaticus*, the antagonistic facet PR-dl on the M1 of *Dinictis* sp. wraps around the lingual paracone flank, shown in the same specimen in D. The dashed line marks the visible edge of the facet. Solid lines indicate the inclination of striations. All pictures taken from epoxy casts.
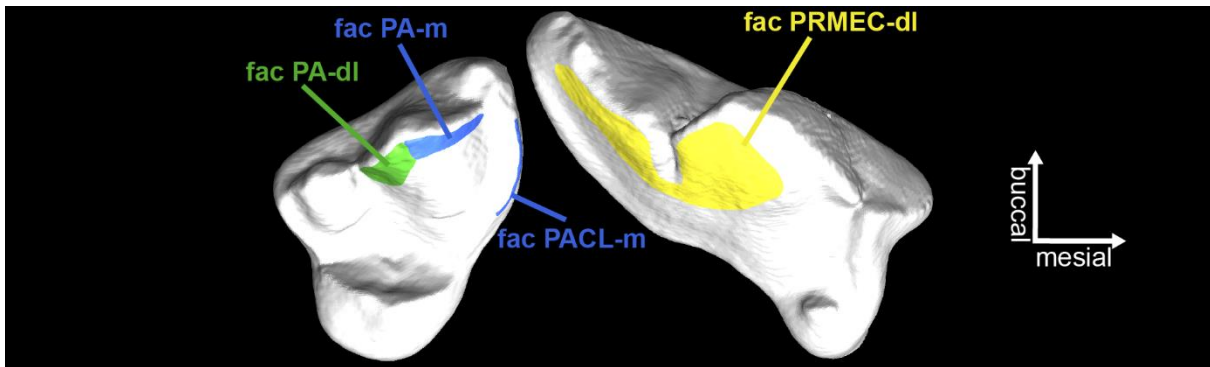
Fig. 37: Facets on the upper distal cheek dentition of a taxon with one derived carnassial and a post-carnassial, as exemplified by the distal cheek dentition (P4 – M1) of *Speothos venaticus*. Rendering of µCT data.
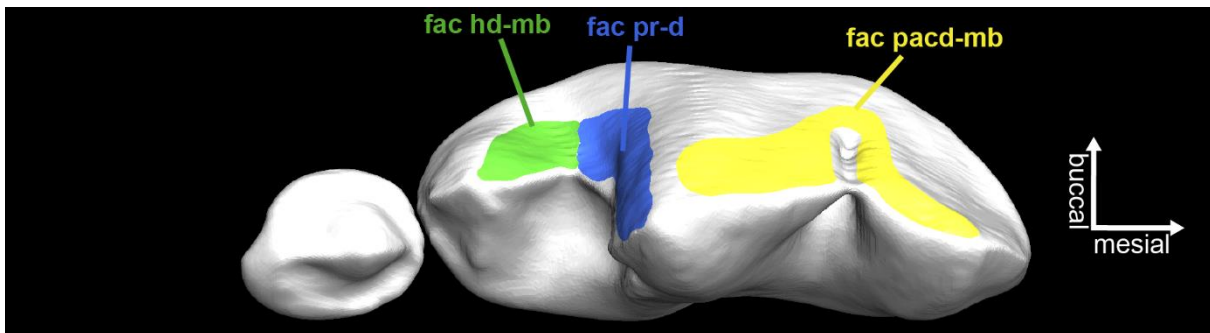
Fig. 38: Facets on the lower distal cheek dentition of a taxon with one derived carnassial with a trenchant heel and a post-carnassial, as exemplified by the distal cheek dentition (m1 – m2) of *Speothos venaticus*. Rendering of µCT data.

4.1.6 OFA Analysis of *Dasyurus viverrinus*

An OFA analysis was carried out with the dentition of *Dasyurus viverrinus* as a representative of a taxon with multiple basal carnassial teeth. The teeth of specimen SMF 1480 were chosen for the analysis. The complete length of the chewing path comprises 231 steps (Fig. 39). Phase I ends at timestep 162, which is the point of centric occlusion. Initial contact occurs between the m4 mesial carnassial blade, at the distalmost point of the paracristid below the paraconid and the M3 distal blade, at the mesial-most point of the metacrista at the metastyle. With the upwards movement of the lower molar, this area of occlusal contact is expanding lingually and thus the active point of cutting is also moving in lingual direction along the paracristid and the metacrista. Initial contact between the paraconid of the m4 and the metacone of the M3 occurs at timestep 18. This area of occlusal contact is moving in buccal direction with further upwards movement of the lower molar. Starting with timestep 18, there are two points of active cutting between the paracristid and the metacrista, which are both successively expanding their areas

towards the center of the two antagonistic cutting blades. At timestep 19, the initial contact between the metacristid of the m3, starting at the protoconid, and the praeparacrista of the M3, starting at the parastyle, is calculated. With a further upwards movement of the lower molar, cutting beween the metacristid and the praeparacrista eventually includes the whole mesial paracone flank. First occlusal contact between the paracristid of the m3 and the metacrista of the M2 is calculated at timestep 24, beginning with the lingual point of contact between the paraconid and the metacone. A second part of contact on the buccal side between the protoconid and the metastyle is calculated at timestep 30. These two contact areas expand with further upwards movement of the lower molar towards the center of the carnassial blade. At timestep 25, initial contact between the metacristid of the m4 and the paracrista of the M4 is calculated between the apex of the protoconid and the parastyle. This area of occlusal contact successively expands lingually and eventually involves the paracone occluding with the distal carnassial notch. At timestep 96, a second occlusal contact is calculated between the metacristid of the m4 and the praeprotocrista of the M4, starting with the occlusion of the apices of the protocone and the metaconid. An additional point of contact between the praeprotocrista and the metacristid, occurring buccally from the metacristid carnassial notch, is calculated at timestep 109. These two points of cutting between the praeprotocrista and the metacristid are moving towards the carnassial notch with further upwards movement of the lower molar. The initial occlusal contact between the paracristid of the m2, starting at the apex of the protoconid and the metacrista of the M1, starting at the metastyle, is calculated at timestep 73. At timestep 76, a second contact between the paracristid and the metacrista is calculated, occurring between the metacone and the paraconid. These two points of occlusal contact are moving towards the center of the carnassial blade with further upwards movement of the lower molar. With this contact, the carnassial blades of the m4, m3 and m2 all perform a cutting function while the lower jaw is moving upwards. Initial contact between the metacristid of the m2 and the praeparacrista of the M2 is calculated at timestep 86. This area of contact expands with further tooth movement towards lingual along the distal paracone flank. A second point of occlusal contact along the metacristid is calculated at timestep 97 and it involves the praeprotocrista. Further upwards movement of the lower jaw results in these two areas of contact moving towards the carnassial notch of the metacristid. The cutting function of the m3 metacristid is enhanced by occlusal contact with the praeparacrista of the M3 at timestep 102. This area of contact on the lingual part of the metacristid is expanding buccally with further tooth movement, while the occlusal contact with the mesial paracone flank expands lingually onto the mesial protocone flank, with both areas expanding towards the carnassial notch of the lower molar. With this contact, the distal trigonid blades of all lower carnassials perform a cutting function during further tooth movement.

In addition to the cutting contacts that are calculated at the mesial and distal trigonid flanks, occlusion also occurs on the talonid.

At timestep 91, the first contact between the praemetacrista of the M3 and the posthypocristid of the m3 occurs. Further upwards movement of the m2 results in contact between the praemetacrista of the M2 and the posthypocristid of the m2 at timestep 100. Initial contact between the postparacrista of the M3 and the praehypocristid of the m3 occurs at timestep 103. A similar contact at timestep 110 occurs between the postparacrista of the M2 and the praehypocristid of the m2. With further upwards movement of the lower jaw, the protocones of the M2, M3 and M4 move into the talonid basins of the antagonistic lower molars. Occlusal contact in the talonid basin successively occurs with the occlusion of the buccal entoconid flank and the postprotocrista. This contact occurs between the M3 and the m3 in timestep 110, between the M2 and the m2 in timestep 117 and between the M4 and the m4 in timestep 131. The calculated contact area shifts into the talonid basins of all lower molars and onto the buccal protocone flank of the upper molars with further upwards movement of the lower jaw. This upwards movement is stopped at timestep 162, when the downwards movement of the lower jaw of phase II starts. From this point on, the hypoconid tips are dragged along the buccal protocone flanks. Due to the small size of the m4 talonid, the occlusal contact between the M4 protocone and the m4 talonid remains only for a short time until timestep 167. Contact between the protocone of the M3 and the m3 talonid remains up until timestep 195, and the final contact between the M2 protocone and the m2 talonid occurs at timestep 231. The movement of the lower jaw during phase I is directed in upwards in lingual direction, and has a movement vector with a slight distal direction. The tooth movement is only slightly altered from the marked-out trajectory path. During phase II, the inclination is a bit compared to phase I and directed downwards in lingual direction. This movement is deflecting more clearly from the marked-out trajectory path and thus is clearly influenced by the morphology of the occluding crown structures, which are the protocones of the upper molars and the talonid basins of the lower molars.
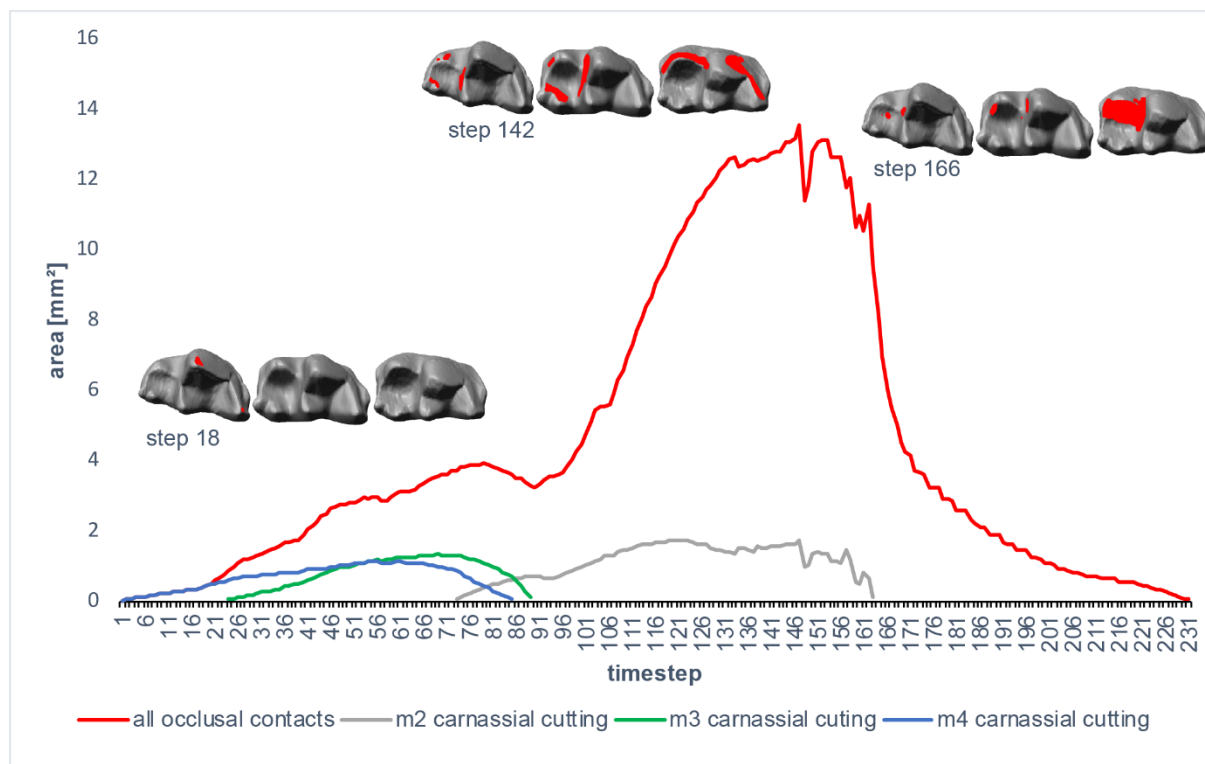
Fig. 39: Diagram of occlusal area size per timestep in the OFA analysis for *Dasyurus viverrinus*. The detected contacts at the lower carnassial blades show a successive cutting function of the carnassials from the distal to the mesial carnassial blades. Carnassial cutting is always initiated by two points of occlusion, as seen in timestep 18, which shift to the center of the carnassial blades with further movement. The first 100 timesteps are mostly characterized by a slow increase of the area of occlusal contact, which is dominated by carnassial cutting. Secondary cutting contacts start to occur at the paracone and metacone flanks around timestep 100, which results in the area of total occlusal contact increasing more rapidly in the following timesteps. Additionally, the first occlusion within the talonid basins is detected (timestep 142). Around timestep 162, which marks the point of centric occlusion, the area of occlusal contact is rapidly decreasing. In the second phase of the power stroke, no carnassial cutting occurs. The detected contacts are dominated by occlusion within the talonid basins, as seen in timestep 166. Rendering of µCT data.

4.1.4 OFA Analysis of *Thylacinus cynocephalus*

An OFA analysis was carried out with *Thylacinus cynocephalus* as a representative with multiple derived carnassials and a still functional talonid. For the analysis, specimen ZMB_Mam_036877 was chosen. The complete chewing path is comprised of 168 steps and consists of one single phase until the point of centric occlusion is reached (Fig. 40). Initial occlusal contact occurs between the metacrista of the M3, starting on the buccal side in proximity to the metastyle, and the distalmost point of the m4 paracristid, in proximity to the apex of the paraconid. With further upwards movement of the lower molars, this contact area expands in mesial direction towards the carnassial notch of the m4 and in direction of the

metacone of the M3. In timestep 18 the first contact between the M3 metacone and the m4 protoconid occurs, marking a second point of occlusion between the M3 and m4 carnassial blades. Both contact areas keep expanding on the occluding flanks and approach each other with further tooth movement, eventually wrapping around the carnassial notch of the lower molar and fusing in timestep 58. In timestep 31, occlusal contact occurs between the mesial paracone flank of the M3 and the distal trigonid flank of the m3. With further tooth movement, this contact area expands along the praeparacrista and postparacrista of the M3 and along the distal trigonid flank of the m3 in cervical direction. This occlusal contact remains up until timestep 120. In timestep 61, two points of contact between the carnassial blades of the M2 and the m3 are detected. The first occurs on the buccal side, respectively in proximity to the metastyle and the protoconid. The second contact occurs on the lingual side, respectively in proximity to the metacone and the paraconid. Both contacts expand with further tooth movement, approximating each other along the metacrista and the paracristid. Eventually, they wrap around the carnassial notch of the m3 and fuse in timestep 99. First contact between the mesial paracone flank of the M2 and the distal trigonid blade of the m2 occurs in timestep 62. With further tooth movement, the area of occlusal contact expands along the postparacrista and the praepacacrista of the M2 and expands in cervical direction of both antagonistic flanks and remains up until timestep 127. In timestep 86, the first occlusal contact between the carnassial blades of the M1 and the m2 is detected. It occurs on the buccal side of the blades between the metastyle of the M1 and the protoconid of the m2. With further upwards movement of the lower molars, this contact area expands in lingual direction along the metacrista and the paracristid. A second point of contact on the lingual side is detected in timestep 97. It occurs between the metacone of the M1 and the paraconid of the m2. With further tooth movement, this contact expands in lingual direction. Both areas of contact approximate each other in the following timesteps and merge in timestep 118, wrapping around the carnassial notch of the lower molar. The first contact between the mesial paracone flank of the M4 and the distal trigonid flank of the m4 occurs in timestep 53. This contact remains during the entire rest of the chewing path, with the distal trigonid flank of the m4 occluding along the paracone of the M4. Eventually, the contact wraps around the paracone and covers the hypoflexid. In addition to the trigonids occluding with the paracones and metacones, there are occlusal contacts between the talonids and the paracones and metacones. The first one occurs in timestep 63 between the distal talonid flank of the m3 and the mesial metacone flank of the M3. It starts on the lingual side, along the praemetacrista in proximity to me metacone and along the posthypocristid in proximity to the hypoconulid. With further tooth movement, this occlusal contact expands in buccal direction along the praemetacrista and along the posthypocristid towards the hypocone. This occlusion remains until timestep 112. In timestep 100, the first occlusal contact between the distal paracone flank of the M3 and the mesial talonid flank of

the m3 is detected. This contact area remains small and is only active for a shorter duration, up until timestep 136. The first occlusal contact between the distal talonid flank of the m2 and the mesial metacone flank of the M2 occurs in timestep 107 on the lingual side. The area of contact expands with further tooth movement along the praemetacrista in lingual direction from the metacone and from the hypoconulid towards the hypocone. It remains active until timestep 131.The mesial talonid flank of the m2 occludes with the distal paracone flank of the M2 first in timestep 133. The area of contact remains small and is active until timestep 155.
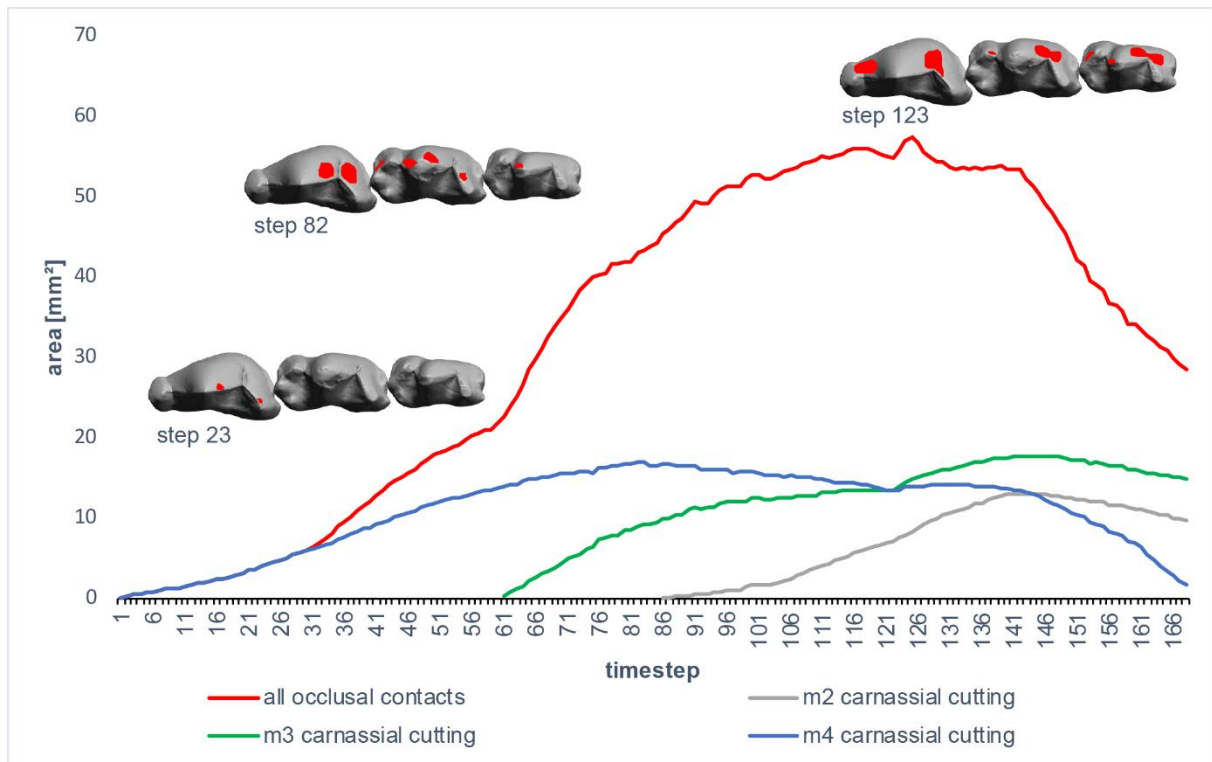
Fig. 40: Diagram of occlusal area size per timestep in the OFA analysis for *Thylacinus cynocephalus*. The successive carnassial cutting from distal to mesial can be seen by the detected occlusion of the respective lower carnassial blades. The occlusion is throughout dominated by carnassial cutting, which is initiated by two points of contact on the respective carnassial blades (as seen in timesteps 23 and 82). Secondary cutting of the paracones and metacones only makes up a small portion of total occlusal contact, protocone/talonid occlusion is absent entirely. Occlusion between the M4 paracone and the m4 hypoflexid occurs at the end of the power stroke (timestep 123). Rendering of µCT data.

4.1.8 OFA Analysis of *Hyaenodon exiguus*

The hyaenodont *Hyaenodon exiguus* with derived carnassial teeth was used in an OFA analysis as a representative with multiple derived carnassials without a functional talonid present. For the upper dentition, specimen NMB Q.C.938 was chosen and for the lower dentition, specimen NMB Q.B.771 was chosen. The complete chewing path is comprised of

202 timesteps (Fig. 41). Occlusion occurs during one single phase of movement until the point of centric occlusion is reached. The occlusion in *H. exiguus* is solely attributed to cutting contacts of the carnassial blades. Initial occlusal contact is detected between the apex of the M2 amphicone and the paracristid near the apex of the m3 paraconid. In timestep 34, the apex of the M1 amphicone occludes with the apex of the m2 paraconid. With further upwards movement of the lower jaw, both of these contact areas keep expanding along the paracristid and the metacrista, respectively in distal direction. A second occlusal contact between the apex of the M2 metastyle and the apex of the m3 protoconid is detected in timestep 56. This area of contact keeps expanding in mesial direction with further tooth movement, fusing with the mesial contact area in timestep 136. This is also the point when the carnassial notches of the M2 and the m3 pass each other. In timestep 71, the first occlusal contact between the apex of the P4 amphicone and the apex of the m1 paraconid is detected. The first contact between the apex of the M1 metastyle and the m2 protoconid is detected in timestep 117. It expands in mesial direction with further tooth movement, respectively along the paracristid and the metacrista. The two areas of occlusal contact between the carnassial blades of the M1 and the m2 fuse in timestep 143, which is when the carnassial notches of the upper and lower molars pass each other. In timestep 163, the apex of the P4 metastyle occludes with the m1 paracristid, in distal direction from the carnassial notch. This marks a second point of contact between the P4 and the m1 carnassial blades. While the mesial contact keeps restricted to the mesial-most points of the occluding carnassial blades, the distal area of contact keeps expanding in mesial direction with further tooth movement towards the carnassial notches. Both areas of contact fuse only in the last timestep of the chewing path. In addition to the carnassial cutting between the metacristae and paracristids, secondary occlusal contacts are detected at the end of the chewing path. Since the talonid basins are absent, they do not pose a "stopping" point for tooth movement. The point of centric occlusion is thus hard to determine. There are however some structures, which to hinder further tooth movement. The most obvious one is the peculiar large protocone of the P4. It is so large that, if the carnassial notches of the P4 and the m1 are placed in the closest possible proximity, which would result in the most effective cutting function, the apex of the m1 paraconid is pushed against the distal margin of the P4 protocone. At this point, further upwards movement of the lower molars is only possible if the lower jaw is displaced distally to allow the m1 paraconid to pass the P4 protocone. It is highly unlikely that such movement occurs. In addition to this, the vestigial protocones of the m1 and the M2 also come in contact with the lower molars. In timestep 191, the M2 protocone occludes with the apex of the m2 protoconid. Further, the M1 protocone occludes with the m1 protoconid in timestep 197. Although these contacts could not be confirmed by the presence of attributed facets, there are "dents" near the apices of the m1 and m2 protoconids which can

be interpreted as wear resulting from repeated occlusal contact with the protocones (discussed in 5.1).
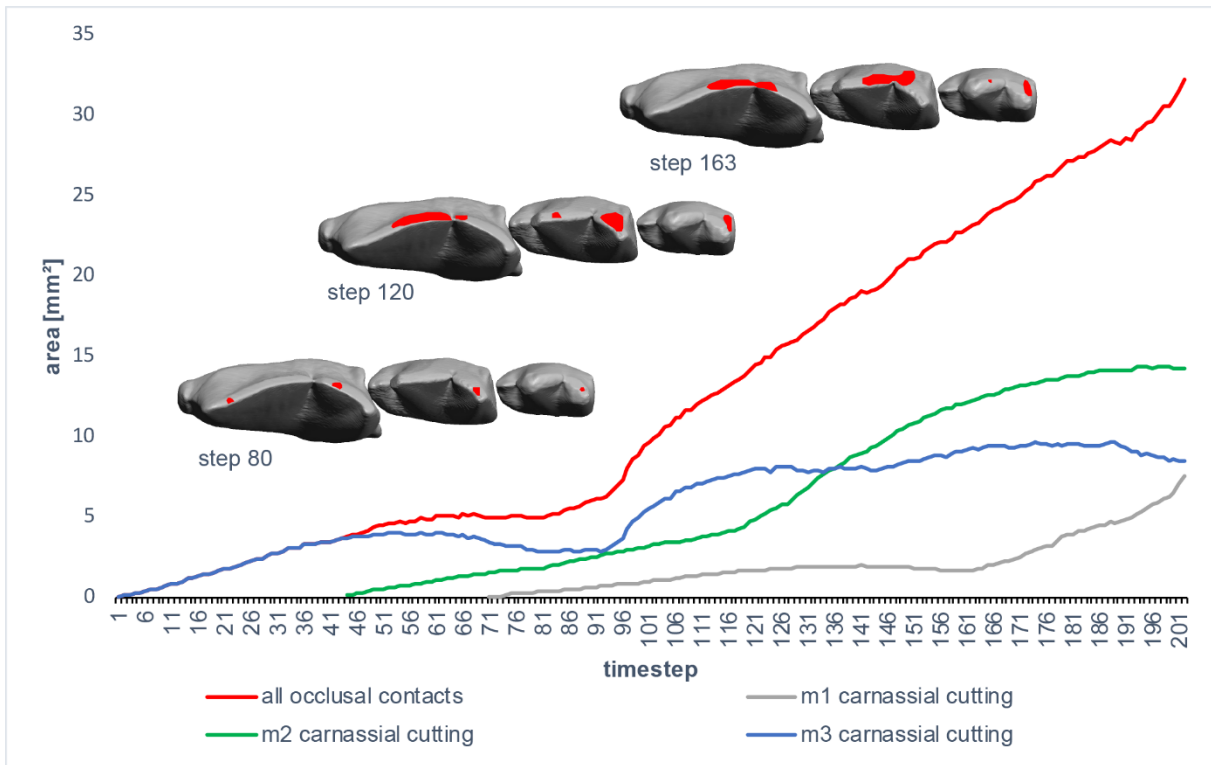
Fig. 41: Diagram of occlusal area size per timestep in the OFA analysis for *Hyaenodon exiguus*. The complete power stroke is dominated by carnassial cutting, which occurs successively from the distal to the mesial carnassial. The cutting function is initiated by two points of contact on the respective carnassial blade, as seen in timestep 80, which then shift towards the center of the blade (timesteps 120 and 163). Up until the end of the power stroke, the total area of occlusion is steadily increasing. Rendering of µCT data.

4.1.9 OFA Analysis of *Viverra tangalunga*

The viverrid *Viverra tangalunga* has a basal carnivoran dentition with weakly specialized carnassials. For the OFA analysis, specimen SMF 697 was chosen. The m1 talonid and the P4 protocone as well as the post-carnassial molars (M1, M2 and m2) are well developed. The complete power stroke comprises 142 timesteps (Fig. 42). The initial occlusal contact occurs between the apex of the P4 paracone and the apex of the m1 paraconid, which results in a first point of cutting between the carnassial blades on the buccal side. In timestep 6, a second occlusal cutting contact on the lingual side is initiated between the apices of the metacone and the protoconid. With further upwards movement of the lower jaw, these two occlusal contacts expand along the carnassial blades towards the location of the carnassial notches. The occlusal contact between the carnassial blades remains active up until timestep 119. Occlusal contact between the parastyle of the M1 and the distal protoconid flank of the m1 is also initiated in timestep 6. This area of contact shifts in cervical direction along the distal protoconid flank with further upwards movement of the lower molar and extends into the hypoflexid around timestep 107, whereas it shifts in lingual direction along the praeparacrista towards the paracone apex on the M1. In timestep 30, the buccal flank of the protoconid apex of the m1 occludes with the postcingulum of the P4, which aids in guiding the lower jaw during further upwards movement, as it restricts the freedom of movement. A second point of occlusion on the distal protoconid flank of the m1 occurs with the paracingulum of the M1 at timestep 32. With further tooth movement it shifts in cervical direction along the same area of the distal protoconid flank that occludes with the parastyle and paracone. The occlusal contacts between the M1 and the distal protoconid flank remain active until the point of centric occlusion. Between timesteps 99 and 125, occlusal contact between the mesial paracone flank along the praeparacrista and the distal hypoconid flank along the posthypocristid occurs. In timestep 82, a first contact occurs between the mesial protocone flank of the M1 and the apex of the m1 metaconid. With further tooth movement, this area of contact expands to cover the entire distal metaconid flank and most of the distal protocone flank up to the point of centric occlusion. Initial occlusal contact in the m1 talonid basin occurs in timestep 121 between the entoconid and the distal M1 protocone flank. This area of contact expands to cover the entire entoconid flank with further tooth movement and a second occlusal contact between the mesial protocone flank and the hypoconulid is initiated in timestep 126. These contacts remain active up until the point of centric occlusion. Additional contacts during centric occlusion are detected at the apex of the M1 protocone, which occludes into the m1 talonid basin, as well as the tip of the m1 hypoconid, which occludes into the M1 talon basin. Also, small contacts are detected between the M2 and the m2, respectively in the trigonid and trigon basins of the molars.
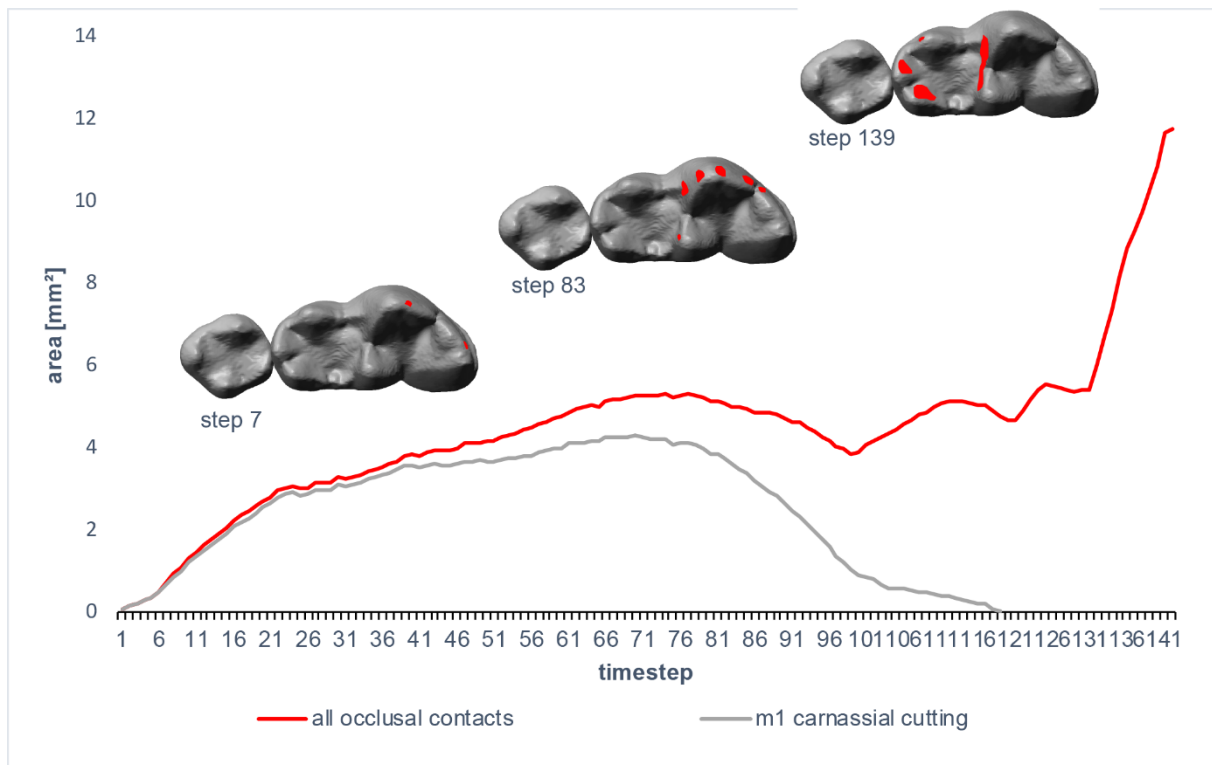
Fig. 42: Diagram of occlusal area size per timestep in the OFA analysis for *Viverra tangalunga*. Initial contact starts at the carnassial blade, where two points of contact (timestep 7) are shifting to the center of the blade with further tooth movement. About half of the duration of the power stroke is dominated mainly by carnassial cutting. Secondary cutting occurs as the mesial protocone and paracone flanks, as well as the paracingulum, occlude with the distal m1 trigonid flank, as seen in timestep 83. Around timestep 71, the portion of carnassial cutting contacts as part of the total occlusal contact is steadily decreasing, as occlusion at the distal trigonid and in the m1 talonid occurs. In the last section of the power stroke, carnassial cutting is not present (timestep 139). In addition to occlusion within the m1 talonid, where a crushing function is performed, occlusion between the m2 and the M2 occurs, which can be attributed to additional crushing. The last timesteps before the point of centric occlusion is reached are characterized by a drastic increase of occlusal contact area. Rendering of µCT data.

4.1.10 OFA Analysis of *Speothos venaticus*

The power stroke of the canid *Speothos venaticus* (specimen ZFMK MAM 1987-0386) is comprised of 102 timesteps (Fig. 43). Initial occlusal contact occurs between the carnassial blades of the P4 and the m1. It is detected between the metacone and the protoconid and with further upwards movement of the lower jaw a second contact is detected between the paracone and the metaconid in timestep 6. As the lower molar is moved upwards, these contact areas keep expanding towards the center of the carnassial blades respectively along the metacrista and the paracristid in direction of the carnassial notches. Around timestep 33, the carnassial notches of the P4 and the m1 pass each other. Carnassial occlusal contact remains active up until timestep 90. In timestep 13, the first postcarnassial occlusion is

detected between the M1 praeparacrista and the distal m1 trigonid flank. With further upwards movement of the lower jaw this contact area shifts in cervical direction along the distal trigonid flank and expands on the mesial paracone flank. Eventually, this contact area shifts into the hypoflexid groove around timestep 86. An additional contact area at the distal trigonid flank is detected at timestep 34 with the M1 paracingulum, which occludes with the apex of the protoconid. This contact area also shifts in cervical direction with further tooth movement along the distal trigonid flank and remains active up until timestep 94. Initial occlusion between the M1 postparacrista and the m1 praehypocristid is detected at timestep 55. This area of contact increases in size with further tooth movement on the mesial hypoconid flank and the distal paracone flank, and eventually shifts into the hypoflexid. Occlusion between the hypoflexid and the paracone remains active up until the end of the power stroke and is functioning as a guiding contact for the direction of tooth movement. The point of centric occlusion, if it is reached in the dentition of *S. speothos*, can only be approximated, as there are no post carnassial crushing contacts, which are also functioning as a stopping mechanism. In the OFA analysis, tooth movement was stopped occlusion of the tip of the m2 main cusp with the distal protocone flank of the M1. It is possible that the in vivo power stroke movement is aborted at an earlier point. The extensive wear that was documented in the hypoflexid shows that the occlusion detected in the OFA analysis is very plausible up until timestep 94.
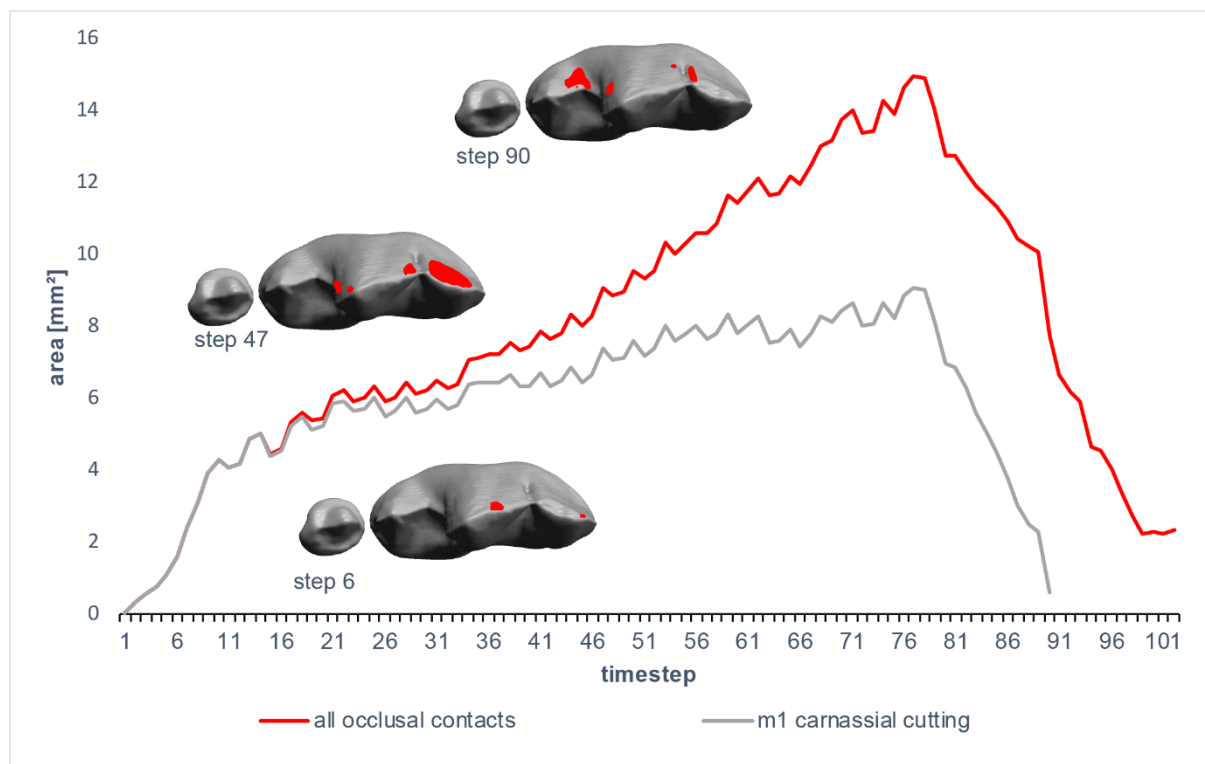
Fig. 43: Diagram of occlusal area size per timestep in the OFA analysis for *Speothos venaticus*. The initial occlusal contact occurs on two points on the carnassial blade (timestep 6). These contacts shift towards the center of the blade with further tooth movement and make up the largest amount of total occlusal contact up until timestep 79. In addition to carnassial cutting, occlusion between the M1 mesial paracone flank and paracingulum with the distal m1 trigonid flank occurs starting around timestep 15. These secondary cutting contacts steadily keep making up a greater portion of total occlusal contact as they shift from the apex of the protoconid in cervical direction towards the hypoflexid (timestep 47). Eventually, occlusion between the M1 paracone and the m1 hypoflexid occurs (timestep 90), whereas the size of the area of carnassial cutting abruptly decreases and in the last ten timesteps of the power stroke is absent. Rendering of μCT data.

4.1.11 OFA Analysis of *Felis silvestris*

The dentition of *Felis silvestris* is highly carnassialized, with the P4 protocone being reduced in size and the m1 talonid completely absent. For the OFA analysis, specimen ZFMK MAM 2018.0102 was chosen. The post-carnassial molars are also largely reduced, with only the vestigial M1 being present. The power-stroke comprises 212 timesteps (Fig. 44). It is dominated by the P4/m1 carnassial cutting function, which is performed from the initial occlusal contact to the last. The first contact is detected between the apex of the P4 paracone and the m1 paraconid. This area of occlusion expands in the distal direction towards the location of the carnassial notch with further tooth movement. In timestep 9, a second occlusal contact is detected between the apex of the P4 metacone and the apex of the m1 protoconid. It extends with further tooth movement in mesial direction towards the carnassial notch. The occlusal

contact areas between the carnassial blades keep wrapping around the carnassial notch up until timestep 155. Around timestep 159, carnassial cutting on the mesial part extends back from the carnassial notches in mesial direction, respectively towards the P4 protocone and the m1 paraconid. Integration of the P4 distal protocone flank occurs around timestep 195, when the contact area of carnassial cutting extends to the postprotocrista. Protocone cutting remains active up until the last timestep of the power-stroke. In addition to the carnassial cutting, an occlusal contact is detected between the mesial flank of the M1 and the distal flank of the m1 trigonid, at the apex of the protoconid. This contact is detected between the timesteps 41 and 99.
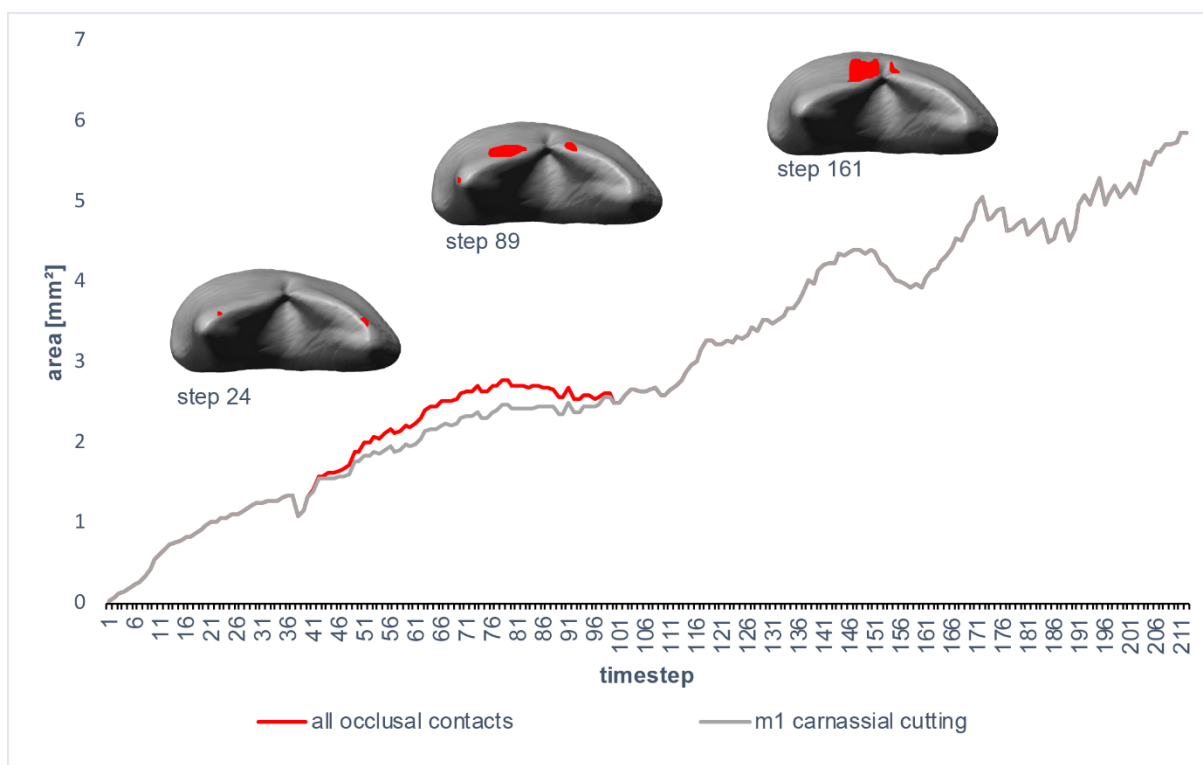
Fig. 44: Diagram of occlusal area size per timestep in the OFA analysis for *Felis silvestris*. The power stroke is dominated almost entirely by carnassial cutting. The two initial points of contact between the m1 and the P4 (timestep 24) keep shifting towards the center of the carnassial blade. Between timesteps 43 and 100, a vestigial contact between the mesial flank of the M1 and the distal m1 trigonid is detected (as seen in timestep 89), making up a small portion of total occlusal contacts. Throughout the power stroke, the area of carnassial contact attributed to a cutting function is nearly constantly increasing (see sizes of contact areas in timestep 161). Rendering of µCT data.

4.1.12 Analysis of carnassial cutting ratio

In taxa with multiple carnassial teeth (*D. viverrinus*, *T. cynocephalus*, *H. exiguus*), the OFA analysis showed that carnassial cutting is performed constantly from the initial occlusal contact up to the point of centric occlusion. The cutting function remains active due to the sequential occlusion of individual antagonistic carnassial blades from distal to mesial in all taxa. However,

there are differences in the amount of occlusal contacts related to carnassial cutting over time during the power stroke (Fig. 45). In *D. viverrinus*, exhibiting the least carnassialized adaptation, occlusion is associated with carnassial cutting for the first 10% of the power stroke up until centric occlusion, performed by the most distal carnassial blades (m4/M3). With further tooth movement, non-carnassial occlusal contacts related to the secondary cutting function of the paracone and the metacone begin to make up around 30% of the total occlusal contact. The carnassial cutting between the m3/M2 and m2/M1 is performed with further tooth movement. Despite that, the amount of carnassial occlusal contact related to the total occlusal contact keeps dropping up until the point of centric occlusion when phase I ends, as more "secondary" cutting occlusal contacts as well as crushing contacts of the protocones entering the talonid basins occur. At the end of phase I, the amount of carnassial occlusion makes up less than 10% of total occlusion. In phase II of the power stroke, no carnassial occlusal contact is detected, as the jaw is opening. In contrast to this, carnassial cutting remains a greater portion of the total occlusal contact throughout the power stroke of *T. cynocephalus*. Although for a short period, the portion of carnassial cutting remains slightly greater in *D. viverrinus*, the amount of "secondary" cutting contacts in *T. cynocephalus* remains smaller in*,* resulting in a higher and steadier portion of carnassial occlusal contacts throughout the power stroke. After the M3 and M2 paracones and metacones occlude with the mesial and distal talonid flanks, the amount of carnassial occlusal contact steadily increases from around 60% to 100%. This can be explained as talonid basins with the associated occlusion of the protocone are not present in *T. cynocephalus*. The last "secondary" cutting contact is performed when the m4 distal trigonid flank is moved along the M4 paracone, which eventually occludes along the hypoflexid groove. A drop in carnassial occlusion at the end of the power stroke in *T. cynocephalus* occurs as the protocone of the M4 occludes with the m4 hypoconid, preventing further tooth movement. The power stroke of *H. exiguus* is dominated by carnassial occlusion, which makes up 100% of the total occlusal contacts for over 90% of the power stroke duration. Occlusion of the mesial M1 and M2 protocone flanks with the respective antagonistic lower distal trigonid flanks can be interpreted as a "secondary" contact not related to carnassial cutting. Thus, the amount of carnassial occlusion drops at the end of the power stroke of *H. exiguus*, though still remains greater than 90%.

Fig. 45: Diagram of the ratio of carnassial cutting, as percentage of the area of total occlusal contact, plotted against the duration of the power stroke, as percentage from initial contact to centric occlusion. The percentage of occlusal carnassial cutting area in the taxon with basal carnassials (*Dasyurus viverrinus*) drops earlier in the duration of the power stroke in comparison to the taxon with more derived carnassials (*Thylacinus cynocephalus*), where the percentage is rising again as the point of centric occlusion is approached. In the taxon with the most derived carnassials (*Hyaenodon exiguus*), the percentage of occlusal carnassial cutting area stays at 100% for almost the entire duration of the power stroke.

The power stroke of carnivoran taxa, where only one carnassial per tooth row is present, generally shows an occlusal shift from the initial contact to the point of centric occlusion (Fig. 46). As seen in *V. tangalunga*, *S. speothos,* and *F. silvestris*, initial contact occurs between the P4 and m1 canrassial blades. This short period of pure carnassial cutting is then followed by occlusion of the mesial M1 paracone flank with the distal m1 trigonid flank. In *V. tangalunga,* this secondary cutting occurs at around 4% of power stroke duration, whereas it occurs a bit later in *S. venaticus,* at about 9%. In *F. silvestris*, this contact occurs at around 20% of power stroke duration. As the M1 in *F. silvestris* is drastically reduced in size, the occlusal contact

with the distal m1 trigonid blade is only maintained for a comparatively short period. The amount of carnassial contact drops to around 85% of total occlusal contact in *F. silvestris*, at around 35% of power stroke duration, and subsequently keeps increasing again to 100% at 47% of power stroke duration. From this point on, the power stroke in *F. silvestris* is a pure cutting function performed by the P4 and m1 carnassial blades. This differs from the power stroke in *V. tangalunga* and *S. venaticus*, where the post-carnassial dentition is not as reduced as in *F. silvestris*. The amount of carnassial occlusion as part of total occlusion is steadily decreasing with progressing tooth movement in both taxa, resulting from occlusion of the mesial paracone flank as well as the paracingulum of the M1 with the distal m1 trigonid flank. Eventually, the amount of carnassial occlusion drops significantly in *V. tangalunga* at around 60% of power stroke duration and in *S. venaticus* at around 80 % of power stroke duration. This marks the point in the power stroke, where occlusion with the m1 talonid occurs. In *V. tangalunga*, occlusion of the M1 distal paracone flank and the mesial metacone flank with the buccal m1 talonid flank makes up an increasing proportion of total occlusal contact. This differs from the power stroke of *S. venaticus*, where no occlusal contact between the M1 metacone and the m1 talonid occurs. At the end of the power stroke of *V. tangalunga* and *S. venaticus*, between 70% and 80% of power stroke duration, carnassial cutting does no longer occur. In *V. tangalunga*, the remaining occlusal contacts up to the point of centric occlusion occur in the m1 talonid basin. As the talonid in *S. venaticus* is reduced to a unicuspid trenchant heel, a basin structure with the associated occlusion is missing. However, occlusion between the M1 mesial paracone flank and the distal m1 trigonid as well as the distal M1 paracone flank and the mesial talonid flank fuse along the hypoflexid groove and are maintained up to the hypothetical point of centric occlusion.
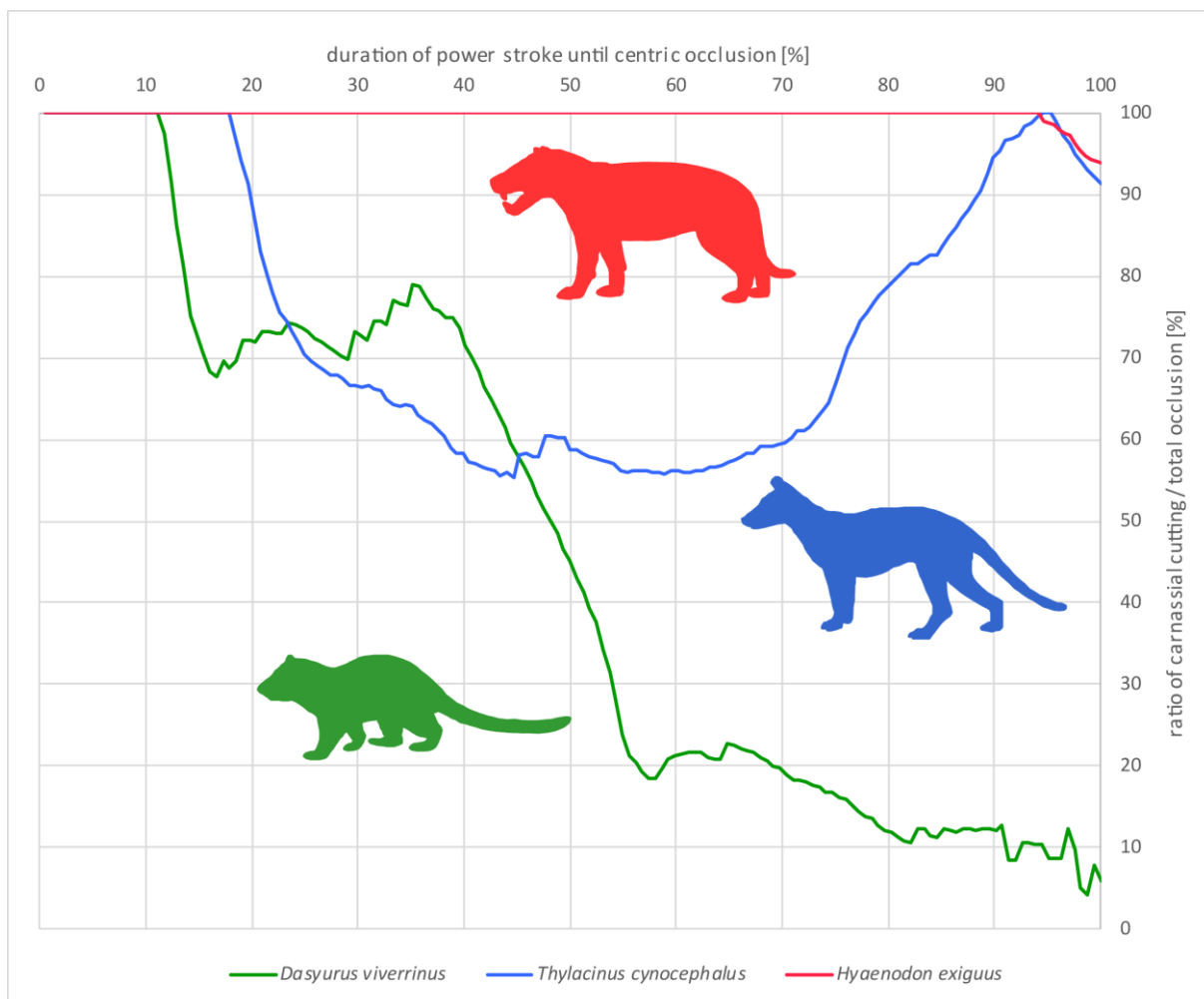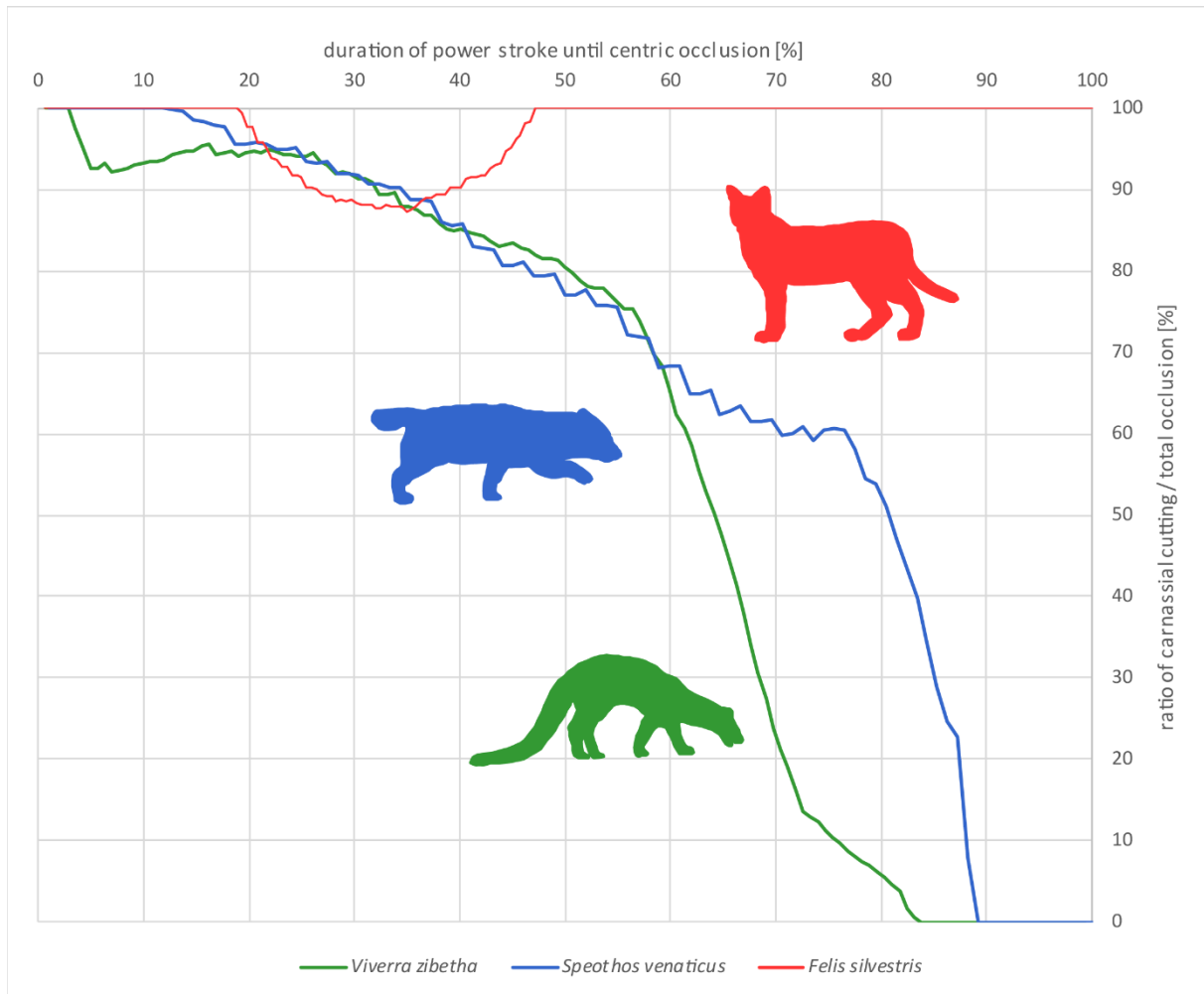
Fig. 46: Diagram of the ratio of carnassial cutting, as percentage of the area of total occlusal contact, plotted against the duration of the power stroke, as percentage from initial contact to centric occlusion. The percentage of occlusal carnassial cutting area in the taxon with basal carnassials and functional post carnassials which contribute to the crushing function (*Viverra tangalunga*) drops earlier in the duration of the power stroke in comparison to the taxon with more derived carnassials (*Speothos speothos*), where the post carnassial teeth are more reduced and mainly used for hypoflexid occlusion. In the taxon with the most derived carnassials (*Felis silvestris*), the percentage of occlusal carnassial cutting area stays virtually at 100% for most of the power stroke, with exception of a short period where the vestigial M1 is occluding with the m1.

4.2 Crown curvature in carnassial teeth

4.2.1 Distribution of ariaDNE values

Section 4.2.1 has been modified and published in: Lang, A. J., Engler, T., & Martin, T. (2021). Dental topographic and three-dimensional geometric morphometric analysis of carnassialization in different clades of carnivorous mammals (Dasyuromorphia, Carnivora, Hyaenodonta). *Journal of Morphology*, 283(1), 91 – 108.

The DTA analysis included 109 individual teeth belonging to 71 specimens (Tab. 1). The calculated ariaDNE values show a shift between the distribution of the basal and the derived groups (Fig. 47). This shift indicates that relatively high ariaDNE values are present in basal carnassials with all cusps present and relatively low ariaDNE values in derived carnassials with at least one cusp reduced. Carnassials with different conditions of metaconid and talonid reduction, representing the morphological changes associated with increasing carnassialization, show a similar pattern of reduction of crown curvature values in all three taxonomic orders (Fig. 48). Within Carnivora, the highest curvature values are found among genera with little specialized teeth (*Civettictis*, *Ichneumia*, *Viverra*, *Vulpes*), while genera with more specialized teeth with a functional but reduced talonid (*Canis*, *Dinictis*, *Lycaon*, *Nimravus*, *Mustela*, *Speothos*) show lower values; the lowest are present in genera where the talonid is non-functional or where the talonid and the metaconid are absent (*Crocuta*, *Cryptoprocta*, *Felis*, *Neofelis*, *Otocolobus*, *Panthera*). Among dasyuromorphs, the highest values are present in the basal carnassials of the various species of *Dasyurus*, while lower curvature values are present in the derived carnassials of *Sarcophilus* and *Thylacinus*. In Hyaenodonta, the highest curvature values are present in the basal carnassials of *Proviverra*, whereas lower values are present in the derived carnassials of *Hyaenodon*, *Oxyaenoides* and *Pterodon*.

Fig. 47: Distribution of ariaDNE values shown as a density estimation for "basal" and "derived" carnassial teeth. Solid lines indicate group means. This figure is published in Lang et al. (2021).

Fig. 48: Distribution of ariaDNE values in different groups of carnassial functional morphotypes. Carnivoran functional morphotypes: (A) all talonid cusps and metaconid present (*Ichneumia albicauda, Civettictis civetta, Viverra* spp., *Vulpes* spp.); (B) metaconid present, at least one talonid cusp reduced (*Canis lupus*, *Dinictis* sp., *Lycaon pictus, Mustela* spp., *Nimravus* sp., *Speothos venaticus*); (C) metaconid absent, talonid present but vestigial (*Crocuta crocuta*, *Cryptoprocta ferox*); (D) metaconid and talonid absent (*Felis silvestris*, *Neofelis nebulosa*, *Otocolobus manul*, *Panthera* spp.). Dasyuromorph functional morphotypes: (E) all talonid cusps and metaconid present (*Dasyurus* spp.); (F) metaconid present, at least one talonid cusp reduced (*Sarcophilus harrisii*); (G) metaconid absent, at least one talonid cusp reduced (*Thylacinus cynocephalus*). Hyaenodont functional morphotypes: (H) all talonid cusps and metaconid present (*Proviverra typica*); (I) metaconid absent, at least one talonid cusp reduced (*Hyaenodon* spp., *Oxyaenoides bicuspidens*, *Pterodon dasyuroides*). Median and interquartile range are drawn for each value distribution except for *Proviverra* (n = 1 per tooth). This figure is published in Lang et al. (2021).
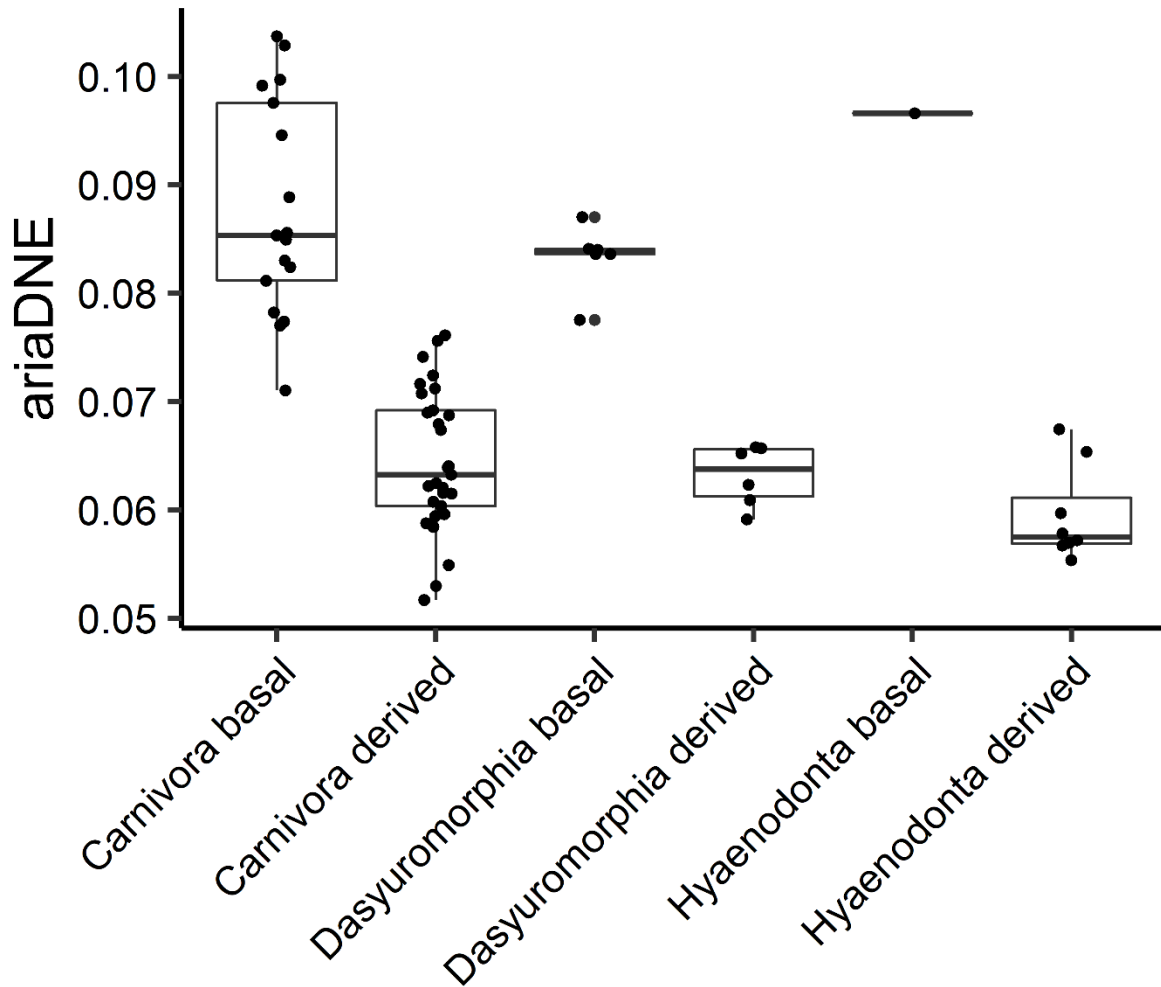
Fig. 49: Boxplot of ariaDNE values of basal and derived principal carnassials within the three major clades (Carnivora, Dasyuromorphia, Hyaenodonta).

The distribution of local ariaDNE values shows differences between the basal and derived carnassial morphotypes (Fig. 49). In carnassials with a basal morphology, where all talonid cusps and the metaconid are present, high curvature values are widely spread over the surface of the crown relief (Figs. 50, 51, 52). High ariaDNE values are found around the tips of trigonid and talonid cusps as well as crown areas that are concavely or convexly curved, such as the mesial, distal and lingual edges of the trigonid (e.g. *Ichneumia*, *Dasyurus*, *Proviverra*). In the basal morphotype, low curvature values are restricted to relatively small areas on flat surfaces like the mesial and distal trigonid and talonid blades, as well as within the talonid and trigonid basins. Compared to the derived morphotype, areas of low curvature appear more punctiform and values of extreme low curvature are rare. In contrast to this, areas of low curvature values are more widespread on carnassials with a derived morphology (e.g., *Felis*, *Thylacinus*, *Hyaenodon*). The size reduction of talonid cusps and the metaconid is reflected by smaller areas with high curvature values around the tips of those cusps. Areas with low curvature values appear more widespread, especially on the lingual and buccal flanks of the trigonid and

talonid. As the metaconid is reduced, the lingual and buccal flanks of the trigonid appear more continuous, which is reflected by a reduction of areas with high curvature. Likewise, carnassials with a reduced talonid have smoother lingual and buccal talonid flanks, which additionally reduces areas of high curvature. Relative to the basal morphotype, areas with low ariaDNE values are more abundant and extreme low curvature values are more common. The distinction of morphotypes via local ariaDNE values is not clear-cut in every case. For example, even though the molars of *Canis* exhibit a derived carnassial morphology, low curvature values are not as widely spread as in the carnassials of *Speothos* or *Mustela* (Fig. 50). Also, while the derived carnassials of *Pterodon* show more abundant areas with low ariaDNE values in comparison to *Proviverra*, they are not as widespread as on the carnassials of *Hyaenodon* (Fig. 52). There is overlap in total ariaDNE values of some basal and derived carnassials. Within the tooth rows of taxa with multiple carnassials, the areas with low ariaDNE values are increasing in size on the distal carnassials, especially on the principal carnassials. Thus, the distribution of local ariaDNE in the basal PCPs of *Dasyurus* or *Proviverra* are more similar to the derived MCPs of *Sarcophilus* and *Pterodon* than any other tooth positions of these taxa compared to one another.
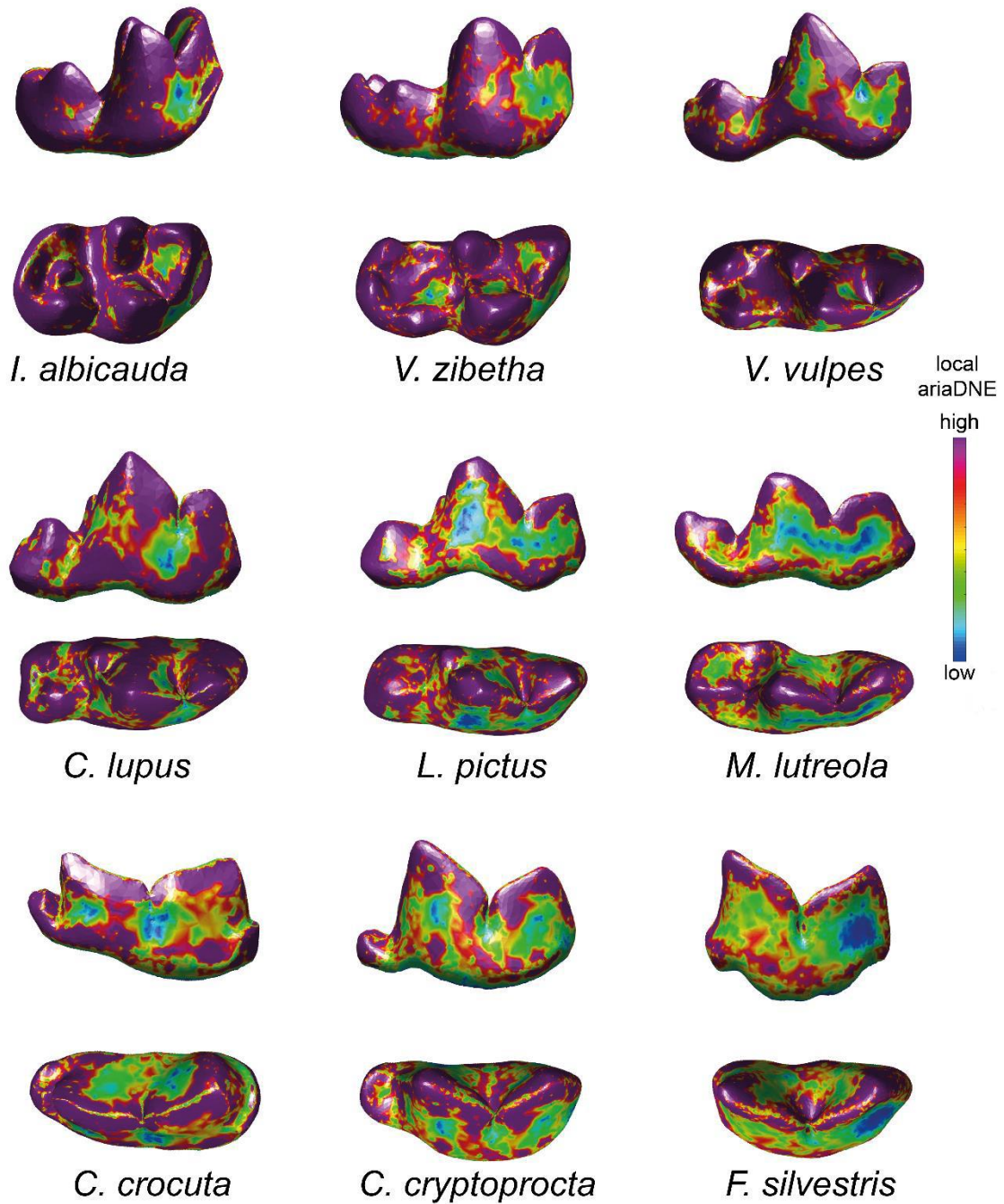
Fig. 50: The distribution of local ariaDNE values shown on the surface of carnivoran carnassials. Note the more widely distributed areas of high ariaDNE values, shown in red and violet colour, in basal carnassials (*Ichneumia. albicauda*, *Viverra zibetha*, *Vulpes vulpes*) in comparison to the more widely distributed low ariaDNE values, shown in green and blue colours, in more derived carnassials (*Canis lupus*, *Lycaon. pictus*, *Mustela lutreola*, *Crocuta crocuta*, *Crocuta cryptoprocta*, *Felis silvestris*). Rendering of µCT data.
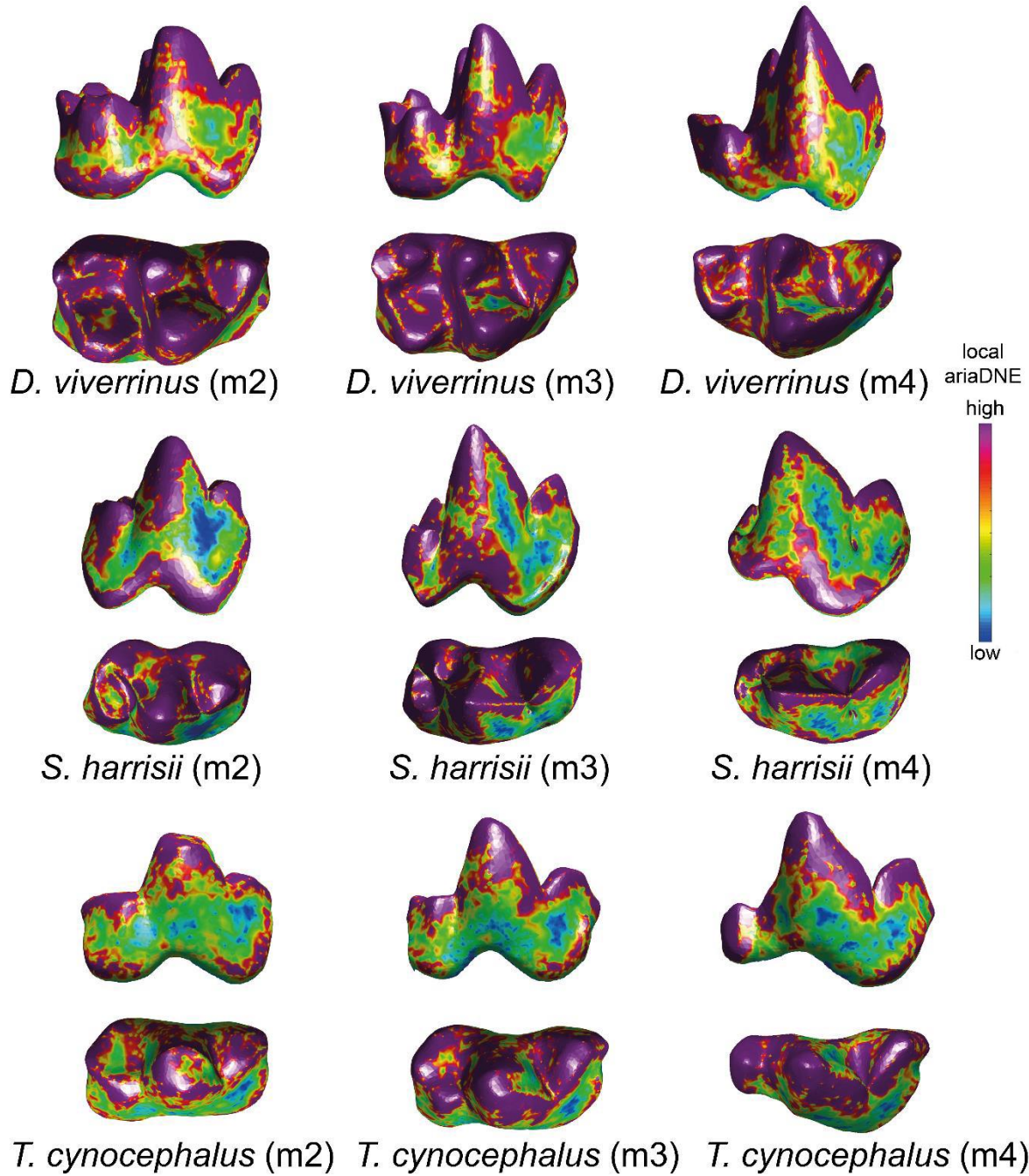
Fig. 51: The distribution of local ariaDNE values shown on the surface of carnivoran carnassials. Note the more widely distributed areas of high ariaDNE values, shown in red and violet colour, in basal carnassials (m2, m3 and m4 of *Dasyurus viverrinus*) in comparison to the more widely distributed low ariaDNE values, shown in green and blue colours, in more derived carnassials (m2, m3 and m4 of *Sarcophilus harrisii* and *Thylacinus cynocephalus*). Rendering of µCT data.
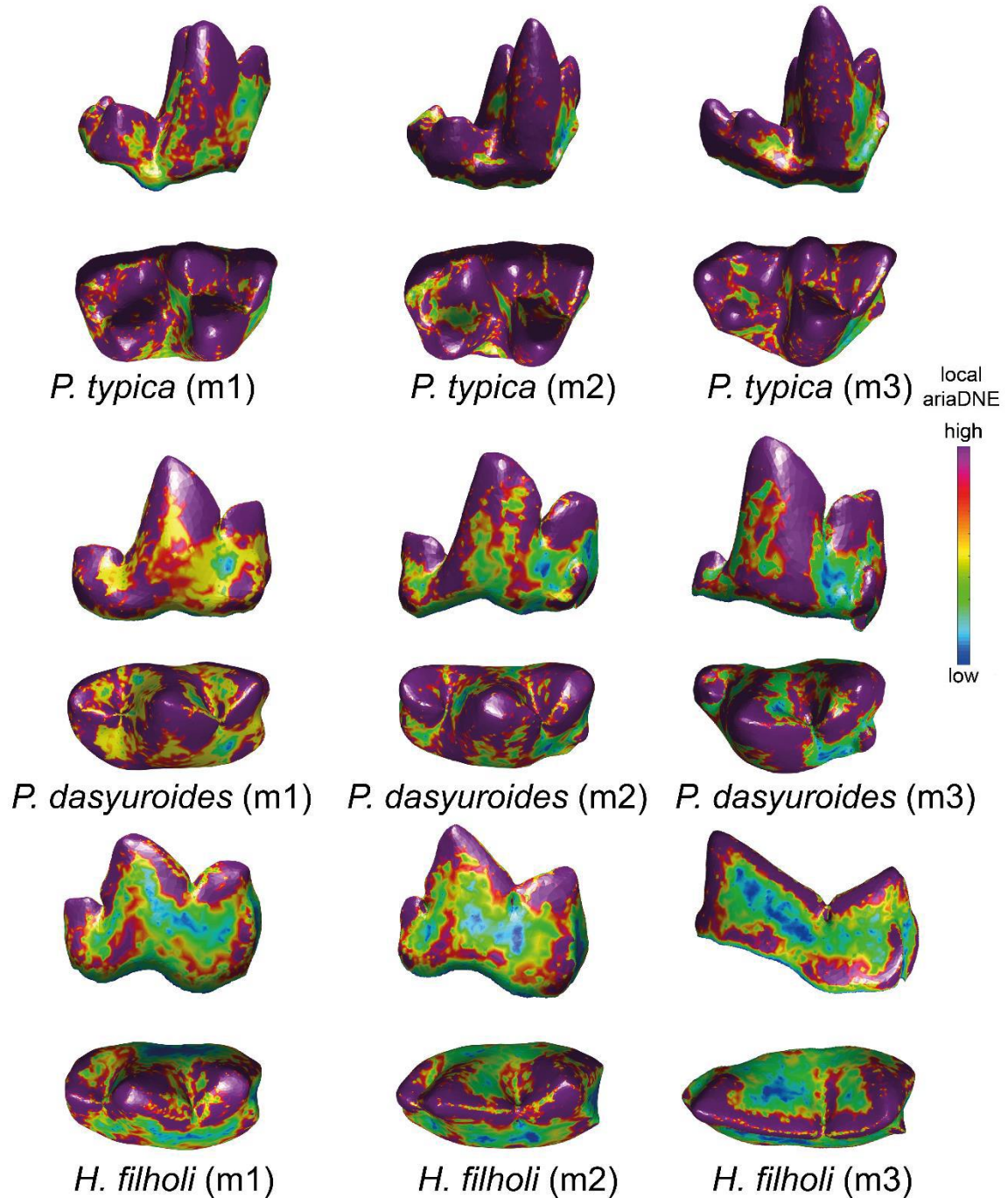
Fig. 52: The distribution of local ariaDNE values shown on the surface of carnivoran carnassials. Note the more widely distributed areas of high ariaDNE values, shown in red and violet colour, in basal carnassials (m1, m2 and m3 of *Proviverra typica*) in comparison to the more widely distributed low ariaDNE values, shown in green and blue colours, in more derived carnassials (m1, m2 and m3 of *Pterodon dasyuroides* and *Hyaenodon filholi*). Rendering of μCT data.

4.2.2 ANOVA

Comparing the calculated values of those groups which are interpreted to be functionally analogous, there is a clear pattern of high ariaDNE values in the basal groups compared to low values in the derived groups (Fig. 49). ANOVA for ariaDNE was significant ($p < 0.05$), thus rejecting group equality of the calculated values of curvature. A post-hoc pairwise group comparison using Tukey's honest-significant-difference-test rejected group equality for all possible combinations of a derived and a basal group for ariaDNE as a quantifier, while all combinations of similar functional groups were not significantly different. For the ariaDNE values of the derived Hyaenodonta, the Shapiro-Wilk-Test rejected group normality. Further, the Levene's test rejected homoscedasticity. Since this can be problematic for a one-way ANOVA, an additional Welch's heteroscedastic F omnibus test was applied to the ariaDNE values, as this test is relatively robust against non-normality (Keselman *et al.*, 2008). Using this test, group equality for ariaDNE values was rejected. As a second post-hoc pairwise group comparison, the Games-Howell test, which also appears robust against non-normality, was used (Day & Quinn, 1989). The results for the pairwise comparisons of the ariaDNE groups confirmed the results of the first post-hoc test, rejecting equality for all combinations of different functional but not for same functional groups.

4.2.3 LDA and predicted group assignment

The basal and derived groups of ariaDNE values of principal carnassials show a minor overlap in value distribution and the Shapiro-Wilk-Test indicates no significant deviation from a normal distribution for either of the groups. Using the calculated decision boundary of the complete dataset in a predict function, 65 values are correctly assigned to the a priori defined groups. One basal principal carnassial is incorrectly assigned to the derived group. Grouping accuracy estimated with cross validation did not differ from the results for the complete original data. Of the correctly assigned teeth, 58 (89%) are classified with a probability of >75%. Using the calculated decision boundary to classify the basal hyaenodont principal carnassial (m3 of *Proviverra typica*), it is assigned to the basal group with >99% probability. Bootstrap samples with leave-one-out cross validation, repeated 1000 times, returned estimations for correct classification accuracy between 88.2% and 100%, with a mean accuracy of 96.4%.

A second LDA was used on the complete raw dataset of lower carnassials except for the basal hyaenodont carnassials, disregarding both phylogeny and tooth position. No deviation from a normal distribution for both resulting groups of ariaDNE values is indicated by the Shapiro-Wilk-Test. The proportion of overlapping values of the resulting group distributions in comparison to the principal carnassial groups does not change significantly. Predicted classification based on the calculated decision boundary assigns 102 (96%) values to the a priori predicted groups. Two basal and two derived teeth are assigned to the incorrect group.

96 (94%) of the correctly classified teeth were classified with a probability of >75% with a cross validated LDA. The predicted group affinity for the three basal hyaenodont carnassials (m1, m2 and m3 of *Proviverra typica*) is the basal group with a probability of >99% for each tooth. Bootstrap cross validation repeated 1000 times estimated an accuracy for correct classification between 85.4% and 100%, with a mean accuracy of 95.7%.

4.3 Geometric morphometric analysis

4.3.1 Landmark based morphospace analysis

Section 4.3.1 has been modified and published in: Lang, A. J., Engler, T., & Martin, T. (2021). Dental topographic and three-dimensional geometric morphometric analysis of carnassialization in different clades of carnivorous mammals (Dasyuromorphia, Carnivora, Hyaenodonta). *Journal of Morphology*, 283(1), 91 – 108.

The landmark-based GMA analysis was conducted on 106 individual teeth belonging to 68 individuals (Tab. 1). The first five PCs identified by the GMA explain more than 75% of total variation, with PC1 accounting for 41.4% and PC2 accounting for 13.9% (Fig. 53). In the morphospace of carnassial molars, basal molars are found mostly in the positive morphospace along PC1 and derived carnassials are found mostly in the negative morphospace (Fig. 54). This shift is also present when taking only basal and derived carnassials within the Caniformia and Feliformia into account, or when comparing the scores of the basal carnassials of dasyuromorphs and hyaenodonts with derived carnassials of the respective groups (Fig. 55). Further, a procrustes ANOVA with 1000 iterations for significance testing of the aligned shape data indicates a significant difference between basal and derived carnassials (p = 0.001).

The landmark shift along PC1 from positive to negative describes a distal elongation of the carnassial blade with a distally displaced carnassial notch and protoconid, a reduction in size of the talonid basin and a change from a cervix line with equally pronounced mesial and distal flexures to an enlarged mesial flexure and a reduced distal flexure (Fig. 54).

Along the axis of PC2, unspecialized carnivorans with basal carnassials (*Civettictis*, *Ichneumia*, *Viverra*, *Vulpes*) and specialized caniformians with derived carnassials (*Canis*, *Lycaon*, *Mustela*, *Speothos*) are largely separated from the rest of the dataset (Fig. 53). PC2 describes the shape change from a carnassial with a relatively high cutting blade and an approximately round crown base (marked by the cervix line) in the more positive morphospace to a relatively low cutting blade and a crown base displaying a bucco-lingual compression and mesio-distal elongation in the more negative morphospace (Fig. 54).

Allometry was tested by the regression of shape versus centroid size and is significant (p = 0.01). However, the coefficient of determination is low (R^2 = 0.137). The smallest teeth are the basal carnassials of *Dasyurus* and *Proviverra*, whereas the largest ones are large caniforms

(*Canis*) and feliforms (*Crocuta* and *Panthera*), with frequent of overlap between taxa and teeth of different carnassialization types in between.
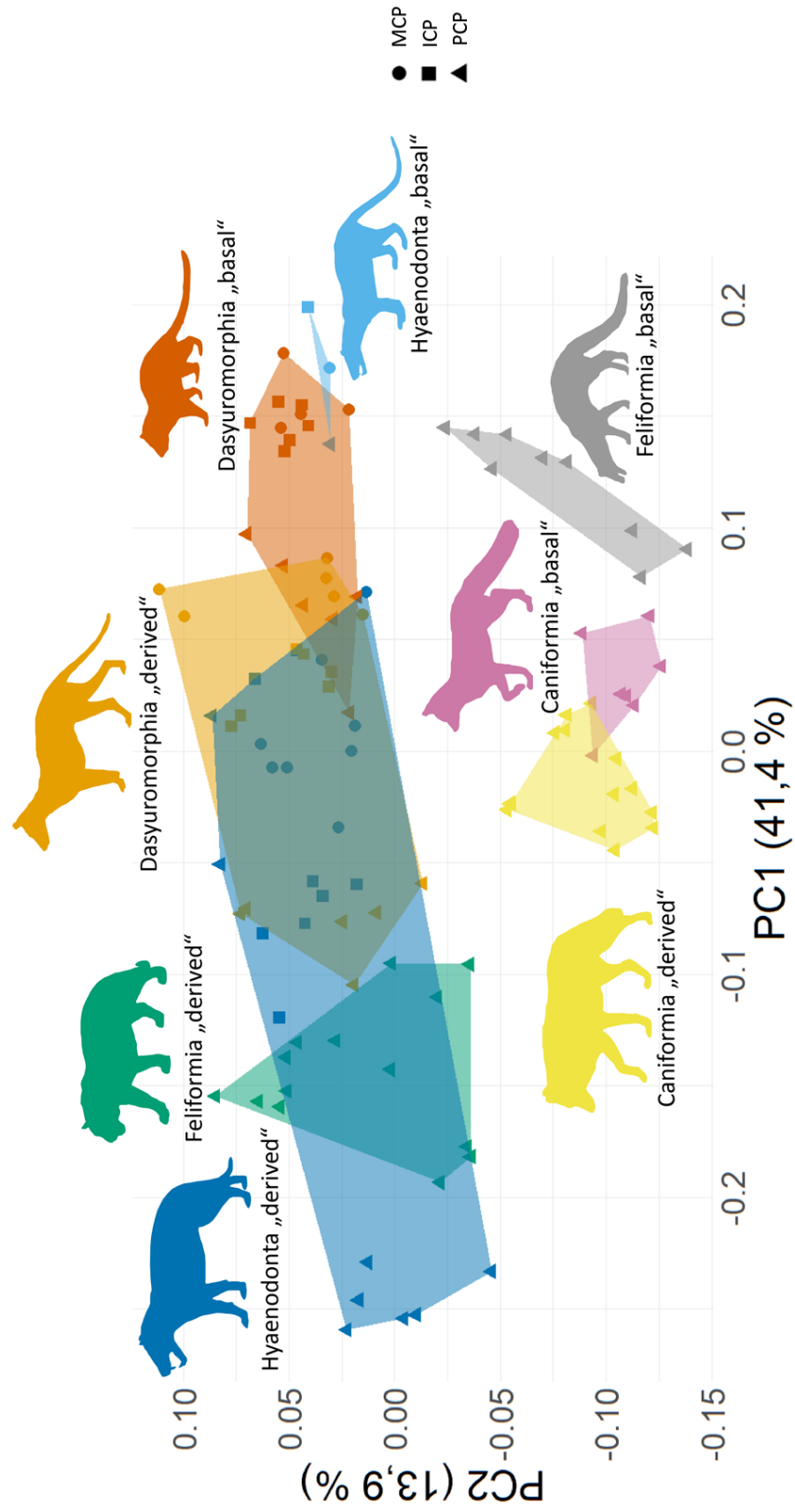
Fig. 53: Bivariate plot of principal components 1 and 2 of the Procrustes aligned shape data, showing the distribution of "basal" and "derived" carnassials within taxonomic orders. This figure is published in Lang et al. (2021).
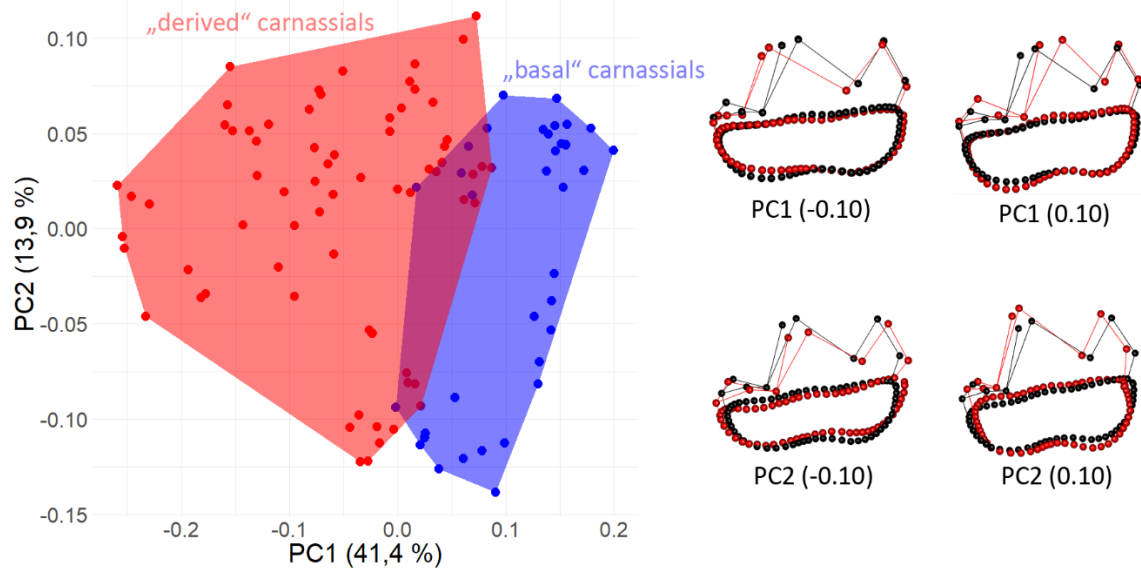
Fig. 54: Bivariate plot of principal components 1 and 2 of the Procrustes aligned shape data, showing the distribution of "basal" and "derived" carnassials. Deformed shapes along the principal components (red) are shown in comparison to the consensus shape (black). This figure is published in Lang et al. (2021).

The distribution of values for taxa with multiple carnassials was analyzed on the genus level (Fig. 55). In all genera with multiple carnassial teeth, the PCPs are the teeth with the lowest PC1 scores. In four genera with derived carnassials (*Hyaenodon*, *Oxyaenoides*, *Sarcophilus*, *Thylacinus*), there is a successive shift from high to low PC1 scores from the mesial to the more distal carnassial positions. This successive value shift is not present in the genera with basal carnassials (*Dasyurus* and *Proviverra*) and one genus with derived carnassials (*Pterodon*).
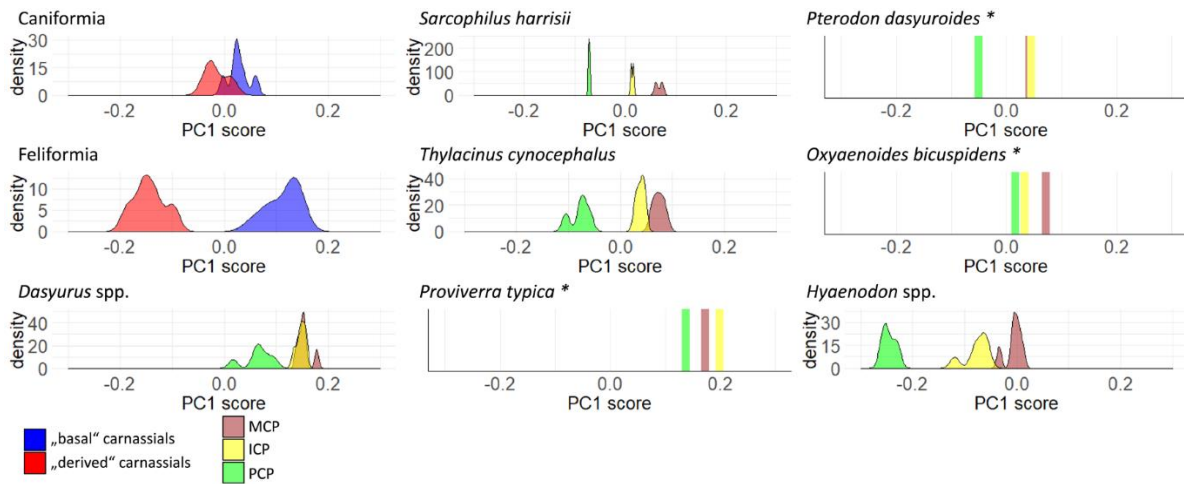
Fig. 55: Distribution of scores for different types of carnassials along the first principal component, shown as density estimations. Asterisks indicate taxa for which only the distributions of single values are shown. This figure is published in Lang et al. (2021).

4.3.2 Carnassial blade angle

The calculated carnassial blade angle in carnivoran, dasyuromorph and hyaenodont principal carnassials, based on the landmarks used in the GMA, ranges between a maximum of 50.1° in *Ichneumia albicauda* and a minimum of <0.1° in *Felis silvestris* and *Hyaenodon exiguus*.

In the rose diagrams, petals with a carnassial blade angle higher than 10° are marked green and the petal below 10°, indicating an exact buccal shearing blade orientation, is marked red (Fig. 56). Overall, the carnassial blade orientation is more transversely aligned in basal carnassials, with a higher tendency to be facing in buccal direction. In contrast to this, the carnassial blade in derived carnassials is aligned with a higher tendency in mesio-distal direction. A deviation from this general pattern can be observed in basal carnivoran carnassials, where mesio-distal blade orientations are also occurring. These were calculated for the carnassials of *Vulpes lagopus* and *Vulpes vulpes*.
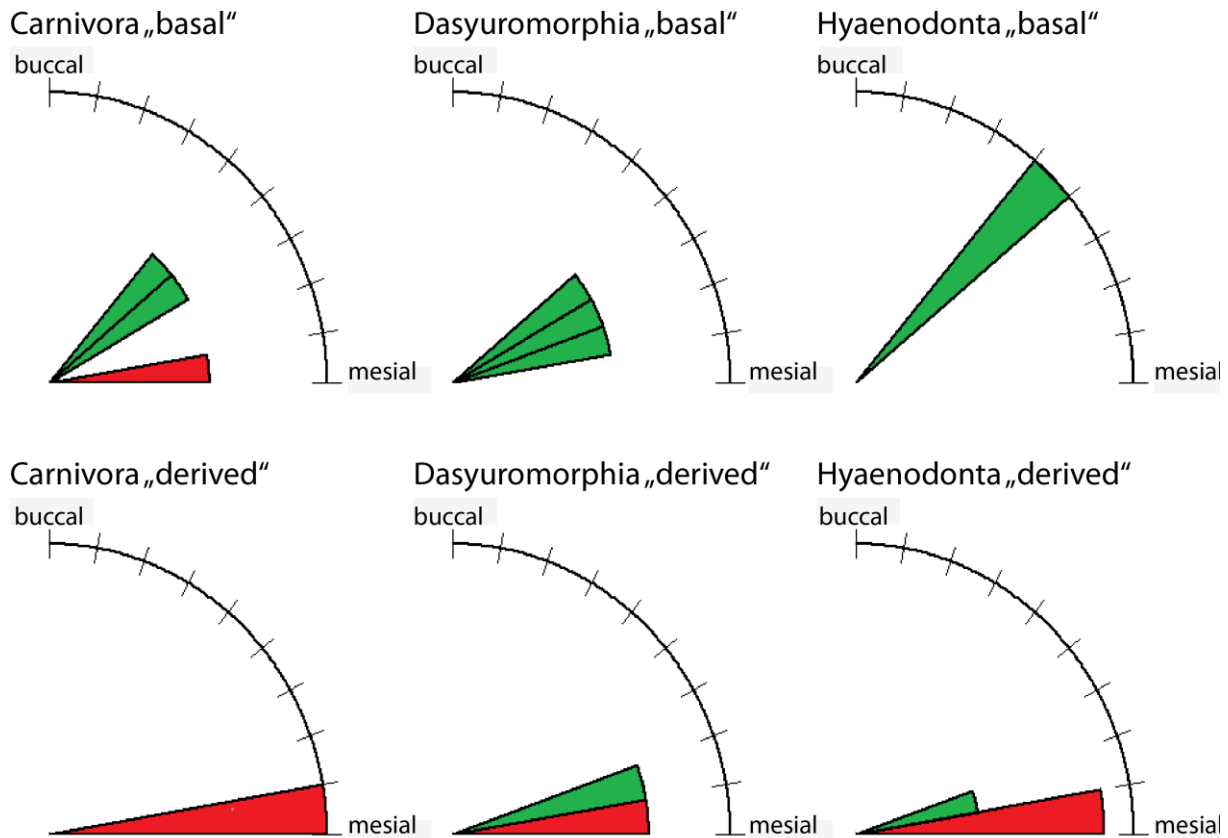
Fig. 56: Rose diagrams of the carnassial blade angle in basal and derived carnassials in the Carnivora, Dasyuromorphia and Hyaenodonta. Green: blade orientation >10°; red: blade orientation <10°.

4.3.3 Shape comparison by Cloud-to-Cloud distance

By cloud-to-cloud distance comparison of the individual carnassial tooth surfaces within the tooth row of taxa with multiple carnassials, local tendencies of surface differences are visualized on the tooth relief and the distances of individual points, grouped in 100 distance classes from 0 to maximum distance, are visualized in area charts. For each reference tooth, the same color scale is used to visualize local distances. Thus, the surface distances of two teeth compared to the same reference tooth are easier to compare. In CloudCompare, the distances are expressed in a unit based on the point coordinates that are stored in the original 3D surface models, which is in mm for the models used in this study. However, since the teeth were rescaled for the surface comparison, only the relative differences between distances rather than absolute distance is relevant for the interpretation.

In *Dasyurus viverrinus*, there is little difference between the surfaces of the m2 (specimen SMF 1480) and m3 (same specimen), using the m2 as a reference. The apices of cusps, especially of the protoconid, entoconid and hypoconulid show some minor local differences. Distance maxima are between 0.21 and 0.29. The comparison between the m2 and the m4 (same specimen) shows differences along the cervix line, within the trigonid and talonid basin and on the tip of the protoconid and of all talonid cusps. The whole lingual, distal and buccal talonid

margin shows high distance values, with the highest values occurring along the distolingual cervix line. Point distances exceed those of the m2/m3 comparison and stretch to a maximum of 1.05 (Fig. 57).

Using the m3 as a reference for the m2, the highest surface deviations are calculated at the tip of the protoconid and the metaconid, however the overall differences are rather low. The maximum calculated differences are between 0.29 and 0.4. The m4 compared to the m3 as a reference shows a surface deviation along the cervix line and minor deviations on the protoconid and the metaconid. A large area of deviation is present along the outer margin of the talonid and on all talonid cusps, with the highest values occurring at the distal and lingual edges of the talonid. The point distances stretch to a maximum of 0.89, much higher than in the m3/m2 comparison (Fig. 57).

Fig. 57: Cloud-to-cloud distance (dist.) of the lower carnassials of *Dasyurus viverrinus*, measured with the m2 as a reference respectively to the m3 and m4, and with the m3 as a reference respectively to the m2 and the m4. Rendering of µCT data.

The m2 of *Sarcophilus harrisii* (specimen ZMB_MAM_001733) compared to the m3 (same specimen) shows little surface deviations on the apical part of the crown (Fig. 58). Higher distances are found in proximity to the cervix line, all around the molar. The highest distances occur at the most cervical part of the cervix flexures on the buccal side of the crown. The maximum distance between points stretches to 2.05. Distances of the m2 compared to the m4 (same specimen) show more deviations on the apical part of the crown. Surface deviations occur at the tips of the protoconid and the paraconid and on the lingual side of the trigonid. Additional deviations occur around the cervix line and on the hypoconid. The highest deviations are found at in the most cervical part of the distal cervix flexure on the buccal side of the crown. Distances between points reach their maximum at 3.93.

The m2 compared to the m3 as a reference shows relatively low local distances at the tip of the protoconid, on the lingual side of the trigonid, on the hypoconid and on the lingual and bucco-mesial parts of the cervix line. The maximum distance between points is 1.25. Using the m3 as a reference for the m4, low distances are found on the lingual side of the trigonid, in the talonid basin and around the lingual, distal and buccal talonid margin. High distances occur at the distal flexure of the cervix line in the most cervical part on the buccal side of the crown. These high distances stretch to a maximum of 2.83. Overall, the calculated distances to the most distal molar are higher both in the m2/m4 and in the m3/m4 comparisons (Fig. 58).

Fig. 58: Cloud-to-cloud distance (dist.) of the lower carnassials of *Sarcophilus harrisii*, measured with the m2 as a reference respectively to the m3 and m4, and with the m3 as a reference respectively to the m2 and the m4. Rendering of µCT data.

In the tooth row of *Thylacinus cynocephalus*, the m3 (specimen ZMB_MAM_036877) compared to the m2 (same specimen) shows generally minor surface deviations. The tips of the protoconid and of the paraconid show slightly increased surface distances. The same is true for the tips of the hypoconid and hypoconulid, as well as the buccal side of the trigonid. Slightly higher distances occur along the mesial and distal part of the cervix line. Overall, the distances are relatively low and reach maximum values at 1.23. When compared to the m2 as a reference, moderate distances to the m4 (same specimen) occur at the lingual side of the trigonid, the paraconid and protoconid tips and along the mesial side of the cervix line. Additionally, moderate distances can be found on the hypoconid, in the talonid basin and around the buccal, distal and lingual margin of the talonid. High surface deviations are found on the mesial and distal part of the talonid basin, near the cervix line. Maximum distances between points reach to 3.32, which is higher than in the m2/m3 comparison (Fig. 59).

The m2 compared to the m3 as a reference results in overall minor surface deviations. Slightly increased areas of higher local surface distances are punctiformly distributed over the crown on the tips of the protoconid and the paraconid, the lingual side of the trigonid and on the talonid cusps (hypoconid, hypoconulid, entoconid). Additionally, slightly increased distances are found on the buccal flank of the talonid and on the bucco-distal part of the cervix line. The maximum distance is 0.8. When compared to the m3 as a reference, the distances to the m4 are distinctively higher. The tip of the protoconid shows a moderate deviation, as does the lingual trigonid flank. Further, an area of moderate surface deviation is found on the mesio-buccal part of the cervix line. Around the buccal, distal and lingual margin of the talonid, huge areas of moderate surface deviation occur. These stretch onto the tip of the entoconid and the hypoconid. High distance values occur bucco-distal part of the cervix line. The distances between points stretch to a maximum of 3.18, exceeding the maximum of the m3/m2 comparison. Thus, for both comparisons with the m2 and the m3 as a reference, the respective comparison with the m4 yielded the highest and most abundant surface distance values (Fig. 59).
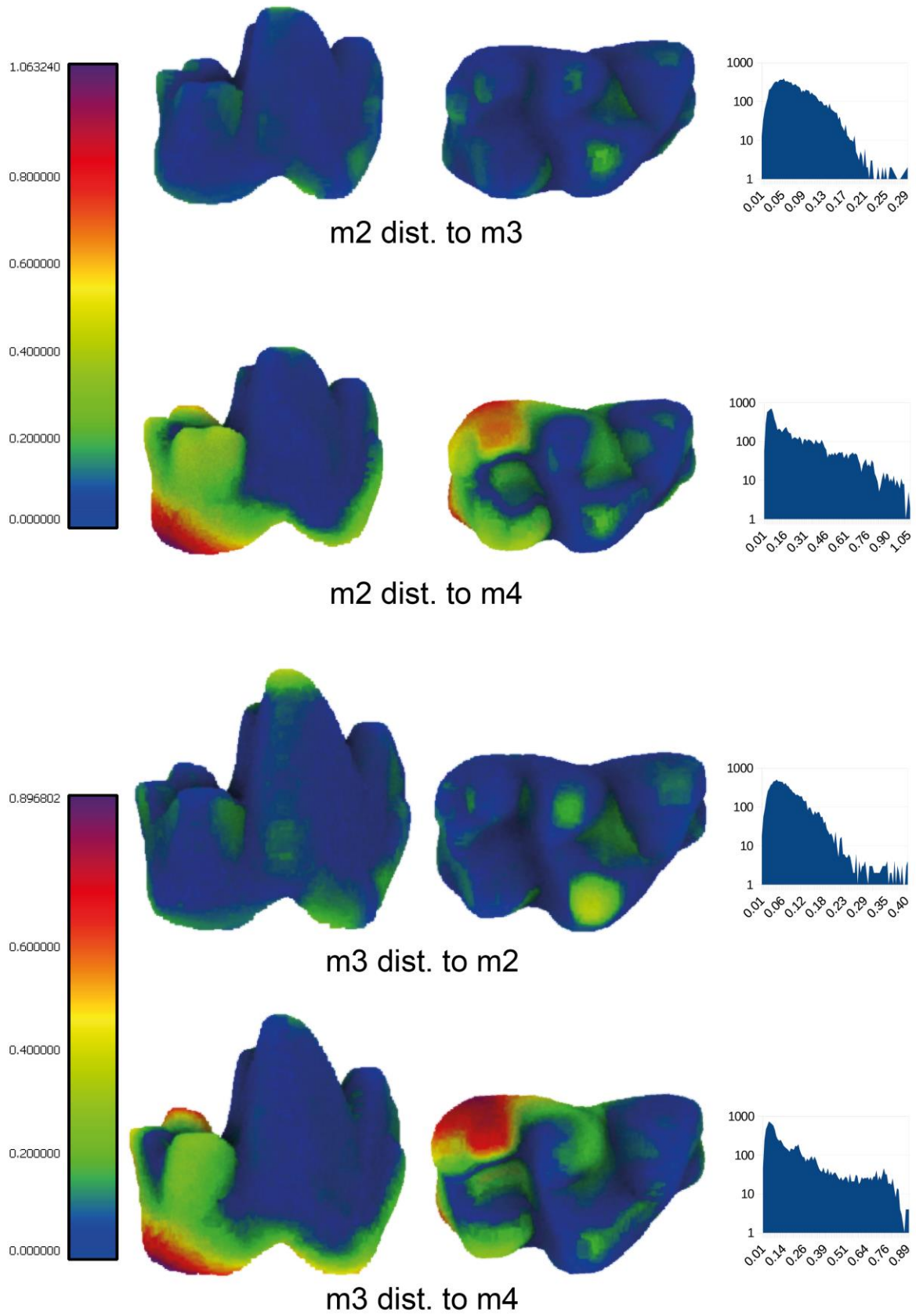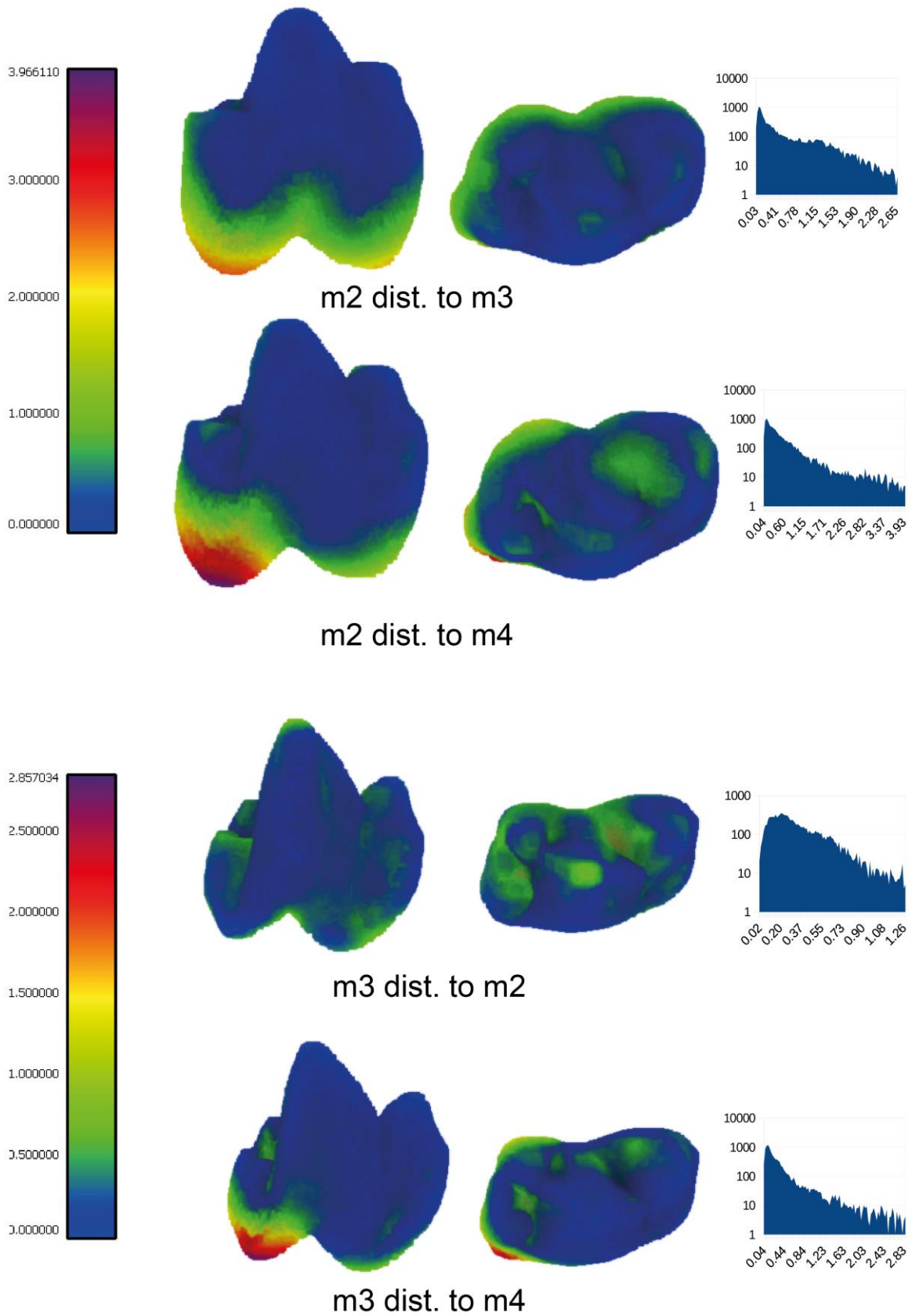
Fig. 59: Cloud-to-cloud distance (dist.) of the lower carnassials of *Thylacinus cynocephalus*, measured with the m2 as a reference respectively to the m3 and m4, and with the m3 as a reference respectively to the m2 and the m4. Rendering of µCT data.

The surface deviations of the m2 of *Proviverra typica* (specimen NMB En.130) compared to the m1 (specimen NMB En.176) as a reference are generally low to moderate. Slightly increased deviations are present on the paraconid, protoconid and metaconid tips, within the talonid basin and along the cervix line. Maximum distances between points are 0.38. The surface deviations of the m3 (specimen NMB En.179) compared to the m1 as a reference are higher. While areas with moderate distances are found on all of the trigonid and talonid cusps, high distances occur at the metaconid, within the talonid basin and around the lingual, distal and buccal margin of the talonid basin along the cervix line. The between point distances reach maximum values of 0.74. When compared to the m2 as a reference, low to moderate surface deviations to the m1 are calculated. Moderate distances are present along the paracristid, the tip of the protoconid and the tip of the paraconid. Additionally, moderate distances occur on the tip of the hypoconid and the hypoconulid as well as within the trigonid basin. The distances between points reach maximum values of 0.39. In contrast to this, the distanced between the m2 and the m3 show more abundant areas of moderate surface deviations and also some areas with high deviations. Moderate distances occur at the tips of the trigonid and talonid cusps and within the trigonid and talonid basins. Additonally, all around the margin of the talonid, moderate surface deviations are present with high deviations occurring on the buccal side of the talonid as well as on the lingual side, expanding onto the hypoconulid. The calculated distances between points reach maximum values of 0.69. The distances calculated when comparing the m3 with either the m1 or the m2 as a reference were thus respectively higher than those calculated comparing the m1 to the m2 (Fig. 60).

Fig. 60: Cloud-to-cloud distance (dist.) of the lower carnassials of *Proviverra typica*, measured with the m1 as a reference respectively to the m2 and m3, and with the m2 as a reference respectively to the m1 and the m3. Rendering of µCT data.

The m2 of *Pterodon dasyuroides* compared to the m1 (NMB Q.B.606) as a reference shows generally very low differences in surface distance. These areas of low deviation are present on the distal part of the talonid basin, the buccal margin of the cervix line and the lingual margin of the cervix line. The maximum distance between points is 1.48. In contrast to this, the comparison of the m3 to the m1 (NMB Q.C.413) shows areas of much higher surface deviations. While on the protoconid apex and on the lingual margin of the cervix line, moderate surface deviations are present, the surface differences are higher on the talonid. The calculated distances on the talonid increase from mesial to distal, with the highest distances occurring on the hypoconid and around the distal margin of the talonid. The highest values of distances between points are at 2.63. The m1 compared to the m2 as a reference shows again a low abundance of surface deviations, except for one small area at the most mesial tip of the cervix line, where the distance between surfaces is high. The maximum distance between points is 2.25. Compared to the m2 as a reference, the surface distance to the m3 is moderate to high. The areas of moderate surface deviation occur at the protoconid apex and on the talonid, encompassing the whole hypoconid. Around the distal margin of the talonid, the surface distance is significantly higher. The maximum calculated distance between points is 3.23 and thus exceeds the maximum distance of the m2/m1 comparison. Surface comparisons with the m3 yield higher distances than the comparisons between m1 and m2 (Fig. 61).
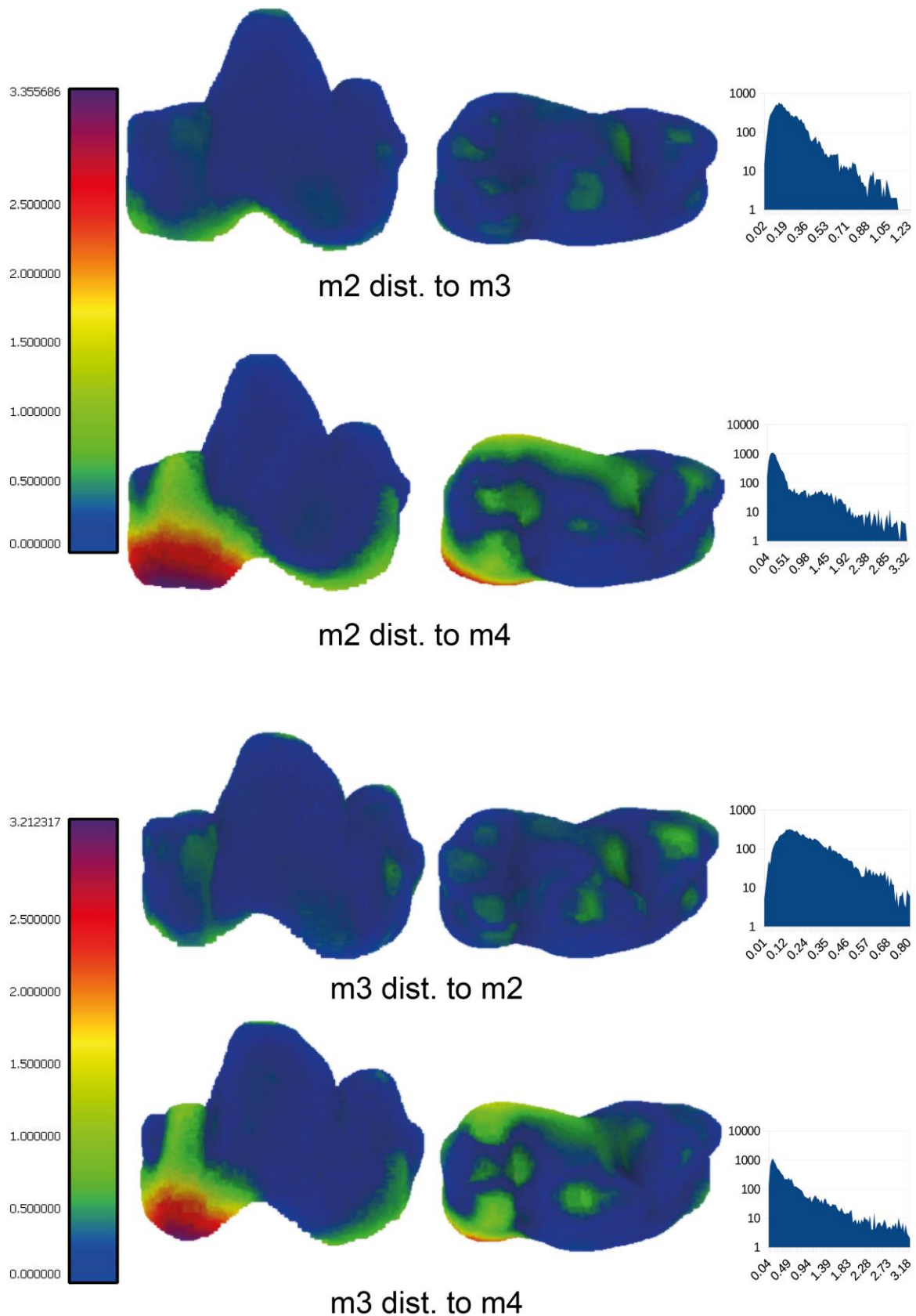
Fig. 61: Cloud-to-cloud distance (dist.) of the lower carnassials of *Pterodon dasyuroides*, measured with the m1 as a reference respectively to the m2 and m3, and with the m2 as a reference respectively to the m1 and the m3. Rendering of µCT data.

The m2 of *Oxyaenoides bicuspidens* (GMH XIV-2909-1954) compared to the m1 as a reference shows low surface deviations, with the highest distances occurring on the protoconid apex and the distal part of the talonid. Some punctiform areas of relatively increased distance are additionally found at the buccal side of the cervix line. The maximum calculated point to point distance is 1.18. The m3 compared to the m1 as a reference shows significantly higher surface deviations. Moderately high differences are found at the protoconid apex as well as the paraconid apex and around the cervix line. Very high deviations occur at the mesial and distal parts of the cervix line. On the talonid, the calculated distance increases from mesial to distal, with the highest distances on the distal talonid flank. The point to point distance extends to a maximum of 2.23. The m1 compared to the m2 as a reference results in generally low to moderate surface distances. Moderate differences occur at the mesial trigonid flank in the proximity of the cervix line as well as punctiformly on the lingual trigonid flank and the bucco-distal edge of the trigonid. Further, the distal margin of the talonid and tip of the hypoconid show moderate surface deviations. High surface deviations are found on the apex of the protoconid. The maximum point to point distance is 1.52. The m3 compared to the m2 as a reference shows almost no surface deviations on the trigonid. Moderate surface deviations occur all around the cervix line and increase to the bucco-mesial edge of the cervix line as well as the bucco-distal margin of the cervix line. Additionally, moderate surface deviations are found on the talonid, encompassing the hypoconid and increasing towards the cervix line. The maximum calculated point to point distance is 1.78. The highest surface distances are calculated for comparisons to the m3 in contrast to comparisons with the mesial tooth positions (Fig. 62).
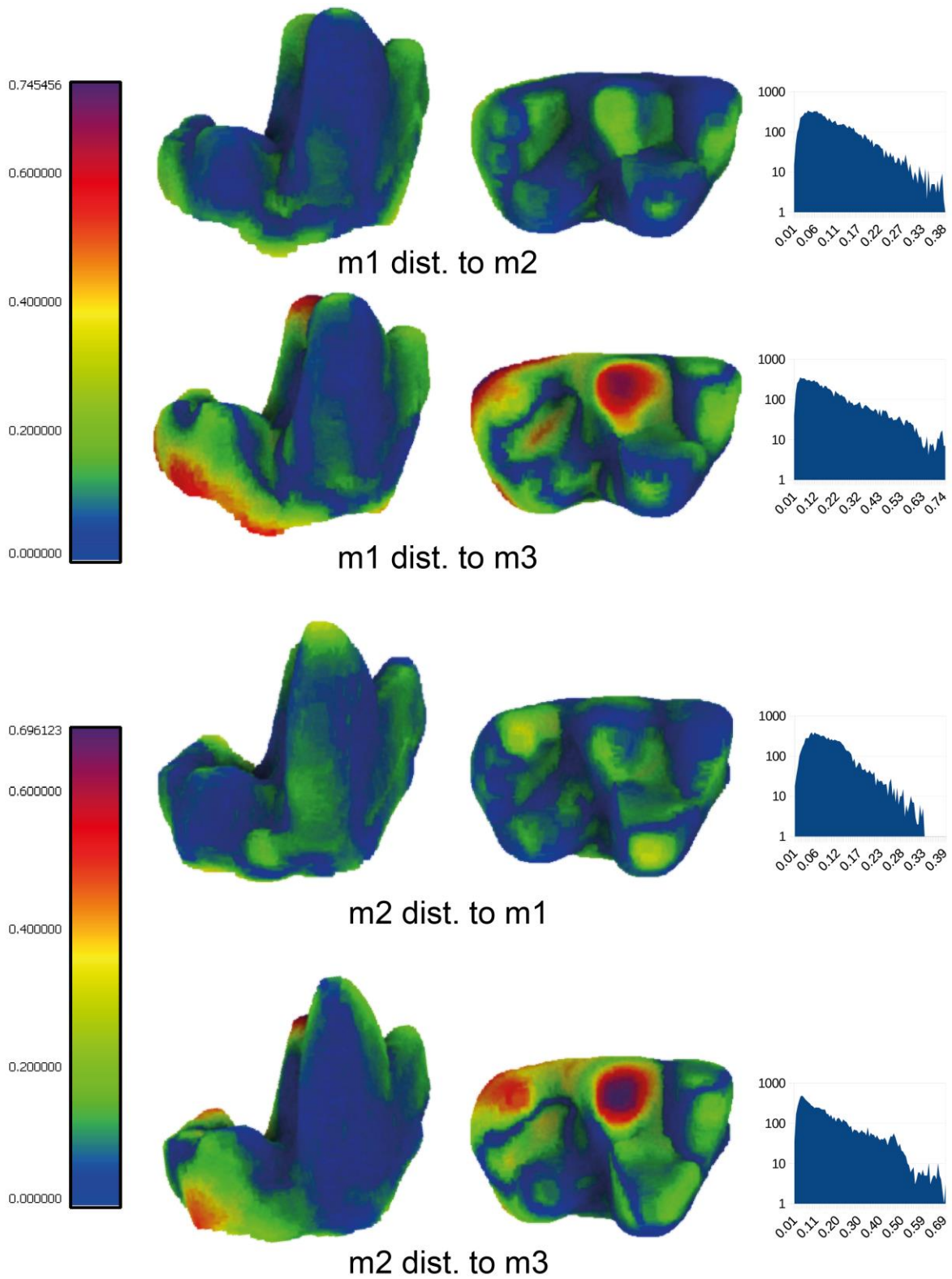
Fig. 62: Cloud-to-cloud distance (dist.) of the lower carnassials of *Oxyaenoides bicuspidens*, measured with the m1 as a reference respectively to the m2 and m3, and with the m2 as a reference respectively to the m1 and the m3. Rendering of µCT data.

The m2 of *Hyaenodon exiguus* (NMB Q.C.221) compared to the m1 as a reference shows almost no surface deviations on the trigonid, except for a small area of minor distance on the apex of the paraconid. Around the distal part of the crown, an area of moderate surface deviation extends along the cervix line on the buccal, distal and lingual side of the talonid. The maximum point to point distance is 1.17. The areas of higher surface deviations are more abundant when comparing the m3 to the m1 as a reference. The highest surface deviations are calculated at the talonid along the cervix line, running from buccal along the distal side to lingual. The area extending apically and mesially shows successively decreasing surface distances, but it covers a much greater part of the crown than in the m1/m2 comparison. Moderate surface deviations are fond all over the talonid, including the whole hypoconid cusp and wrap around the whole mesial part of the crown, extending along the cervix line below the trigonid. The point to point distance extends to a maximum of 3.15. The m1 compared to the m2 as a reference results in overall low surface deviations. On the paraconid and the protoconid, a small area of minor surface deviation is respectively found on the apices. The maximum calculated point to point distance is 1.0. In contrast to this, the m3 compared to the m2 as a reference shows a larger area of moderate to high surface distance that runs along the cervix line. The mesial part of this area, running below the paraconid, shows a moderate surface deviation. Below the talonid, the surface deviations are increasing in cervical direction, with an area of high surface distance that covers the lingual, distal and buccal side of the talonid. The area of moderate surface distance extends to the hypoconid. The maximum point to point distance is 3.03. Thus, surface distances for the m1/m2 comparisons show lower distance maxima than the respective comparisons with the m3 (Fig. 63).

For all taxa, the cloud-to-cloud distance comparisons show minor to moderate surface deviations when comparing the two mesial carnassials (m2/m3 in dasyuromorphs and m1/m2 in hyaenodonts) and shows significantly higher deviations when comparing any of the two mesial carnassials to the most distal carnassial (m4 in dasyuromorphs and m3 in hyaenodonts). This is seen both in the size differences of the visualized areas for surface deviations as well as the values of the calculated point-to-point distances, which consistently show higher maxima for the comparisons with the most distal carnassial.

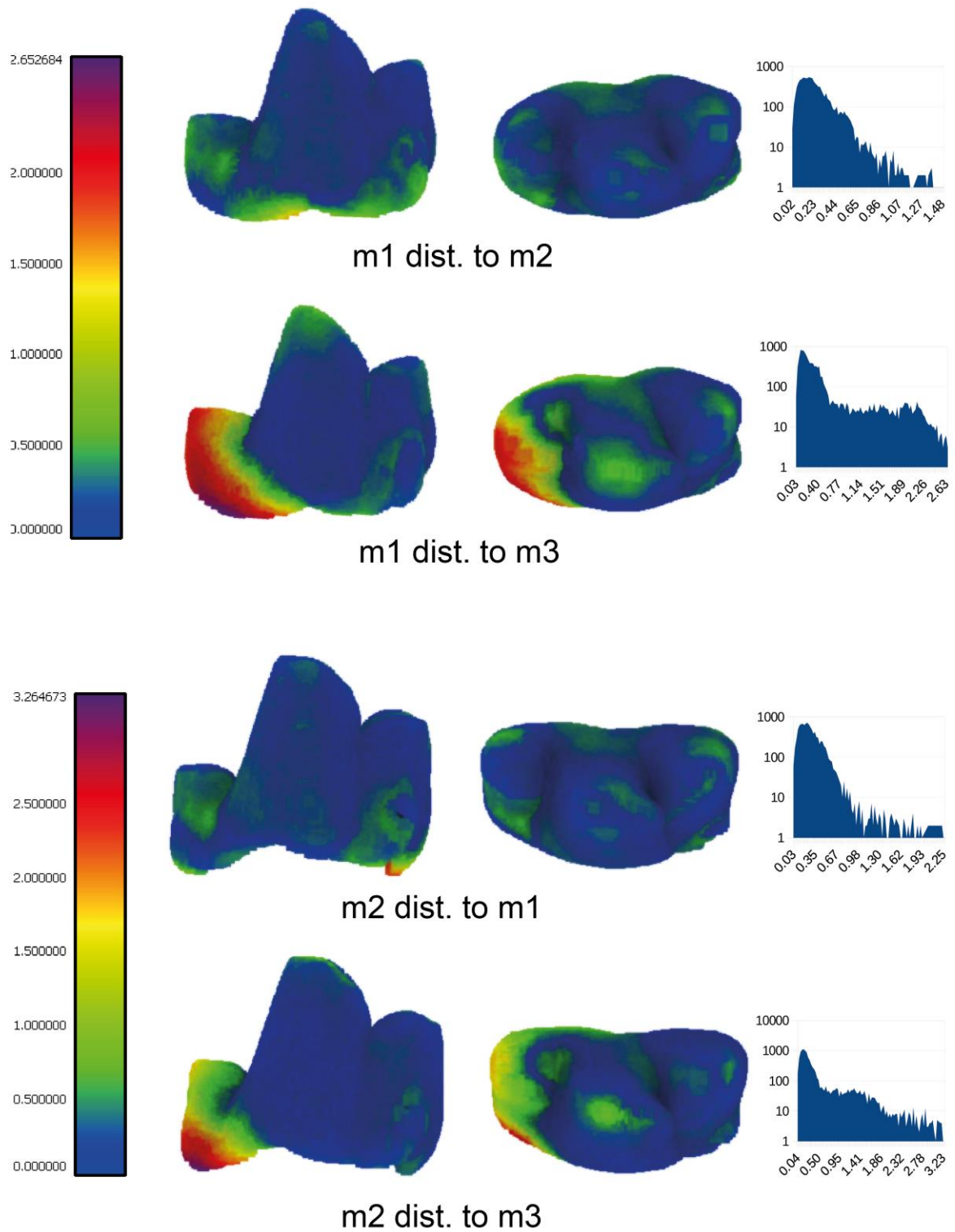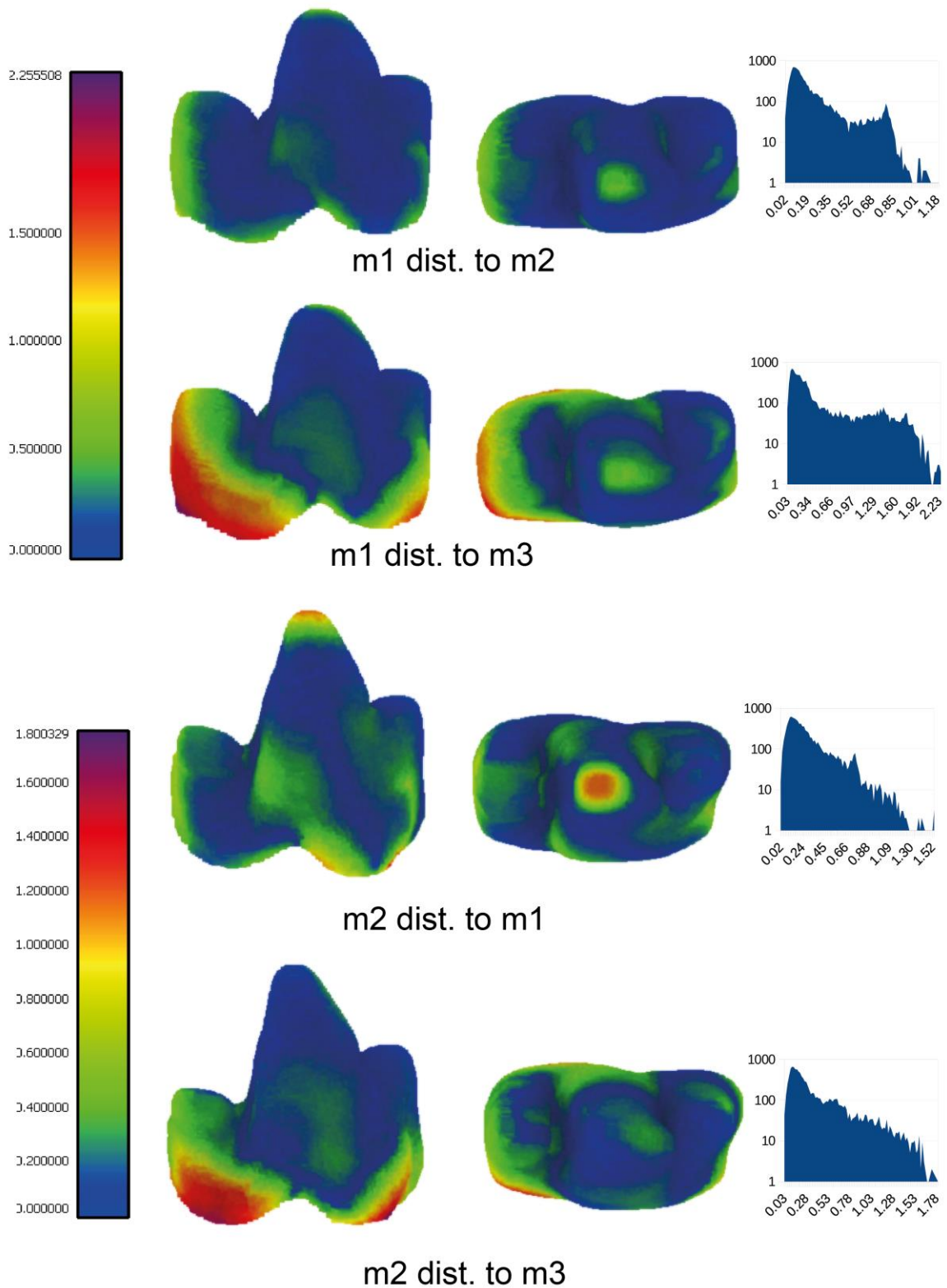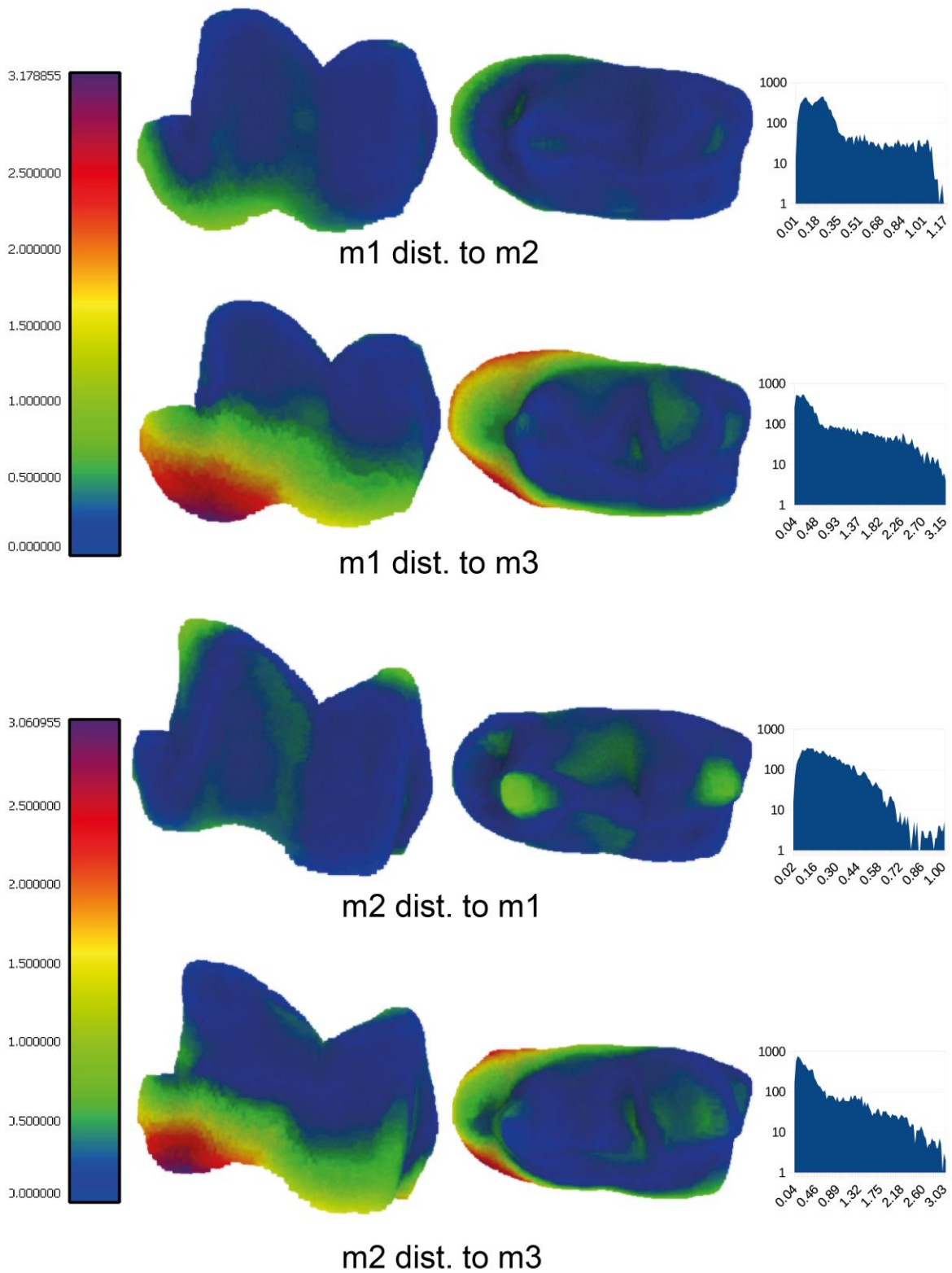**Fig. 63**: Cloud-to-cloud distance (dist.) of the lower carnassials of *Hyaenodon exiguus*, measured with the m1 as a reference respectively to the m2 and m3, and with the m2 as a reference respectively to the m1 and the m3. Rendering of µCT data.

4.4 Phylogenetic distribution of shape signals

4.4.1 Ancestral state reconstruction

Section 4.4.1 has been modified and published in: Lang, A. J., Engler, T., & Martin, T. (2021). Dental topographic and three-dimensional geometric morphometric analysis of carnassialization in different clades of carnivorous mammals (Dasyuromorphia, Carnivora, Hyaenodonta). *Journal of Morphology*, 283(1), 91 – 108.

Ancestral state reconstructions were calculated for the carnivoran, dasyuromorph and hyaenodont ariaDNE values and scores of PC1 and PC2 (Fig. 64), using the mean values of species. PCPs were chosen for this analysis because they are interpreted to be the most specialized carnassial teeth in taxa with multiple carnassials (see 5.4).

The distribution of ariaDNE values ranges from a minimum value of 0.0517 (*Panthera pardus*) to a maximum value of 0.1006 (*Viverra tangalunga*) with a total range of 0.0489. The calculated value for the base of the tree is 0.0723. From the base value of the tree, the base value of the Carnivora (0.0706) has a deviation of 3.4%, the base value of the Hyaenodonta (0.0748) has a deviation of 5.1% and the base value of the Dasyuromorphia (0.0707) has a deviation of 3.2%. Extreme high values occur within the Carnivora in the clade of the Felidae (*Felis*, *Neofelis*, *Otocolobus*, *Panthera*) and in within the Hyaenodonta in the species of *Hyaenodon*. Values in the lower side of the spectrum are found in the species of *Dasyurus* and *Vulpes*, as well as in the Viverridae (*Civettictis*, *Viverra*), the Herpestidae (*Ichneumia*) and in the proviverrine hyaenodont *Proviverra*.

The minimum value of PC1 is -0.25 (*Hyaenodon exiguus*) and the maximum value is 0.14 (*Ichneumia albicauda*), spanning a total range of 0.39. The base of the tree has a calculated value of -0.0229. The base value of the Carnivora (-0.0531) has a deviation of 7.7% from the base of the tree, while the base value of the Hyaenodonta (-0.0024) has a deviation of 5.3% and the base value of the Dasyuromorphia (-0.0275) has a deviation of 1.2%. The highest values occur in the species of *Hyaenodon*. Moderately high values are found in the Felidae, Hyaenidae, Mustelidae, Nimravidae, some of the Canidae (*Lycaon* and *Speothos*), the Mustelidae, as well as the hyaenodonts *Oxyaenoides* and *Pterodon* and in the dasyuromorphs *Sarcophilus* and *Thylacinus*. Low values are found in the Viverridae, Herpestidae, the Vulpini, the hyaenodont *Proviverra* and the dasyuromorph species of *Dasyurus*.

The PC2 values range from a minimum of -0.1276 (*Viverra tangalunga*) to a maximum of 0.0862 (*Oxyaenoides bicuspidens*) with a total range of 0.2138. For the base of the tree, the calculated value is 0.0196. From the base value of the tree, the base value of the Carnivora (-0.0355) has a divergence of 25.8%, while the base value of the Hyaenodonta (0.0419) has a deviation of 10.4% and the base value of the Dasyuromorphia (0.026) has a deviation of 3%. High values are restricted to the Carnivora, where they appear in all Caniformia, the

Nimravidae, the Viverridae and the Herpestidae. Within the Carnivora, values on the low part of the spectrum are found in the Felidae and the Hyaenidae.
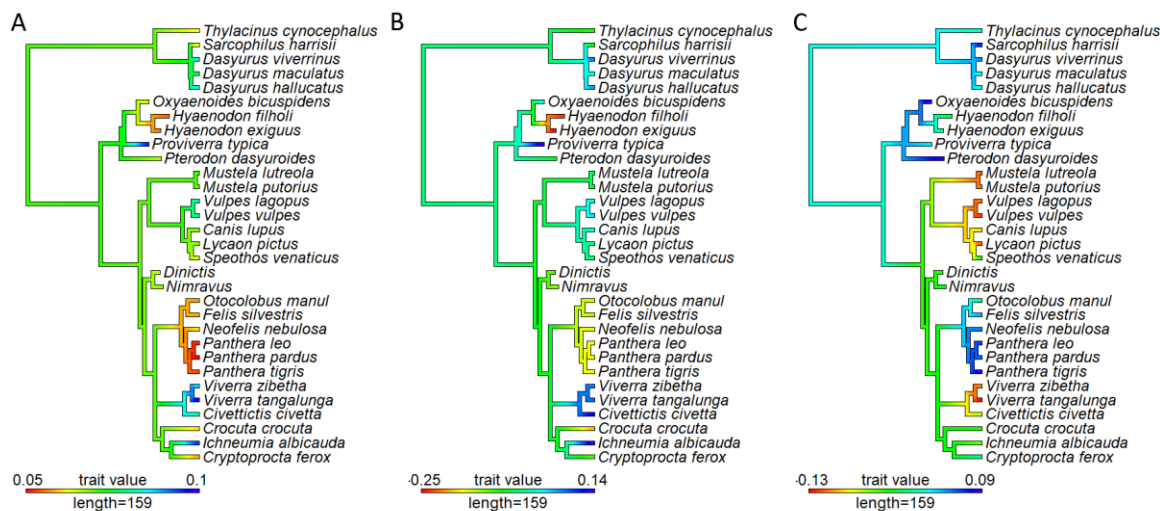
Fig. 64: Ancestral state reconstruction of A ariaDNE, B carnassial crown shape PC1 and C carnassial crown shape PC2. Estimated evolutionary history of each trait is mapped onto the phylogeny. This figure is published in Lang et al. (2021).

4.4.2 Traitgram analysis

Traitgrams using the dated phylogeny of the investigated taxa were used to investigate the dispersal of principal carnassials defined either as "basal" or as "derived" dependent on ariaDNE values as well as PC1 and PC2 scores. The dispersal of teeth depending on the ariaDNE values shows a strict divide between basal and derived carnassials (Fig. 65). A phylogenetic pattern specific for the Carnivora, Dasyuromophia of the Hyaenodonta cannot be identified, as the phylogeny in all three clades is distorted by the scattering of ariaDNE values. A similar pattern can be observed in the traitgram of the PC1 scores (Fig. 66). Although the division is not as strict, as two basal with basal carnassials and two taxa with derived carnassials are overlapping with their PC1 scores, the general divide between basal and derived carnassials is still clearly observable. Like in the ariaDNE traitgram, the phylogeny is distorted by the scattering of PC1 scores.

In contrast to this, there is no clear division between basal carnassials and derived carnassials in the traitgram of PC2 scores (Fig. 67). Although the phylogeny is also distorted by the scattering of PC2 scores, a phylogenetic patterning in the low spectrum of PC2 scores can be identified, as this part of the spectrum is purely occupied by carnivoran taxa. Basal and derived carnivoran carnassials make up roughly the lower 50% of the range of PC2 scores. Further, it can be observed that the only carnivoran taxa overlapping with dasyuromorph and hyaenodont taxa belong to the Felidae.
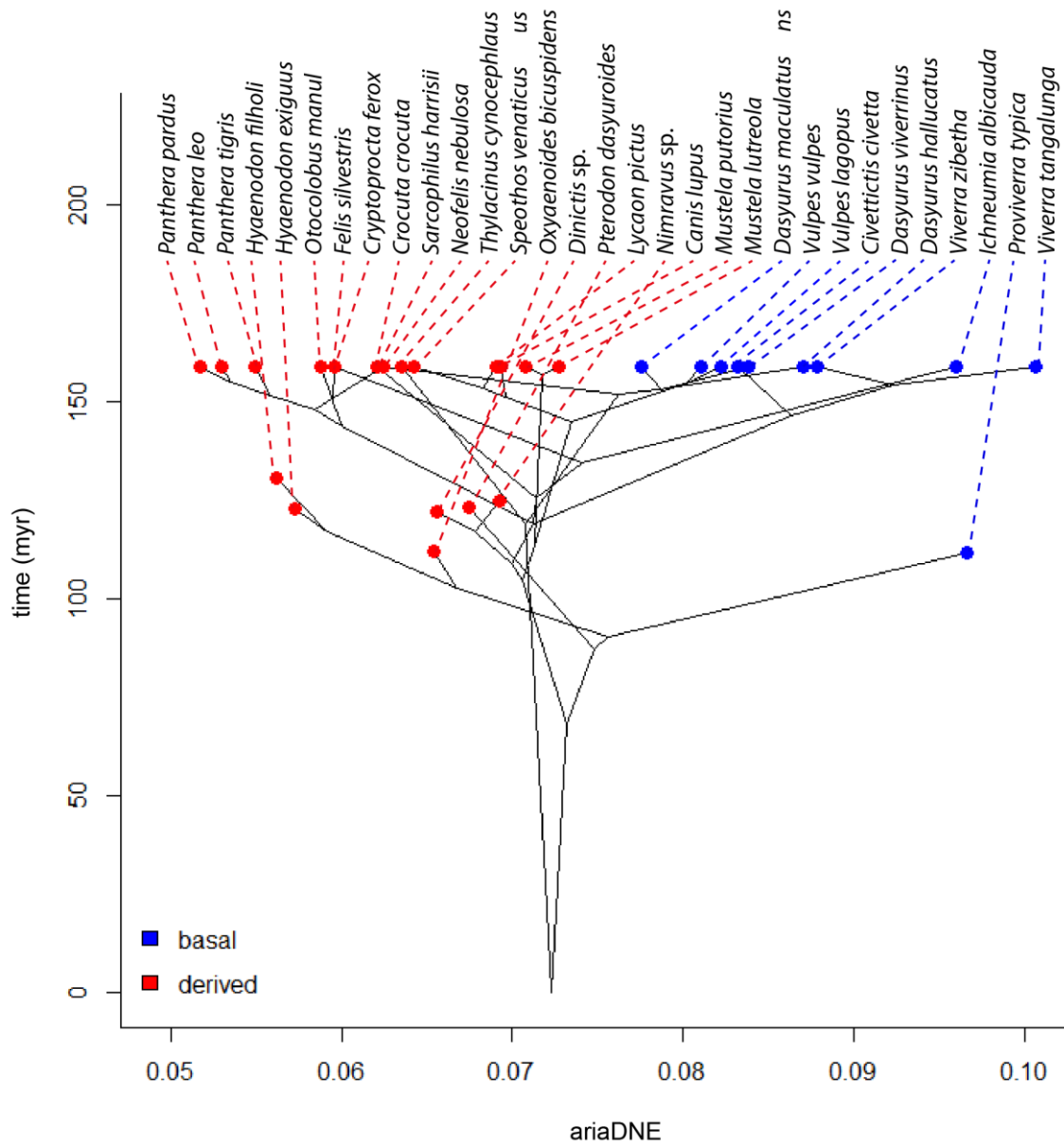
Fig. 65: Traitgram of basal of principal carnassial teeth, with tip distribution corresponding to the respectively calculated ariaDNE mean of species. The length of branches is based on the time calibrated phylogenetic data.
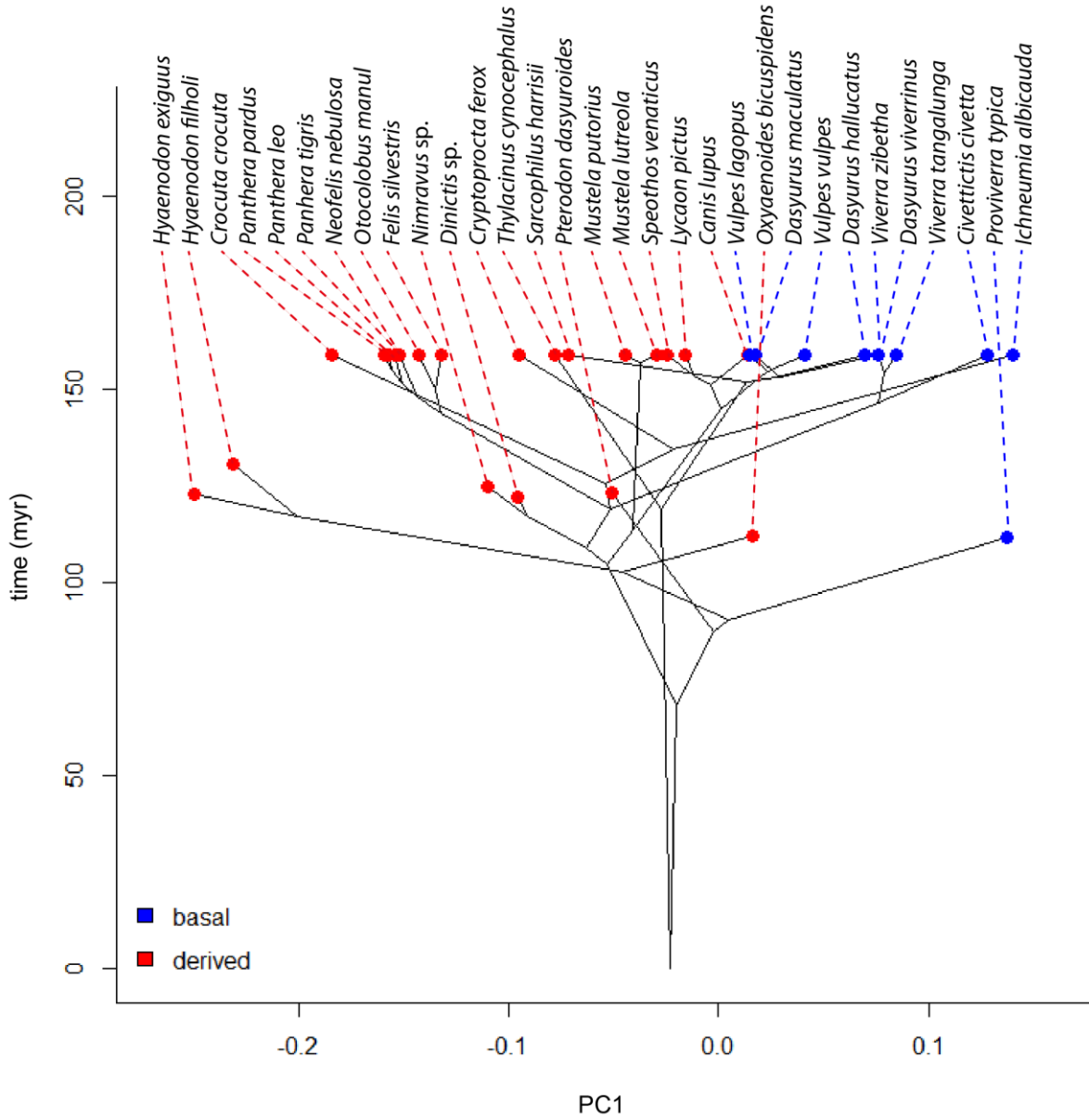
Fig. 66: Traitgram of basal of principal carnassial teeth, with tip distribution corresponding to the respectively calculated PC1 mean of species. The length of branches is based on the time calibrated phylogenetic data.
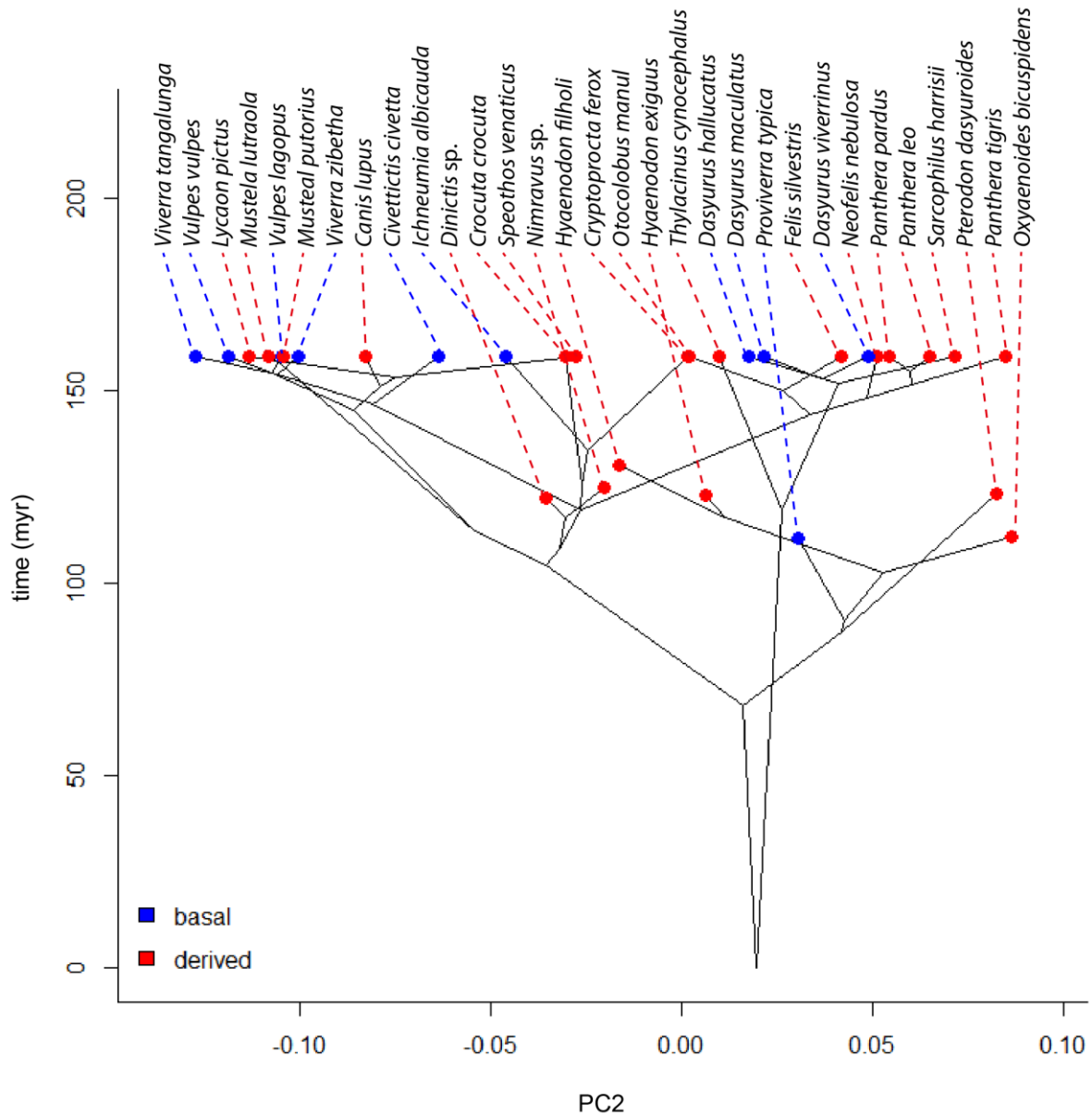
Fig. 67: Traitgram of basal of principal carnassial teeth, with tip distribution corresponding to the respectively calculated PC2 mean of species. The length of branches is based on the time calibrated phylogenetic data.

4.4.3 Cluster analysis

Section 4.4.3 has been modified and published in: Lang, A. J., Engler, T., & Martin, T. (2021). Dental topographic and three-dimensional geometric morphometric analysis of carnassialization in different clades of carnivorous mammals (Dasyuromorphia, Carnivora, Hyaenodonta). *Journal of Morphology*, 283(1), 91 – 108.

The UPGMA cluster analysis of the mean values of the first five PCs for basal and derived MCPs, ICPs and PCPs calculated a fundamental division between all basal (cluster A) and all

derived carnassials (cluster G) (Fig. 68). Within the cluster of basal carnassials, the hyaenodont and dasyuromorph carnassials form a cluster of their own (cluster B), which is separated from that of the basal carnivoran carnassial. Within the cluster B, there is a division between a cluster comprising the hyaenodont carnassials (cluster C) and a cluster comprising the dasyuromorph carnassials (cluster D). The hyaenodont MCP and ICP form a cluster of their own (cluster E) within the hyaenodont cluster (cluster C), as do the dasyuromorph MCP and ICP (cluster F) within the dasyuromorph cluster (cluster D).

Within the cluster of derived carnassials (cluster G), there is a division between a cluster uniting the dasyuromorph and hyaenodont IPCs and MCPs (cluster H) and a cluster uniting all PCPs (cluster I). Within cluster H, the dasyuromorph ICP and MCP are forming a cluster of their own (cluster J), separated from the cluster uniting the hyaenodont ICP and MCP (cluster K). Within the cluster of PCPs, the dasyuromorph PCP and the carnivoran PCP are forming a cluster (L) separate from the hyaenodont PCP.
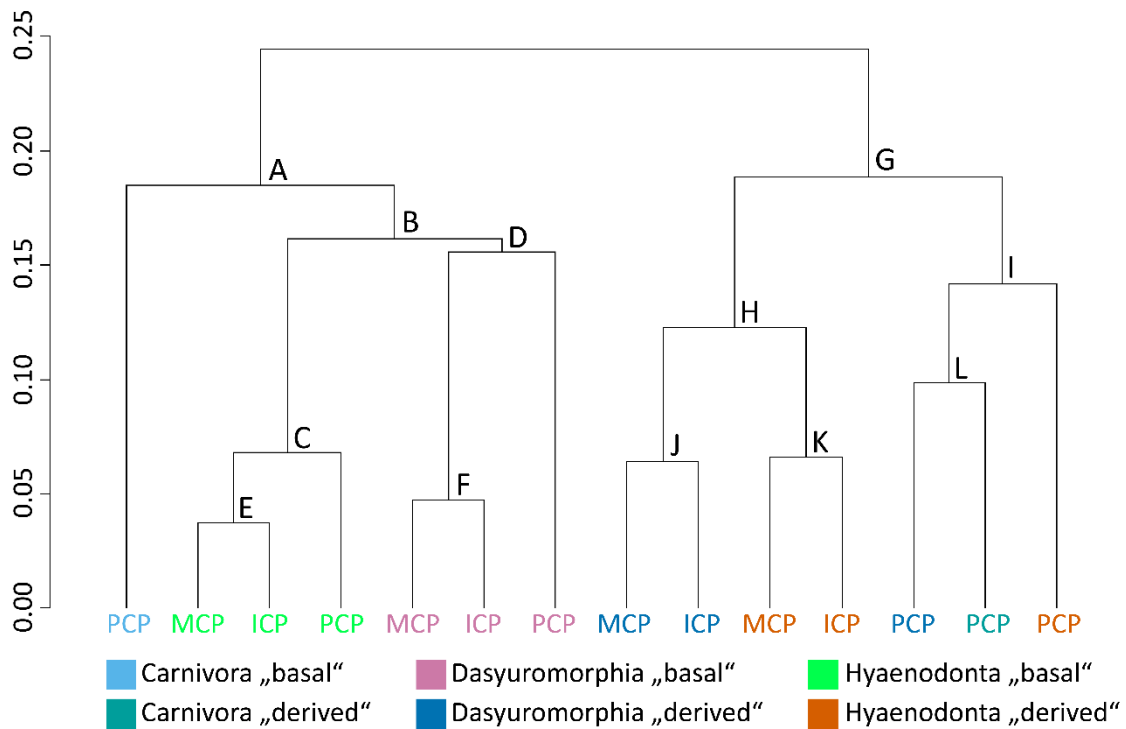
Fig. 68: Dendrogram of the UPGMA cluster analysis on the mean PC scores from the first five PCs for different carnassial tooth positions of type "basal" and "derived" per taxonomic order. This figure is published in Lang et al. (2021).

5. Discussion

5.1 Occlusion in carnassial dentitions

The documentation of tooth wear and simulation of chewing cycles using the OFA software reveal a fundamental difference regarding occlusal contacts between heterodont cheek dentitions, as in carnivorans, and more homodont cheek dentitions, as in dasyuromorphs and hyaenodonts. The occlusal pattern that is most similar to the plesiomorphic tribosphenic condition is found in the carnassials of the hyaenodont *Proviverra typica* and the various species of *Dasyurus.* The crown structure has all the characters of a tribosphenic condition, with the trigon, trigonid and talonid fully developed. The talonid on the distalmost lower carnassial is reduced in size, with the antagonistic distalmost upper molar also showing a reduction of the trigon, as the metacone is vestigial. The resulting occlusal patterns in the OFA analysis of *Dasyurus viverrinus* show that besides the primary carnassial cutting between the metacrista of the upper carnassials and the paracristid on the lower carnassials, there are also secondary cutting contacts present, evidenced by associated attritional wear. These result from the occlusion of the mesial paracone and metacone flanks with the distal trigonid flank and the mesial and distal talonid flanks. Further, occlusion of the protocone with the lower molars results in occlusion with the distal trigonid flank as well as the buccal entoconid flank and the lingual hypoconid flank within the talonid basin. Wear within the talonid basin was not found on the m4, however the OFA analysis shows that the M4 protocone does occlude into the talonid basin at the end of the power stroke and produces a small area of occlusal contact. This contact can be interpreted as vestigial and is one trait that is in the process of reduction already in "basal" carnassial dentitions.

Increasing carnassialization results in a reduction of these secondary contacts, as seen in the wear on the carnassials of *Hyaenodon exiguus*, *Hyaenodon filholi*, *Oxyaenoides bicuspidens*, *Sarcophilus harrisii,* and *Thylacinus cynocephalus*. The simplified occlusal pattern can be linked to the reduction of the talonid, which is either approximating the condition of a unicuspid "trenchant heel" (see discussion below) or is absent entirely, as in the distalmost carnassials of *Hyaenodon* spp. The lack of protocone/talonid occlusion explains the absence of associated wear. On the upper molars, reduction of secondary cutting is associated with the paracone being further reduced in size in dasyuromorphs or fusion of the paracone and metacone into an amphicone in hyaenodonts. The OFA analysis of *T. cynocephalus* shows that carnassial cutting during the power stroke is overall responsible for a greater proportion of occlusal contact than in the more basal carnassial dentition of *D. viverrinus*. In *H. exiguus*, almost the entirety of occlusal contact can be attributed to carnassial cutting, while secondary cutting contacts are absent. A point of centric occlusion in highly carnassialized dentitions is hard to define, if it is present at all, as the structures that are involved in maximum intercuspation in

tribosphenic molars, the talonid and the protocone, are reduced in carnassials. Definite stopping points in the OFA analysis are produced by occlusion of the M4 protocone with the m4 hypoconid in *T. cynocephalus* and by occlusion of the vestigial M1 and M2 protocones with the m1 and m2 protoconids in *H. exiguus*. There is evidence that the latter contacts might have occurred in the power stroke of the living animal, as "dents" can be found on the protoconid apices of the m1 and m2 in one specimen of *H. exiguus* (Fig. 69). These might have been produced by occlusion with the lingual protocone flanks of the antagonistic upper molars, although attritional wear could not be documented on these areas of inferred occlusal contact.
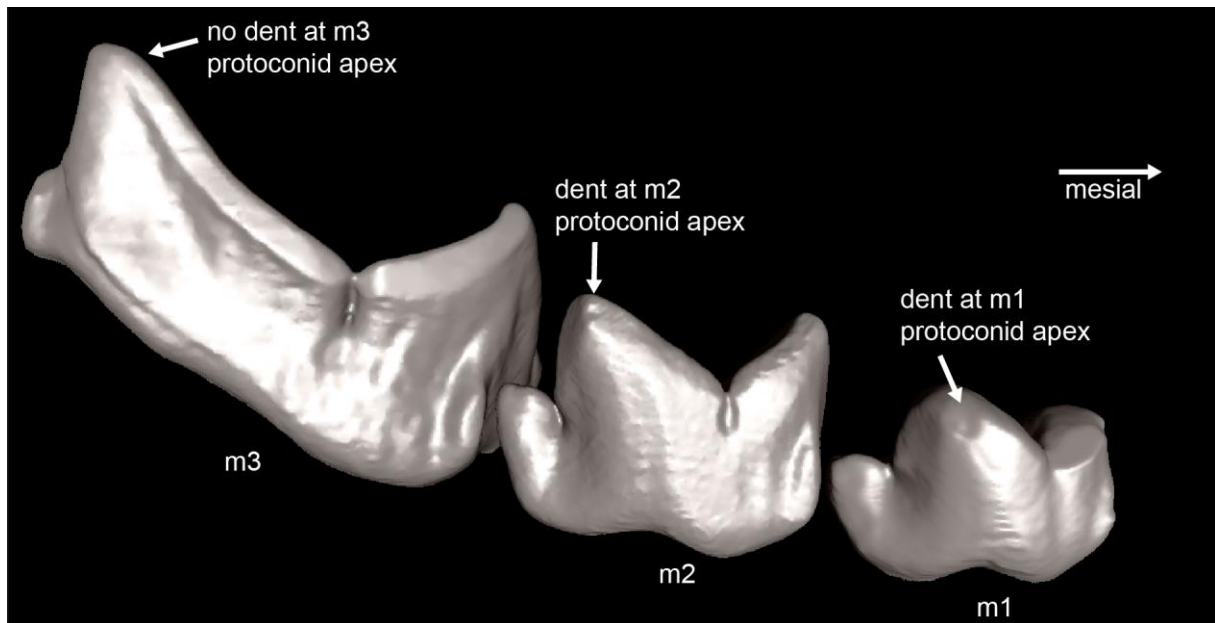
Fig. 69: The lower molar dentition on *Hyaenodon exiguus* (NMB Q.B.771; picture taken in OFA) showing dents near the protoconid apices of the m1 and m2. The dents appear at the locations where the protocones of the upper M1 and M2 occlude at the end of the power stroke in the OFA analysis, indicating that occlusion might be the reason for the presence of the dents. The m3, lacking an antagonist, is also lacking a dent.

In carnivoran taxa, the division along the cheek dentition between the mesial P4/m1 carnassial blades and the distal post-carnassial dentition results in a specific occlusal pattern. In the basal condition of *Ichneumia albicauda* and *Viverra zibetha*, in addition to the carnassial contact between the P4 praemetacrista and the m1 paracristid, there are secondary contacts occurring between the M1 and the m1 distal trigonid and talonid flanks. The M1 protocone occludes with the distal m1 trigonid flank and with the buccal entoconid and hypoconulid flanks, producing distinctive facets. Further, the distal paracone and mesial metacone flanks occlude with the buccal talonid flanks. In the OFA analysis of *Viverra tangalunga* and *Speothos venaticus*, carnassial cutting is responsible for the majority of occlusal contacts for about half the duration of the power stroke, with the duration of cutting being slightly longer in the more derived

carnassial condition of *S. venaticus*. Though, occlusion related to the post carnassial dentition in both taxa is linked to different crown structures. In *V. tangalunga*, the talonid is basin shaped, with the hypoconulid and entoconid present. Occlusion of the buccal entoconid and hypoconulid flanks is documented by wear and is also reconstructed in the OFA analysis. However, no facet forms on the m1 lingual hypoconid flank and the M1 buccal protocone flank. Although occlusion of the M1 protocone into the m1 talonid basin is reconstructed in the OFA analysis, the calculated contact areas remain small. The combination of calculated contact in the OFA and absence of attritional wear on the actual tooth surface point to the flat post carnassial molar surface performing a crushing function which is compressing food without tooth-tooth-contact. This type of function has been described as "puncture-crushing" (Hiiemae, 1976). There is no wear indicating a second phase after the point of centric occlusion, thus it is inferred that the power stroke is terminated with the puncture-crushing within the talonid basin in *V. tangalunga,* without a second phase. The post carnassial occlusion occurring in *S. venaticus* shows a different occlusal pattern. The m1 talonid basin is reduced, but occlusion does occur between the M1 paracone and the m1 hypoflexid. In fact, the mesial talonid blade, spanning half of the hypoflexid groove, is enlarged in *S. venaticus* in comparison to *V. tangalunga*, thus a bigger area of occlusion is calculated on this structure in the OFA analysis. In the OFA analysis of *Felis silvestris*, the occlusal contacts are attributed almost entirely to carnassial cutting with the post carnassial occlusion being reduced to small areas of contact. These can be interpreted as vestigial contacts of the reduced M1 with the distal m1 trigonid flank.

For all dentitions, the OFA analysis calculated two points of initial contact between the respective antagonistic carnassial blades which shift towards the carnassial notch with further tooth movement during the power stroke. As described by Evans and Sanson (2006), the occlusion of carnassial notches concentrates the bite forces, as the amount of material is reduced. This occlusal pattern is found on all carnassial blades. In carnivoran and hyaenodont carnassials, notches form on the lower and upper blades which results in the occlusion of two V-shaped crests. This is in contrast to dasyuromorph carnassials, where a notch only forms on the lower carnassials, while the upper carnassial blade (praemetacrista) is U-shaped. One explanation for this structural difference is that a U-shaped blade is less prone to breakage and to misalignment with progressing tooth wear (Evans & Sanson, 2006). It has to be considered that the U-shaped upper praemetacrista might be a plesiomorphic trait among marsupials, as it did not evolve in hyaenodonts, despite having an otherwise very similar structural and functional resemblance. There is a difference in the timing of carnassial cutting between homodont cheek dentitions and heterodont cheek dentitions. The carnassial cutting in all OFA analyses of homodont carnivoran carnassial dentitions follows a similar occlusal pattern. This pattern is present both in basal carnassial dentitions and in more derived ones.

In the Carnivora, occlusion of the single carnassial P4/m1 blades initiates the power stroke, thus carnassial cutting is performed early on in the power stroke and is then replaced by secondary contacts, related to talonid occlusion (except for *F. silvestris*). In the homodont Dasyuromorphia and the Hyaenodonta, there is a sequential cutting of the individual carnassial blades from distal to mesial during the power stroke. Initial contact always occurs at the distalmost carnassial blades.

5.2 Hypoflexid occlusion in the "trenchant heel" and "morphogenetic reversal"

The reduction of crown features in carnassial teeth results in a simplified morphology that in some aspects resembles a primitive pretribosphenic molar condition. The aspect of structural reversal in carnassial teeth to a more plesiomorphic condition has been discussed in detail by Solé and Ladevèze (2017), who conclude that a possible inhibition of the development of certain crown features reverses the carnassial crown structure to a more ancestral condition. Thus, there is likely a direct link between the ontogenetic development of the crown structure of carnassial teeth and the evolutionary succession of structural changes that led to the emergence of carnassials in different clades of mammals. Solé and Ladevèze (2017) base their conclusion solely on morphological observations. Based on the observations in this study, I propose a possible "functional reversal" in some carnassials, which is linked to the presence of a "trenchant heel", as first described by Wortman & Matthew (1899). Trenchant talonids convergently evolved in multiple lineages of mammals. They usually are interpreted as a secondary cutting feature, whereby the unicuspid talonid is functioning as an additional cutting blade via the presence of an enlarged hypoconid (Van Valkenburgh, 1991; Solé & Ladevèze, 2017). The observed presence of facets along the praehypocristid, extending into the hypoflexid and on the antagonistic upper molar extend from the distal to the lingual paracone flank, suggests that the trenchant heel occlusion may play a more crucial role in the carnassial power stroke than simple cutting. Striations observed in the caniform *Speothos venaticus* as well as the feliform *Dinictis* sp. with a trenchant heel showed striations present on the distal flank of the trigonid, which indicate a slightly inclined tooth movement that is parallel to the inclination of the hypoflexid groove. Hypoflexid occlusion played a crucial role in pretribosphenic teeth, for example in dryolestids, where it is interpreted that the hypoflexid groove served as a guiding structure for tooth movement during the power stroke and performed a shearing function with a crushing component, from which the crushing talonid basin of the tribosphenic molar eventually evolved (Schultz & Martin, 2011). This guiding, shearing and possibly to a certain extent crushing function is reactivated in the trenchant heel of carnassials. This is interesting, especially because the inclination of the groove prevents the tooth movement during the power stroke to have a mostly orthal orientation and induces a more transversal component. As seen in the OFA analysis of *Thylacinus cynocephalus* and

Speothos venaticus, paracone/hypoflexid occlusion occurs after the primary carnassial cutting is performed, and thus maintains a slightly transversal tooth movement. Although the retention of a vestigial crushing function is a possibility for the presence of hypoflexid shearing, in case of the carnassials it seems unlikely that it is linked mainly to the processing of food, as there is an overall tendency to reduce the crushing function. One explanation for the presence of hypoflexid shearing may be to prevent the carnassial blades from moving into the gum by slightly inclining tooth movement. In mammals, the term "autocclusion" has been coined to refer to the occlusal alignment of cusps being controlled by the morphology of the teeth (Mellett, 1985). This limits the neurological requirements for tooth alignment to the initial occlusal contact (Evans & Sanson, 2006). The hypoflexid seems to be an ancient structure that serves in autocclusion, which is re-activated in the trenchant heel. It is also possible that the developmental "reversal" of tooth structures may have led to the development of hypoflexid shearing as a genetic remnant. In the Carnivora this is plausible, because the plesiomorphic occluding structures (paracone and unicuspid talonid) are present. In case of the Hyaenodonta, the occlusal relationships get somewhat more complex. Pairing and eventual fusion of the metacone and the paracone are an apomorphic condition of the Hyaenodonta, resulting in a condition different from the one found in carnivorans and ancestral pretribosphenic taxa. The tooth wear suggests that both the metacone and the paracone occlude with the trenchant heel in the Hyaenodonta, such as in *Oxyaenooides bicuspidens*, and the resulting facet covers the hypoflexid along the praehypocristid, wrapping around the buccal hypoconid flank and extending along the posthypocristid. On the antagonistic molar, a facet that connects the paracone and the metacone lingually indicates that both cusps occlude with the trenchant heel. Thus, hypoflexid occlusion is also present in hyaenodont taxa with a trenchant heel, but differs from the occlusion of carnivoran carnassials. Hypoflexid shearing appears to be an intermediate condition in the evolution of carnassial teeth from molars with a crushing talonid to molars without talonid (Fig. 70). To further confirm this, an examination on the successive evolution of carnassial teeth in multiple lineages which completely reduced the taloned will be necessary.

The picture, however, gets more complicated when the Dasyuromorphia are included. In the multiple carnassial teeth of *Sarcophilus harrisii* and *Thylacinus cynocephalus*, hypoflexid occlusion seems to play a subordinate role, but this is only the case when occlusion of the mesial carnassials (m2/M2, m3/M3) is considered. Tooth wear implies that occlusion along the distal postparacrista and the praehypocristid does occur, but the resulting facet remains small on the m2 and the m3. With progressing wear, the facet may extend into the small hypoflexid groove of the m3, though it is unlikely that it has a crucial function in terms of guiding or food processing. In dasyuromorphs, there is a tendency of metacone hypertrophy and paracone reduction, very similar to the condition in the Didelphidae (Thenius, 1989). It is thus not

surprising that occlusion of the small paracone with the hypoflexid is not well pronounced in the carnassials of dasyuromorphs. Wear along the posthypocristid and the metacrista instead shows a generally more well pronounced occlusion between these structures. Given all these observations, it is surprising to find wear in the hypoflexid of the m4 in both *S. harrisii* and *T. cynocephalus*. The upper M4 has most of its crown structures reduced, showing a vestigial morphology. Unfortunately, there has been no detailed examination of its occlusal function so far, it even has been assumed to have "no opponent" (Berkovitz & Shellis, 2018). The tooth wear that was observed, however, shows that the praeparacrista of the M4 occludes with the distal trigonid flank, and the paracone occludes along the hypoflexid of the m4. Striations are present on the distal trigonid flank of the m4 of *S. harrisii* and *T. cynocephalus*, and in both cases, they show a slight transversal inclination parallel to the hypoflexid groove. It is possible that the hypotrophy of the paracone in dasyuromorphs has posed an obstacle to re-emerge hypoflexid occlusion in the evolution of the carnassials. If the reappearance of hypoflexid occlusion would be driven purely by genetics, an enlargement of the paracone and a well pronounced postparacrista/praehypocristid occlusion would be the expected result. Instead, the Dasyuromorphia seem to have evolved an apomorphic "solution" for this problem independently, by employing the paracone of the vestigial M4 in hypoflexid occlusion. Again, this suggests some functional importance of the hypoflexid groove for the guiding of the chewing motion. Further, it has to be noted that the m4 is the principal carnassial in dasyuromorphs, exhibiting the most carnassialized crown structure (see discussion below). The presence of prominent paracone/hypoflexid occlusion on the most carnassialized tooth position suggests that a link between this feature and the degree of carnassialization exists.

These observations support the hypothesis of morphogenetic reversal by Solé & Ladevèze (2017) by revealing that during carnassialization, morphogenetic reversal does not only reduce, but also re-emerge some characters. What role exactly genetics plays in the development of carnassial teeth with possible structural and functional reversals to ancestral conditions is an interesting field of future research.
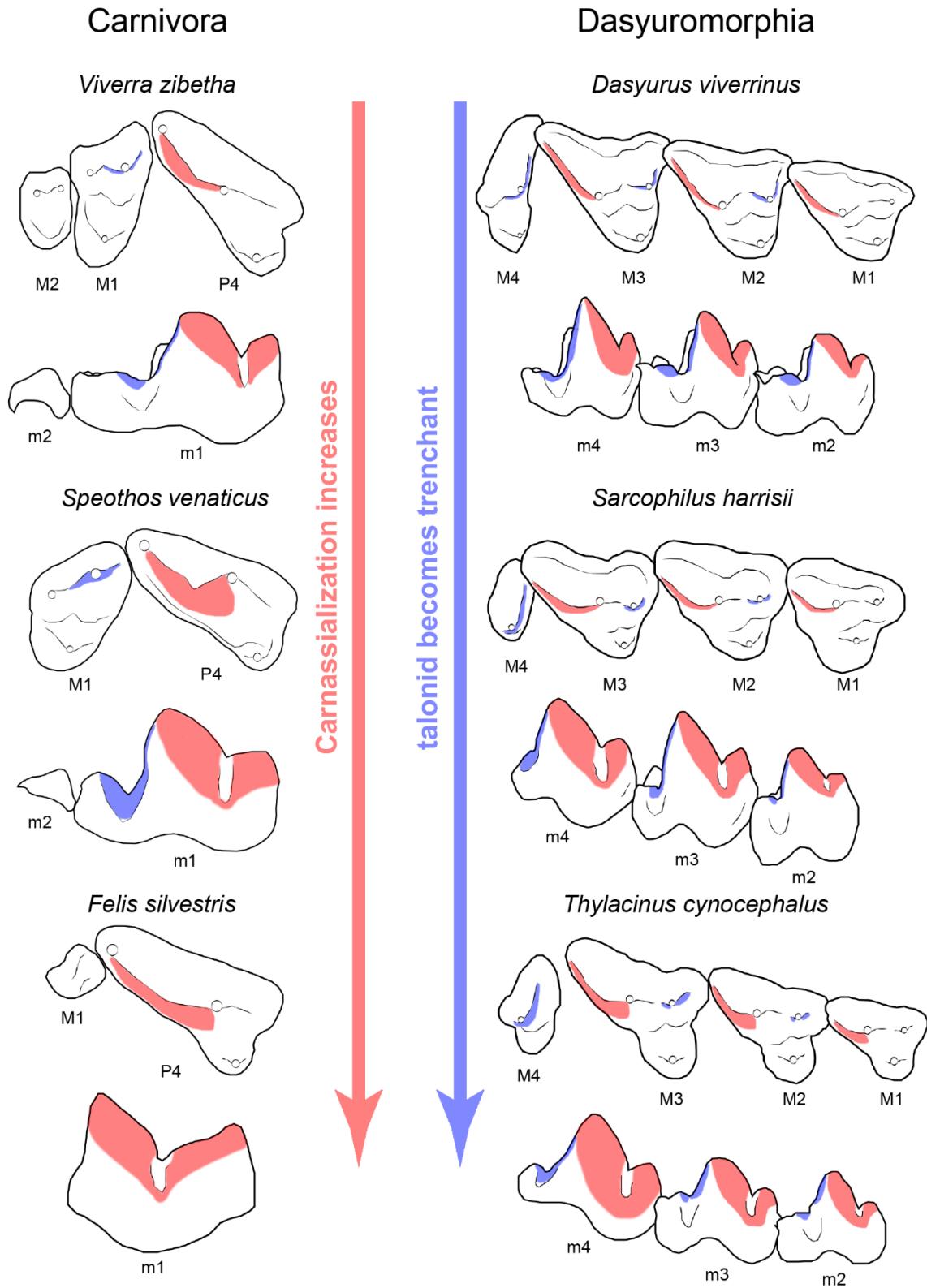
Fig. 70: Evolutive connection of carnassialization and the "trenchant" talonid heel as exemplified in carnivoran and dasyuromorph taxa. Carnassial occlusal contact (red) and paracone/hypoflexid occlusal contact on the talonid (blue) both increase up to the point where the talonid is completely reduced (as in *Felis silvestris*). Upper molars in occlusal view, lower molars in buccal view. Mesial is to the right.

As discussed by Davis (2011), the homology of the first singular pretribosphenic talonid cusp is not resolved, it may be identical with either the hypoconid or the hypoconulid of tribosphenic molars. If the structural reversal of carnassial teeth, as discussed above, is true and the hypoflexid groove in the trenchant heel is indeed homologous to the pretribosphenic hypoflexid groove, then the cusp bordering this groove may also be homologous to the pretriboshenic single talonid cusp (hypoconid) (Fig. 71).
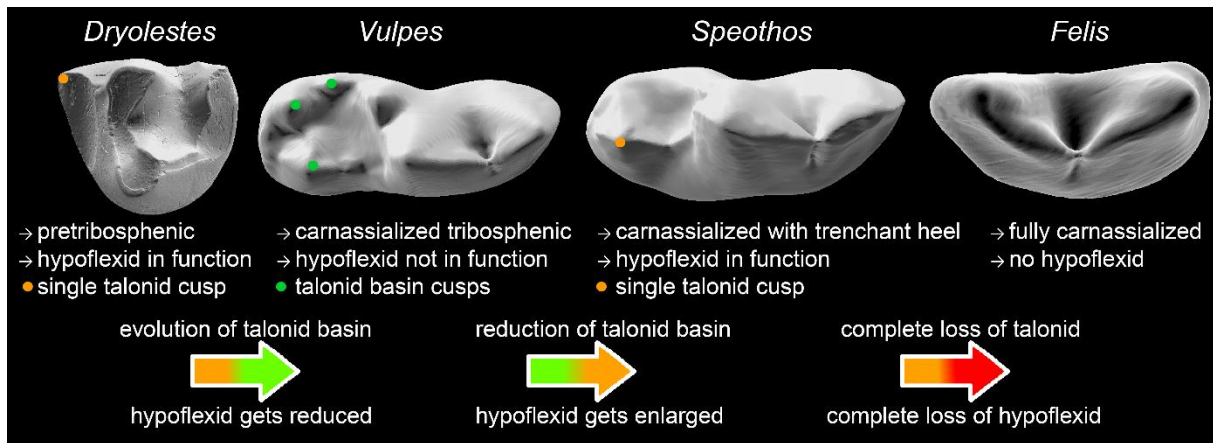
Fig. 71: Hypothetical sequence of evolution of the lower tooth-crown from pretribosphenic to tribosphenic to carnassial with trenchant heel to carnassial without talonid, shown in exemplaric taxa. Teeth in occlusal view, mesial is to the right. Not to scale. *Dryolestes leiriensis* scan of specimen Gui Mam 1196 provided by Julia Schultz. Rendering of µCT data.

5.3 The influence of functional morphology on corwn DNE

Section 5.3 has been modified and published in: Lang, A. J., Engler, T., & Martin, T. (2021). Dental topographic and three-dimensional geometric morphometric analysis of carnassialization in different clades of carnivorous mammals (Dasyuromorphia, Carnivora, Hyaenodonta). *Journal of Morphology*, 283(1), 91 – 108.

Crown curvature of carnassials as quantified by ariaDNE is related to changes in functional morphology associated with carnassialization. These include the reduction of the metaconid and of the talonid cusps in highly carnassialized teeth. The interordinal convergent evolutionary trend observed in the molars of Dasyuromorphia, Carnivora and Hyaenodonta is indicated by the respective crown curvature values. In all orders, carnassial molars with basal morphotypes show significantly higher ariaDNE values than molars with a more derived carnassialized crown morphology. The ariaDNE value shift from less to higher carnassialized teeth is unidirectional in all included taxa, regardless of phylogeny. This indicates that ariaDNE quantifies the convergent morphological conditions of low and highly carnassialized teeth and is a proxy for the relative reduction of functional occlusal structures. Relatively high ariaDNE

values point to a crown morphology with a more complex crown and a potentially more diverse function, including not only a simple shearing but also a crushing function, because talonid cusps are still present. Low ariaDNE values are very unlikely to occur in carnassial teeth which retain crushing structures, and if they do, they are reduced in relation to those with higher ariaDNE values (as in *Mustela* and *Canis*, both lacking at least one talonid cusp). The ariaDNE values are interpreted as a strong indicator for functional reduction. Results of the one-way ANOVA and Welch's heteroscedastic F tests using the ariaDNE values of lower principal carnassials support the indication of carnassialization as the primary influence on ariaDNE values. After being classified as either "basal" or "derived" carnassialized, basal and derived groups within the same taxon were significantly different, but groups of the same carnassialization category were not. All taxa with a relatively reduced metaconid and talonid, even if still functional, can be separated with a high probability from basal morphotypes via ariaDNE, as shown by the results of the ANOVA and Welch test. This is further supported by the results of the LDA. Even though there is a small fraction of overlap of values of the basal and derived groups of carnassial teeth, the misclassification rate using ariaDNE values is low (2% using only lower principal carnassials, 4% using all lower carnassials). The discrete group assignment of ariaDNE values is not expected to correctly classify every carnassial tooth, since carnassialization is not a binary character state but rather a dynamic character shift. Naturally, when examining conditions along a spectrum of functional morphological adaptation, overlap between subjectively defined groups will be common. Nonetheless, ariaDNE values of carnassial teeth will give a good indication as to whether a tooth is closer to a weakly or highly carnassialized condition.

Studies applying DTA methods to carnassial teeth prior to this are relatively rare. The Orientation Patch Count (OPC) method was used as a proxy for complexity to compare carnivoran and rodent molar tooth rows of taxa with different dietary adaptations and was able to distinguish carnivorous, omnivorous and herbivorous taxa in both groups (Evans et al., 2007). Further, the Orientation Patch Count Rotated (OPCR) of carnivoran and rodent molar tooth rows and individual molars confirmed the results of the former study, showing that lower molars are better indicators of diet and isolated molars show a stronger phylogenetic signal (Evans & Jernvall, 2009). The OPCR was used to measure the complexity of the molar tooth rows of carnivoran and dasyuromorph taxa. The OPCR values showed overlapping values of the carnivoran and dasyuromorph taxa, which could be a result of sampling rather than an actual adaptive signal (Smits & Evans, 2012). Pineda-Munoz et al. (2017) included carnivoran taxa among Rodentia, Primates and Diprotodontia to compare dietary adaptations of a total of 134 species using the OPCR of individual teeth as well as complete post-canine tooth rows, showing that dental topography is well correlated with dietary

adaptations in all included groups. Hyaenodont teeth have not yet been included in studies employing DTA.

DNE quantification has mostly been applied to Primates so far (Bunn et al., 2011; Winchester et al., 2014; Prufrock et al., 2016; Berthaume, & Schroer, 2017; López-Torres et al., 2017; Berthaume et al., 2018; Pampush et al., 2018; Berthaume et al., 2019; Fulwood, 2020; Li et al., 2020), although it has also been used for rodents (Renaud & Ledevin, 2017), meridiolestidans (Harper et al., 2019), scandentians (Selig et al., 2018; Selig et al., 2019b; Selig et al., 2020) and suids (Rannikko et al., 2020). Typically, DNE is interpreted as being sensitive to height and sharpness of cusps, and therefore the overall shearing ability (Bunn et al., 2011). However, my study implies that the number of functional features (namely crests and cusps) on the occlusal surface of a molar has an equally high impact on calculated DNE. As shown by Winchester et al. (2014), molars of insectivorous platyrrhines and "prosimians" with multiple steep cusps have significantly higher DNE values than molars of hard object feeders, which have a blunted occlusal surface. In this case, the occlusal surface may be interpreted as "low-cusped" (in comparison to the insectivorous condition) or "simplified", as the individual cusps are largely reduced or absent. In the case of highly derived carnassialized teeth, only the latter can be attributed to the molar morphology. The surface is simplified, as multiple cusps have been reduced, but the molar crown itself shows a high relief with steep shearing walls, exhibiting a large simple shearing blade. Thus, surface areas with high curvature are less abundant. The functional result found in the cheek teeth of hard object feeders and highly specialized meat eaters can equally be described as "simplified". In case of hard object feeders, tooth function is reduced to a simple crushing function, in case of meat eaters tooth function is a simple shearing function. Both cases of functional reduction are reflected by low ariaDNE values.

The distribution of ariaDNE values of carnassials with different functional structures present supports this assertion. Presence of higher ariaDNE values in Carnivora with specialized carnassials and a still functional talonid (as in canids) compared to carnassials where the talonid is absent (as in felids) thus implies a potential difference in functional, and ultimately adaptive versatility. Teeth with a functional talonid are able to process food via crushing, which expands the range of potential food items. This may be one explanation as to why specialized clades of North American canids over the last 40 million years were less prone to extinction than saber toothed cats, as discussed in Balisi & Van Valkenburgh (2020).

5.4 Morphospace analysis

A large proportion of variance (41.4 %) in the morphospace is explained by enlargement of the carnassial blade and reduction of the talonid. The change in the cervix line from an approximately symmetrical shape (with mesial and distal flexures of similar size) to an asymmetrical shape (with an enlarged mesial flexure and a reduced distal flexure) also accounts for the variance. The shape change of the cervix line can be explained by the presence of a mesial and a distal root of similar size in basal carnassials, while in derived carnassials, there is a tendency to enlargement of the mesial root and reduction of the distal root. Relative size changes of the mesial carnassial blade and the distal talonid basin cause similar size changes in the respective roots, which act as mechanical support for the crown structures. The cervix line, marking the intersection of crown and root, captures these relative size changes. The shape change along the axis of PC1 divides basal carnassials from derived carnassials in Carnivora, Dasyuromorphia and Hyaenodonta and can be interpreted as a signal of functional adaptation to a more or less pronounced carnivorous diet. The carnassial shape analysis of the carnivoran m1 and the didelphimorph and dasyuromorph m3 and m4 by Tarquini et al. (2020) indicates an overarching signal of carnassial blade enlargement as well as metaconid and talonid reduction (Fig. 72). The results of the morphospace analysis are consistent with this observation. The most extreme values in the analysis are found in *Hyaenodon* spp., *Crocuta* and Felidae with derived carnassials in the negative morphospace, and in *Proviverra*, Feliformia with basal carnassials and the MCPs and ICPs of *Dasyurus* spp. in the positive morphospace. There is an overlap of the dasyuromorph basal PCPs with the dasyuromorph derived MCPs and ICPs. This indicates that within the Dasyuromorphia, basal PCPs are as specialized as the derived MCPs and ICPs. Basal caniform carnassials occupy a spectrum between the most unspecialized carnivoran carnassials (viverrids and herpestids) and caniforms with derived carnassials (*Canis*, *Lycaon*, *Speothos*). None of the caniform carnassials are as specialized as the carnassials of feliforms with derived carnassials, which occupy a spectrum of lower PC1 scores. Two hyaenodonts with derived carnassials (*Oxyaenoides* and *Pterodon*) overlap with the Caniformia. The dasyuromorph derived PCPs of *Sarcophilus* and *Thylacinus* are more specialized than that of the Caniformia and overlap with some derived carnassials of the Feliformia. The successive mesio-distal shape shift observed in the distribution of PC1 scores of the lower carnassials of *Hyaenodon*, *Oxyaenoides*, *Sarcophilus* and *Thylacinus* indicates a differential adaptation of the individual

carnassials in more specialized taxa (see discussion below). Tarquini et al. (2020) concluded, that the m4 of didelphimorphs and dasyuromorphs is a better analogue to the carnivoran m1 and is more modified than the m3. This conclusion is supported by the results of the morphospace analysis, indicating that the PCP in dasyuromorphs as well as hyaenodonts is indeed the most specialized in all taxa that were examined, with the two mesial carnassials being less specialized.

The shape change along the axis of PC2 indicates slightly longitudinally elongated carnassials, as delineated by the cervix line in the Caniformia and the Feliformia with basal carnassials, scoring low values. These overlap with the carnassials of *Hyaenodon*, *Crocuta* and *Dinictis*, while the remaining data points have much higher PC2 scores, which indicates slightly mesio-distally compressed carnassials (Fig. 72). Highest PC2 scores are found among the derived carnassials of Feliformia (e.g., *Felis silvestris*), Dasyuromorphia (e.g., *Sarcophilus*) and Hyaenodonta (e.g., *Oxyaenoides* and *Pterodon*).
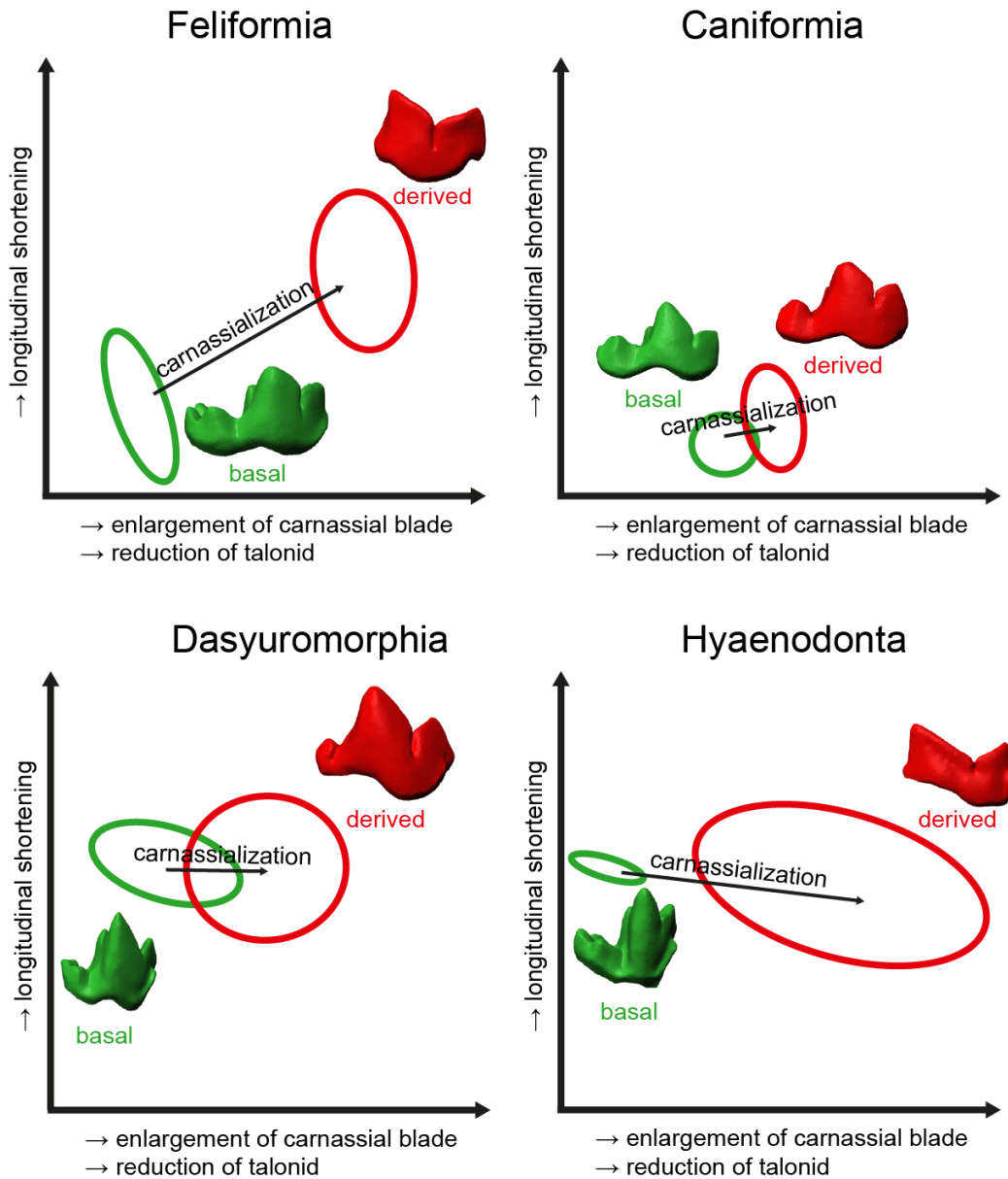
Fig. 72: Schematic illustration of the carnassial shape changes observed in the morphospace analysis in the Feliformia, with examples of an m1 of *Viverra tangalunga* (SMF 697) and *Felis silvestris* (ZFMK MAM 2018.0106), in the Caniformia, with examples of an m1 of *Vulpes vulpes* (IGPB M 6238) and *Canis lupus* (, SMF 15 699), in the Dasyuromorphia, with examples of an m4 of *Dasyurus viverrinus* (SMF 1480) and *Thylacinus cynocephalus* (ZMB_Mam_036877) and in the Hyaenodonta, with examples of an m3 of *Proviverra typica* (NMB En.179) and *Hyaenodon filholi* (MNHN.F.Qu 8421). Rendering of µCT data.

5.5 Mesio-distal carnassialization in the Dasyuromorphia and Hyaenodonta

Section 5.5 has been modified and published in: Lang, A. J., Engler, T., & Martin, T. (2021). Dental topographic and three-dimensional geometric morphometric analysis of carnassialization in different clades of carnivorous mammals (Dasyuromorphia, Carnivora, Hyaenodonta). *Journal of Morphology*, 283(1), 91 – 108.

Carnassialization along the tooth row of dasyuromorph and hyaenodont dentitions increases from the mesial to the distal tooth positions. This is indicated by the shift of PC1 scores within the lower tooth row of most investigated taxa with derived carnassial dentitions (*Hyaenodon* spp., *Oxyaenoides bicuspidens*, *Sarcophilus harrisii*, *Thylacinus cynocephalus*) with the exception of *Pterodon dasyuroides*. The shift is not present in basal carnassial dentitions (*Dasyurus* spp. and *Proviverra typica*). *In all taxa with multiple carnassials, the PCP is the most specialized, indicated by the most negative PC1 score among all teeth of the individual molar row.* This indicates that a successive mesio-distal shift is expressed with increasing carnassialization of the overall tooth row. Increasing carnassialization on the most distal (principal) carnassial is further indicated by the cloud-to-cloud comparison of molars of individual tooth rows. In all taxa, the MCPs and the ICPs show low surface deviations to one another, while the deviations in the MCP/PCP and ICP/PCP comparisons are respectively higher. The highest deviation values consistently occur at the distal end of the teeth, in the talonid region. The calculated distance values mainly show differences in the distal flexure of the carnassial, which is explained by a reduction of the distal flexure in the more carnassialized PCP. Additionally, high distances are calculated on the cusps of the talonid (hypoconid, hypoconulid, entoconid), which indicates the reduction of these cusps in the PCP. It has to be considered that differential tooth wear also has some influence on the calculated surface deviations. Apical wear typically advances from the mesial to the distal tooth position, and some punctiform areas of high distance values on the apices of trigonid cusps, especially the paraconid and protoconid, may be explained by tooth wear. Further, in two taxa (*P. dasyuroides* and *P. typica*) teeth of multiple specimens were used for the surface comparison. Some of the higher surface deviations in these two taxa may also be explained by differences in tooth wear based on different ontogenetic stages of the specimens. The most extreme scattering of high surface deviations can be found in *P. typica*, where the teeth of three specimens were included in the analysis. Nonetheless, high surface deviations also occur around the talonid, which is consistent with the pattern seen in the other taxa.

5.6 Phylogenetic signal

Section 5.6 has been modified and published in: Lang, A. J., Engler, T., & Martin, T. (2021). Dental topographic and three-dimensional geometric morphometric analysis of carnassialization in different clades of carnivorous mammals (Dasyuromorphia, Carnivora, Hyaenodonta). *Journal of Morphology*, 283(1), 91 – 108.

The ancestral state reconstruction for the PCPs of Carnivora, Dasyuromorphia and Hyaenodonta indicates that the basal carnassial state for all three groups is not much different from the base state of the mammalian tree (split point of Eutheria and Metatheria) for ariaDNE values and PC1 scores. The deviation for ariaDNE values from the base of the tree is around 3.2% to 5.1% for all orders, with the highest difference between Carnivora and Hyaenodonta (8.5%). For the PC1 scores, the ancestral state of the individual orders deviates between 1.2% and 7.7% from the base state of the tree, with the highest difference between Carnivora and Hyaenodonta (13%). Thus, moderate deviation around 10% indicates that the ancestral conditions for the studied higher taxa were generally similar. Reduced crown curvature and carnassial blade enlargement relative to a reduced talonid basin in highly carnassialized teeth within the different taxonomic groups points to a uniform ancestral state regarding this aspect of morphology.

The ancestral state reconstruction for the PC2 scores indicates a high deviation of the carnivoran base state from the base state of the tree (25.8%), whereas it is much lower in Hyaenodonta and Dasyuromorphia (3.0% respectively 10.4%). The deviation of the base state of the Carnivora to that of the Dasyuromorphia is 36.2% and to that of the Hyaenodonta it is 28.7%, whereas it is 7.4% between the Dasyuromorphia and the Hyaenodonta. All this points to an ancestral state of the Carnivora within the morphospace of PC2 scores which differs considerably from that of the Hyaenodonta and the Dasyuromorphia, as well as the base of the tree. The presence of carnassials with a somewhat mesio-distally (longitudinally) elongated crown base (Fig. 73) may thus be a plesiomorphic feature of the Carnivora. If this is true, a carnassial with a slightly mesio-distally compressed crown base evolved multiple times in the Feliformia with derived carnassials (Eupleridae, Felidae, Hyaenidae, Nimravidae) and is a specific derived state within the Carnivora. One possible explanation for this adaptation is the shortening of the rostrum in cat-like ecomorphs (see discussion below).

Tarquini et al. (2020) found a dietary signal of dasyuromorph and carnivoran carnassials to be phylogenetically structured. The morphospace analysis indicates that a phylogenetic structuring is also present between weakly and strongly carnassialized molars, and that hyaenodont carnassials are generally more similar in shape to those of dasyuromorphs than of carnivorans.

Further, the UPGMA cluster analysis points to a difference between basal carnassial morphotypes and a signal of convergence with increasing carnassialization. The individual basal carnassial tooth positions of the tooth row of dasyuromorphs and hyaenodonts respectively cluster together, and they are recovered together in a cluster separate from the basal carnivoran m1. This indicates that the basal dasyuromorph m2, m3 and m4 shapes are more similar to the basal hyaenodont m1, m2 and m3 shapes than to the basal carnivoran m1 shape. This difference can be explained with the observed shape changes in the PC2 dimension, with the basal carnivoran m1 occupying the more negative spectrum. In addition to this, the phylogenetic clustering of the dasyuromorph and hyaenodont carnassials is only partially maintained in derived carnassials. Only the dasyuromorph m2 and m3 are clustering together, which is in congruence with the hyaenodont m1 and m2 clustering together. As discussed above, this can be explained with the differential shape shift of dasyuromorph and hyaenodont carnassials in the PC1 dimension which correlates with increasing carnassialization (enlagement of the carnassial blade, reduction of the talonid basin). The most carnassialized teeth of the dasyuromorph and hyaenodont tooth row are the most distal tooth positions. In the cluster analysis, these are forming a cluster together with the derived carnivoran m1. This indicates an increasing signal of convergent evolution with increasing carnassialization, where the initial apomorphic structural differences are lost and the teeth approximate a similar, simplified shape.
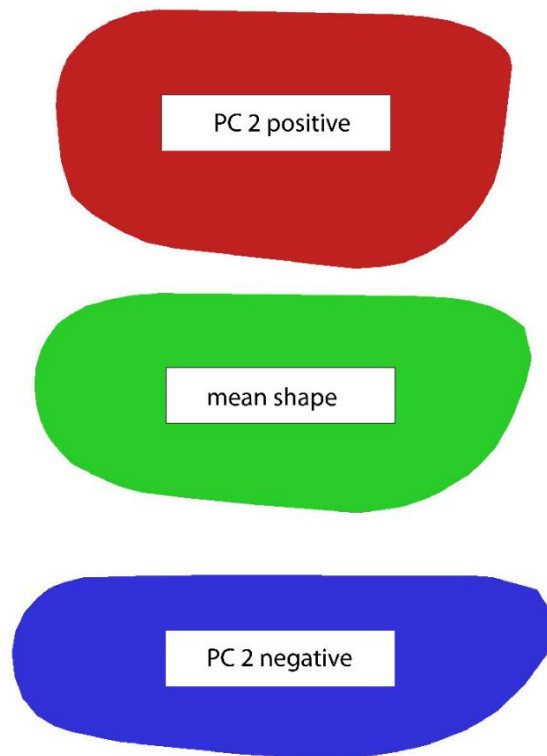
Fig. 73: "Footprint" of the shape of lower right carnassials based on the shape of the cervix line in the PC2 dimension at a positive score (0.1), the mean shape score (0) and a negative score (-0.1). The planes were created as mean planes of the cervix line in PolyWorks and are shown in occlusal view. A relative mesio-distal compression can be seen in the shape with a positive score, whereas the shape with a negative score is mesio-distally elongated. Mesial is to the right.

5.7 Blade alignment and reduction of "secondary occlusal features"

In carnassial dentitions, "secondary occlusion" not related to carnassial cutting is being reduced with increasing carnassialization. Selective pressure is driving enlargement of the carnassial blades and reduction of protocone/talonid occlusion. Although the overarching changes in carnassial crown structure and function indicate a convergent pattern, the specific carnassial shape that is found among carnivoran carnassials is an indicator for a different functional effectiveness, especially in basal carnivoran carnassials. The calculated carnassial blade angles for lower carnassials reveal some general trends for blade alignment:

1. A longitudinal (mesio-distal) blade alignment is approximated with increasing carnassialization.
2. A transversal blade alignment is typical for weakly carnassialized teeth.
3. A longitudinal blade alignment in weakly carnassialized teeth is only found among carnivorans.

This indicates a link between the more longitudinal elongated carnassial shape in carnivorans and the presence of a longitudinally aligned carnassial blade in combination with a fully functional talonid basin. A possible difference between the homodont cheek dentitions of

dasyuromorphs and hyaenodonts to the heterodont cheek dentitions of carnivorans regarding selective pressure may be present resulting from the number of carnassial teeth present in the tooth row. In tribosphenic dentitions, the individual teeth perform cutting and crushing functions (Schultz & Martin 2014). The occlusal pattern of basal carnassial dasyuromorph and hyaenodont teeth is generally similar to the tribosphenic occlusion. The presence of a functional talonid basin poses both an advantage regarding multifunctionality, as a crushing can be performed, as well as an obstacle in the enlargement and realignment of the carnassial blades, hindering a more effective processing of meat. The reason for this is that "embrasure shearing", defined by one lower molar occluding between two upper antagonists, is a plesiomorphic condition in therians (Kielan-Jaworowska et al. 2004). Embrasure shearing requires the shearing blades to be transversally oriented in relation to the mesio-distal axis of the tooth. This pattern is also present in the basal carnassial dentitions of dasyuromorphs and hyaenodonts, but in carnivorans the P4/m1 carnassial blades bay be longitudinally realigned and perform a more effective cutting. Thus, a carnassial cutting function can be performed while the blunt post-carnassial teeth perform a crushing function. The selective pressure to evolve a more carnassialized morphology being present in just one tooth position of the tooth row in carnivorans enabled the re-alignment of the carnassial blade while maintaining multifunctionality. This explains the elongated carnassial shape, giving space to a mesio-distally aligned carnassial blade and a crushing basin. In contrast to this, dasyuromorph and hyaenodont lineages had to overcome embrasure shearing by realigning the carnassial blades on all carnassial tooth positions. Thus, there may have been a greater selective pressure to reduce the talonid basin and the associated crushing function. A tooth row with multiple carnassial blades, all with a longitudinal alignment, is approximated with increasing carnassialization, with the most extreme condition found in the various species of *Hyaenodon*. Instead of embrasure shearing, a continuous cutting function is performed with the mesio-distally oriented carnassial blades, at expense of the crushing talonid structures of the individual teeth which get reduced.

5.8 Implications for functional constraints

Section 5.8 has been modified and published in: Lang, A. J., Engler, T., & Martin, T. (2021). Dental topographic and three-dimensional geometric morphometric analysis of carnassialization in different clades of carnivorous mammals (Dasyuromorphia, Carnivora, Hyaenodonta). *Journal of Morphology*, 283(1), 91 – 108.

The results of the DTA (ariaDNE) and the GMA (PC1 scores) indicate a functional reduction of highly carnassialized molars relative to more basal carnassial conditions for dasyuromorph, carnivoran and hyaenodont taxa. It is most likely that all late surviving Hyaenodonta (which

include one species of *Hyaenodon*) were affected by this functional reduction. Interestingly, the carnivoran taxa in this study for which a basal carnassialized and potentially multifunctional crown is indicated, are all extant taxa (*Civettictis*, *Ichneumia*, *Viverra*, *Vulpes*). The cheek dentition of these taxa is overall very close to the plesiomorphic heterodont, "generalized" condition (Gregory & Hellman, 1939). This ancestral condition of the Carnivora, inherited from the Carnivoramorpha, is characterized by restricted shear at one pair of carnassial teeth (P4/m1) (Flynn & Wesley-Hunt, 2005). All derived specialized carnivorous or herbivorous carnivoran dentitions evolved from this carnassial type. The ancestral condition of the Carnivora is thus a heterodont cheek dentition formed by cutting carnassials and crushing post-carnassials in contrast to the homodont ancestral condition of the Hyaenodonta and Dasyuromorphia, which is closer to the plesiomorphic homodont tribosphenic cheek dentition (although the most distal upper molars may become vestigial). The limited adaptive diversity of marsupial carnivores has been linked to their molar dentition, as it is interpreted as less versatile than that of (non-specialized) carnivorans (Van Valkenburgh, 1999). It is indicated that in the generalized carnivoran taxa not only the heterodont condition of the cheek dentition, but also the functional morphology of the carnassial tooth itself points to a higher versatility in function. Within multiple carnivoran lineages (Vulpini, Herpestidae, and Viverridae) the ancestral and more versatile carnassial morphotype has been retained. The presence of a talonid in these longitudinally elongated carnassials makes it possible to crush a more diverse range of food items in addition to carnassial meat cutting. This is in conformity with the results of the DTA, where the lowest values of crown curvature within the Carnivora, indicating a reduction or absence of talonid function, are found in specialized feliforms, whereas caniforms and non-specialized feliforms show higher values. The DTA can, however, not distinguish unspecialized carnassials of the longitudinally elongated type in carnivorans from unspecialized carnassials which are longitudinally short, as seen in dasyuromorphs and hyaenodonts. The evolutionary success of the Carnivora in comparison to the Hyaenodonta may have been largely influenced by the retention of the ancestral ("basal") morphotype throughout their evolutionary history.

The significance of an adaptive difference in carnassial dentitions has been discussed for almost a century now. Butler (1946) proposed that the dental condition of the modern Carnivora and their ancestors has more evolutionary plasticity as it provides more functional diversity compared to the functionally restricted condition of the extinct Hyaenodonta and Oxyaenodonta. From this functionally versatile condition, carnivorans were able to evolve more carnassialized cheek teeth as well as adaptations with a greater emphasis on the crushing function and reduced carnassial cutting multiple times throughout the Cenozoic (Van Valkenburgh, 2007). The fact that specialized carnivorous "Creodonta" were replaced by carnivorans which retained more generalized adaptations during the Eocene in North America

(Friscia & Van Valkenburgh, 2010) supports the idea of more plasticity in the ancestral heterodont condition of the Carnivora. Afro-Arabian hyainailouroid taxa survived into the Middle Miocene, but if the dispersal of Carnivora played a role in their eventual demise is not known (Borths & Stevens, 2017a). The Carnivora very likely contributed in some way to the extinction of the Hyaenodonta. A difference in the functional morphology and the resulting adaptive potential of the carnassials is one possible factor to consider.

There have been numerous ways to assess the evolutionary pros and cons of the specialization to a carnivorous diet among mammals. The overarching picture of the "costs of carnivory" indicates that specialization to a carnivorous diet hinders a subsequent adaptation to another diet, mostly due to craniodental modifications (Holliday & Steppan, 2004). In the fossil record, this results in a repeated pattern of carnivorous clades specializing to a highly carnivorous diet, going extinct and getting replaced by another clade (Van Valkenburgh, 2007). Holliday (2010) also detected a morphological constraint in the molars of Carnivora with a specialized carnivorous diet, which inhibits reversal to a more generalized condition. It is of great importance to note that the pattern of evolutionary constraint in molars of carnivorous mammals is most likely not restricted to the Carnivora alone, but applies to all carnivorous groups with highly carnassialized cheek teeth. This is due to the highly convergent character of molar functional morphology among even the most distantly related taxa with carnivorous adaptations (e.g., metatherians and eutherians).

Studies on the character change of specialized carnivorous molars indicate that inhibited reversed evolution to a more generalized condition has a greater influence on the evolution of increasingly specialized carnassials than directional selection (Holliday, 2010). The tendency of specialized carnivorous lineages to go extinct rather than responding by increased phenotypic specialization has been described as an "evolutionary ratchet" by Van Valkenburgh et al. (2004). The Hyaenodonta may have been influenced to a higher degree by increased vulnerability to extinction. By looking at the evolutionary history of the Carnivora and the Hyaenodonta and comparing changes in tooth morphology as well as adaptive and taxonomic diversity, it seems that due to higher ecomorphological diversity the Carnivora were less severely influenced by constraints of extreme carnivorous specialization in their dentition, and as a group recovered from intraphyletic extinctions. The Hyaenodonta showed lower adaptive diversity and this may have been an evolutionary disadvantage.

The cause for functional restriction in dasyuromorph and hyaenodont carnassial dentitions, reflected by similar morphospace occupancy in this study, does not seem to be the pattern of tooth eruption which differs greatly between both groups. Both the morphological confinement to the carnassialized condition as well as the eruption patterns themselves seem to be the result of the selective pressure to extend carnassial functionality during ontogeny. Werdelin (1987) proposed the hypothesis that the successive eruption of carnassials in the

Dasyuromorphia forces each carnassial to function as the main cutting tooth until this function is taken over by the subsequently erupting distal carnassial until all molars are erupted, thus forcing all molars to become highly carnassialized. It seems plausible that the resulting functional constraint may be a result of the reduced marsupial tooth replacement. In the Hyaenodonta, however, the picture is quite the opposite. In *Hyaenodon* and specialized hyainailourid taxa, deciduous carnassials are replaced late in ontogeny, and there is always one premolar position (p3 or p4) which erupts after the last permanent carnassial (m3) has erupted (Bastl & Nagel, 2013; Borths & Stevens, 2017b). Adaptations for longevity of the carnassial function during ontogeny have been demonstrated in other examples, such as wide and stout metastyles in *Hyainailouros* providing more enamel for abrasion (Borths & Stevens, 2019) or the extreme example of upper carnassial rotation in the late ontogeny of *Hyaenodon* (Mellett, 1977). All these adaptations, including the tooth eruption, seem to contribute to extended carnassial functionality and play a role in the resulting functional constraint and the morphological similarities that were observed in dasyuromorphs and hyaenodonts, namely longitudinally shortened carnassials (in contrast to carnivorans except specialized feliforms) and increasing carnassialization from the mesial to the distal carnassial positions in specialized taxa.

The question remains, what enabled the carnivoran carnassial to remain in a functional-morphological equilibrium in several lineages up until present times. Previous studies have pointed out an affinity between the carnassial morphology of caniform and unspecialized feliform taxa (namely viverrids and herpestids) (Crusafont-Pairó & Truyols-Santonya*, 1956;* Meloro & Raia, 2010; Tarquini et al. 2020). Caniform, viverrid and herpestid taxa also occupy a unique morphospace in the GMA, separate from all carnassials of dasyuromorphs, hyaenodonts and specialized feliforms. The analysis of ancestral state reconstructions points to a possible retention of a plesiomorphic carnivoran trait in these taxa. This trait, associated with a longitudinally elongated crown base and a low cutting blade which enables the presence of a cutting blade in mesio-distal orientation as well as a fully functional talonid basin, may have played a key role in the adaptive success of the Carnivora (Fig. 74).

Vulpes vulpes (m1)

functional talonid basin: carnassial blade / mesial vector angle:
efficient crushing   low → efficient cutting
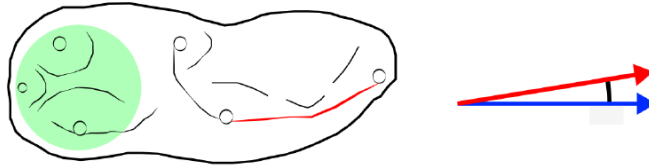
Felis silvestris (m1)

no talonid basin: carnassial blade / mesial vector angle:
no crushing   low → efficient cutting
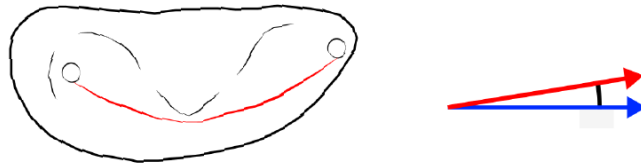
Proviverra typica (m1 - m3)

functional talonid basin: carnassial blade / mesial vector angle:
efficient crushing   high → inefficient cutting
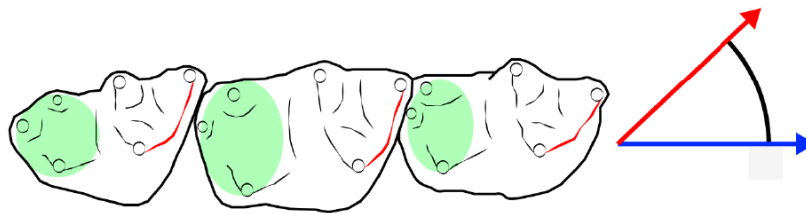
Hyaenodon exiguus (m1 - m3)

no talonid basin: carnassial blade / mesial vector angle:
no crushing   low → efficient cutting

mesial
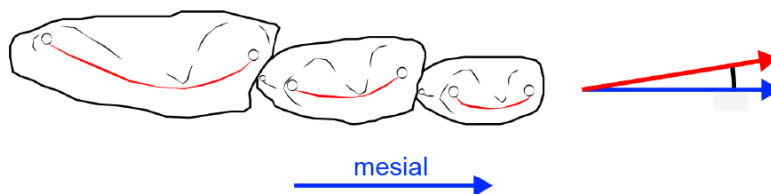
Fig. 74: The differences of functionality between the basal carnivoran carnassial condition with a longitudinally oriented carnassial blade (*Vulpes vulpes*), the basal hyaenodont carnassial condition with transversally oriented carnassial blades (*Proviverra typica*) and two taxa with a derived carnassial condition (*Felis silvestris* and *Hyaenodon exiguus*). The basal carnivoran condition combines a crushing function of the talonid with an efficient carnassial cutting, which his enabled by a longitudinal elongation of the tooth. Teeth in occlusal view.

5.9 Linkage between carnassial and skull shape

The foreshortening of the rostrum enables greater bite forces at the anterior section of the jaw, e.g. the incisors and canines, as they are positioned closer to the jaw joint (Van Valkenburgh, 2007). The most extreme modifications linked to this evolutionary trend of rostrum-foreshortening are found in saber-tooth adaptations, where the canines are elongated in an extreme way. Within the Feliformia, saber-tooth dentitions evolved in the Felidae (Machairodontinae) (Barycka, 2007) and, if classified as feliforms, also the Nimravidae including the Barbourofelinae (after Wang et al., 2020). From personal observation, when overall comparing the relative canine size of felids to the relative canine size of canids, a general trend to exhibit larger canines can be seen in felids. The extant felid *Neofelis nebulosa* even shares some dental and other cranial affinities with extinct saber-toothed taxa (Christiansen, 2006). The carnassials of saber-toothed felids will very likely occupy a morphospace together with the other felids, as they exhibit highly similar craniodental adaptations. Further, highly specialized carnivorous Hyaenids such as *Crocuta crocuta* have foreshortened rostra, which makes them employ their premolars in a bone-crushing function, unlike in the extinct caniform Borophaginae which used the more distal molars (Van Valkenburgh, 2007). And even in the euplerid *Cryotoprocta ferox*, rostrum-foreshortening due to a high adaptation to a carnivorous diet evolved convergently (Van Valkenburgh, 2007). It may thus be postulated, that within the Feliformia, taxa that become specialized to a carnivorous diet generally show a tendency to rostrum-foreshortening, as seen in felids, hyaenids, nimravids and one euplerid taxon. All these taxa converge in the same morphospace in my analysis (see Fig. 75).

Interestingly, saber-tooth modifications also evolved in the oxyaenodont Machaeroidinae (Zack et al., 2021). This group offers an opportunity to test the proposed hypothesis. Oxyaenodonts differ from hyaenodonts by the reduction of their posterior molars (M3/m3) and they tend to foreshorten the rostrum (Thenius, 1989). Thus, in terms of skull morphology, the Oxyaendonta share many similarities with the Felidae. If included in the geometric morphometric analysis of carnassials, it is here postulated that oxyaenodont carnassials may occupy a similar morphospace to the specialized Feliformia. From the perspective of adaptive versatility, the Oxyaenodonta share the worst of both worlds. They have a reduced posterior dentition and an emphasis on rostrum-foreshortening, as seen in specialized Feliformia, and all their remaining molars are carnassialized, as seen in the Hyaenodonta and specialized Dasyuromorphia. Thus, selective pressure would have resulted in quick carnassialization and reduction of dental multifunctionality, weakening the adaptive potential.
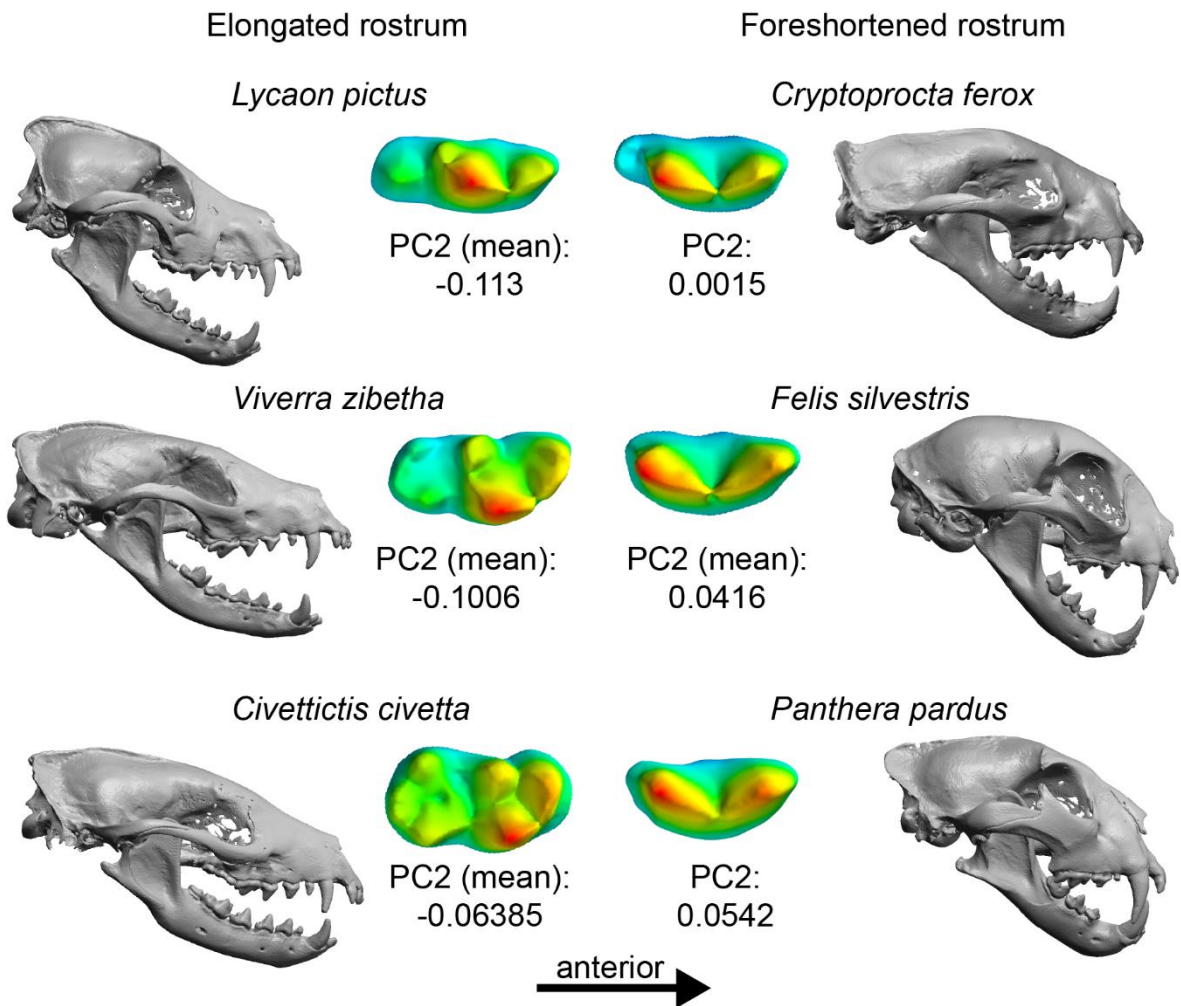
Fig. 75: Carnivoran skulls with an elongated rostrum, as exemplified by *Lycaon pictus* (ZFMK MAM 2001.0275), *Viverra zibetha* (ZFMK MAM 1968.0085) and *Civettictis civetta* (ZFMK MAM 1993.0705), compared to carnivoran skulls with a foreshortened rostrum, as exemplified by *Cryptoprocta ferox* (ZFMK MAM 1987.0584), *Felis silvestris* (ZFMK MAM 2018.0100) and *Panthera pardus* (ZFMK MAM 1997.0547) in lateral view. Next to the skull the respective right side m1 position is shown in occlusal view as a topographic height model. Lower PC2 values correspond with a relative mesio-distal elongation of the tooth. Pictures not to scale. Rendering of μCT data..

6. Conclusion

Carnassialization in Carnivora, Dasyuromorphia and Hyaenodonta involves specific changes of dental functionality, topography and shape, which have evolved independently of phylogeny and tooth position. In dasyuromorph and hyaenodont taxa, which have multiple carnassials per tooth row, the most distal carnassial is the most specialized, which exhibits the same shape changes that occur between taxa with weak and strong carnassialization. In more specialized taxa, there is a tendency to a successively increasing mesio-distal carnassialization along the tooth row.

The overall convergent adaptive trend of carnassialization can be described as a simplification of tooth morphology, resulting in teeth with less structural complexity and functional versatility. The simplification occurs specifically in regards to the protocone/talonid crushing function. Moreover, there is a tendency to switch from a plesiomorphic "embrasure shearing" of tribosphenic teeth to a cutting function with mesio-distally oriented blades. There are indications that the changes of crown morphology linked to carnassialization follow a pattern of structural reversal to an ancestral pretribosphenic condition, with the possible re-emergence of pretribosphenic molar functionality in carnassials that exhibit a functional unicuspid talonid. Despite carnassialization being mainly driven by convergent evolution, differences are apparent in the basal carnivoran carnassial condition in comparison to dasyuromorphs and hyaenodonts. It seems that carnivorans, having evolved only one carnassial within the tooth row, may have diminished the functional obstacles linked to carnassialization to some extent. Basal carnivoran carnassials exhibit a mesio-distal elongation, enabling a mesio-distal alignment of the carnassial blade, which increases the carnassial cutting function. At the same time, the crushing structures of the carnassial tooth and the post-carnassial teeth are maintained, preserving multifunctionality of the dentition. In contrast to this, mesio-distal re-alignment of the multiple carnassial teeth in the tooth row of dasyuromorphs and hyaenodonts may have resulted in more frequent loss of multifunctionality, as selective pressure would favor the evolution of mesio-distally oriented carnassial blades on the individual tooth positions at expense of the crushing function. This study further solidifies a unique morphospace occupancy of caniform and unspecialized feliform carnassials, based on longitudinal elongation and a low carnassial blade, which is not present in dasyuromorphs and hyaenodonts.

7. References

Adams, D., Collyer, M., Kaliontzoloulou, A., & Baken, E. (2021). Package "geomorph": Read, manipulate and digitize landmark data, generate shape variables via Procrustes analysis for points, curves and surfaces, perform shape analyses, and provide graphical depictions of shapes and patterns of shape variation. *R package version 4.0.0*. Retrieved from https://cran.r-project.org/web/packages/geomorph.

Archer, M. (1976). The dasyurid dentition and its relationships to that of didelphids, thylacinids, borhyaenids (Marsupicarnivora) and peramelids (Peramelina: Marsupialia). *Australian Journal of Zoology Supplementary Series*, 24(39), 1 – 34.   https://doi.org/10.1071/AJZS039

Archer, M., Christmas, O., Hand, S. J., Black, K., Creaser, P., Godthelp, H., Graham, I. T., Cohen, D. R., Arena, D. A., Anderson, C., Soares, G. G., Machin, N., Beck, R. M., Wilson, L. A., Myers, T. J., Gillespie, A. K., Khoo, B. Y., & Travouillon, K. J. (2016). Earliest known record of a hypercarnivorous dasyurid (Marsupialia), from newly discovered carbonates beyond the Riversleigh world Heritage area, north Queensland. *Memoirs of the Museum of Victoria*, 74, 137 – 150.

Asher, R. J., Horovitz, I., & Sánchez-Villagra, M. R. (2004). First combined cladistic analysis of marsupial mammal interrelationships. *Molecular Phylogenetics and Evolution*, 33, 240 – 250. https://doi.org/10.1016/j.ympev.2004.05.004

Averianov, A., Obraztsova, E., Danilov, I., Skutschas, S., & Jin, J. (2016). First nimravid skull from Asia. *Scientific Reports*, 6, 25812. https://doi.org/10.1038/srep25812

Balisi, M.A., & Van Valkenburgh, B. (2020). Iterative evolution of large-bodied hypercarnivory in canids benefits species but not clades. *Communications Biology*, 3, 461. https://doi.org/10.1038/s42003-020-01193-9

Barrett, P. Z. (2016). Taxonomic and systematic revisions to the North American Nimravidae (Mammalia, Carnivora). *PeerJ*, 4:e1658. https://doi.org/10.7717/peerj.1658

Barry, J. C. (1988). *Dissopsalis*, a middle and late Miocene proviverrine creodont (Mammalia) from Pakistan and Kenya. *Journal of Vertebrate Paleontology*, 8, 25 – 45. https://doi.org/10.1080/02724634.1988.10011682

References

Barry, J. C., Behremsmeyer, A. K., & Monaghan, M. (1980). A geologic and biostratigraphic framework for Miocene sediments near Khaur Village, northern Pakistan. *Postilla*, 183, 1 – 19.

Barycka, E. (2007). Evolution and systematics of the feliform Carnivora. *Mammalian Biology*, 72, 257 – 282. https://doi.org/10.1016/j.mambio.2006.10.011

Bastl, K., & Nagel, D. (2013). First evidence of the tooth eruption sequence of the upper jaw in *Hyaenodon* (Hyaenodontidae, Mammalia) and new information on the ontogenetic development of its dentition. *Paläontologische Zeitschrift*, 88, 481 – 494. https://doi.org/10.1007/s12542-013-0207-z

Bastl, K., Nagel, D., & Peigné, S. (2014). Milk tooth morphology of small-sized *Hyaenodon* (Hyaenodontidae, Mammalia) from the European Oligocene – evidence of a *Hyaenodon* lineage in Europe. *Palaeontographica*, 303, 61 – 84. https://doi.org/10.1127/pala/303/2014/61

Beck, R. M. D., Godthelp, H., Weisbecker, V., Archer, M., & Hand, S. J. (2008). Australia's Oldest Marsupial Fossils and their Biogeographical Implications. PLoS ONE, 3(3), e1858. https://doi.org/10.1371/journal.pone.0001858

Benazzi, S., Kullmer, O., Grosse, I. R., & Weber, G. W. (2011). Using occlusal wear information and finite element analysis to investigate stress distributions in human molars. *J Anat*, 219(3), 259 – 72. https://doi.org/10.1111/j.1469-7580.2011.01396.x

Benton, M. J., & Donoghue, P. C. J. (2007). Paleontological evidence to date the tree of life. Mol. Biol. Evol., 24(1), 26 – 53. https://doi.org/10.1093/molbev/msl150

Berkovitz, B., & Shellis, P. (2018). Chapter 4 – Monotremata and Marsupialia. In Berkovitz, B., & Shellis, P. (Eds.), *The Teeth of Mammalian Vertebrates* (pp. 57 – 74). Academic Press. https://doi.org/10.1016/B978-0-12-802818-6.00004-1

Berta, A., Chuchill, M., & Boessenecker, R. W. (2018). The Origin and Evolutionary Biology of Pinnipeds: Seals, Sea Lions, and Walruses. *Annual Review of Earth and Planetary Sciences*. 46, 203 – 228. https://doi.org/10.1146/annurev-earth-082517-010009

References

Berthaume, M. A., & Schroer, K. (2017). Extant ape dental topography and its implications for reconstructing the emergence of early *Homo*. *Journal of Human Evolution*, 112, 15 – 29. https://doi.org/10.1016/j.jhevol.2017.09.001

Berthaume, M. A., Delezene, L. K., & Kupczik, K. (2018). Dental topography and the diet of *Homo naledi*. *Journal of Human Evolution*, 118, 14 – 26. https://doi.org/10.1016/j.jhevol.2018.02.006

Berthaume, M. A., Winchester, J., & Kupczik, K. (2019). Effects of cropping, smoothing, triangle count, and mesh resolution on 6 dental topographic metrics. *PLoS ONE*, 14(5), e0216229. https://doi.org/10.1371/journal.pone.0216229

Biknevicius, A. R. & Van Valkenburgh, B. (1996). Design for Killing: Craniodental Adaptations of Predators. In Gitleman, J. L. (Ed.), *Carnivore behavior, ecology, and evolution* (pp. 393 – 428). Ithaca, NY: Cornell University Press. https://doi.org/10.7591/9781501745829-019

Borths, M. R., & Stevens, N. J. (2017a). The first hyaenodont from the Late Oligocene Nsungwe Formation of Tanzania: Paleoecological insights into the Paleogene-Neogene carnivore transition. *PLoS ONE*, 12(10), e0185301. https://doi.org/10.1371/journal.pone.0185301

Binfield, P., Archer, M., Hand, S.J., Black, K. H., Myers, T.J., Gillespie, A. K., & Arena, D. A. (2016). A new Miocene carnivorous marsupial, *Barinya kutjamarpensis* (Dasyuromorphia), from central Australia. *Alcheringa*, 41, 46 – 53. https://doi.org/10.1080/03115518.2016.1180029

Bon, C., Berthonaud, V., Maksud, F., Labadie, K., Poulian, J., Artiguenave, F., Wincker, P., Aury., J.-M., & Elalouf, J.-M. (2012). Coprolites as a source of information on the genome and diet of the cave hyena. *Proc. R. Soc. B.*, 279, 2825 – 2830. https://doi.org/10.1098/rspb.2012.0358

Borths, M. R., & Stevens, N. J. (2017b). Deciduous dentition and dental eruption of Hyainailouroidea (Hyaenodonta, "Creodonta", Placentalia, Mammalia). *Palaeontologica Electronica*, 20.3.55A, 1 – 34. https://doi.org/10.26879/776

References

Borths, M. R., & Stevens, N. L. (2019). *Simbakubwa kutokaafrika*, gen. et sp. nov. (Hyainailourinae, Hyaenodonta, 'Creodonta,' Mammalia), a gigantic carnivore from the earliest Miocene of Kenya. *Journal of Vertebrate Paleontology*, 39, e1570222. https://doi.org/10.1080/02724634.2019.1570222

Bunn, J. M., Boyer, D. M., Lipman, Y., St Clair, E. M., Jernvall, J., & Daubechies, I. (2011). Comparing Dirichlet normal surface energy of tooth crowns, a new technique of molar shape quantification for dietary inference, with previous methods in isolation and in combination. *American Journal of Physical Anthropology*, 145, 247 – 261. https://doi.org/10.1002/ajpa.21489

Butler, P. M. (1946). The Evolution of carnassial dentitions in the Mammalia. *Proceedings of the Zoological Society of London*, 116, 198 – 220. https://doi.org/10.1111/j.1096-3642.1946.tb00117.x

Butler, P. M. (1952). The milk-molars of Perissodactyla, with remarks on molar occlusion. *Journal of Zoology*, 121(4), 777 – 817. http://dx.doi.org/10.1111/j.1096-3642.1952.tb00784.x

Butler, P. M. (1972). Some functional aspects of molar evolution. *Evolution*, 26, 474 – 483. https://doi.org/10.1111/j.1558-5646.1972.tb01951.x

Christiansen, P. (2006). Sabertooth Characters in the Clouded Leopard (*Neofelis nebulosa* Griffiths 1821). *Journal of Morphology*, 267, 1186 – 1198. https://doi.org/10.1002/jmor.10468

Christiansen, P. (2013). Phylogeny of the sabertoothed felids (Carnivora: Felidae: Machairodontinae). *Cladistics*, 29(5), 543 – 559. https://doi.org/10.1111/cla.12008

Cope, E.D. (1879). The origin of the specialized teeth of the Carnivora. *Annals and Magazine of Natural History*, 3, 391 – 392. https://doi.org/10.1080/00222937908694109

Cope, E. D. (1884). The Creodonta. *The American Naturalist*, Vol. 18(4), 344 – 353.

Crusafont-Pairó, M., & Truyols-Santonja, J. (1956). A Biometric study of the evolution of fissiped carnivores. *Evolution*, 10, 314 – 332. https://doi.org/10.2307/2406015

Crompton, A. W. (1971). The origin of the tribosphenic molar. *Zoological Journal of the Linnean Society*, 50 (Suppl. 1): 65-87.

References

Crompton, A., & Hiiemae, K. (1969). Functional Occlusion in Tribosphenic Molars. *Nature*, 222, 678 – 679. https://doi.org/10.1038/222678b0

Crompton, A., & Hiiemae, K. (1970). Molar occlusion and mandibular movements during occlusion in the American opossum, *Didelphis marsupialis* L. *Zoological Journal of the Linnean Society*, 49, 21 – 47. https://doi.org/10.1111/j.1096-3642.1970.tb00728.x

Cuvier, F. (1825). Des dents des mammifères considérées comme caractères zoologiques. Strasbourg, Paris: F. G. Levrault, Le normant.

Dag, O., Dolgun, A., Konar, N. M., Weerahandi, S., & Ananda, M. (2019). Package "onewaytests": One-way tests in independent groups designs. *R package 2.4*. Retrieved from https://cran.r-project.org/web/packages/onewaytests.

Day, R. W., & Quinn, G. O. (1989). Comparisons of treatments after an analysis of variance in ecology. *Ecological Monographs*, 59, 433 – 463. https://doi.org/10.2307/1943075

Dickman, C., & Russell, E. (2006). Marsupials. In MacDonald, D. W. (Ed.), *The Encyclopedia of Mammals*. Oxford University Press. https://doi.org/10.1093/acref/9780199206087.001.0001

Evans, A. R. (2013). Shape descriptors as ecometrics in dental ecology. *Hystrix, the Italian Journal of mammalogy*, 24, 133 – 140. https://doi.org/10.4404/hystrix-24.1-6363

Evans, A. R., & Sanson, G. D. (2006). Spatial and functional modeling of carnivore and insectivore molariform teeth. *Journal of Morphology*, 267(6), 649 – 662. https://doi.org/10.1002/jmor.10285

Evans, A. R., & Jernvall, J. (2009). Patterns and constraints in carnivoran and rodent dental complexity and relative tooth size. *Journal of Vertebrate Paleontology*, 29, 92A. https://doi.org/10.1080/02724634.2009.10411818

Evans, A. R., Wilson, G. P., Fortelius, M., & Jernvall, J. (2006). High-level similarity of dentitions in carnivorans and rodents. *Nature*, 445, 78 – 81. https://doi.org/10.1038/nature05433

Fernandez, A., & Gomez, S. (2018). Package "mdendro": Variable-group methods for hierarchical clustering. *R package version 1.0.1*. Retrieved from https://cran.r-project.org/web/packages/mdendro.

Friscia, A. R., & Van Valkenburgh, B. (2010). Ecomorphology of North American Eocene carnivores: evidence for competition between carnivorans and creodonts. In A. Goswami & A. Friscia (Eds.), *Carnivoran evolution: new views on phylogeny, form, and function* (pp. 311 – 341). Cambridge, UK: Cambridge University Press. https://doi.org/10.1017/CBO9781139193436.012

Flynn, J. J., & Wesley-Hunt, G. D. (2005). Carnivora. In K. D. Rose & D. Archibald (Eds.), *Origin, timing, and relationships of the major clades of extant placental mammals* (pp. 175 – 198). Baltimore, MD: Johns Hopkins University Press.

Flynn, J. J., Finarelli, J. A., & Spaulding, M. (2010). Phylogeny of the Carnivora and Carnivoramorpha, and the use of the fossil record to enhance understanding of evolutionary transformations. In A. Goswami & A. Friscia (Eds.), *Carnivoran evolution: new views on phylogeny, form, and function* (pp. 25 – 63). Cambridge, UK: Cambridge University Press. https://doi.org/10.1017/CBO9781139193436.003

Fox, R. C. (2015). A revision of the Late Cretaceous–Paleocene eutherian mammal *Cimolestes* Marsh, 1889. *Canadian Journal of Earth Sciences*, 52(12), 1 – 13. https://doi.org/10.1139/cjes-2015-0113

Fox, J., & Weisberg, S. (2019). An R Companion to applied regression, Third edition. Thousand Oaks, CA: Sage.

Fu, W. J., Carroll, R. J., & Wang, S. (2005). Estimating misclassification error with small samples via bootstrap cross-validation. *Bioinformatics*, 21, 1979 – 1986. https://doi.org/10.1093/bioinformatics/bti294

Fulwood, E. L. (2020). Ecometric modelling of tooth shape and precipitation gradients among lemurs on Madagascar. *Biological Journal of the Linnean Society*, 129, 26 – 40. https://doi.org/10.1093/biolinnean/blz158

Gerdtz, W. R. & Archbold, N. W. (2003). *Glaucodon ballaratensis* (Marsupialia, Dasyuridae), a Late Pliocene 'devil' from Batesford, Victoria. *Proceedings of The Royal Society of Victoria*, 115(2).

Gillespie, A. K., Archer, M., & Hand, S. J. (2019). A new Oligo-Miocene marsupial lion from Australia and revision of the family Thylacoleonidae. *Journal of Systematic Palaeontology*, 17, 59 – 89. https://doi.org/10.1080/14772019.2017.1391885

Gheebrant, E., Iarochene, M., Amaghzaz, M., & Bouya, B. (2006). Early African hyaenodontid mammals and their bearing on the origin of the Creodonta. *Geological Magazine*, 143, 475 – 489. https://doi.org/10.1017/S0016756806002032

Gingerich, P. D. (1980). *Tytthaena parrisi*, oldest known oxyaenid (Mammalia, Creodonta) from the Late Paleocene of western America. *Journal of Paleontology*, 54, 570 – 576.

Godthelp, H., Wroe, S., & Archer, M. (1999). A New Marsupial from the Early Eocene Tingamarra Local Fauna of Murgon, Southeastern Queensland: A Prototypical Australian Marsupial? *Journal of Mammalian Evolution*, 6(3), 289 – 313. https://doi.org/10.1023/A:1020517808869

Goin, F. J., Woodburne, M. O., Zimicz, A. N., Martin, G. M., & Chornogubsky, L. (2016). Paleobiology and Adaptations of Paleogene Metatherians. *A Brief History of South American Metatherians.* Dordrecht: Springer Earth System Sciences. https://doi.org/10.1007/978-94-017-7420-8_6

Gregory, W. K., & Hellmann, M. (1939). On the Evolution and major classification of the civets (Viverridae) and allied fossil and recent Carnivora: A phylogenetic study of the skull and dentition. *Proceedings of the American Philosophical Society*, 81, 309 – 392.

Grohé, C., Morlo, M., Chaimanee, Y., Blondel, C., Coster, P., Valentin, X., Salem, M., Bilal, A. A., Jaeger, J.-J., & Brunet, M. (2012). New Apterodontinae (Hyaenodontida) from the Eocene Locality of Dur At-Talah (Libya): Systematic, Paleoecological and Phylogenetical Implications. PLoS ONE, 7(11), e49054. https://doi.org/10.1371/journal.pone.0049054

Harper, T., Parras, A., & Rougier, G. W. (2019). *Reigitherium* (Meridiolestida, Mesungulatoidea), an enigmatic Late Cretaceous mammal from Patagonia, Argentina: Morphology, affinities, and dental evolution. *Journal of Mammalian Evolution*, 26, 447 – 478. https://doi.org/10.1007/s10914-018-9437-x

Hassanin, A., Veron, G., Ropiquet, A., Van Vuuren, B. J., Lécu, A., Goodman, St, M., Haider, J., & Nguyen, T. T. (2021). Evolutionary history of Carnivora (Mammalia, Laurasiatheria) inferred from mitochondrial genomes. *PLoS ONE*, 16(2), e0240770. https://doi.org/10.1371/journal.pone.0240770

Hiiemae, K. M. (1976). Masticatory movements in primitive mammals. In Anderson, D. J., & Matthews, B. (Eds.), *Mastication* (pp. 105 – 118). Bristol: John Wright and Sons.

Holliday, J. A. (2010). Evolution in Carnivora: identifying a morphological bias. In A. Goswami & A. Friscia (Eds.), *Carnivoran evolution: new views on phylogeny, form, and function* (pp. 189 – 224). Cambridge, UK: Cambridge University Press. https://doi.org/10.1017/CBO9781139193436.008

Holliday, J. A., & Steppan, S. J. (2004). Evolution of hypercarnivory: The effect of specialization on morphological and taxonomic diversity. *Paleobiology*, 30, 108 – 128. https://doi.org/10.1666/0094-8373(2004)030<0108:EOHTEO>2.0.CO;2

Hu, Y., Meng, J., Wang, Y., & Li, C. (2005). Large Mesozoic mammals fed on young dinosaurs. *Nature*, 433, 149 – 152. https://doi.org/10.1038/nature03102

Hunt, R. M. (1996). Biogeography of the Order Carnivora. In Gitleman, J. L. (Ed.), *Carnivore behavior, ecology, and evolution* (pp. 458 – 541). Ithaca, NY: Cornell University Press. https://doi.org/10.7591/9781501745829-022

Hunt, R. M. (1998). Evolution of the aeluroid Carnivora. Diversity of the earliest aeluroids from Eurasia (Quercy, Hsanda-Gol) and the origin of felids. *American Museum Novitates*, 3252, 1 – 65. http://hdl.handle.net/2246/3156

Hutchins, M., Thoney, D. A., & Schlager, N. (2003). Grzimek's Animal Life Encyclopedia Volumes 12–16, Mammals I–V (2nd ed.). Farmington Hills, MI: Gale Group.

Janis, C. M., & Fortelius, M. (1988). On the means whereby mammals achieve increased functional durability of their dentitions, with special reference to limiting factors. *Biol Rev Camb Philos Soc.*, 63(2), 197 – 230. https://doi.org/10.1111/j.1469-185x.1988.tb00630.x

Jones, M. E., & Stoddart, D. M. (1998). Reconstruction of the predatory behaviour of the extinct marsupial thylacine (*Thylacinus cynocephalus*). *Journal of Zoology*, 246, 239 – 256. https://doi.org/10.1111/j.1469-7998.1998.tb00152.x

Kay, R. F. & Hiiemae, K. M. (1974). Jaw movement and tooth use in recent and fossil primates. *Am. J. Phys. Anthropol.*, 40, 227 – 256. https://doi.org/10.1002/ajpa.1330400210

Keselman, H. J., Algina, J., Lix, L. M., Wilcox, R. R., & Deering, K. N. (2008). A generally robust approach for testing hypotheses and setting confidence intervals for effect sizes. *Psychological Methods*, 13, 110–129. https://doi.org/10.1037/1082-989X.13.2.110

Kielan-Jaworowska, Z., Cifelli, R. L., & Luo, Z.-X. (2004). Mammals from the Age of Dinosaurs: Origins, Evolution, and Structure. Columbia University Press. https://doi.org/10.7312/kiel11918

Kitchener, A. C., Breitenmoser-Würsten, C., Eizirik, E., Gentry, A., Werdelin, Lars, Wilting, A., Yamaguchi, N., Abramov, A. V., Christiansen, P., Driscoll, C., Duckworth, J. W., Johnson, Warren E., Luo, S. J., Meijaard, E., O'Donoghue, P., Sanderson, J., Seymour, K., Bruford, M., Groves, C., Hoffmann, M., Nowell, K., Timmons, Z., & Tobe, S. (2017). A revised taxonomy of the Felidae: The final report of the Cat Classification Task Force of the IUCN Cat Specialist Group. *Cat News*, Special Issue 11, 1 – 80. http://researchrepository.murdoch.edu.au/id/eprint/45096

Kumar, S., Stecher, G., Suleski, M., & Hedges, S.B. (2017). TimeTree: A resource for timelines, timetrees, and divergence times. *Molecular Biology and Evolution*, 1812 – 1819. https://doi.org/10.1093/molbev/msx116

References
_____

Kullmer, O., Menz, U., & Fiorenza, L. (2020). Occlusal Fingerprint Analysis (OFA) reveals dental occlusal behavior in primate molars. In Martin, T., & Koenigswald, W. v. (Eds.) *Mammalian Teeth — Form and Function* (pp. 25 – 43). Mpnchen: Verlag Dr. Friedrich Pfeil. http://dx.doi.org/10.23788/mammteeth.02

Lambert, J. E., Fellner, V., McKenney, E., & Hartstone-Rose, A. (2014). Binturong (*Arctictis binturong*) and Kinkajou (*Potos flavus*) Digestive Strategy: Implications for Interpreting Frugivory in Carnivora and Primates. PLoS ONE, 9(8), e105415. https://doi.org/10.1371/journal.pone.0105415

Lang, A. J., Engler, T., & Martin, T. (2021). Dental topographic and three-dimensional geometric morphometric analysis of carnassialization in different clades of carnivorous mammals (Dasyuromorphia, Carnivora, Hyaenodonta). *Journal of Morphology*, 283(1), 91 – 108. https://doi.org/10.1002/jmor.21429

Lange-Badré, B. & Dashzeveg, D. (1989). On some Oligocene carnivorous mammals from Central Asia. *Acta Palaeontologica Polonica*, 34(2), 125 – 148.

Law, C. J., Slater, G. J., & Mehta, R. S. (2018). Lineage Diversity and Size Disparity in Musteloidea: Testing Patterns of Adaptive Radiation Using Molecular and Fossil-Based Methods. *Systematic Biology*, 67(1), 127 – 144. https://doi.org/10.1093/sysbio/syx047

Li, P., Morse, P. E., & Kay, R. F. (2020). Dental topographic change with macrowear and dietary inference in *Homunculus patagonicus*. *Journal of Human Evolution*, 144, 102786. https://doi.org/10.1016/j.jhevol.2020.102786

Long, J., Archer, M., Flannery, T., & hand, S. (2003). Prehistoric Mammals of Australia and New Guinea: One Hundred Million Years of Evolution. Baltimore, MD: Johns Hopkins University Press.

López-Torres, S., Selig, K. R., Prufrock, K. A., Lin, D., & Silcox, M. T. (2017). Dental topographic analysis of paromomyid (Plesiadapiformes, Primates) cheek teeth: more than 15 million years of changing surfaces and shifting ecologies. *Historical Biology*, 30, 76 – 88. https://doi.org/10.1080/08912963.2017.1289378

Lund, U., Agostinelli, C., Arai, H., Gagliardi, A., García-Portugués, E., Giunchi, D., Irisson, J.-O., Pocernich, M., & Rotolo, F. (2022). Package "circular": Circular statistics. *R package 0.4-95*. Retrieved from https://cran.r-project.org/web/packages/circular.

Luo, Z.-X., Yuan, C.-X., Meng, Q.-J., & Ji, Q. (2011). A Jurassic eutherian mammal and divergence of marsupials and placentals. *Nature*, 476, 442 – 445. https://doi.org/10.1038/nature10291

Maindonald, J. (2008*). R exercises Part VI: Linear Discriminant Analysis – Using lda()*. Retrieved from: https://maths-people.anu.edu.au/~johnm/courses/dm/math3346/2008/pdf/.

Mallett, J. S. (1969). Carnassial Rotation in a Fossil Carnivore. *The American Midland Naturalist*, 82(1), 287 – 289. https://doi.org/10.2307/2423840

Martín-Serra, A., Figueirido, B., & Palmqvist, P. (2014). A three-dimensional analysis of the morphological evolution and locomotor behaviour of the carnivoran hind limb. *BMC Evolutionary Biology*, 14, 129. https://doi.org/10.1186/1471-2148-14-129

Matthew, W. D. (1901). Additional observations on the Creodonta. *Bulletin of the American Museum of Natural History*, 14, 1 – 38. http://hdl.handle.net/2246/1542

Matthew, W. D. (1909). The Carnivora and Insectivora of the Bridger Basin, middle Eocene. *Memoirs of the American Museum of Natural History*, 9, 291 – 567. http://hdl.handle.net/2246/5744

May-Collado, L. J., Kilpatrick, C. W., & Agnarsson, I. (2015). Mammals from 'down under': a multi-gene species-level phylogeny of marsupial mammals (Mammalia, Metatheria). *PeerJ*, 3:e805. https://doi.org/10.7717/peerj.805

Mellett, J. S. (1985). Autocclusal mechanisms in the carnivore dentition. *Australian Mammalogy*, 8(4), 233 – 238. https://doi.org/10.1071/AM85022

Meloro, C., & Raia, P. (2010). Cats and dogs down the tree: The tempo and mode of evolution in the lower carnassial of fossil and living Carnivora. *Evolutionary Biology*, 37, 177 – 186. https://doi.org/10.1007/s11692-010-9094-3

Meng, J., Zhai, R., & Wyss, A. R. (1998). The late Paleocene Bayan Ulan Fauna of inner Mongolia, China. *Bulletin of Carnegie Museum of Natural History*, 34, 148 – 185.

Mills, J. R. E. (1955). Ideal dental occlusion in the primates. *Dental Practitioner*, 6(2), 47 – 63.

Mills, J. R. E. (1966), The functional occlusion of the teeth of Insectivora. *Zoological Journal of the Linnean Society of London*, 46, 1 – 25. https://doi.org/10.1111/j.1096-3642.1966.tb00081.x

Morales, J., & Pickford, M. (2021). Taxonomic revision of the genus Leptoplesictis (Viverridae, Mammalia) with description of new fossils from Grillental VI (Namibia) and Moratilla 2 (Spain). *Communications of the Geological Survey of Namibia*, 23, 161 – 176.

Morlo, M. (1999). Niche structure and evolution in creodont (Mammalia) faunas of the European and North American Eocene. *Geobios*, 32, 297 – 305. https://doi.org/10.1016/S0016-6995(99)80043-6

Muizon, C. De, & Lange-Badré, B. (1997). Carnivorous dental adaptations in tribosphenic mammals and phylogenetic reconstruction. *Lethaia*, 30, 353 – 366. https://doi.org/10.1111/j.1502-3931.1997.tb00481.x

Osborn, H. F. (1907). Evolution of mammalian teeth to and from the triangular type. New York: The Macmillian Company.

O'Leary, M. A., Bloch, J. I., Flynn, J. J., Gaudin, T. J., Giallombardo, A., Giannini, N. P., Goldberg, S. L., Kraatz, B. P., Luo, Z.-X., Meng, J., Ni, X., Novacek, M. J., Perini, F. A., Randall, Z. S., Rougier, G. W., Sargis, E. J., Silcox, M. T., Simmons, N. B., Spaulding, M., Velazco, P. M., Weksler, M., Wible, J. R., & Cirranello, A. L. (2013). The placental mammal ancestor and the Post-K-Pg radiation of placentals. *Science*, 339, 662 – 667. https://doi.org/10.1126/science.1229237

Osborn, H. F. (1888). The Evolution of Mammalian Molars To and From the Tritubercular Type. *The American Naturalist*, 22, 1067 – 1079.

Owen, R. (1840). Odontography; Or, a treatise on the comparative anatomy of the teeth, their physiological relations, mode of development and microscopic structure, in the vertebrate animals. London: Hippolyte Bailliere.

Owen, R. (1868). On the anatomy of vertebrates, volume 3: mammals. London: Longmans, Green and Co. https://doi.org/10.5962/bhl.title.990

Pampush, J. D., Winchester, J. M., Morse, P. E., Vining, A. Q., Boyer, D. M., & Kay, R. F. (2016). Introducing molaR: A new R package for quantitative topographic analysis of teeth (and other topographic surfaces). *Journal of Mammalian Evolution*, 23, 397 – 412. https://doi.org/10.13140/RG.2.1.3284.9687

Pampush, J. D., Spradley, J. P., Morse, P. E., Griffith, D., Gladman, J. T., Gonzales, L. A., & Kay, R. F. (2018). Adaptive wear-based changes in dental topography associated with atelid (Mammalia: Primates) diets. *Biological Journal of the Linnean Society*, 124, 587 – 606. https://doi.org/10.1093/biolinnean/bly069

Paterson, R., Samuels, J. X., Rybczynski, N., Ryan, M. J., & Maddin, H. C. (2020). The earliest mustelid in North America. *Zoological Journal of the Linnean Society*, 188, 1318 – 1339. https://doi.org/10.1093/zoolinnean/zlz091

Pineda-Munoz, S., Lazagabaster, I. A., Alroy, J., & Evans, A. (2017). Inferring diet from dental morphology in terrestrial mammals. *Methods in Ecology and Evolution*, 8, 481 – 491. https://doi.org/10.1111/2041-210X.12691

Pires, A. M., Silvestro, D., & Quental, T. B. (2015). Continental faunal exchange and the asymmetrical radiation of carnivores. *Proceedings of the Royal Society B*, 282, 20151952. https://doi.org/10.13140/RG.2.1.3284.9687doi.org/10.1098/rspb.2015.1952

Prevosti, F. J., & Forasiepi, A. M. (2018). Evolution of South American Mammalian predators during the Cenozoic: Paleobiogeographic and paleoenvironmental contingencies. Springer International Publishing. https://doi.org/10.1007/978-3-319-03701-1_3

Prevosti, F. J., Turazzini, G. F., Ercoli, M. D., & Hingst-Zaher, E. (2012). Mandible shape in marsupial and placental carnivorous mammals: a morphological comparative study using geometric morphometrics. *Zoological Journal of the Linnean Society*, 164, 836 – 855. https://doi.org/10.1111/j.1096-3642.2011.00785.x

Prufrock, K. A., Boyer, D. M., & Silcox, M. T. (2016). The first major primate extinction: An evaluation of paleoecological dynamics of North American stem Primates using a homology free measure of tooth shape. *American Journal of Physical Anthropology*, 159, 683 – 697. https://doi.org/10.1002/ajpa.22927

R Core Team. (2020). R: A language and environment for statistical computing. Vienna, Austria. Retrieved from http://R-project.org/: R Foundation for Statistical Computing.

Rannikko, J., Adhikari, A., Karme, A., Žliobaitė, I. & Fortelius, M. (2020). The case of the grass-eating suids in the Plio-Pleistocene Turkana Basin: 3D dental topography in relation to diet in extant and fossil pigs. *Journal of Morphology*, 281, 348 – 364. https://doi.org/10.1002/jmor.21103

Reig, O. A. & Simpson, G. G. (1972). *Sparassocynus* (Marsupialia, Didelphidae), a peculiar mammal from the late Cenozoic of Argentina. *Journal of Zoology*, 167(4), 511 – 539. https://doi.org/10.1111/j.1469-7998.1972.tb01742.x

Ripley, B., Venables, B., Bates, D. M., Hornik, K., Gebhart, A., & Firth, D. (2020). Package "MASS": Support functions and datasets for Venables and Ripley's MASS. *R package version 7.3-53*. Retrieved from https://cran.r-project.org/web/packages/MASS.

Rovinsky, D. S., Evans, A. R., & Adams, J. W. (2019). The pre-Pleistocene fossil thylacinids (Dasyuromorphia: Thylacinidae) and the evolutionary context of the modern thylacine. *PeerJ*, 7:e7457. https://doi.org/10.7717/peerj.7457

Rovinsky, D. S., Evans, A. R., & Adams, J. W. (2021). Functional ecological convergence between the thylacine and small prey-focused canids. *BMC Ecology and Evolution*, 21, 58. https://doi.org/10.1186/s12862-021-01788-8

Rose, K. D. (2006). The Beginning of the Age of Mammals. Baltimore, MD: Johns Hopkins University Press.

Renaud, S., & Ledevin, R. (2017). Impact of wear and diet on molar row geometry and topography in the house mouse. *Archives of Oral Biology*, 81, 31 – 40. https://doi.org/10.1016/j.archoralbio.2017.04.028

References

Revell, L. J. (2020). Package "phytools": Phylogenetic tools for comparative biology (and other things). *R package version 0.7-70.* Retrieved from https://cran.r-project.org/web/packages/phytools.

Sacco, T., & Van Valkenburgh, B. (2004). Ecomorphological indicators of feeding behaviour in the bears (Carnivora: Ursidae). *J. Zool., Lond.*, 263, 41 – 54. https://doi.org/10.1017/S0952836904004856

Salesa, M. J., Peigné, S., Anton, M., & Morales, J. (2011). Evolution of the Family Ailuridae: Origins and Old- World Fossil Record. In Gatston, A. R. (Ed.), *Red Panda, Biology and Conservation of the First* (pp. 27 – 41). Academic Press. https://doi.org/10.1016/B978-1-4377-7813-7.00003-3

Savage, R. J. G. (1977). Evolution in carnivorous mammals. *Paleontology*, 20(2), 237 – 271.

Schlager, S., Jefferis, G., & Dryden, I. (2020). Package "Morpho": Calculations and visualisations related to geometric morphometrics. *R package version 2.8.* Retrieved from https://cran.r-project.org/web/packages/Morpho.

Schlegel, A. (2016). *R function for performing Games-Howell post-hoc test.* Retrieved from https://gist.github.com/aschleg/ea7942efc6108aedfa9ec98aeb6c2096.

Schultz, J. A., & Martin, T. (2011). Wear pattern and functional morphology of dryolestoid molars (Mammalia, Cladotheria). *Paläontologische Zeitschrift*, 85, 269 – 285. https://doi.org/10.1007/s12542-010-0091-8

Schultz, J. A., & Martin, T. (2014). Function of pretribosphenic and tribosphenic mammalian molars inferred from 3D animation. *Naturwissenschaften*, 101, 771 – 781. https://doi.org/10.1007/s00114-014-1214-y

Schultz, J. A., Menz, U., Winkler, D. E., Schulz-Kornas, E., Engels, S., Kalthoff, D. C., Koenigswald, W. v., Ruf, I., Kaiser, T. M., Kullmer, O., Südekum, K.-H., & Martin, T. (2018) Modular Wear Facet Nomenclature for mammalian post-canine dentitions, *Historical Biology*, 30(1-2), 30 – 41. https://doi.org/10.1080/08912963.2017.1302442

Schultz, J. A., Anders, U., Braune, C., Brinkkötter, J. J., Calandra, I., Engels, S., Findeisen, E., Gailer, J.-P., Hummel, J., Jäger, K. R. K., Kaiser, T. M., Kalthoff, D. C., Koenigswald, W. v., Kullmer, O., Landwehr, C., Mau, M., Menz, U., Ruf, I., Schubert, A. M., Schulz-Kornas, E., Schwermann, A. H., Schwermann, L. C., Skiba, M., Steuer, P., Südekum, K.-H., Winkler, D. E., & Martin, T. (2020). A new wear facet terminology for mammalian dentitions. In Martin, T., & Koenigswald, W. v. (Eds.) *Mammalian Teeth — Form and Function* (pp. 11 – 24). Mpnchen: Verlag Dr. Friedrich Pfeil. http://dx.doi.org/10.23788/mammteeth.01

Selig, K. R., López-Torres, S., Sargis, E. J., & Silcox, M. T. (2018). First 3D dental topographic analysis of the enamel-dentine junction in non-primate euarchontans: Contribution of the enamel-dentine junction to molar morphology. *Journal of Mammalian Evolution*, 26, 587 – 598. https://doi.org/10.1007/s10914-018-9440-2

Selig, K. R., López-Torres, S., Sargis, E. J., & Silcox, M. T. (2019a). First 3D dental topographic analysis of the enamel–dentine junction in non-primate euarchontans: contribution of the enamel-dentine junction to molar morphology. *Journal of Mammalian Evolution*, 26, 587 – 598. https://doi.org/10.1007/s10914-018-9440-2

Selig, K. R., Sargis, E. J., & Silcox, M. T. (2019b). The frugivorous insectivores? Functional morphological analysis of molar topography for inferring diet in extant treeshrews (Scandentia). *Journal of Mammalogy*, 100, 1901 – 1917.   https://doi.org/10.1093/jmammal/gyz151

Selig, K. R., Sargis, E. J., Chester, S. G. B., & Silcox, M. T. (2020). Using three-dimensional geometric morphometric and dental topographic analyses to infer the systematics and paleoecology of fossil treeshrews (Mammalia, Scandentia). *Journal of Paleontology*, 94, 1202 – 1212. https://doi.org/10.1017/jpa.2020.36

Shan, S., Kovalsky, S. Z., Winchester, J. M., Boyer, D.M., & Daubechies, I. (2019). ariaDNE: A robustly implemented algorithm for Dirichlet energy of the normal. *Methods in Ecology and Evolution*, 10, 541 – 552. https://doi.org/10.1111/2041-210X.13148

Simpson, G. G. (1959). The nature and origin of supraspecific taxa. *Cold Spring Harbor Symposia on Quantitative Biology*, 24, 255 – 271. https://doi.org/10.1101/SQB.1959.024.01.025

Smits, P. D., & Evans, A. (2012). Functional constraints on tooth morphology in carnivorous mammals. *BMC Evolutionary Biology*, 12, 146. https://doi.org/10.1186/1471-2148-12-146

Solé, F., & Ladevèze, S. (2017). Evolution of the hypercarnivorous dentition in mammals (Metatheria, Eutheria) and its bearing on the development of tribosphenic molars. *Evolution & Development*, 19, 56 – 68. https://doi.org/10.1111/ede.12219

Solé, F., & Mennecart, B. (2019). A large hyaenodont from the Lutetian of Switzerland expands the body mass range of the European mammalian predators during the Eocene. *Acta Palaeontologica Polonica*, 64, 275 – 290. https://doi.org/10.4202/app.00581.2018

Solé, F., Gheerbrant, E., Amaghzaz, M., & Bouya, B. (2009). Further evidence of the African antiquity of hyaenodontid ('Creodonta', Mammalia) evolution. *Zoological Journal of the Linnean Society*, 156, 827 – 846. https://doi.org/10.1111/j.1096-3642.2008.00501.x

Solé, F., Smith, R., Coillot, T., de Bast, E., & Smith, T. (2014). Dental and tarsal anatomy of '*Miacis*' *latouri* and a phylogenetic analysis of the earliest carnivoraforms (Mammalia, Carnivoramorpha). *Journal of Vertebrate Paleontology*, 34(1), 1 – 21. https://doi.org/10.1080/02724634.2013.793195

Solé, F., Smith, T., de Bast, E., Codrea, V., & Gheerbrant, E. (2016). New carnivoraforms from the latest Paleocene of Europe and their bearing on the origin and radiation of Carnivoraformes (Carnivoramorpha, Mammalia). *Journal of Vertebrate Paleontology*, 36(2), e1082480. https://doi.org/10.1080/02724634.2016.1082480

Solé, F., Morgane, D., Le Verger, K., & Mennecart, B. (2018). Niche partitioning of the European carnivorous mammals during the Paleogene. *PALAIOS*, 33, 514 – 523. https://doi.org/10.2110/palo.2018.022

Solé, F., Marandat, B., & Lihoreau, F. (2020). The hyaenodonts (Mammalia) from the French locality of Aumelas (Hérault), with possible new representatives from the late Ypresian. *Geodiversitas*, 42(13), 185 – 214. https://doi.org/10.5252/geodiversitas2020v42a13

Solé, F., Morlo, M., Schaal, T., & Lehmann, T. (2021). New hyaenodonts (Mammalia) from the late Ypresian locality of Prémontré (France) support a radiation of the hyaenodonts in Europe already at the end of the early Eocene. *Geobios*, 66 – 67, 119 – 141. https://doi.org/10.1016/j.geobios.2021.02.004

References

Strahan, R. 2000. The mammals of Australia. Sydney: Reed New Holland.

Szalay, F. S. (1993). Metatherian Taxon Phylogeny: Evidence and Interpretation from the Cranioskeletal System. In Szalay, F.S., Novacek, M.J., & McKenna, M.C. (Eds.), *Mammal Phylogeny*. New York, NY: Springer. https://doi.org/10.1007/978-1-4613-9249-1_15

Szalay, F. S., & Gould, S. J. (1966). Asiatic Mesonychidae (Mammalia, Condylarthra). *Bulletin of the American Museum of Natural History*, 132, 127 – 174.

Tarquini, S. D., Chemisquy, M. A., & Prevosti, F. J. (2020). Evolution of the carnassial in living mammalian carnivores (Carnivora, Didelphimorphia, Dasyuromorphia): Diet, phylogeny, and allometry. *Journal of Mammalian Evolution*, 27, 95 – 109. https://doi.org/10.1007/s10914-018-9448-7

Thenius, E. (1989). Tlbd/Part 56 Zähne und Gebiss der Säugetiere. Berlin, Boston: De Gruyter. https://doi.org/10.1515/9783110856927

Tomiya, S. (2011). A new basal caniform (Mammalia: Carnivora) from the Middle Eocene of North America and remarks on the phylogeny of early carnivorans. *PLoS ONE*, 6(9), e24146. https://doi.org/10.1371/journal.pone.0024146

Tomiya, S., & Tseng, Z. J. (2016). Whence the beardogs? Reappraisal of the Middle to Late Eocene '*Miacis'* from Texas, USA, and the origin of Amphicyonidae (Mammalia, Carnivora). *R. Soc. open sci.*, 3, 160518. http://dx.doi.org/10.1098/rsos.160518

Ungar, P. S. (2019). Mammalian Teeth: Origin, Evolution, and Diversity. Baltimore, MD: Johns Hopkins University Press.

Ungar, P. S. (2018). Tooth surface topography. In R. L. Anemone & G. C. Conroy (Eds.), *New geospatial approaches to the anthropological sciences* (pp. 101 – 120). Albuquerque: University of New Mexico Press.

Van Valkenburgh, B. (1988). Trophic Diversity in past and present guilds of large predatory mammals. *Paleobiology*, 14(2), 155 – 173. https://doi.org/10.1017/S0094837300011891

Van Valkenburgh, B. (1989). Carnivore dental adaptations and diet: A study of trophic diversity within guilds. In Gitleman, J. L. (Ed.), *Carnivore behavior, ecology, and evolution* (pp. 410 – 436). Boston, MA: Springer. https://doi.org/10.1007/978-1-4757-4716-4_16

Van Valkenburgh, B. (1991). Iterative evolution of hypercarnivory in canids (Mammalia: Carnivora): evolutionary interactions among sympatric predators. *Paleobiology*, 17(4), 340 – 362. https://doi.org/10.1017/S0094837300010691

Van Valkenburgh, B. (1999). Major Patterns in the history of carnivorous mammals. *Annual Review of Earth and Planetary Sciences*, 27, 463 – 493. https://doi.org/10.1146/annurev.earth.27.1.463

Van Valkenburgh, B. (2007). Déjà vu: the evolution of feeding morphologies in the Carnivora. *Integrative and Comparative Biology*, 47, 147 – 163. https://doi.org/10.1093/icb/icm016

Van Valkenburgh, B., & Wayne, R. K. (2010). Carnivores. *Current Biology*, 20(21), R915 – R919. https://doi.org/10.1016/j.cub.2010.09.013

Van Valkenburgh, B., Wang, X., & Damuth, J. (2004). Cope's Rule, hypercarnivory, and extinction in North American canids. *Science*, 306, 101 – 104. https://doi.org/10.1126/science.1102417

Voss, R. S., & Jansa, S. A. (2003). Phylogenetic studies on didelphid marsupials II. Nonmolecular data and new IRBP sequences: Separate and combined analyses of didelphine relationships with denser taxon sampling. *Bulletin of the American Museum of Natural History*, 276, 1 – 82. https://doi.org/10.1206/0003-0090(2003)276%3C0001:PSODMI%3E2.0.CO;2

Voss, R. S., Gardner, A. L., & Jansa, S. A. (2004). On the relationships of 'Marmosa' formosa Shamel, 1930 (Marsupialia: Didelphidae), a phylogenetic puzzle from the Chaco of northern Argentina. *American Museum Novitates*, 3442, 1 – 18. https://doi.org/10.1206/0003-0082(2004)442%3C0001:OTROMF%3E2.0.CO;2

Wang, X. (1994). Phylogenetic systematics of the Hesperocyoninae (Carnivora, Canidae). *Bulletin of the American Museum of Natural History*, 221, 1 – 207. http://hdl.handle.net/2246/829

References

Wang, X., & Tedford, R. H. (2007). Evolutionary History of Canids. In Jensen, P. (Ed.), *The Behavioural Biology of Dogs* (pp. 3 – 22). CABI Publishing. https://doi.org/10.1079/9781845931872.0003

Wang, X., & Tedford, R. H. (2008). Dogs: Their Fossil Relatives and Evolutionary History. New York, Columbia University Press.

Wang, X., McKenna, M. C., & Dashzeveg, D. (2005a). *Amphicticeps* and *Amphicynodon* (Arctoidea, Carnivora) from Hsanda Gol Formation, Central Mongolia and Phylogeny of Basal Arctoids with Comments on Zoogeography. *American Museum Novitates*, 3483, 1 – 60. https://doi.org/10.1206/0003-0082(2005)483[0001:AAAACF]2.0.CO;2

Wang, X., Whistler, D. P., & Takeyuchi, G. T. (2005b). A new basal skunk *Martinogale* (Carnivora, Mephitinae) from Late Miocene Dove Spring Formation, California, and origin of New World mephitines. *Journal of Vertebrate Paleontology*, 25(4), 936 – 949. https://doi.org/10.1671/0272-4634(2005)025[0936:ANBSMC]2.0.CO;2

Wang, X., Qiu, Z., & Wang, B. (2005c). Hyaenodonts and carnivorans from the early Oligocene to early Miocene of Xianshuihe Formation, Lanzhou Basin, Gansu Province, China. *Palaeontologica Electronica*, 8(1), 6A.

Wang, X., White, S. C., & Guan, J. (2020). A new genus and species of sabretooth, Oriensmilus liupanensis (Barbourofelinae, Nimravidae, Carnivora), from the middle Miocene of China suggests barbourofelines are nimravids, not felids. *Journal of Systematic Palaeontology*, 18(9), 783 – 803. https://doi.org/10.1080/14772019.2019.1691066

Werdelin, L. (1986). Comparison of skull shape in marsupial and placental carnivores. *Australian Journal of Zoology*, 34, 109 – 117. https://doi.org/10.1071/ZO9860109

Werdelin, L. (1987). Jaw geometry and molar morphology in marsupial carnivores: Analysis of a constraint and Its macroevolutionary consequences. *Paleobiology*, 13, 342 – 350. https://doi.org/10.1017/S0094837300008915

Wesley-Hunt, G. D. (2005). The morphological diversification of carnivores in North America. *Paleobiology*, 31, 35 – 55. https://doi.org/10.1666/0094-8373(2005)031%3C0035:TMDOCI%3E2.0.CO;2

Wesley-Hunt, G. D., & Flynn, J. J. (2005). Phylogeny of the Carnivora: Basal relationships among the carnivoramorphans, and assessment of the position of '*Miacoidea*' relative to Carnivora. *Journal of Systematic Palaeontology*, 3, 1 – 28. https://doi.org/10.1017/S1477201904001518

Winchester, J. M. (2016). MorphoTester: An open source application for morphological topographic analysis. *PLoS ONE*, 11(2), e0147649. https://doi.org/10.1371/journal.pone.0147649

Winchester, J. M., Boyer, D. M., St Clair, E. M., Gosselin-Ildari, A. D., Cooke, S. B., & Ledogar, J. A. (2014). Dental topography of platyrrhines and prosimians: Convergence and contrasts. *American Journal of Physical Anthropology*, 153, 29 – 44. https://doi.org/10.1002/ajpa.223

Wolsan, M. (1999). Oldest mephitine cranium and its implications for the origin of skunks. *Acta Palaeontologica Polonica*, 44(2), 223 – 230.

Wortman, J. L. (1899). Restoration of *Oxyaena lupina* Cope, with descriptions of certain new species of Eocene creodonts. *Bulletin of the American Museum of Natural History*, 12, 139 – 148. http://hdl.handle.net/2246/1536

Wortman, J. L. (1901). Studies of Eocene Mammalia in the Marsh Collection, Peabody Museum. *American Journal of Science*, s4-12(72), 421 – 432. https://doi.org/10.2475/ajs.s4-12.72.421

Wortman, J. L. & Matthew, W. D. (1899). The ancestry of certain members of the Canidae, the Viverridae, and Procyonidae. *Bulletin of the American Museum of Natural History*, 12, 109 – 138. http://hdl.handle.net/2246/1535

Wroe, S. (1998). A new 'bone-cracking' dasyurid from the Miocene of Riversleigh, northwestern Queensland. *Alcheringa*, 22, 277 – 284. https://doi.org/10.1080/03115519808619205

Zack, S. P., Poust, A. W., & Wagner, H. (2022). *Diegoaelurus*, a new machaeroidine (Oxyaenidae) from the Santiago Formation (late Uintan) of southern California and the relationships of Machaeroidinae, the oldest group of sabertooth mammals. *PeerJ*, 10:e13032 https://doi.org/10.7717/peerj.13032

Zhou, Y., Wang, S.-R., & Ma, J.-Z. (2017). Comprehensive species set revealing the phylogeny and biogeography of Feliformia (Mammalia, Carnivora) based on mitochondrial DNA. *PLoS ONE*, 12(3), e0174902. https://doi.org/10.1371/journal.pone.0174902

10. Acknowledgements

11. Appendix

Table S1: Calculated ariaDNE (using the script by Shan et al. 2019 for Matlab version 9.10.0.1710957 R2021a) for the individual teeth per specimen.

Taxon	Specimen	ariaDNE			
		m1	m2	m3	m4
Canis lupus	SMF 36 408	0.07613			
Canis lupus	SMF 15 699	0.07562			
Canis lupus	ZFMK MAM 1988.0151	0.06404			
Canis lupus	ZFMK MAM 1978.0268	0.06153			
Civettictis civetta	ZFMK MAM 1958.0015	0.08494			
Civettictis civetta	ZFMK MAM 1993.0705	0.08558			
Civettictis civetta	ZFMK MAM 1958.0012	0.07104			
Crocuta crocuta	IGPB M 427	0.06391			
Crocuta crocuta	IGPB M 418	0.06207			
Crocuta crocuta	IGPB M 5997	0.06038			
Cryptoprocta ferox	ZFMK MAM 1987.0584	0.05963			
Dinictis sp.	SMNK-PAL 35102	0.06222			
Dinictis sp.	SMNK-PAL 35101	0.06899			
Felis silvestris	ZFMK MAM 2018.0106	0.05946			
Felis silvestris	ZFMK MAM 2018.0102	0.06077			
Felis silvestris	ZFMK MAM 2018.0100	0.05846			
Otocolobus manul	ZFMK MAM 1965.0510	0.05880			
Ichneumia albicauda	SMF 32 733	-			
Ichneumia albicauda	SMF 32 735	0.09916			
Ichneumia albicauda	SMF 16 553	0.10289			
Ichneumia albicauda	ZFMK MAM 1976.0125	0.09970			
Ichneumia albicauda	ZFMK MAM 1931.0056	0.08242			
Lycaon pictus	ZFMK MAM 2001.0275	0.06738			

Lycaon pictus	ZFMK MAM 1981.0527	0.06877			
Lycaon pictus	ZFMK MAM 1956.0888	0.07121			
Mustela lutreola	IGPB M 2151a	0.07243			
Mustela lutreola	IGPB M 2151b	0.07163			
Mustela lutreola	IGPB M 2151c	0.07415			
Mustela lutreola	IGPB M 335	0.07077			
Neofelis nebulosa	ZFMK 1984.0337	0.06248			
Nimravus sp.	IGPB M 6134	0.06921			
Panthera leo	ZFMK MAM 2006.0031	0.05300			
Panthera pardus	ZFMK MAM 1997.0547	0.05169			
Panthera tigris	ZFMK MAM 1986.0118	0.05493			
Speothos venaticus	ZFMK MAM 1954.0154	0.06325			
Speothos venaticus	ZFMK MAM 1987.0386	0.06794			
Speothos venaticus	ZFMK MAM 1992.0565	0.06157			
Viverra tangalunga	SMF 697	0.09758			
Viverra tangalunga	SMF 20 928	0.10372			
Viverra zibetha	SMF 16 516	0.09459			
Viverra zibetha	ZFMK MAM 1968.0085	0.08116			
Vulpes laogpus	IGPB M 553	0.08535			
Vulpes laogpus	IGPB M 4005	0.08301			
Vulpes laogpus	IGPB M 4007	0.07823			
Vulpes vulpes	IGPB M 6238	0.08888			
Vulpes vulpes	IGPB M 6258	0.07739			
Vulpes vulpes	IGPB M 6182	0.07702			
Dasyurus viverrinus	SMF 378		0.08132	0.09264	0.08403
Dasyurus viverrinus	SMF 1480		0.08901	0.09555	0.08364
Dasyurus viverrinus	SMF 1485		0.08236	0.08964	0.08411

Dasyurus viverrinus	SMF 15505		0.09432	0.09730	0.08362
Dasyurus hallucatus	TMM M-6921		0.09381	0.09436	0.08704
Dasyurus maculatus	UMZC A6.10/3		0.07760	0.08688	0.07755
Sarcophilus harrisii	ZMB_Mam_001733		0.07036	0.08119	0.06570
Sarcophilus harrisii	ZMB_Mam_002343		0.07455	0.07906	0.05914
Thylacinus cynocephalus	HLMD-M-1250		0.06125	0.06824	0.06091
Thylacinus cynocephalus	NMB 2526		0.05260	0.06165	0.06522
Thylacinus cynocephalus	ZMB_Mam_036877		0.06736	0.07072	0.06580
Thylacinus cynocephalus	ZMB_Mam_047902		0.06368	0.06888	0.06235
Hyaenodon sp.	MNHN.F.Qu 8467	0.04953	0.05904	0.05720	
Hyaenodon sp.	MNHN.F.Qu 8471	0.05675	0.06209	0.05972	
Hyaenodon exiguus	NMB Q.B.603	0.05103	0.05812	0.05785	
Hyaenodon exiguus	NMB Q.C.221	0.05624	0.06388	0.05674	
Hyaenodon filholi	MNHN.F.Qu 8421	0.05513	0.05612	0.05536	
Hyaenodon filholi	NMB Q.B.771	0.05192	0.06457	0.05696	
Oxyaenoides bicuspidens	GMH XIV-2909-1954	0.06348	0.06888	0.06538	
Proviverra typica	NMB En.130		0.09475		
Proviverra typica	NMB En.176	0.08887			
Proviverra typica	NMB En.179			0.09660	
Pterodon dasyuroides	NMB Q.B.606		0.06842	0.06747	
Pterodon dasyuroides	NMB Q.C. 413	0.06595			

Table S2: Calculated Principal component of the GMA (using "geomorph" package for R) for the individual teeth per specimen.

Taxon	Specimen	PC1 of GMA				PC2 of GMA			
		m1	m2	m3	m4	m1	m2	m3	m4
Canis lupus	SMF 36 408	0.0163				-0.0815			
Canis lupus	SMF 15 699	0.0215				-0.0931			
Canis lupus	ZFMK MAM 1988.0151	0.0095				-0.0810			
Canis lupus	ZFMK MAM 1978.0268	0.0082				-0.0758			
Civettictis civetta	ZFMK MAM 1958.0015	0.1296				-0.0816			
Civettictis civetta	ZFMK MAM 1993.0705	0.1265				-0.0461			
Crocuta crocuta	IGPB M 427	-0.1772				-0.0343			
Crocuta crocuta	IGPB M 418	-0.1933				-0.0215			
Crocuta crocuta	IGPB M 5997	-0.1817				-0.0361			
Cryptoprocta ferox	ZFMK MAM 1987.0584	-0.0950				0.0015			
Dinictis sp.	SMNK-PAL 35102	-0.0955				-0.0356			
Felis silvestris	ZFMK MAM 2018.0106	-0.1296				0.0278			
Felis silvestris	ZFMK MAM 2018.0102	-0.1304				0.0458			
Felis silvestris	ZFMK MAM 2018.0100	-0.1372				0.0512			
Otocolobus manul	ZFMK MAM 1965.0510	-0.1426				0.0018			
Ichneumia albicauda	SMF 32 733	0.1420				-0.0531			
Ichneumia albicauda	SMF 32 735	0.1313				-0.0701			
Ichneumia albicauda	SMF 16 553	0.1421				-0.0379			
Ichneumia albicauda	ZFMK MAM 1976.0125	0.1450				-0.0238			
Lycaon pictus	ZFMK MAM 2001.0275	-0.0166				-0.1124			
Lycaon pictus	ZFMK MAM 1981.0527	-0.0033				-0.1053			
Lycaon pictus	ZFMK MAM 1956.0888	-0.0274				-0.122			
Mustela lutreola	IGPB M 2151a	-0.0358				-0.0979			
Mustela lutreola	IGPB M 2151b	-0.0193				-0.1041			
Mustela lutreola	IGPB M 2151c	-0.0342				-0.1225			

Species	Specimen							
Mustela lutreola	IGPB M 335	-0.0443				-0.1045			
Neofelis nebulosa	ZFMK 1984.0337	-0.1522				0.0511			
Nimravus sp.	IGPB M 6134	-0.1102				-0.0204			
Panthera leo	ZFMK MAM 2006.0031	-0.1569				0.0647			
Panthera pardus	ZFMK MAM 1997.0547	-0.1594				0.0542			
Panthera tigris	ZFMK MAM 1986.0118	0.0542				0.0848			
Speothos venaticus	ZFMK MAM 1954.0154	-0.0236				-0.0551			
Speothos venaticus	ZFMK MAM 1987.0386	-0.0233				-0.0549			
Speothos venaticus	ZFMK MAM 1992.0565	-0.0263				-0.0532			
Viverra tangalunga	SMF 697	0.078				-0.1166			
Viverra tangalunga	SMF 20 928	0.0905				-0.1385			
Viverra zibetha	SMF 16 516	0.099				-0.1125			
Viverra zibetha	ZFMK MAM 1968.0085	0.0528				-0.0887			
Vulpes laogpus	IGPB M 553	0.0206				-0.1135			
Vulpes laogpus	IGPB M 4005	0.0256				-0.1072			
Vulpes laogpus	IGPB M 4007	-0.0018				-0.0939			
Vulpes vulpes	IGPB M 6238	0.0607				-0.1206			
Vulpes vulpes	IGPB M 6258	0.0249				-0.1097			
Vulpes vulpes	IGPB M 6182	0.0381				-0.1262			
Dasyurus viverrinus	SMF 378			0.1396	0.0592			0.0495	0.0289
Dasyurus viverrinus	SMF 1480		0.1515	0.1473	0.0974		0.1515	0.0683	0.0699
Dasyurus viverrinus	SMF 1485		0.1532	0.1461	0.0831		0.0215	0.0407	0.0526
Dasyurus viverrinus	SMF 15505		0.1785	0.1568	0.0654		0.0524	0.0548	0.043
Dasyurus hallucatus	TMM M-6921		0.1553	0.1554	0.0692		0.0439	0.0437	0.0174
Dasyurus maculatus	UMZC A6.10/3		0.1452	0.1346	0.0173		0.0538	0.0519	0.0214
Sarcophilus harrisii	ZMB_Mam_001733		0.0607	0.0114	-0.0728		0.0993	0.0771	0.0726
Sarcophilus harrisii	ZMB_Mam_002343		0.0727	0.0161	-0.0707		0.1113	0.0728	0.0702

Thylacinus cynocephalus	HLMD-M-1250		0.0612	0.029	-0.1047		0.015	0.031	0.0192
Thylacinus cynocephalus	NMB 2526		0.0867	0.046	-0.0592		0.0319	0.0463	-0.0134
Thylacinus cynocephalus	ZMB_Mam_036877		0.0779	0.0358	-0.0723		0.0324	0.0298	0.0087
Thylacinus cynocephalus	ZMB_Mam_047902		0.0695	0.0437	-0.0765		0.0285	0.0431	0.0246
Hyaenodon sp.	MNHN.F.Qu 8467	0.0003	-0.0594	-0.2524		0.0205	0.0178	-0.0102	
Hyaenodon sp.	MNHN.F.Qu 8471	0.0118	-0.0581	-0.2593		0.0188	0.0387	0.0226	
Hyaenodon exiguus	NMB Q.B.603	-0.0069	-0.0646	-0.2459		0.0509	0.0338	0.0169	
Hyaenodon exiguus	NMB Q.C.221	-0.0338	-0.1191	-0.2542		0.0266	0.0545	-0.0043	
Hyaenodon filholi	MNHN.F.Qu 8421	-0.007	-0.0815	-0.229		0.058	0.0625	0.0127	
Hyaenodon filholi	NMB Q.B.771	-0.0338	-0.1191	-0.2542		0.0266	0.0545	-0.0043	
Oxyaenoides bicuspidens	GMH XIV-2909-1954	0.0714	0.0327	0.0158		0.0134	0.0661	0.0862	
Proviverra typica	NMB En.130		0.1993			0.0409			
Proviverra typica	NMB En.176	0.172				0.0305			
Proviverra typica	NMB En.179			0.1376				0.0302	
Pterodon dasyuroides	NMB Q.B.606		0.0456	-0.0507			0.0464	0.0824	
Pterodon dasyuroides	NMB Q.C. 413	0.0412				0.0345			

Table S3: Constructed carnassial blade angle per specimen.

Species	Specimen number	Constructed carnassial blade angle
Canis lupus	ZFMK MAM 1988.0151	5.375
Canis lupus	ZFMK MAM 1978.0268	4.365
Canis lupus	SMF 36408	2.981
Civettictis civetta	ZFMK MAM 1958.0015	41.239
Civettictis civetta	ZFMK MAM 1993.0705	49.491
Crocuta crocuta	IGPB M 5997	7.581
Crocuta crocuta	IGPB M 418	1.41
Crocuta crocuta	IGPB M 427	7.764
Cryptoprocta ferox	ZFMK MAM 1987.0584	3.313
Dasyurus hallucatus	TMM M-6921	30.588
Dasyurus maculatus	UMZC A6.10/3	19.736
Dasyurus viverrinus	SMF 1485	18.936
Dasyurus viverrinus	SMF 378	23.128
Dasyurus viverrinus	SMF 1480	13.144
Dasyurus viverrinus	SMF 15505	33.811
Dinictis sp.	SMNK-PAL 35101	4.09
Felis silvestris	ZFMK MAM 2018.0100	1.93
Felis silvestris	ZFMK MAM 2018.0102	1.942
Felis silvestris	ZFMK MAM 2018.0106	0.003
Hyaenodon exiguus	NMB Q.C.221	5.5
Hyaenodon exiguus	NMB Q.B.603	0.004
Hyaenodon filholi	NMB Q.B.771	1.997
Hyaenodon filholi	MNHN.F.Qu 8421	1.644
Hyaenodon sp.	MNHN.F.Qu 8467	3.961
Hyaenodon sp.	MNHN.F.Qu 8471	3.966
Ichneumia albicauda	SMF 16553	49.283
Ichneumia albicauda	SMF 32733	48.984
Ichneumia albicauda	SMF 32735,	41.06
Ichneumia albicauda	ZFMK MAM 1976.0125	50.125
Lycaon pictus	ZFMK MAM 1956.0888	4.928
Lycaon pictus	ZFMK MAM 1981.0527	6.238
Lycaon pictus	ZFMK MAM 2001.0275	5.287
Mustela lutreola	IGPB M 2151c	2.251
Mustela lutreola	IGPB M 2151b	11.101
Mustela lutreola	IGPB M 2151a	7.765
Mustela putorius	IGPB M 335	5.189
Neofelis nebulosa	ZFMK 1984.0337	2.048
Nimravus sp.	IGPB M 6134	1.949
Otocolobus manul	ZFMK MAM 1965.0510	4.241
Oxyaenoides bicuspidens	GMH XIV-2909-1954	2.363
Panthera leo	ZFMK MAM 2006.0031	2.27
Panthera pardus	ZFMK MAM 1997.0547	2.347

Panthera tigris	ZFMK MAM 1986.0118	1.16
Proviverra typica	NMB En.179	43
Pterodon dasyuroides	NMB Q.B.606	19.029
Sarcophilus harrisii	ZMB_Mam_002343	3.095
Sarcophilus harrisii	ZMB_Mam_001733	0.147
Speothos venaticus	ZFMK MAM 1954.0154	4.49
Speothos venaticus	ZFMK MAM 1987.0386	2.0248
Speothos venaticus	ZFMK MAM 1992.0565	0.688
Thylacinus cynocephalus	NMB 2526	15
Thylacinus cynocephalus	ZMB_Mam_036877	12
Thylacinus cynocephalus	ZMB_Mam_047902	17.162
Thylacinus cynocephalus	HLMD-M-1250	19.144
Viverra tangalunga	SMF 697	33.213
Viverra tangalunga	SMF 20928	29.656
Viverra zibetha	ZFMK MAM 1968.0085	29
Viverra zibetha	SMF 16516	37.487
Vulpes lagopus	IGPB M 4005	2.427
Vulpes lagopus	IGPB M 4007	3.429
Vulpes lagopus	IGPB M 553	7.086
Vulpes vulpes	IGPB M 6238	0.599
Vulpes vulpes	IGPB M 6182	0.549
Vulpes vulpes	IGPB M 6258	3.043

Testing for landmark repeatability

The digitized landmarks were tested for repeatability based on the procedure described in the supplementary data of Tarquini et al. (2020). All landmarks were digitized by myself in order to prevent errors of subjective placement. The first test included only the fixed landmarks on the crown (landmarks 1 to 9). Landmarks of three specimens belonging to three different genera (*Hyaenodon*, *Felis* and *Dasyurus*), using the principal carnassial tooth of each taxon, were digitized on three different days, randomizing the order of digitization on each date. Then, a Procrustes ANOVA of the geomorph library for the software R was used to perform two tests for significance. The ANOVA testing the landmarks for interdigitization differences of the three different days was not significant ($p = 0.943$), whereas it was significant when checking for intertaxonomic difference between the three genera ($p = 0.001$).

Taxon	Specimen	Tooth position
Hyaenodon	MNHN.F.Qu 8471	m3
Hyaenodon	NMB Q.C.221	m3
Hyaenodon	MNHN.F.Qu 8421	m3
Dasyurus	SMF 15505	m4
Dasyurus	SMF 1480	m4
Dasyurus	SMF 378	m4
Felis	ZFMK MAM 2018.0100	m1
Felis	ZFMK MAM 2018.0102	m1
Felis	ZFMK MAM 2018.0106	m1

Table S4: Specimens used for the first repeatability test, using only fixed landmarks.

Subsequently, all 69 landmarks, including semi-landmarks along the cervix line, were digitized for 11 different tooth positions (including carnivoran m1, dasyuromorph m2, m3, m4 and hyaenodont m1, m2 and m3) for two specimens per tooth on two different days, randomizing the order of digitization on each day. A Procrustes ANOVA checking the digitized landmarks for interdigitization differences on the two days was not significant ($p = 1$), whereas it was significant when testing for differences between the different tooth positions ($p = 0.001$).

Taxon	Specimen	Tooth position
Hyaenodon	MNHN.F.Qu 8421	m1, m2, m3
Hyaenodon	NMB Q.B.771	m1, m2, m3
Dasyurus	SMF 15505	m2, m3, m4
Dasyurus	SMF 1480	m2, m3, m4
Thylacinus	ZMB_Mam_036877	m2, m3, m4
Thylacinus	HLMD-M-1250	m2, m3, m4
Vulpes	IGPB M 6182	m1
Vulpes	IGPB M 6238	m1
Lycaon	ZFMK MAM 2001.0275	m1
Lycaon	ZFMK MAM 1981.0527	m1

Table S5: Specimens used for the second repeatability test, using fixed and semi-landmarks.

Figure S1: Distribution of carnivoran teeth (red dots) in the PCA morphospace. Non-carnivoran teeth are displayed as gray dots. *Canis lupus* = ca_lu, *Civettictis civetta* = ci_ci, *Cryptoprocta ferox* = cr_fe, *Crocuta Crocuta* = cr_cr, *Dinictis sp.* = di_sp, *Felis silvestris* = fe_si, *Ichneumia albicauda* = ic_al, *Lycaon pictus* = ly_pi, *Mustela lutreola* = mu_lu, *Mustela putorius* = mu_pu, *Neofelis nebulosa* = ne_ne, *Nimravus sp.* = ni_sp, *Otocolobus manul* = ot_ma, *Panthera leo* = pa_le, *Panthera pardus* = pa_pa, *Panthera tigris* = pa_ti, *Speothos venaticus* = sp_ve, *Viverra tangalunga* = vi_ta, *Viverra zibetha* = vi_zi, *Vulpes lagopus* = vu_la, *Vulpes vulpes* = vu_vu.

Figure S2: Distribution of dasyuromorph teeth (red dots) in the PCA morphospace. Non-dasyuromorph teeth are displayed as gray dots. *Dasyurus hallucatus* = da_ha, *Dasyurus maculatus* = da_my, *Dasyurus viverrinus* = da_vi, *Sarcophilus harrisii* = sa_ha, *Thylacinus cynocephalus* = th_cy.
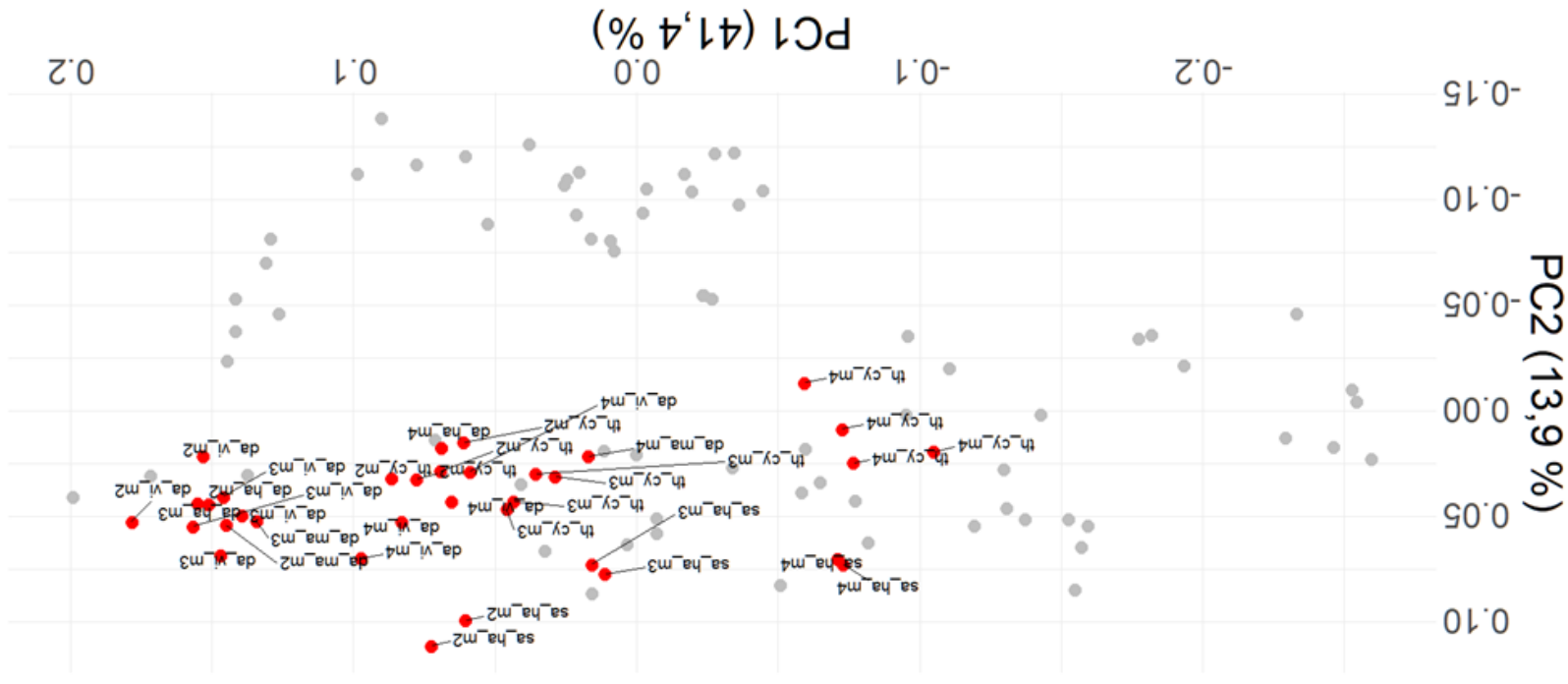
Figure S3: Distribution of hyaenodont teeth (red dots) in the PCA morphospace. Non-hyaenodont teeth are displayed as gray dots. *Hyaenodon exiguus* = hy_ex, *Hyaenodon filholi* = hy_fi, *Hyaenodon* sp. = hy_sp, *Oxyaenoides bicuspidens* = ox_bi, *Proviverra typica* = pr_ty, *Pterodon dasyuroides* = pt_da.
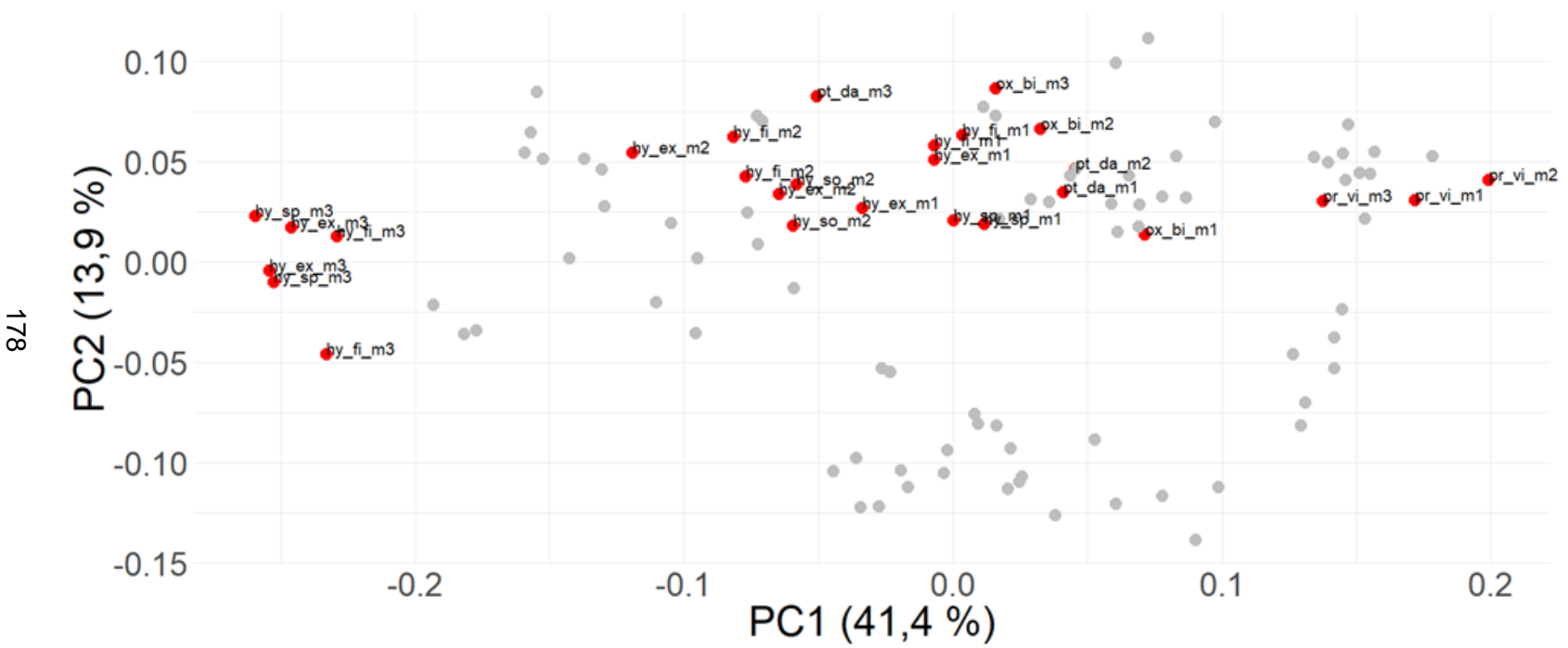
Figure S4: Shape scores of shape regression on size plotted against centroid size. ● Hyaenodonta (basal), ● Dasyuromorphia (basal), ● Carnivora (basal), ● Hyaenodonta (derived), ● Dasyuromorphia (derived), ● Carnivora (derived).
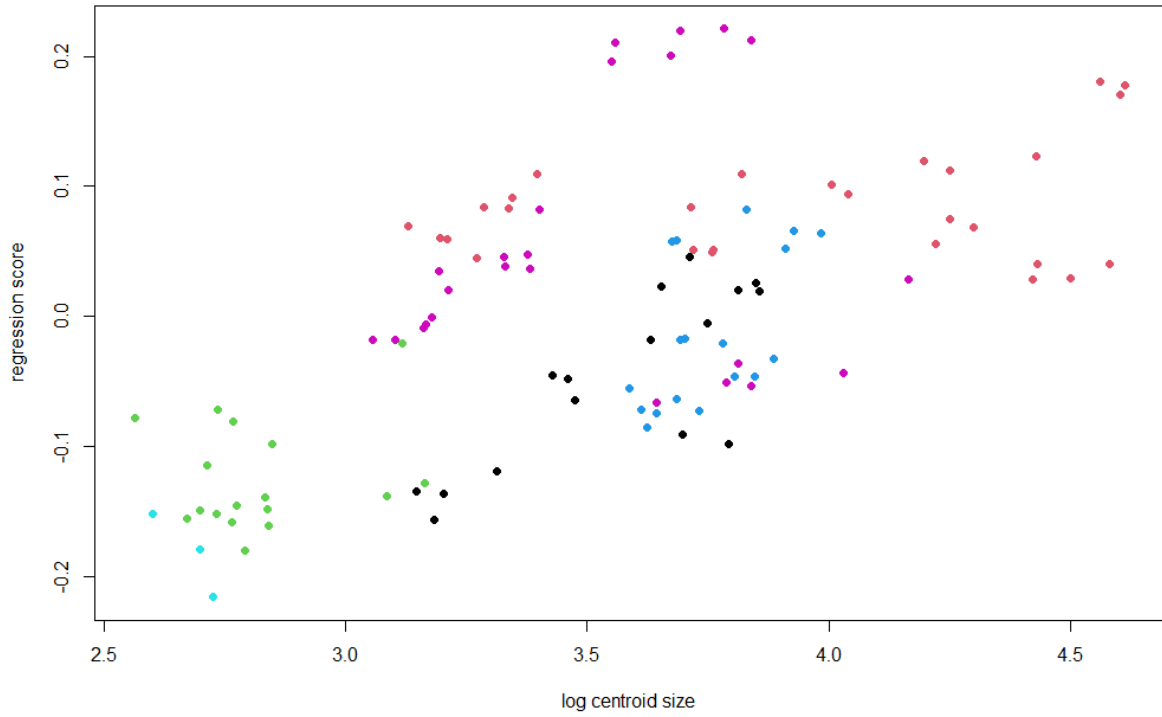
Table S6: Results of one way ANOVA, Welch's heteroscedastic F test and Levene's test for ariaDNE values, calculated with R.

	one way ANOVA					Welch's heteroscedastic F test				Levene's test		
	DF	Sum. Sq.	Mean Sq.	F value	p value	statistic	DF	denom. DF	p value	DF	F value	p value
ariaDNE	4	0.0083	0.0021	41.74	<0.001	59.607	4	20.2734	<0.001	4	6.0572	<0.001

Table S7: Results of the Shapiro-Wilk test for ariaDNE values of principal carnassials (divided into five groups based on functional morphology and phylogeny), calculated with R.

	Shapiro-Wilk test									
	Carnivora (basal)		Carnivora (derived)		Dasyuromorphia (basal)		Dasyuromorphia (derived)		Hyaenodonta (derived)	
	W value	p value	W value	p value	W value	p value	W value	p value	W value	p value
ariaDNE	0.9382	0.2977	0.9689	0.5307	0.8119	0.0751	0.8742	0.2436	0.8151	0.0414

Table S8: Results of the Shapiro-Wilk test for ariaDNE values of principal carnassials and all carnassials (respectively divided into two groups based on functional morphology) calculated with R.

	Shapiro-Wilk test							
	principal carnassials (basal)		principal carnassials (derived)		all carnassials (basal)		all carnassials (derived)	
	W value	p value	W value	p value	W value	p value	W value	p value
ariaDNE	0.9222	0.0742	0.9805	0.6661	0.9694	0.4273	0.9894	0.8147

Table S9: Results of Tukey's honest-significant-difference-test for ariaDNE values, calculated with R.

	Tukey's honest-significant-difference-test				
	Compared groups	diff	lwr.	upr.	p adj
ariaDNE	Carnivora (derived) + Carnivora (basal)	-0.0232	-0.0293	-0.0172	<0.001
	Carnivora (derived) + Dasyuromorphia (basal)	0.0188	0.0099	0.0277	<0.001
	Carnivora (derived) + Dasyuromorphia (derived)	-0.0014	-0.0103	0.0075	0.9923
	Carnivora (derived) + Hyaenodonta (derived)	-0.0050	-0.0129	0.0029	0.4010
	Carnivora (basal) + Dasyuromorphia (basal)	-0.0045	-0.0139	0.0049	0.6703
	Carnivora (basal) + Dasyuromorphia (derived)	-0.0246	-0.0340	-0.0152	<0.001
	Carnivora (basal) + Hyaenodonta (derived)	-0.0282	-0.0367	-0.0197	<0.001
	Dasyuromorphia (basal) + Dasyuromorphia (derived)	-0.0201	-0.0316	-0.0087	0.0001
	Dasyuromorphia (basal) + Hyaenodonta (derived)	-0.0237	-0.0345	-0.0130	<0.001
	Dasyuromorphia (derived) + Hyaenodonta (derived)	-0.0036	-0.0143	0.0071	0.8776

Table S10: Results of the Games-Howell test for ariaDNE values, calculated with R.

	Games-Howell test							
	Compared groups	Mean Difference	Standard Error	t	df	p	upper limit	lower limit
ariaDNE	Carnivora (derived) + Carnivora (basal)	0.023	0.002	8.551	24.16	<0.001	0.031	0.015
	Carnivora (derived) + Dasyuromorphia (basal)	0.019	0.001	10.667	15.979	<0.001	0.024	0.013
	Carnivora (derived) + Dasyuromorphia (derived)	-0.001	0.001	0.824	18.402	0.92	0.004	-0.006
	Carnivora (derived) + Hyaenodonta (derived)	-0.005	0.001	2.512	16.502	0.136	0.001	-0.011
	Carnivora (basal) + Dasyuromorphia (basal)	-0.004	0.002	1.631	20.937	0.495	0.004	-0.013
	Carnivora (basal) + Dasyuromorphia (derived)	-0.025	0.002	9.159	20.647	<0.001	-0.017	-0.033
	Carnivora (basal) + Hyaenodonta (derived)	-0.028	0.002	9.761	22.987	<0.001	-0.02	-0.037
	Dasyuromorphia (basal) + Dasyuromorphia (derived)	-0.02	0.001	11.765	9.899	<0.001	-0.014	-0.026
	Dasyuromorphia (basal) + Hyaenodonta (derived)	-0.024	0.001	11.777	11.981	<0.001	-0.017	-0.03
	Dasyuromorphia (derived) + Hyaenodonta (derived)	-0.004	0.001	1.856	11.781	0.389	0.003	-0.01

Table S11: Results of the linear discriminant analysis of ariaDNE for principal carnassials, calculated in R.

ariaDNE	a priori group	calculated with original data	posterior probability calculated with CV	
		LD1	basal	derived
0.0517	derived	-2.7715	0.0000	1.0000
0.0530	derived	-2.5893	0.0000	1.0000
0.0549	derived	-2.3192	0.0001	0.9999
0.0554	derived	-2.2585	0.0001	0.9999
0.0567	derived	-2.0668	0.0001	0.9999
0.0570	derived	-2.0359	0.0002	0.9998
0.0572	derived	-2.0018	0.0002	0.9998
0.0578	derived	-1.9115	0.0002	0.9998
0.0585	derived	-1.8258	0.0003	0.9997
0.0588	derived	-1.7789	0.0004	0.9996
0.0591	derived	-1.7309	0.0004	0.9996
0.0595	derived	-1.6867	0.0005	0.9995
0.0596	derived	-1.6617	0.0005	0.9995
0.0597	derived	-1.6494	0.0006	0.9994
0.0604	derived	-1.5581	0.0008	0.9992
0.0608	derived	-1.5033	0.0009	0.9991

0.0609	derived	-1.4829	0.0010	0.9990
0.0615	derived	-1.3968	0.0013	0.9987
0.0616	derived	-1.3912	0.0013	0.9987
0.0621	derived	-1.3219	0.0016	0.9984
0.0622	derived	-1.3003	0.0018	0.9982
0.0623	derived	-1.2824	0.0019	0.9981
0.0625	derived	-1.2637	0.0020	0.9980
0.0633	derived	-1.1561	0.0028	0.9972
0.0639	derived	-1.0637	0.0037	0.9963
0.0640	derived	-1.0461	0.0040	0.9960
0.0652	derived	-0.8813	0.0067	0.9933
0.0654	derived	-0.8588	0.0071	0.9929
0.0657	derived	-0.8139	0.0082	0.9918
0.0658	derived	-0.8007	0.0086	0.9914
0.0674	derived	-0.5802	0.0171	0.9829
0.0675	derived	-0.5673	0.0178	0.9822
0.0679	derived	-0.5018	0.0218	0.9782
0.0688	derived	-0.3860	0.0312	0.9688
0.0690	derived	-0.3548	0.0344	0.9656
0.0692	derived	-0.3244	0.0378	0.9622
0.0708	derived	-0.1066	0.0732	0.9268
0.0710	basal	-0.0677	0.0577	0.9423
0.0712	derived	-0.0440	0.0882	0.9118
0.0716	derived	0.0146	0.1047	0.8953
0.0724	derived	0.1259	0.1441	0.8559
0.0741	derived	0.3662	0.2723	0.7277
0.0756	derived	0.5712	0.4291	0.5709
0.0761	derived	0.6429	0.4907	0.5093
0.0770	basal	0.7678	0.5496	0.4504
0.0774	basal	0.8192	0.5920	0.4080
0.0776	basal	0.8414	0.6098	0.3902
0.0782	basal	0.9367	0.6823	0.3177
0.0812	basal	1.3459	0.8910	0.1090
0.0824	basal	1.5220	0.9350	0.0650
0.0830	basal	1.6047	0.9493	0.0507
0.0836	basal	1.6895	0.9608	0.0392
0.0836	basal	1.6926	0.9612	0.0388
0.0840	basal	1.7471	0.9672	0.0328
0.0841	basal	1.7573	0.9682	0.0318
0.0849	basal	1.8743	0.9779	0.0221
0.0853	basal	1.9311	0.9815	0.0185
0.0856	basal	1.9632	0.9832	0.0168
0.0870	basal	2.1669	0.9912	0.0088
0.0889	basal	2.4243	0.9961	0.0039
0.0946	basal	3.2223	0.9997	0.0003

0.0976	basal	3.6396	0.9999	0.0001
0.0992	basal	3.8605	1.0000	0.0000
0.0997	basal	3.9358	1.0000	0.0000
0.1029	basal	4.3814	1.0000	0.0000
0.1037	basal	4.4975	1.0000	0.0000

Table S12: Results of the linear discriminant analysis of ariaDNE for all carnassials, calculated in R.

ariaDNE	a priori group	calculated with original data	posterior probability calculated with CV	
		LD1	basal	derived
0.0495	derived	-2.9844	0.0000	1.0000
0.0510	derived	-2.7799	0.0000	1.0000
0.0517	derived	-2.6896	0.0000	1.0000
0.0519	derived	-2.6585	0.0000	1.0000
0.0526	derived	-2.5661	0.0000	1.0000
0.0530	derived	-2.5115	0.0000	1.0000
0.0549	derived	-2.2474	0.0000	1.0000
0.0551	derived	-2.2196	0.0000	1.0000
0.0554	derived	-2.1880	0.0001	0.9999
0.0561	derived	-2.0841	0.0001	0.9999
0.0562	derived	-2.0686	0.0001	0.9999
0.0567	derived	-2.0006	0.0001	0.9999
0.0568	derived	-1.9986	0.0001	0.9999
0.0570	derived	-1.9704	0.0001	0.9999
0.0572	derived	-1.9371	0.0001	0.9999
0.0578	derived	-1.8488	0.0002	0.9998
0.0581	derived	-1.8111	0.0002	0.9998
0.0585	derived	-1.7650	0.0002	0.9998
0.0588	derived	-1.7192	0.0003	0.9997
0.0590	derived	-1.6857	0.0003	0.9997
0.0591	derived	-1.6722	0.0003	0.9997
0.0595	derived	-1.6290	0.0004	0.9996
0.0596	derived	-1.6046	0.0004	0.9996
0.0597	derived	-1.5926	0.0004	0.9996
0.0604	derived	-1.5032	0.0006	0.9994
0.0608	derived	-1.4497	0.0007	0.9993
0.0609	derived	-1.4297	0.0007	0.9993
0.0613	derived	-1.3834	0.0008	0.9992
0.0615	derived	-1.3456	0.0009	0.9991
0.0616	derived	-1.3401	0.0009	0.9991
0.0616	derived	-1.3295	0.0010	0.9990
0.0621	derived	-1.2724	0.0012	0.9988
0.0621	derived	-1.2696	0.0012	0.9988

0.0622	derived	-1.2512	0.0013	0.9987
0.0623	derived	-1.2337	0.0013	0.9987
0.0625	derived	-1.2154	0.0014	0.9986
0.0633	derived	-1.1102	0.0020	0.9980
0.0635	derived	-1.0787	0.0022	0.9978
0.0637	derived	-1.0524	0.0024	0.9976
0.0639	derived	-1.0246	0.0027	0.9973
0.0639	derived	-1.0199	0.0027	0.9973
0.0640	derived	-1.0027	0.0029	0.9971
0.0646	derived	-0.9298	0.0036	0.9964
0.0652	derived	-0.8415	0.0049	0.9951
0.0654	derived	-0.8195	0.0052	0.9948
0.0657	derived	-0.7757	0.0060	0.9940
0.0658	derived	-0.7627	0.0063	0.9937
0.0660	derived	-0.7418	0.0067	0.9933
0.0674	derived	-0.5492	0.0125	0.9875
0.0674	derived	-0.5471	0.0126	0.9874
0.0675	derived	-0.5346	0.0131	0.9869
0.0679	derived	-0.4705	0.0161	0.9839
0.0682	derived	-0.4286	0.0185	0.9815
0.0684	derived	-0.4038	0.0200	0.9800
0.0688	derived	-0.3573	0.0232	0.9768
0.0689	derived	-0.3417	0.0244	0.9756
0.0689	derived	-0.3414	0.0244	0.9756
0.0690	derived	-0.3268	0.0256	0.9744
0.0692	derived	-0.2970	0.0282	0.9718
0.0704	derived	-0.1390	0.0465	0.9535
0.0707	derived	-0.0903	0.0541	0.9459
0.0708	derived	-0.0840	0.0552	0.9448
0.0710	basal	-0.0461	0.0485	0.9515
0.0712	derived	-0.0228	0.0668	0.9332
0.0716	derived	0.0344	0.0796	0.9204
0.0724	derived	0.1433	0.1105	0.8895
0.0741	derived	0.3782	0.2148	0.7852
0.0746	derived	0.4330	0.2477	0.7523
0.0756	derived	0.5786	0.3511	0.6489
0.0761	derived	0.6487	0.4078	0.5922
0.0770	basal	0.7708	0.4814	0.5186
0.0774	basal	0.8211	0.5244	0.4756
0.0776	basal	0.8428	0.5428	0.4572
0.0776	basal	0.8494	0.5483	0.4517
0.0782	basal	0.9360	0.6196	0.3804
0.0791	derived	1.0487	0.7371	0.2629
0.0812	basal	1.3361	0.8615	0.1385
0.0812	derived	1.3396	0.8898	0.1102

0.0813	basal	1.3577	0.8698	0.1302
0.0824	basal	1.4992	0.9143	0.0857
0.0824	basal	1.5082	0.9166	0.0834
0.0830	basal	1.5891	0.9349	0.0651
0.0836	basal	1.6720	0.9496	0.0504
0.0836	basal	1.6750	0.9501	0.0499
0.0840	basal	1.7283	0.9578	0.0422
0.0841	basal	1.7383	0.9591	0.0409
0.0849	basal	1.8527	0.9715	0.0285
0.0853	basal	1.9082	0.9761	0.0239
0.0856	basal	1.9396	0.9784	0.0216
0.0869	basal	2.1171	0.9878	0.0122
0.0870	basal	2.1388	0.9887	0.0113
0.0889	basal	2.3904	0.9950	0.0050
0.0890	basal	2.4083	0.9953	0.0047
0.0896	basal	2.4949	0.9965	0.0035
0.0926	basal	2.9046	0.9991	0.0009
0.0938	basal	3.0644	0.9995	0.0005
0.0943	basal	3.1335	0.9996	0.0004
0.0944	basal	3.1390	0.9996	0.0004
0.0946	basal	3.1707	0.9996	0.0004
0.0956	basal	3.3017	0.9998	0.0002
0.0973	basal	3.5407	0.9999	0.0001
0.0976	basal	3.5787	0.9999	0.0001
0.0992	basal	3.7947	1.0000	0.0000
0.0997	basal	3.8683	1.0000	0.0000
0.1029	basal	4.3039	1.0000	0.0000
0.1037	basal	4.4175	1.0000	0.0000

Table S13: Predicted group assignment of basal hyaenodont (*Proviverra*) principal carnassial (m3) and all carnassials (m1, m2, m3), based on the LDA of ariaDNE.

	predicted group probability for principal carnassial (based on training data using only principal carnassials)		predicted group probability (based on training data using all carnassias)					
			m1		m2		m3	
	basal	derived	basal	derived	basal	derived	basal	derived
LDA of ariaDNE	0.9999	0.0001	0.9953	0.0047	0.9997	0.0003	0.9999	0.0001

Supplementary CD

Table S14: Files stored on the added CD.

File	Description
Dasyurus.ofaproject	OFA project file for *Dasyurus viverrinus*
Felis.ofaproject	OFA project file for *Felis silvestris*
Hyaenodon.ofaproject	OFA project file for *Hyaenodon exiguus*
Speothos.ofaproject	OFA project file for *Speothos venaticus*
Thylacinus.ofaproject	OFA project file for *Thylacinus cynocephalus*
Viverra.ofaproject	OFA project file for *Viverra tangalunga*
fixed_landmarks.RData	Handplaced fixed landmarks, to be imported in R as an object of class "array"
semilandmarks.RData	Handplaced semi-landmarks, to be imported in R as an object of class "array"
tree_export.RData	Phylogenetic tree used in this study, to be imported in R as an object of class "phylo"
gpa_output.RData	Output of the Procrustes analysis, to be imported in R as an object of class "gpagen" (requires the package "geomorph")

Appendix References

Adams, D., Collyer, M., Kaliontzoloulou, A., & Baken, E. (2021). Package "geomorph": Read, manipulate and digitize landmark data, generate shape variables via Procrustes analysis for points, curves and surfaces, perform shape analyses, and provide graphical depictions of shapes and patterns of shape variation. *R package version 4.0.0*. Retrieved from https://cran.r-project.org/web/packages/geomorph.

R Core Team. (2020). R: A language and environment for statistical computing. Vienna, Austria. Retrieved from http://R-project.org/: R Foundation for Statistical Computing.

Shan, S., Kovalsky, S. Z., Winchester, J. M., Boyer, D.M., & Daubechies, I. (2019). ariaDNE: A robustly implemented algorithm for Dirichlet energy of the normal. *Methods in Ecology and Evolution*, 10, 541 – 552. https://doi.org/10.1111/2041-210X.13148

Shan, S., Kovalsky, S. Z., Winchester, J. M., Boyer, D.M., & Daubechies, I. (2019). ariaDNE: A robustly implemented algorithm for Dirichlet energy of the normal. *Methods in Ecology and Evolution*, 10, 541 – 552. https://doi.org/10.1111/2041-210X.13148

Tarquini, S. D., Chemisquy, M. A., & Prevosti, F. J. (2020). Evolution of the carnassial in living mammalian carnivores (Carnivora, Didelphimorphia, Dasyuromorphia): Diet, phylogeny, and allometry. *Journal of Mammalian Evolution*, 27, 95 – 109. https://doi.org/10.1007/s10914-018-9448-7

Associated Publication

Lang, A. J., Engler, T., & Martin, T. (2021). Dental topographic and three-dimensional geometric morphometric analysis of carnassialization in different clades of carnivorous mammals (Dasyuromorphia, Carnivora, Hyaenodonta). *Journal of Morphology*, 283(1), 91 – 108. https://doi.org/10.1002/jmor.21429

RESEARCH ARTICLE

Dental topographic and three-dimensional geometric morphometric analysis of carnassialization in different clades of carnivorous mammals (Dasyuromorphia, Carnivora, Hyaenodonta)

Andreas Johann Lang [ORCID] | Thomas Engler | Thomas Martin

Institute of Geosciences, Section Paleontology, Rheinische Friedrich-Wilhelms-Universität Bonn, Bonn, Germany

Correspondence
Andreas Johann Lang, Institute of Geosciences, Section Paleontology, Rheinische Friedrich-Wilhelms-Universität Bonn, Nussallee 8, 53115 Bonn, Germany.
Email: ajlang@gmx.de

Abstract
The evolution of carnassial teeth in mammals, especially in the Carnivora, has been subject of many morphometric and some dental topographic studies. Here, we use a combination of dental topographic analysis (Dirichlet normal energy) and 3D geometric morphometrics of less and high carnassialized lower teeth of carnivoran, dasyuromorph and hyaenodont taxa. Carnassial crown curvature, as indicated by Dirichlet normal energy, is high in lesser carnassialized teeth and low in higher carnassialized teeth, where it is influenced by the reduction of crown features such as cusps and crests. PC1 of the geometric morphometric analysis is linked to enlargement of the carnassial blade, reduction of the talonid crushing basin and an increasingly asymmetric cervix line with an enlarged mesial flexure in more carnassialized teeth. Distribution of PC1 values further indicates that along the tooth row of dasyuromorphs (m2–m4) and hyaenodonts (m1–m3) the most distal carnassial is the most carnassialized (principal carnassial), and in most taxa with overall higher carnassialized teeth, carnassialization successively increases from the anterior to the posterior tooth position along the tooth row. PC2 indicates that a longitudinal elongated carnassial is present in caniforms and in unspecialized feliforms, which separates these taxa in morphospace from all dasyuromorphs, hyaenodonts and specialized feliforms. An ancestral state reconstruction shows that this longitudinal elongation may be a plesiomorphic ancestral state for the Carnivora, which is different from the Dasyuromorphia and the Hyaenodonta. This elongation, enabling the presence of a longitudinally aligned carnassial blade as well as a complete talonid basin, might have provided the Carnivora with an advantage in terms of adaptive versatility.

KEYWORDS
carnassials, dental topographic analysis, functional morphology, geometric morphometrics

1 | INTRODUCTION

1.1 | Carnivory in mammals

Carnivory in terms of a diet comprised of vertebrate meat has evolved multiple times within different clades of mammals and resulted in repeated convergent morphological adaptations (De Muizon & Lange-Badré, 1997). The oldest evidence for carnivory in mammals is known from the Early Cretaceous eutriconodontan *Repenomamus* (Hu et al., 2005). Members of the Late Cretaceous metatherian taxa Deltatheroidea and Stagodontidae also show carnivorous adaptations, with molars of several species showing an emphasis on the shearing function (De Muizon & Lange-Badré, 1997). After the extinction of the non-avian dinosaurs at the end of the Cretaceous, many therian lineages started to occupy the vacant niches of meat eaters as predators and/or scavengers. Among the earliest were the Mesonychia, a group of carnivorous ungulates, which evolved a greater emphasis on piercing and bone-crushing rather than precise shearing (Szalay & Gould, 1966). By the end of the Paleocene, clades which possessed true carnassial molars with a much higher emphasis on precise shearing and a much higher degree of morphological convergence evolved. These early Paleocene taxa comprise the first representatives of Oxyaenodonta (Gingerich, 1980), Hyaenodonta (Gheebrant et al., 2006; Meng et al., 1998) and Carnivoramorpha (Flynn & Wesley-Hunt, 2005), the latter including the ancestors of the modern Carnivora (Flynn et al., 2010). In South America, the metatherian Sparassodonta showed similar dental adaptations and occupied the carnivorous niche until they went extinct in the early Pliocene (Prevosti & Forasiepi, 2018). In Australia, the highly specialized metatherian Thylacoleonidae appeared in the late Oligocene and were probably the top carnivorous mammals in Australia in the later Cenozoic (Gillespie et al., 2019).

The dominant extant group of carnivorous mammals are the eutherian Carnivora, which comprise the doglike (Caniformia) and cat-like (Feliformia) carnivorans as well as several extinct lineages (Flynn et al., 2010). All other aforementioned groups of carnivorous mammals went extinct. However, among extant mammals, carnivorous proclivities are also present in the South American didelphid *Lutreolina crassicaudata* (Goin et al., 2016).

Furthermore, the australidelphian order Dasyuromorphia includes particularly highly specialized carnivorous species within two families (Dasyuridae and Thylacinidae) that survived into historic times whereby the family Dasyuridae is still present in Australia today. The Dasyuridae include a large variety of small insectivorous species, of which some may occasionally consume vertebrate meat, as well as the exclusively carnivorous Tasmanian devil (*Sarcophilus harrisii*) and the quolls (*Dasyurus* spp.), including at least one species (*D. maculatus*) which relies exclusively on vertebrate meat (Hutchins et al., 2003). Thylacinidae are known since the late Oligocene (Ravinsky et al., 2019). The last member, the Tasmanian tiger (*Thylacinus cynocephalus*), which went extinct in 1936, was a specialized carnivorous dasyuromorph, probably relying predominantly on small vertebrate prey (Jones & Stoddart, 1998).

Of special interest to our study is the extinct placental order Hyaenodonta, as it coexisted with the Carnivora throughout the Cenozoic up until its extinction in the Miocene. Although the fossil record of the Hyaenodonta remains fragmentary, new findings during the last decade have improved our knowledge on the evolutionary history of this enigmatic group. After their most likely European origin in the early Paleocene, the Hyaenodonta dispersed into North America, Asia and Africa, forming endemic Northern American, Afro-Arabian and European clades during the Eocene (Borths & Stevens, 2019). Throughout the Eocene, hyaenodont taxa were present in Europe, where they filled the niches of top predators, and were also present in North America, where they competed with early carnivoran and oxyaenodont taxa (Morlo, 1999). In North America, there is a drastic decline of hyaenodont diversity at the end of the Eocene, which coincided with the radiation of early Canidae, while the decline of hyaenodont taxa in Europe was less abrupt and in steady progress throughout the Oligocene (Pires et al., 2015). Additionally, the fossil record shows a significant isolated radiation of the hyaenodont Hyainailouroidea in Afro-Arabia during the Paleogene and Neogene and points to a decline of African hyainailouroid diversity only after carnivoran taxa dispersed into Africa around the Oligocene-Miocene boundary (Borths & Stevens, 2017a). Miocene hyainailouroid taxa include some of the largest mammalian land predators (Borths & Stevens, 2019). Only a few remaining hyaenodont lineages kept coexisting with the Carnivora up until the extinction of the Hyaenodonta in the late Miocene (Barry, 1988; Wang et al., 2005). Carnivoran diversity increased during the Oligocene and Miocene (Pires et al., 2015). This pattern is in congruence with the idea that hyaenodont taxa evolved specialized carnivorous morphotypes first and were later replaced by carnivoran taxa with similar adaptations (Van Valkenburgh, 1988; Wesley-Hunt, 2005). The iterative evolution of convergent carnivorous morphotypes in different mammalian lineages throughout the Paleogene and Neogene, sometimes in direct competition, has been described as "dynastic replacement" by Van Valkenburgh (1999). According to current knowledge, in comparison to other Paleogene carnivorous mammals, the Carnivora and Hyaenodonta were evolutionarily the most successful in terms of diversity and dispersal in Eurasia, North America and Africa, and competed for the longest time of their existence for the same dietary resource, namely vertebrate meat.

1.2 | Carnassial dentitions

The convergent evolution of morphological characters in carnivorous mammals becomes apparent when looking at their dentitions, especially the cheek teeth. The Premolars and molars become specialized for the processing of meat, which in fact may pose a key factor to our understanding of the evolutionary history of carnivorous mammals. The tribosphenic origin of the molars provided them with a set of tools (cutting crests and a crushing protocone/talonid), which were convergently modified for a carnivorous diet in multiple lineages. These modifications resulted in enlarged distal upper (metacrista) and

mesial lower (paracristid) cutting blades and the reduction of subordinate cutting structures (prevallum/postvallid shearing) as well as the reduction of the crushing protocone-talonid functional complex (De Muizon & Lange-Badré, 1997). Cheek teeth which evolved the aforementioned characters are typically referred to as "carnassials". Modification and reduction of crown features, especially of the talonid cusps, has been demonstrated to follow a patterning cascade mode of successively (most likely genetically) blocked cusp development (Solé & Ladevèze, 2017). In the Carnivora, the last upper premolar (P4) and the first lower molar (m1) form the carnassials (Matthew, 1909). The Hyaenodonta evolved multiple carnassials in their cheek teeth. Commonly, all molars in the Hyaenodonta except for the upper M3 have been described as carnassials (Butler, 1946), although there is no strict consensus about that. Carnivorous marsupials show a similar pattern, possessing multiple carnassial teeth (Werdelin, 1987). In the Hyaenodonta, the distal lower molar (m3) has been described as the most specialized for cutting, also termed "principal carnassial" (Butler, 1946; Matthew, 1909). Likewise, the distal lower molar of dasyuromorphs (m4) is typically interpreted to be the most specialized (Matthew, 1909; Prevosti et al., 2012; Tarquini et al., 2020; Werdelin, 1986, 1987). The adaptation of cheek teeth to a more specialized carnassial condition has been termed "carnassialization" by Simpson (1959). The heterodont cheek dentition of the Carnivora (one mesial carnassial per tooth row and, if present and functional, distal post-carnassials used for crushing) is the main difference to the homodont condition in the Hyaenodonta and the Dasyuromorphia (all distal molars show a degree of carnassialization).

Molar morphology of carnivorous mammals provides crucial information about molar function and dietary adaptation (Cope, 1879; Matthew, 1909; Osborn, 1907). Measurements of specific morphological crown features are usually used to quantify the degree of carnassialization (e.g., Butler, 1946; Crusafont-Pairó & Truyols-Santonja, 1956; Van Valkenburgh, 1988, 1989; Voss et al., 2004; Voss & Jansa, 2003). Dental characters of Hyaenodonta and Oxyaenodonta were also used in combination with locomotory characters to reconstruct morphospaces of North American and European Eocene predatory guilds (Morlo, 1999). Tarquini et al. (2020) further employed geometric morphometric analysis to differentiate carnassial morphotypes of Carnivora, Didelphimorphia and Dasyuromorphia with different diets. These morphometric studies provide crucial information about the paleobiology of extant and extinct carnivorous mammals, especially in terms of dietary and ecomorphological adaptations. Even though over the last two decades the dental topographic analysis of molar crowns, using 3D models of scanned tooth surfaces, has become a well-established method in mammal paleontology (see Ungar, 2018), teeth of carnivorous mammals have been given little attention in this regard.

Our study focuses on the analysis of lower carnassial morphology of carnivoran, dasyuromorph and hyaenodont taxa (Figure 1). We apply a method of virtual 3D crown quantification utilizing a combination of geometric morphometric analysis (GMA) and dental
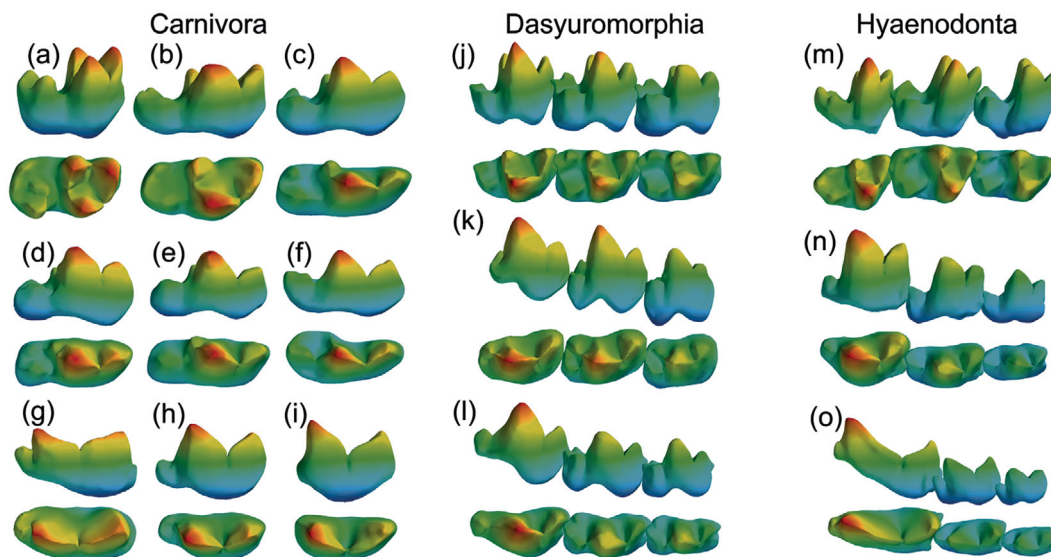

FIGURE 1 Topographic height 3D models, created with MorphoTester (Winchester, 2016), of carnivoran (m1), dasyuromorph (m2 to m4) and hyaenodont (m1 to m3) lower carnassials, showing topographic elevation from low (blue) to high (red) in buccal and occlusal view (mesial is to the right). Basal carnassialized carnivoran condition of (a) *Ichneumia albicauda* (ZFMK MAM 1976.0125), (b) *Viverra zibetha* (ZFMK MAM 1968.0085) and (c) *Vulpes vulpes* (IGPB M 6258); derived carnassialized carnivoran condition of (d) *Canis lupus* (ZFMK MAM 1988.0151), (e) *Lycaon pictus* (ZFMK MAM 2001.0275), (f) *Mustela lutreola* (IGPB M 2151a), (g) *Crocuta crocuta* (IGPB M 5997), (h) *Cryptoprocta ferox* (ZFMK MAM 1987.0584) and (i) *Felis silvestris* (ZFMK MAM 2018.0102); basal carnassialized dasyuromorph condition of (j) *Dasyurus viverrinus* (SMF 1480); derived carnassialized dasyuromorph condition of (k) *Sarcophilus harrisii* (ZMB_Mam_001733) and (l) *Thylacinus cynocephalus* (ZMB_Mam_036877); basal carnassialized hyaenodont condition of (m) *Proviverra typica* (NMB En.130, NMB En.176, NMB En.179); derived carnassialized hyaenodont condition of (n) *Pterodon dasyuroides* (NMB Q.B.606, NMB Q.C. 413) and (o) *Hyaenodon filholi* (NMB Q.B.771). 3D models not to scale

TABLE 1   List of taxa with specimen collection number of which lower carnassials were used for this study

Taxon	Order	Carnassialization type	Specimens	*n* (MCP)	*n* (ICP)	*n* (PCP)
Canis lupus (Linnaeus, 1758)	Carnivora	Derived	ZFMK MAM 1978.0268, ZFMK MAM 1988.0151, SMF 15699, SMF 36408	–	–	4
Civettictis civetta (Schreber, 1776)	Carnivora	Basal	ZFMK MAM 1958.0012[a], ZFMK MAM 1993.0705, ZFMK MAM 1958.0015	–	–	3 (DTA) 2(GMA)
Crocuta crocuta (Erxleben, 1777)	Carnivora	Derived	IGPB M 5997, IGPB M 418, IGPB M 427	–	–	3
Cryptoprocta ferox (Bennett, 1833)	Carnivora	Derived	ZFMK MAM 1987.0584	–	–	1
Dinictis sp. (Leidy, 1854)	Carnivora	Derived	SMNK-PAL 35101; SMNK-PAL 35102[a]	–	–	2 (DTA) 1(GMA)
Felis silvestris (Schreber, 1777)	Carnivora	Derived	ZFMK MAM 2018.0100, ZFMK MAM 2018.0102, ZFMK MAM 2018.0106	–	–	3
Otocolobus manul (Pallas, 1776)	Carnivora	Derived	ZFMK MAM 1965.0510	–	–	1
Ichneumia albicauda (Cuvier, 1829)	Carnivora	Basal	ZFMK MAM 1931.0056[a], ZFMK MAM 1976.0125, SMF 16553, SMF 32735, SMF 32733[b]	–	–	4
Lycaon pictus (Temminck, 1820)	Carnivora	Derived	ZFMK MAM 1956.0888, ZFMK MAM 1981.0527, ZFMK MAM 2001.0275	–	–	3
Mustela lutreola (Linnaeus, 1761)	Carnivora	Derived	IGPB M 2151a, IGPB M 2151b, IGPB M 2151c	–	–	3
Mustela putorius (Linnaeus, 1758)	Carnivora	Derived	IGPB M 335	–	–	1
Neofelis nebulosa (Griffith, 1821)	Carnivora	Derived	ZFMK 1984.0337	–	–	1
Nimravus sp. (Cope, 1879)	Carnivora	Derived	IGPB M 6134	–	–	1
Panthera leo (Linnaeus, 1758)	Carnivora	Derived	ZFMK MAM 2006.0031	–	–	1
Panthera pardus (Linnaeus, 1758)	Carnivora	Derived	ZFMK MAM 1997.0547	–	–	1
Panthera tigris (Linnaeus, 1758)	Carnivora	Derived	ZFMK MAM 1986.0118	–	–	1
Speothos venaticus (Lund, 1842)	Carnivora	Derived	ZFMK MAM 1992.0565, ZFMK MAM 1954.0154, ZFMK MAM 1987.0386	–	–	3
Viverra tangalunga (Gray, 1832)	Carnivora	Basal	SMF 20928, SMF 697	–	–	2
Viverra zibetha (Linnaeus, 1758)	Carnivora	Basal	ZFMK MAM 1968.0085, SMF 16516	–	–	2
Vulpes laogpus (Linnaeus, 1758)	Carnivora	Basal	IGPB M 553, IGPB M 4005, IGPB M 4007	–	–	3
Vulpes vulpes (Frisch, 1775)	Carnivora	Basal	IGPB M 6182, IGPB M 6238, IGPB M 6258	–	–	3
Dasyurus viverrinus (Shaw, 1800)	Dasyuromorphia	Basal	SMF 378[a], SMF 1480, SMF 1485, SMF 15505	4 (DTA) 3 (GMA)	4	4
Dasyurus hallucatus (Gould, 1842)	Dasyuromorphia	Basal	TMM M-6921	1	1	1
Dasyurus maculatus (Kerr, 1792)	Dasyuromorphia	Basal	UMZC A6.10/3	1	1	1
Sarcophilus harrisii (Boitard, 1841)	Dasyuromorphia	Derived	ZMB_Mam_001733, ZMB_Mam_002343	2	2	2
Thylacinus cynocephalus (Harris, 1808)	Dasyuromorphia	Derived	ZMB_Mam_047902, ZMB_Mam_036877, HLMD-M-1250, NMB 2526	4	4	4
Hyaenodon sp. (Laizer & Parieu, 1838)	Hyaenodonta	Derived	MNHN.F.Qu 8471, MNHN.F.Qu 8467	2	2	2
Hyaenodon exiguus (Gervais, 1872)	Hyaenodonta	Derived	NMB Q.B.603, NMB Q.C.221	2	2	2

TABLE 1   (Continued)

Taxon	Order	Carnassialization type	Specimens	n (MCP)	n (ICP)	n (PCP)
Hyaenodon filholi (Schlosser, 1877)	Hyaenodonta	Derived	NMB Q.B.771, MNHN.F.Qu 8421	2	2	2
Oxyaenoides bicuspidens (Matthes, 1967)	Hyaenodonta	Derived	GMH XIV-2909-1954	1	1	1
Proviverra typica (Rütimeyer, 1862)	Hyaenodonta	Basal	NMB En.130, NMB En.176, NMB En.179	1	1	1
Pterodon dasyuroides (Blainville, 1839)	Hyaenodonta	Derived	NMB Q.B.606, NMB Q.C. 413	1	1	1

Abbreviations: GMH = *Geiseltal collection*, Halle an der Saale, Germany; HLMD = Hessisches Landesmuseum Darmstadt, Germany; IGPB = Institute of Geosciences, paleontology, Rheinische Friedrich-Wilhelms-Universität Bonn, Germany; MNHN = Muséum national d'Histoire naturelle, Paris, France; NMB = Naturhistorisches museum Basel, Switzerland; SMF = *Senckenberg Naturmuseum* Frankfurt, Senckenberg Gesellschaft für Naturforschung, Germany; SMNK = Staatliches museum für *Naturkunde Karlsruhe, Germany*; TMM = Texas memorial museum, University of Texas, Austin, USA; UMCZ = University Museum of Zoology, University of Cambridge, United Kingdom; ZFMK = Zoologisches Forschungsmuseum Alexander Koenig, Bonn, Germany; ZMB = m*useum* für Naturkunde, Humboldt-Universität zu *Berlin, Germany*.
[a]Teeth of this specimen were omitted in the GMA.
[b]Teeth of this specimen were omitted in the DTA.

topographic analysis (DTA) to find signals correlated with functional carnassial morphology and the degree of carnassialization. Differences in crown shape and topography of carnassials are observed between different taxa and between different molar positions of taxa with multiple carnassials. A subsequent ancestral state reconstruction of shape and topography parameters is used to identify possible differences in the evolution of principle carnassials.

2 | MATERIALS AND METHODS

2.1 | Carnivorous taxa investigated

A total of 12 dasyuromorph, 47 carnivoran and 12 hyaenodont specimens were included in this study, resulting in 110 individual teeth of 31 species within 23 different genera that were quantified (Table 1). Because in the Carnivora the bunodont post-carnassials are not part of the convergent adaptive spectrum of carnassialization (see introduction) we only included the carnivoran m1 in our study, while we included the complete lower molar series of hyaenodonts (m1–m3) and the three distal molars of the dasyuromorphs (m2–m4; Figure 1). Because the dasyuromorph m1 lacks a complete trigonid and mesial cutting blade with associated attritional shearing wear, we excluded it from our study.

2.2 | Quantification of tooth morphology in carnivorous mammals

We use the quantification of the total Dirichlet Normal Energy (DNE), first introduced by Bunn et al. (2011), as a method of DTA. The DNE method measures curvature (undulation) of a surface as the deviation from a planar surface (Bunn et al., 2011). In the context of dental topography, DNE is interpreted to quantify the change in height and curvature of cusps and crests (Evans, 2013). Dirichlet Normal Energy is a strong indicator for dietary adaptations (e.g., Bunn et al., 2011;

Winchester et al., 2014) and further has been shown to be correlated with other factors such as precipitation seasonality and annuality (Fulwood, 2020). Dirichlet Normal Energy is independent of homolog orientation, which makes it especially suitable for a database as phylogenetically diverse as ours.

For calculation of DNE, we used the implementation of the ariaDNE ("A Robustly Implemented Algorithm for Dirichlet Normal Energy") script for Matlab 9.10.0.1710957 R2021a (The MathWorks Inc.), developed and provided by Shan et al. (2019). The ariaDNE algorithm has the advantage of reducing surface noise, making it less susceptible to the method of surface mesh preparation than earlier algorithms for the calculation of DNE, which results in less scattered values. Furthermore, by implementation of the ϵ parameter, it is possible to selectively increase the weight of small surface fluctuations (low ϵ) or large surface features, potentially ridges, cusps and crests (high ϵ), on the ariaDNE calculation (see Shan et al., 2019 for detailed explanation).

While DTA has been referred to as a "shape descriptor", capturing molar morphology in a landmark-free abstraction, GMA is a "shape specifier", representing the shape via the positions of specific landmarks (Evans, 2013). As both methods capture quite different aspects of morphology, with DTA being useful for measuring a more functional signal and GMA being useful for observing the positions of landmarks within morphospace, they can be used to complement each other (Selig et al., 2020).

The surface meshes used in this study are mostly based on CT-scans conducted with the v|tome|x s 240, situated at the Institute of Geosciences (Rheinische Friedrich-Wilhelms-Universität Bonn). Scan voxel sizes vary between 0.018 and 0.246 mm. Additional scan data were acquired from the digimorph.org (scan of TMM M-6921) and morphosource.org (scan of UMZC A6.10/3) digital databases. Specimen NMB 2526 was scanned at the Naturhistorisches Museum Basel. All carnassials used in this study showed as minimal wear as possible. Some teeth still were slightly more worn than others and while they are not problematic for DTA, they were excluded from the GMA (Selig et al., 2020). Teeth with all landmarks present but other parts of the

crown being damaged were used in the GMA but not in the DTA. Thus, the sample size differs between both analyses. Our mesh preparation protocol is based on to the workflow of previous studies which used DNE (a summary of DNE workflow protocols can be found in Pampush et al., 2016). Individual molars were cropped from segmented scan data at the cervix line, down-sampled to 10,000 faces (or left unchanged if initial face number was lower) using the Poly-Works 2015 IR 13 (InnovMetric Software Inc.) mesh optimization tool and subsequently smoothed using the smooth surface tool in Avizo 8.1 (FEI _Visualization Sciences Group_) with 100 iterations and a lambda of 0.6. Individual tooth models were exported as Stanford Triangle Format (.PLY) files. The ϵ parameter was set to 0.08. The placing of landmarks for the GMA was conducted on the same down-sampled and smoothed meshes, which has been shown to work in previous studies (Selig et al., 2020; Selig, López-Torres, et al., 2019). We used lower left teeth if available and in better condition than the right teeth. Otherwise, right teeth were used and mirrored using PolyWorks.

Our landmark configuration for the GMA is based largely on the workflow applied by Tarquini et al. (2020), using the paraconid (landmark 1), carnassial notch (landmark 2), protoconid (landmark 3), metaconid (landmark 4), distal trigonid edge (landmark 5), hypoconid (landmark 6), entoconid (landmark 7), mesial trigonid edge (landmark 8) and distal talonid edge (landmark 9) as fixed landmarks. The positions of landmarks 5, 8 and 9 were determined in occlusal view. In case of metaconid, hypoconid or entoconid reduction, we placed the missing landmarks as described by Tarquini et al. (2020). To capture the base of the crown in detail, we used 60 semi-landmarks along the cervix line (Figure 2). Landmarks and semi-landmarks were placed using the point placing tool of PolyWorks. For each molar, at least 60 semi-landmark points were placed, starting at the most mesial point. In cases where we placed more than 60 points, these were down-sampled to 60 points and before performing the GMA the semi-landmarks were made equidistant using the equidistantCurve function of the R library Morpho (Schlager et al., 2020) for the software R (R Core Team, 2020; version 4.0.5). The Procrustes alignment and a Procrustes ANOVA of the aligned shape data were carried out with the R library geomorph (Adams et al., 2021).

Topographic height models were created with MorphoTester (Winchester, 2016).

All lower carnassial teeth included in this study were assigned to a "basal" and a "derived" functional group. The criteria we used for a priori grouping are presence of a complete talonid (hypoconid, hypoconulid and entoconid) and presence of the metaconid. The absence of one of the aforementioned cusps was interpreted as a deviation relative to the basal condition to a more derived carnassialized condition.

In taxa with multiple carnassials, we grouped the individual carnassial teeth based on their respective positions in the tooth row. The most mesial carnassials of dasyuromorphs (m2) and hyaenodonts (m1) are referred to as the "mesial carnassial position" (MCP), the intermediate carnassials of dasyuromorphs (m3) and hyaenodonts (m2) are referred to as the "intermediate carnassial position" (ICP) and
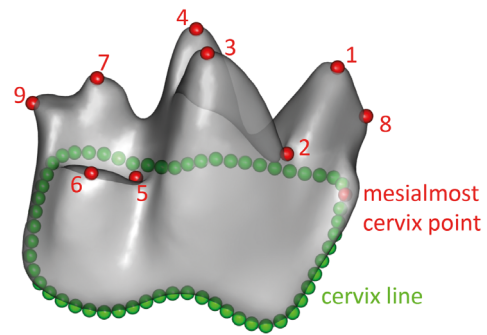

FIGURE 2 3D model of a lower carnassial (m3 of _Dasyurus viverrinus_) showing the placement of fixed landmarks (red) and semi-landmarks (green). The model is in buccal view, mesial is to the right

the distal carnassial of dasyuromorphs (m4) and hyaenodonts (m3) as well as the carnivoran m1 are referred to as the "principal carnassial position" (PCP).

Due to both our study design and the underlying biological circumstances, testing the results of the DTA and GMA values for a phylogenetic signal is not trivial. First of all, our study analyses the morphology of a trait in taxa where it is present multiple times (dasyuromorphs and hyaenodonts with multiple carnassials per tooth row) and compares it with taxa where it is present only once (carnivorans with a single carnassial per tooth row). Thus, in some cases multiple traits are being analyzed both on the individual as well as the species and genus levels. This is further complicated by the fact that the analyzed traits do for the most part not represent homologous anatomical features. While presence of homologous traits (carnassialization of molar positions) on homologous anatomical features can be dependent on phylogenetic history within the respective taxonomic orders, the analyzed anatomical features in the Carnivora (m1), the Hyaenodonta (m1, m2, m3) and the Dasyuromorphia (m2, m3, m4) are mostly present on non-homologous tooth positions and testing them for phylogenetic significance would not yield meaningful results, as no analysis including a single molar position per group would include a homologous tooth position in all taxa.

We analyze the evolution of carnassialization in a phylogenetic context by conducting an ancestral state reconstruction on calculated values of the DTA and GMA (PC values of PCA) for PCPs. We interpret the calculated signal as a functional morphological trait of adaptation, not a homologous anatomical trait or feature. This makes it possible to compare the hypothetical ancestral states of the Carnivora, Hyaenodonta and Dasyuromorphia, although differences or similarities of lineages within these groups could potentially still depend on the respective phylogenetic intrataxon history.

2.3 | Phylogenetic data

A calibrated phylogenetic tree based on mitochondrial data for extant species (all dasyuromorphs and all carnivorans except nimravids) was downloaded from TimeTree.org (Kumar et al., 2017). The root of the

tree is at 159 Ma (split of Eutheria and Metatheria). Absolute ages for *Nimravus* (34 Ma) and *Dinictis* (37 Ma) were taken from the published composite tree of Martín-Serra et al. (2014). We follow the placement of Nimravidae within Feliformia according to Wesley-Hunt and Flynn (2005) and Tomiya (2011), with a split of Nimravidae from the non-nimravid feliforms at 50 Ma. The split of *Nimravus* and *Dinictis* was dated at 42 Ma, according to Wesley-Hunt and Flynn (2005). The phylogeny for the hyaenodont taxa in this study is based on the published calibrated tree of Solé and Mennecart (2019). *Hyaenodon filholi* was not included in the published hyaenodont phylogeny. In our tree, we placed it as a sister taxon to *Hyaenodon exiguus* with a split at the base of the *Hyaenodon* clade. This is based on the interpretation of the European *H. filholi* as an immigrant taxon from Asia with a split from the endemic European *H. exiguus* deep within the *Hyaenodon* clade (Bastl et al., 2014). Since an absolute age of this split was not calculated, the placement within our tree estimates the split between European and Asian *Hyaenodon* clades at the base of the genus. The absolute age for *H. filholi* is 30.9 Ma according to its oldest stratigraphic occurrence in European MP 23 faunas (Bastl et al., 2014; Solé et al., 2018). The oldest internal Hyaenodonta split in the tree of Solé & Mennecart (2019; split between the Tinerhodon/Altacreodus clade and the rest of the Hyaenodonta) was used as the age for the split between the Carnivora and the Hyaenodonta. To our knowledge, there is no comprehensive dated phylogeny for the relationship between Hyaenodonta and Carnivora and the timing of the split of both lineages. We follow the general consensus of placing Hyaenodonta within Ferae, e.g. as proposed by O'Leary et al. (2013), with a split dating back well into the Late Cretaceous.

The two specimens of *Hyaenodon* sp. were excluded from the phylogenetic analysis because of unknown phylogenetic placement and range of stratigraphic age.

Ancestral states at individual nodes of the tree were calculated using the fastAnc function (fast estimation of maximum likelihood ancestral states) of the phytools library (Revell, 2020) for R and were further investigated by using the contMap function for a graphical depiction of trait change.

We measured the difference of the distribution of values for PCPs of the Carnivora, Dasyuromorphia and Hyaenodonta by calculating the deviation of the calculated base value of the respective group from the calculated value of the base (root) of the tree, expressed as percentage of the total range of values of the respective trait (ariaDNE, PC1 or PC2).

2.4 | UPGMA cluster analysis

The mean values of the scores of the first five PCs (explaining more than 75% of total variation) for the MCPs, ICPs and PCPs of Carnivora, Dasyuromorphia and Hyaenodonta, using the a priori classification of "basal" and "derived" (Table 1) within each group, were included in an unweighted pair group method with arithmetic mean

(UPGMA) cluster analysis using the linkage function of the mdendro library (Fernandez & Gomez, 2018) for R to examine shape similarities among the tooth positions.

3 | RESULTS

3.1 | Crown curvature in carnassial teeth

Our DTA analysis included 109 individual teeth belonging to 71 specimens (Table S1). The calculated ariaDNE values show a shift between the distribution of the basal and the derived groups (Figure 3). This shift indicates that relatively high ariaDNE values are present in basal carnassials with all cusps present and relatively low ariaDNE values in derived carnassials with at least one cusp reduced. Carnassials with different conditions of metaconid and talonid reduction, representing the morphological changes associated with increasing carnassialization, show a similar pattern of reduction of crown curvature values in all three taxonomic orders (Figure 4). Within Carnivora, the highest curvature values are found among genera with little specialized teeth (*Civettictis*, *Ichneumia*, *Viverra*, *Vulpes*), while genera with more specialized teeth with a functional but reduced talonid (*Canis*, *Dinictis*, *Lycaon*, *Nimravus*, *Mustela*, *Speothos*) show lower values; the lowest are present in genera where the talonid is non-functional or where the talonid and the metaconid are absent (*Crocuta*, *Cryptoprocta*, *Felis*, *Neofelis*, *Otocolobus*, *Panthera*). Among dasyuromorphs, the highest values are present in the basal carnassials of the various species of *Dasyurus*, while lower curvature values are present in the derived carnassials of *Sarcophilus* and *Thylacinus*. In Hyaenodonta, the highest curvature values are present in the basal carnassials of *Proviverra*, whereas lower values are present in the derived carnassials of *Hyaenodon*, *Oxyaenoides* and *Pterodon*.
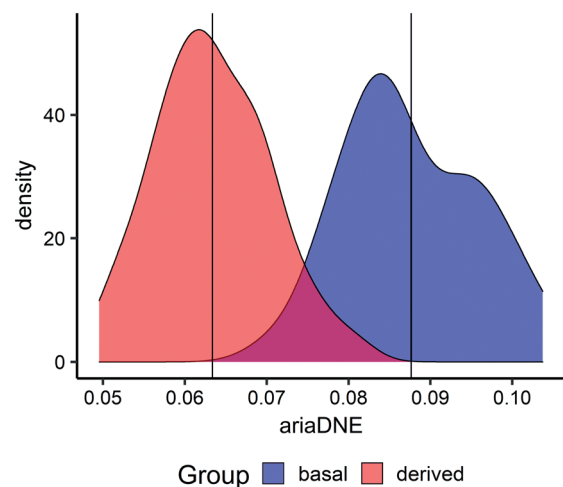

FIGURE 3 Distribution of ariaDNE values shown as a density estimation for "basal" and "derived" carnassial teeth. *Solid lines indicate group means*

3.2 | Carnassial morphospace analysis

The GMA analysis was conducted on 106 individual teeth belonging to 68 individuals (Supporting Information). The first five PCs identified by the GMA explain more than 75% of total variation, with PC1 accounting for 41.4% and PC2 accounting for 13.9%. The landmark shift along PC1 from positive to negative describes a distal elongation of the carnassial blade, a reduction in size of the talonid basin and a change from a cervix line with equally pronounced mesial and distal flexures to an enlarged mesial flexure and a reduced distal flexure (Figure 5). In the morphospace of carnassial molars, basal molars are found mostly in the positive morphospace along PC1 and derived carnassials are found mostly in the negative morphospace. This shift is also present when taking only basal and derived carnassials within the respective orders into account (Figure 6). A procrustes ANOVA with 1000 iterations for significance testing of the aligned shape data indicates a significant difference between basal and derived carnassials ($p = .001$).
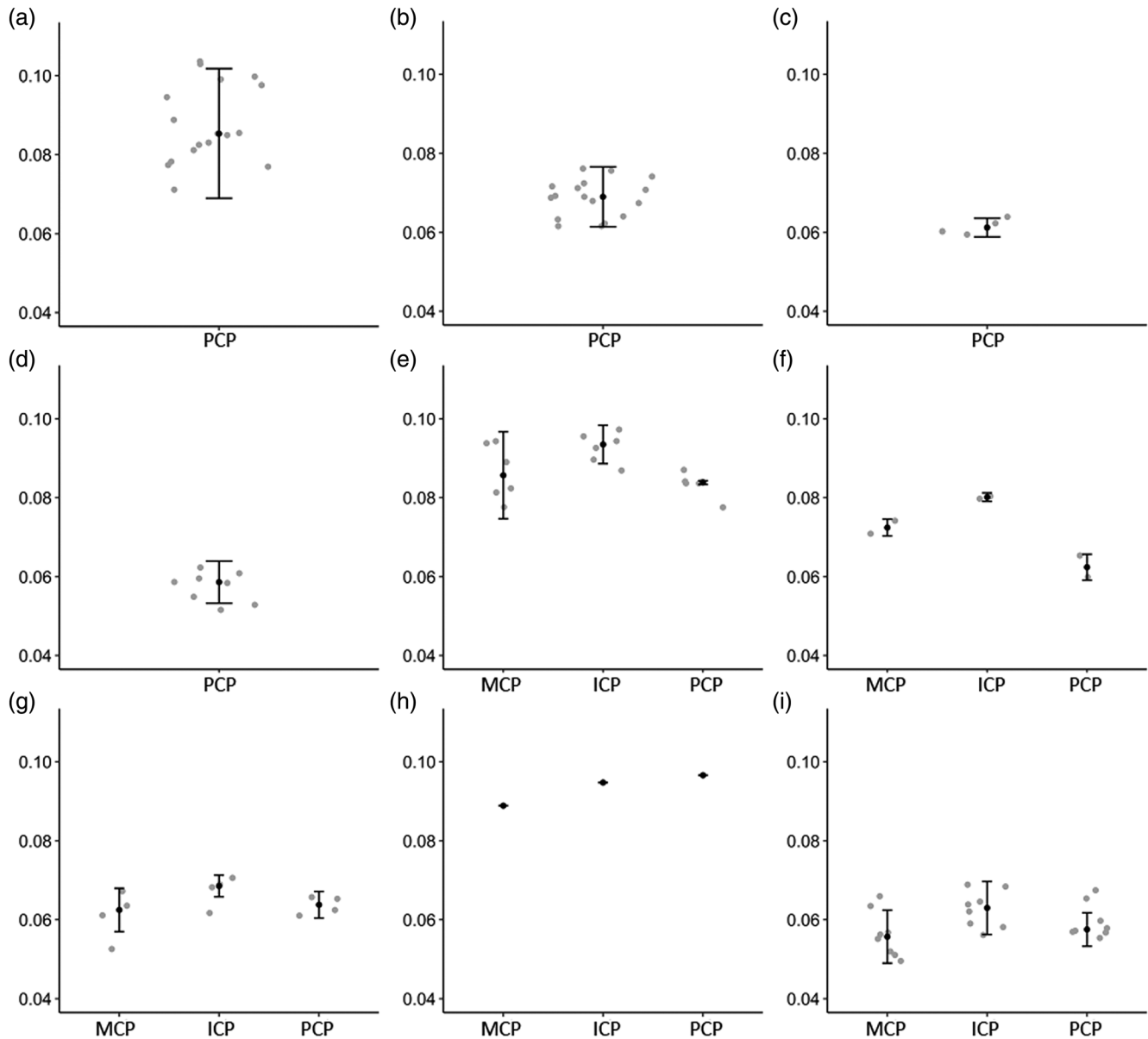
FIGURE 4 Distribution of ariaDNE values in different groups of carnassial functional morphotypes. Carnivoran functional morphotypes: (a) all talonid cusps and metaconid present (*Ichneumia albicauda, Civettictis civetta, Viverra* spp., *Vulpes* spp.); (b) metaconid present, at least one talonid cusp reduced (*Canis lupus, Dinictis* sp., *Lycaon pictus, Mustela* spp., *Nimravus* sp., *Speothos venaticus*); (c) metaconid absent, talonid present but vestigial (*Crocuta crocuta, Cryptoprocta ferox*); (d) metaconid and talonid absent (*Felis silvestris, Neofelis nebulosa, Otocolobus manul, Panthera* spp.). Dasyuromorph functional morphotypes: (e) all talonid cusps and metaconid present (*Dasyurus* spp.); (f) metaconid present, at least one talonid cusp reduced (*Sarcophilus harrisii*); (g) metaconid absent, at least one talonid cusp reduced (*Thylacinus cynocephalus*). Hyaenodont functional morphotypes: (h) all talonid cusps and metaconid present (*Proviverra typica*); (i) metaconid absent, at least one talonid cusp reduced (*Hyaenodon* spp., *Oxyaenoides bicuspidens, Pterodon dasyuroides*). Median and interquartile range are drawn for each value distribution except for *Proviverra* ($n = 1$ per tooth)

The distribution of values for taxa with multiple carnassials was analyzed on the genus level. In all genera with multiple carnassial teeth, the PCPs are the teeth with the lowest PC1 scores. In four genera with derived carnassials (*Hyaenodon, Oxyaenoides, Sarcophilus, Thylacinus*), there is a successive shift of high to low PC1 scores from the mesial to the more distal carnassial positions. This successive value shift is not present in the genera with basal carnassials (*Dasyurus* and *Proviverra*) and one genus with derived carnassials (*Pterodon*).

Along the axis of PC2, unspecialized carnivorans with basal carnassials and specialized carnivorans with derived carnassials are largely separated from the rest of the dataset (Figure 7). Principal

component 2 describes the shape change from a carnassial with a relatively high cutting blade and an approximately round crown base (marked by the cervix line) in the more positive morphospace to a relatively low cutting blade and a crown base displaying a bucco-lingual compression and mesio-distal elongation in the more negative morphospace (Figure 7).

Allometry was tested by the regression of shape versus centroid size and is significant ($p = .01$). However, the coefficient of determination is low ($R^2 = 0.137$). The smallest teeth are the basal carnassials of *Dasyurus* and *Proviverra*, whereas the largest ones are large caniforms (*Canis*) and feliforms (*Crocuta* and *Panthera*), with frequent of
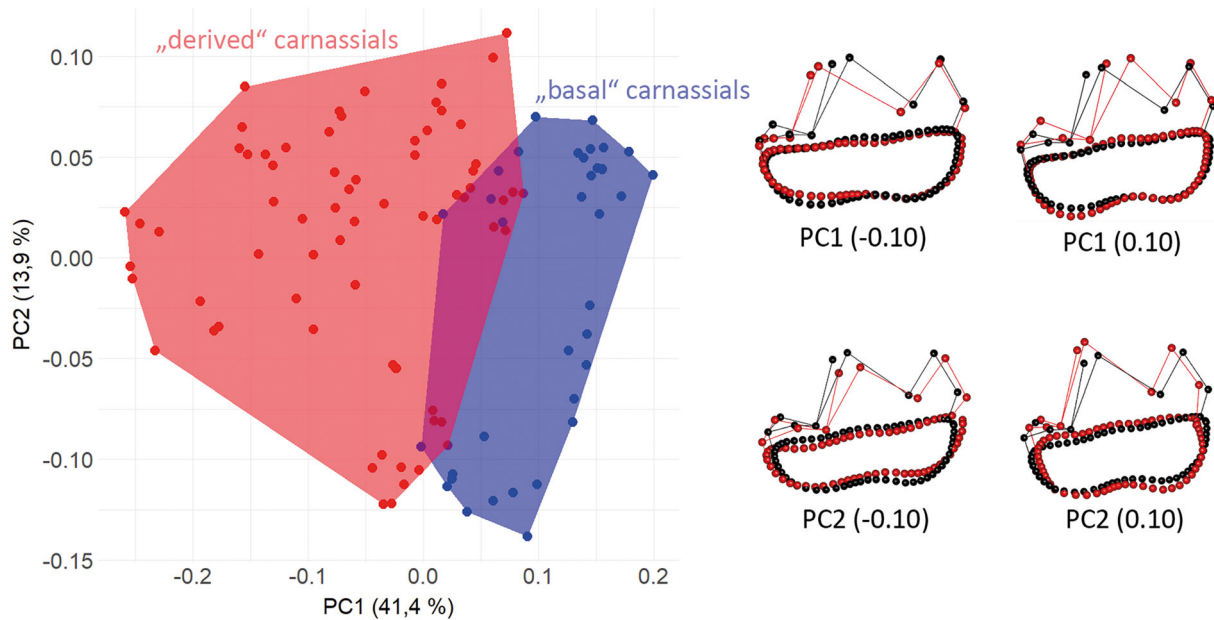
FIGURE 5 Bivariate plot of principal components 1 and 2 of the Procrustes aligned shape data, showing the distribution of "basal" and "derived" carnassials. Deformed shapes along the principal components (red) are shown in comparison to the consensus shape (black)
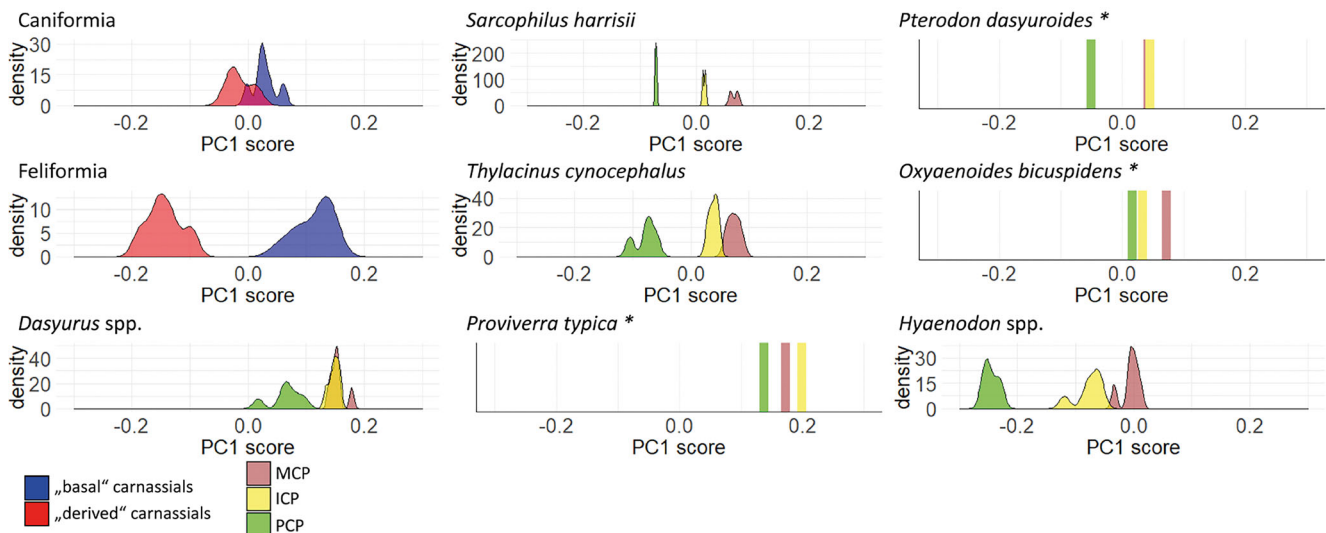

FIGURE 6 Distribution of scores for different types of carnassials along the first principal component, shown as density estimations. Asterisks indicate taxa for which only the distributions of single values are shown

overlap between taxa and teeth of different carnassialization types in between (Figure S4).

3.3 | Phylogenetic distribution of shape signals

Ancestral state reconstructions were calculated for the carnivoran, dasyuromorph and hyaenodont ariaDNE values and scores of PC1

and PC2 (Figure 8), using the mean values of species. PCPs were chosen for this analysis because they are interpreted to be the most specialized carnassial teeth in taxa with multiple carnassials (see discussion).

The distribution of ariaDNE values ranges from a minimum value of 0.0517 (*Panthera pardus*) to a maximum value of 0.1006 (*Viverra tangalunga*) with a total range of 0.0489. The calculated value for the base of the tree is 0.0723. From the base value of the tree, the base
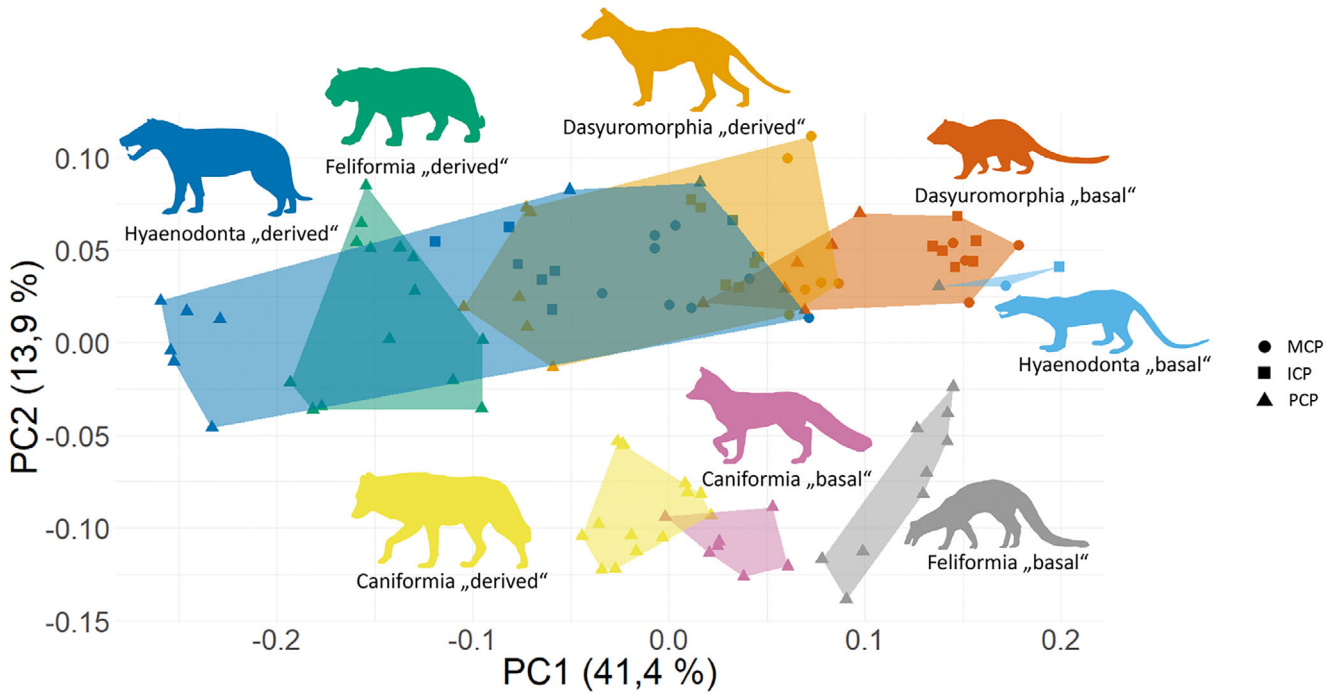
FIGURE 7 Bivariate plot of principal components 1 and 2 of the Procrustes aligned shape data, showing the distribution of "basal" and "derived" carnassials within taxonomic orders
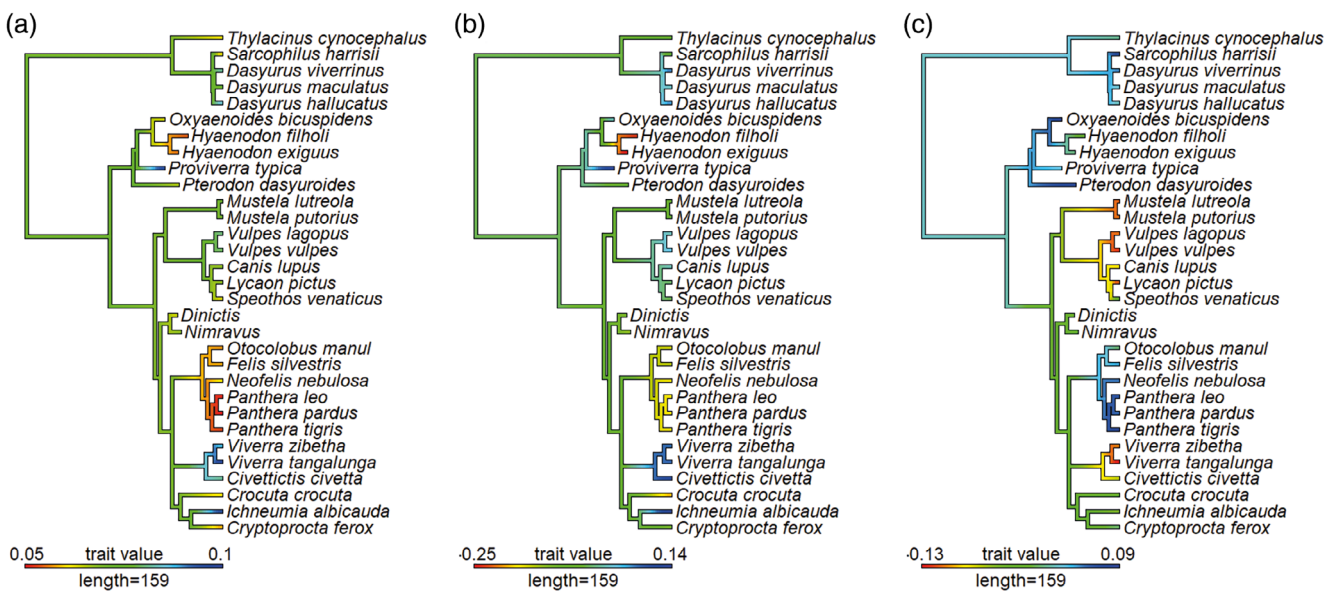
FIGURE 8 Ancestral state reconstruction of (a) ariaDNE, (b) carnassial crown shape PC1 and (c) carnassial crown shape PC2. Estimated evolutionary history of each trait is mapped onto the phylogeny

value of the Carnivora (0.0706) has a deviation of 3.4%, the base value of the Hyaenodonta (0.0748) has a deviation of 5.1% and the base value of the Dasyuromorphia (0.0707) has a deviation of 3.2%.

The minimum value of PC1 is −0.25 (*Hyaenodon exiguus*) and the maximum value is 0.14 (*Ichneumia albicauda*), spanning a total range of 0.39. The base of the tree has a calculated value of −0.0229. The base value of the Carnivora (−0.0531) has a deviation of 7.7% from the base of the tree, while the base value of the Hyaenodonta (−0.0024) has a deviation of 5.3% and the base value of the Dasyuromorphia (−0.0275) has a deviation of 1.2%.

The PC2 values range from a minimum of −0.1276 (*Viverra tangalunga*) to a maximum of 0.0862 (*Oxyaenoides bicuspidens*) with a total range of 0.2138. For the base of the tree, the calculated value is 0.0196. From the base value of the tree, the base value of the Carnivora (−0.0355) has a divergence of 25.8%, while the base value of the Hyaenodonta (0.0419) has a deviation of 10,4% and the base value of the Dasyuromorphia (0.026) has a deviation of 3%.

3.4 | Cluster analysis

The UPGMA cluster analysis of the mean values of the first five PCs for basal and derived MCPs, ICPs and PCPs calculated a division between all basal and all derived carnassials into two clusters (Figure 9). Within the cluster of basal carnassials, the hyaenodont and dasyuromorph carnassials form a cluster of their own, which is separated from that of the carnivoran carnassial. Within the hyaenodont +dasyuromorph basal cluster, the hyaenodont and dasyuromorph carnassials form two separated clusters, with the respective MCP and ICP being more similar to one another than to the PCP.

Within the cluster of derived carnassials, there is a division between a cluster uniting the dasyuromorph and hyaenodont IPCs and MCPs and a cluster uniting all PCPs. The dasyuromorph ICP and MCP are forming a cluster of their own, separated from the cluster

uniting the hyaenodont ICP and MCP. Within the cluster of PCPs, the dasyuromorph PCP and the carnivoran PCP are forming a cluster separate from the hyaenodont PCP.

4 | DISCUSSION

4.1 | The influence of functional morphology on crown DNE

Crown curvature of carnassials as quantified by ariaDNE is related to changes in functional morphology associated with carnassialization. These include the reduction of the metaconid and of talonid cusps in highly carnassialized teeth. The interordinal convergent evolutionary trend observed in the molars of Dasyuromorphia, Carnivora and Hyaenodonta is indicated by the respective crown curvature values. In all orders, carnassial molars with basal morphotypes show significantly higher ariaDNE values than molars with a more derived carnassialized crown morphology. The ariaDNE value shift from less to higher carnassialized teeth is unidirectional in all included taxa, regardless of phylogeny. This indicates that ariaDNE quantifies the convergent morphological conditions of low and high carnassialized teeth and is a proxy for the relative reduction of functional occlusal structures. Relatively high ariaDNE values point to a crown morphology with a more complex crown and a potentially more diverse function, including not only a simple shearing but also a crushing function, because talonid cusps are still present. Low ariaDNE values are unlikely to occur in carnassial teeth which retain crushing structures, and if they do, they are reduced in relation to those with higher ariaDNE values (as in *Mustela* and *Canis*, both lacking at least one talonid cusp). We interpret low ariaDNE values are a strong indicator for functional reduction.

Studies applying DTA methods to carnassial teeth prior to ours are relatively rare. The Orientation Patch Count (OPC) method was
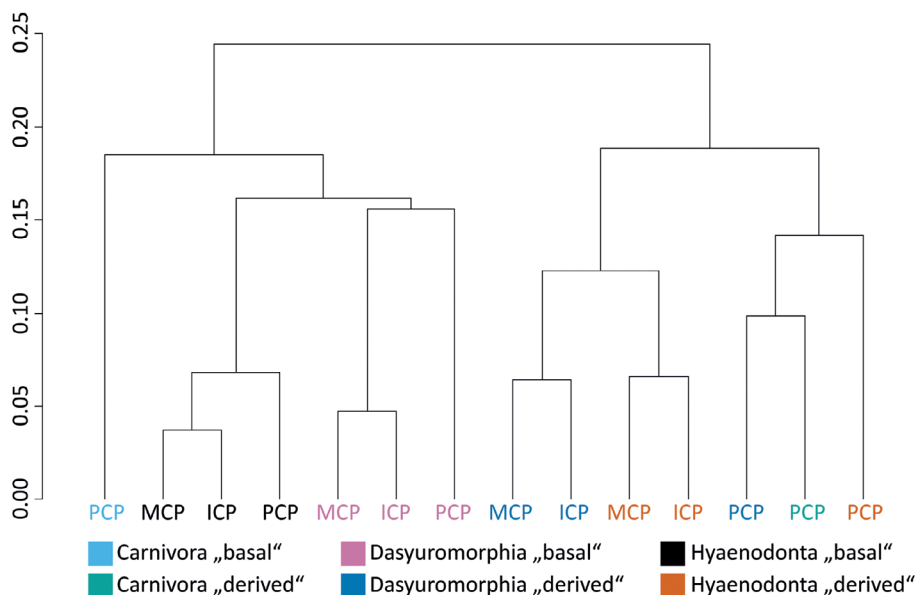

FIGURE 9 Dendrogram of the UPGMA cluster analysis on the mean PC scores from the first five PCs for different carnassial tooth positions of type "basal" and "derived" per taxonomic order

used as a proxy for complexity to compare carnivoran and rodent molar tooth rows of taxa with different dietary adaptations and was able to distinguish carnivorous, omnivorous and herbivorous taxa in both groups (Evans et al., 2006). Furthermore, the Orientation Patch Count Rotated (OPCR) of carnivoran and rodent molar tooth rows and individual molars confirmed the results of the former study, showing that lower molars are better indicators of diet and isolated molars show a stronger phylogenetic signal (Evans & Jernvall, 2009). The OPCR was used to measure the complexity of the molar tooth rows of carnivoran and dasyuromorph taxa. The OPCR values showed overlapping values of the carnivoran and dasyuromorph taxa, which could be a result of sampling rather than an actual adaptive signal (Smits & Evans, 2012). Pineda-Munoz et al. (2017) included carnivoran taxa among Rodentia, Primates and Diprotodontia to compare dietary adaptations of a total of 134 species using the OPCR of individual teeth as well as complete post-canine tooth rows, showing that dental topography is well correlated with dietary adaptations in all included groups. Hyaenodont teeth have not yet been included in studies employing DTA.

DNE quantification so far has mostly been applied to Primates (Berthaume et al., 2018; Berthaume et al., 2019; Berthaume & Schroer, 2017; Bunn et al., 2011; Fulwood, 2020; Li et al., 2020; López-Torres et al., 2017; Pampush et al., 2018; Prufrock et al., 2016; Winchester et al., 2014), although it has also been used for rodents (Renaud & Ledevin, 2017), meridiolestidans (Harper et al., 2019), scandentians (Selig et al., 2018; Selig et al., 2020; Selig, Sargis, & Silcox, 2019) and suids (Rannikko et al., 2020).

Typically, DNE is interpreted as being sensitive to height and sharpness of cusps, and therefore the overall shearing ability (Bunn et al., 2011). However, our study implies that the number of functional features (namely crests and cusps) on the occlusal surface of a molar has an equally high impact on calculated DNE. As shown by Winchester et al. (2014), molars of insectivorous platyrrhines and "prosimians" with multiple steep cusps have significantly higher DNE values than molars of hard object feeders, which have a blunted occlusal surface. In this case, the occlusal surface may be interpreted as "low-cusped" (in comparison to the insectivorous condition) or "simplified", as the individual cusps are largely reduced or absent. In the case of highly derived carnassialized teeth, only the latter can be attributed to the molar morphology. The surface is simplified, as multiple cusps have been reduced, but the molar crown itself shows a high relief with steep shearing walls, exhibiting a large simple shearing blade. Thus, surface areas with high curvature are less abundant. The functional result found in the cheek teeth of hard object feeders and highly specialized meat eaters can equally be described as "simplified". In case of hard object feeders, tooth function is reduced to a simple crushing function, in case of meat eaters tooth function is a simple shearing function. Both cases of functional reduction are reflected by low ariaDNE values.

The distribution of ariaDNE values of carnassials with different functional structures present supports this assertion (Figure 4). Presence of higher ariaDNE values in Carnivora with specialized carnassials and a still functional talonid (as in canids) compared to carnassials

where the talonid is absent (as in felids) thus implies a potential difference in functional, and ultimately adaptive versatility. Teeth with a functional talonid are able to process food via crushing, which expands the range of potential food items. This may be one explanation as to why specialized clades of North American canids over the last 40 million years were less prone to extinction than saber toothed cats, as discussed in Balisi and Van Valkenburgh (2020).

4.2 | Morphospace analysis

A large proportion of variance (41.4%) in the morphospace is explained by enlargement of the carnassial blade and reduction of the talonid. The change in the cervix line from an approximately symmetrical shape (with mesial and distal flexures of similar size) to an asymmetrical shape (with an enlarged mesial flexure and a reduced distal flexure) also accounts for the variance. The shape change of the cervix line can be explained by the presence of a mesial and a distal root of similar size in basal carnassials, while in derived carnassials, there is a tendency to enlargement of the mesial root and reduction of the distal root. Relative size changes of the mesial carnassial blade and the distal talonid basin cause similar size changes in the respective roots, which act as mechanical support for the crown structures. The cervix line, marking the intersection of crown and root, captures these relative size changes. The shape change along the axis of PC1 divides basal carnassials from derived carnassials in Carnivora, Dasyuromorphia and Hyaenodonta and can be interpreted as a signal of functional adaptation to a more or less pronounced carnivorous diet. The carnassial shape analysis of the carnivoran m1 and the didelphimorph and dasyuromorph m3 and m4 by Tarquini et al. (2020) indicates an overarching signal of carnassial blade enlargement as well as metaconid and talonid reduction. Our study is consistent with this observation. The most extreme values in our analysis are found in *Hyaenodon* spp., *Crocuta* and Felidae with derived carnassials in the negative morphospace, and in *Proviverra*, Feliformia with basal carnassials and the MCPs and ICPs of *Dasyurus* spp. in the positive morphospace. There is an overlap of the dasyuromorph basal PCPs with the dasyuromorph derived MCPs and ICPs. This indicates, that within the Dasyuromorphia, basal PCPs are as specialized as the derived MCPs and ICPs. Basal caniform carnassials occupy a spectrum between the most unspecialized carnivoran carnassials (viverrids and herpestids) and caniforms with derived carnassials (*Canis*, *Lycaon*, *Speothos*). None of the caniform carnassials are as specialized as the carnassials of feliforms with derived carnassials, which occupy a spectrum of lower PC1 scores. Two hyaenodonts with derived carnassials (*Oxyaenoides* and *Pterodon*) overlap with the Caniformia. The dasyuromorph derived PCPs of *Sarcophilus* and *Thylacinus* are more specialized than that of the Caniformia and overlap with some derived carnassials of the Feliformia. The successive mesiodistal shape shift observed in the distribution of PC1 scores of the lower carnassials of *Hyaenodon*, *Oxyaenoides*, *Sarcophilus* and *Thylacinus* indicates a differential adaptation of the individual carnassials in more specialized taxa. In all taxa with multiple carnassials, the PCP is the most specialized, indicated by

the most negative PC1 score among all teeth of the individual molar row. Tarquini et al. (2020) concluded, that the m4 of didelphimorphs and dasyuromorphs is a better analogue to the carnivoran m1 and is more modified than the m3. Our study supports this conclusion, indicating that the PCP in dasyuromorphs as well as hyaenodonts is indeed the most specialized in all taxa that we observed, with the two mesial carnassials being less specialized.

The shape change along the axis of PC2 indicates slightly longitudinally elongated carnassials, as delineated by the cervix line in the Caniformia and the Feliformia with basal carnassials, the scoring low values. These overlap with the carnassials of *Hyaenodon*, *Crocuta* and *Dinictis*, while the remaining data points have much higher PC2 scores, which indicates slightly mesio-distally compressed carnassials. Highest PC2 scores are found among the derived carnassials of Feliformia (*Felis silvestris*), Dasyuromorphia (*Sarcophilus*) and Hyaenodonta (*Oxyaenoides* and *Pterodon*).

4.3 | Phylogenetic signal

The ancestral state reconstruction for the PCPs of Carnivora, Dasyuromorphia and Hyaenodonta indicates that the basal carnassial state for all three orders is not much different from the base state of the tree (split point of Eutheria and Metatheria) for ariaDNE values and PC1 scores. The deviation for ariaDNE values from the base of the tree is around 3.2%–5.1% for all orders, with the highest difference between Carnivora and Hyaenodonta (8.5%). For the PC1 scores, the ancestral state of the individual orders deviates between 1.2% and 7.7% from the base state of the tree, with the highest difference between Carnivora and Hyaenodonta (13%). Thus, moderate deviation around 10% indicates that the ancestral conditions for the studied higher taxa were generally similar. Reduced crown curvature and carnassial blade enlargement relative to a reduced talonid basin in highly carnassialized teeth within the different taxonomic groups points to a uniform ancestral state regarding this aspect of morphology.

The ancestral state reconstruction for the PC2 scores indicates a high deviation of the carnivoran base state from the base state of the tree (25.8%), whereas it is much lower in Hyaenodonta and Dasyuromorphia (3.0%, respectively, 10.4%). The deviation of the base state of the Carnivora to that of the Dasyuromorphia is 36.2% and to that of the Hyaenodonta it is 28.7%, whereas it is 7.4% between the Dasyuromorphia and the Hyaenodonta. All this points to an ancestral state of the Carnivora within the morphospace of PC2 scores, which differs considerably from that of the Hyaenodonta and the Dasyuromorphia, as well as the base of the tree. The presence of carnassials with a somewhat mesio-distally (longitudinally) elongated crown base may thus be a plesiomorphic feature of the Carnivora. If this is true, a carnassial with a slightly mesio-distally compressed crown base evolved multiple times in the Feliformia with derived carnassials (Eupleridae, Felidae, Hyaenidae, Nimravidae) and is a specific derived state within the Carnivora. One possible explanation for this adaptation is the shortening of the rostrum in cat-like ecomorphs,

which also evolved in some caniforms (Canidae, Mustelidae, Amphicyonidae), but the shortening of the tooth row linked to this adaptation is most extreme and a reoccurring trend within feliform Carnivora (Van Valkenburgh, 2007). The shortening of the carnassial itself, as indicated by our analysis, may additionally contribute to the shortening of the rostrum.

Tarquini et al. (2020) found a dietary signal of dasyuromorph and carnivoran carnassials to be phylogenetically structured. The morphospace distribution of carnassials in our study indicates that a phylogenetic structuring is also present between weakly and strongly carnassialized molars, and that hyaenodont carnassials are generally more similar in shape to those of dasyuromorphs than of carnivorans.

4.4 | Implications for functional constraints

The results of the DTA (ariaDNE) and the GMA (PC1 scores) indicate a functional reduction of highly carnassialized molars relative to more basal carnassial conditions for dasyuromorph, carnivoran and hyaenodont taxa. It is most likely, that all late surviving Hyaenodonta (which include one species of *Hyaenodon*) were affected by this functional reduction. Interestingly, the carnivoran taxa in our study for which a basal carnassialized and potentially multifunctional crown is indicated, are all extant taxa (*Civettictis*, *Ichneumia*, *Viverra*, *Vulpes*). The cheek dentition of these taxa is overall close to the plesiomorphic heterodont, "generalized" condition (Gregory & Hellmann, 1939). This ancestral condition of the Carnivora, inherited from the Carnivoramorpha, is characterized by restricted shear at one pair of carnassial teeth (P4/m1) (Flynn & Wesley-Hunt, 2005). All derived specialized carnivorous or herbivorous carnivoran dentitions evolved from this carnassial type. The ancestral condition of the Carnivora is thus a heterodont cheek dentition formed by cutting carnassials and crushing post-carnassials in contrast to the homodont ancestral condition of the Hyaenodonta and Dasyuromorphia, which is closer to the plesiomorphic homodont tribosphenic cheek dentition (although the most distal upper molars may become vestigial). The limited adaptive diversity of marsupial carnivores has been linked to their molar dentition, as it is interpreted as less versatile than that of (non-specialized) carnivorans (Van Valkenburgh, 1999). Our results indicate, that in the generalized carnivoran taxa not only the heterodont condition of the cheek dentition, but also the functional morphology of the carnassial tooth itself points to a higher versatility in function. Within multiple carnivoran lineages (Vulpini, Herpestidae and Viverridae) the ancestral and more versatile carnassial morphotype has been retained. The presence of a talonid in these longitudinally elongated carnassials makes it possible to crush a more diverse range of food items in addition to carnassial meat cutting. This is in conformity with the results of our DTA, where the lowest values of crown curvature within the Carnivora, indicating a reduction or absence of talonid function, are found in specialized feliforms, whereas caniforms and non-specialized feliforms show higher values. The DTA can, however, not distinguish unspecialized carnassials of the longitudinally elongated type in carnivorans from unspecialized carnassials which are longitudinally short,

as in dasyuromorphs and hyaenodonts. According to our results, the evolutionary success of the Carnivora in comparison to the Hyaenodonta may have been largely influenced by the retention of the ancestral ("basal") morphotype throughout their evolutionary history.

The significance of an adaptive difference in carnassial dentitions has been discussed for almost a century now. Butler (1946) proposed that the dental condition of the modern Carnivora and their ancestors has more evolutionary plasticity as it provides more functional diversity compared to the functionally restricted condition of the extinct Hyaenodonta and Oxyaenodonta. From this functionally versatile condition, carnivorans were able to evolve more carnassialized cheek teeth as well as adaptations with a greater emphasis on the crushing function and reduced carnassial cutting multiple times throughout the Cenozoic (Van Valkenburgh, 2007). The fact that specialized carnivorous "Creodonta" were replaced by carnivorans which retained more generalized adaptations during the Eocene in North America (Friscia & Van Valkenburgh, 2010) supports the idea of more plasticity in the ancestral heterodont condition of the Carnivora. Afro-Arabian hyainailouroid taxa survived into the middle Miocene, but if the dispersal of Carnivora played a role in their eventual demise is not known (Borths & Stevens, 2017a). The Carnivora likely contributed in some way to the extinction of the Hyaenodonta. A difference in the functional morphology and the resulting adaptive potential of the carnassials is one possible factor to consider.

There have been numerous ways to assess the evolutionary pros and cons of the specialization to a carnivorous diet among mammals. The overarching picture of the "costs of carnivory" indicates that specialization to a carnivorous diet hinders a subsequent adaptation to another diet, mostly due to craniodental modifications (Holliday & Steppan, 2004). In the fossil record, this results in a repeated pattern of carnivorous clades specializing to a highly carnivorous diet, going extinct and getting replaced by another clade (Van Valkenburgh, 2007). Holliday (2010) also detected a morphological constraint in the molars of Carnivora with a specialized carnivorous diet, which inhibits reversal to a more generalized condition. It is of great importance to note that the pattern of evolutionary constraint in molars of carnivorous mammals is most likely not restricted to the Carnivora alone, but applies to all carnivorous groups with highly carnassialized cheek teeth. This is due to the highly convergent character of molar functional morphology among even the most distantly related taxa with carnivorous adaptations (e.g., metatherians and eutherians).

Studies on the character change of specialized carnivorous molars indicate, that inhibited reversed evolution to a more generalized condition has a greater influence on the evolution of increasingly specialized carnassials than directional selection (Holliday, 2010). The tendency of specialized carnivorous lineages to go extinct rather than responding by increased phenotypic specialization has been described as an "evolutionary ratchet" by Van Valkenburgh et al. (2004). The Hyaenodonta may have been influenced to a higher degree by increased vulnerability to extinction. By looking at the evolutionary history of the Carnivora and the Hyaenodonta and comparing changes

in tooth morphology as well as adaptive and taxonomic diversity, it seems that due to higher ecomorphological diversity the Carnivora were less severely influenced by constraints of extreme carnivorous specialization in their dentition, and as a group recovered from intraphyletic extinctions. The Hyaenodonta showed lower adaptive diversity and this may have been an evolutionary disadvantage.

The cause for functional restriction in dasyuromorph and hyaenodont carnassial dentitions, reflected by similar morphospace occupancy in our study, does not seem to be the pattern of tooth eruption, which differs greatly between both groups. Both the morphological confinement to the carnassialized condition as well as the eruption patterns themselves seem to be the result of the selective pressure to extend carnassial functionality during ontogeny. Werdelin (1987) proposed the hypothesis, that the successive eruption of carnassials in the Dasyuromorphia forces each carnassial to function as the main cutting tooth until this function is taken over by the subsequently erupting distal carnassial until all molars are erupted, thus forcing all molars to become highly carnassialized. It seems plausible that the resulting functional constraint may be a result of the reduced marsupial tooth replacement. In the Hyaenodonta however, the picture is quite the opposite. In _Hyaenodon_ and specialized hyainailourid taxa, deciduous carnassials are replaced late in ontogeny, and there is always one premolar position (p3 or p4) which erupts after the last permanent carnassial (m3) has erupted (Bastl & Nagel, 2013; Borths & Stevens, 2017b). Adaptations for longevity of the carnassial function during ontogeny have been demonstrated in other examples, such as wide and stout metastyles in _Hyainailouros_ providing more enamel for abrasion (Borths & Stevens, 2019) or the extreme example of upper carnassial rotation in the late ontogeny of _Hyaenodon_ (Mellett, 1977). All these adaptations, including the tooth eruption, seem to contribute to extended carnassial functionality and play a role in the resulting functional constraint and the morphological similarities that we observed in dasyuromorphs and hyaenodonts, namely longitudinally shortened carnassials (in contrast to carnivorans except specialized feliforms) and increasing carnassialization from the mesial to the distal carnassial positions in specialized taxa.

The question remains, what enabled the carnivoran carnassial to remain in a functional-morphological equilibrium in several lineages up until present times. Previous studies have pointed out an affinity between the carnassial morphology of caniform and unspecialized feliform taxa (namely viverrids and herpestids) (Crusafont-Pairó & Truyols-Santonya, 1956; Meloro & Raia, 2010; Tarquini et al., 2020). Caniform, viverrid and herpestid taxa also occupy a unique morphospace in our GMA, separate from all carnassials of dasyuromorphs, hyaenodonts and specialized feliforms. Our analysis of ancestral state reconstructions points to a possible retention of a plesiomorphic carnivoran trait in these taxa. This trait, associated with a longitudinally elongated crown base and a low cutting blade, which enables the presence of a cutting blade in mesio-distal orientation as well as a fully functional talonid basin, may have played a key role in the adaptive success of the Carnivora.

5 | CONCLUSIONS

We conclude that carnassialization in Carnivora, Dasyuromorphia and Hyaenodonta involves specific changes of crown topography and shape, which have evolved independently of phylogeny and tooth position. In dasyuromorph and hyaenodont taxa, which have multiple carnassials, the most distal carnassial is the most specialized, which exhibits the same shape changes that occur between taxa with weak and strong carnassialization. In more specialized taxa, there is a tendency to a successively increasing mesio-distal carnassialization along the tooth row. Carnassialization is linked with metaconid and talonid reduction and thus a higher specialization to a carnivorous diet and poses a constraint in functionality and adaptive versatility. Thus, late surviving hyaenodont taxa like *Hyaenodon* may have been influenced by an adaptive disadvantage due to a constraint of dental function. Our study further solidifies a unique morphospace occupancy of caniform and unspecialized feliform carnassials, based on longitudinal elongation and a low carnassial blade, which is not present in dasyuromorphs and hyaenodonts.

CONFLICT OF INTEREST

The authors declare no conflict of interest.

AUTHOR CONTRIBUTIONS

Andreas Johann Lang: Conceptualization; data curation; formal analysis; funding acquisition; investigation; methodology; software; validation; visualization; writing original draft; writing-review and editing. Thomas Engler: Methodology; software; validation; writing-review and editing. Thomas Martin: Conceptualization; funding acquisition; project administration; resources; supervision; writing-review and editing.

ORCID

Andreas Johann Lang https://orcid.org/0000-0003-3467-1972

REFERENCES

Adams, D., Collyer, M., Kaliontzoloulou, A., & Baken, E. (2021). Package "geomorph": Read, manipulate and digitize landmark data, generate shape variables via Procrustes analysis for points, curves and surfaces, perform shape analyses, and provide graphical depictions of shapes and patterns of shape variation. R package version 4.0.0. https://cran.r-project.org/web/packages/geomorph.

Balisi, M. A., & Van Valkenburgh, B. (2020). Iterative evolution of large-bodied hypercarnivory in canids benefits species but not clades. *Communications Biology*, *3*, 461. https://doi.org/10.1038/s42003-020-01193-9

Barry, J. C. (1988). *Dissopsalis*, a middle and late Miocene proviverrine creodont (Mammalia) from Pakistan and Kenya. *Journal of Vertebrate Paleontology*, *8*, 25–45. https://doi.org/10.1080/02724634.1988.10011682

Bastl, K., & Nagel, D. (2013). First evidence of the tooth eruption sequence of the upper jaw in *Hyaenodon* (Hyaenodontidae, Mammalia) and new information on the ontogenetic development of its dentition. *Paläontologische Zeitschrift*, *88*, 481–494. https://doi.org/10.1007/s12542-013-0207-z

Bastl, K., Nagel, D., & Peigné, S. (2014). Milk tooth morphology of small-sized *Hyaenodon* (Hyaenodontidae, Mammalia) from the European Oligocene—Evidence of a *Hyaenodon* lineage in Europe. *Palaeontographica*, *303*, 61–84. https://doi.org/10.1127/pala/303/2014/61

Berthaume, M. A., Delezene, L. K., & Kupczik, K. (2018). Dental topography and the diet of *homo Naledi*. *Journal of Human Evolution*, *118*, 14–26. https://doi.org/10.1016/j.jhevol.2018.02.006

Berthaume, M. A., & Schroer, K. (2017). Extant ape dental topography and its implications for reconstructing the emergence of early *Homo*. *Journal of Human Evolution*, *112*, 15–29. https://doi.org/10.1016/j.jhevol.2017.09.001

Berthaume, M. A., Winchester, J., & Kupczik, K. (2019). Effects of cropping, smoothing, triangle count, and mesh resolution on 6 dental topographic metrics. *PLoS One*, *14*(5), e0216229. https://doi.org/10.1371/journal.pone.0216229

Borths, M. R., & Stevens, N. J. (2017a). The first hyaenodont from the late Oligocene Nsungwe formation of Tanzania: Paleoecological insights into the Paleogene-Neogene carnivore transition. *PLoS One*, *12*(10), e0185301. https://doi.org/10.1371/journal.pone.0185301

Borths, M. R., & Stevens, N. J. (2017b). Deciduous dentition and dental eruption of Hyainailouroidea (Hyaenodonta, "Creodonta", Placentalia, Mammalia). *Palaeontologica Electronica*, 20.3.55A, 1–34. https://doi.org/10.26879/776

Borths, M. R., & Stevens, N. L. (2019). *Simbakubwa kutokaafrika*, gen. et sp. nov. (Hyainailourinae, Hyaenodonta, 'Creodonta,' Mammalia), a gigantic carnivore from the earliest Miocene of Kenya. *Journal of Vertebrate Paleontology*, 39, e1570222. https://doi.org/10.1080/02724634.2019.1570222

Bunn, J. M., Boyer, D. M., Lipman, Y., St Clair, E. M., Jernvall, J., & Daubechies, I. (2011). Comparing Dirichlet normal surface energy of tooth crowns, a new technique of molar shape quantification for dietary inference, with previous methods in isolation and in combination. *American Journal of Physical Anthropology*, 145, 247–261. https://doi.org/10.1002/ajpa.21489

Butler, P. M. (1946). The evolution of carnassial dentitions in the Mammalia. *Proceedings of the Zoological Society of London*, 116, 198–220. https://doi.org/10.1111/j.1096-3642.1946.tb00117.x

Cope, E. D. (1879). The origin of the specialized teeth of the Carnivora. *Annals and Magazine of Natural History*, 3, 391–392. https://doi.org/10.1080/00222937908694109

Crusafont-Pairó, M., & Truyols-Santonja, J. (1956). A biometric study of the evolution of fissiped carnivores. *Evolution*, 10, 314–332. https://doi.org/10.2307/2406015

De Muizon, C., & Lange-Badré, B. (1997). Carnivorous dental adaptations in tribosphenic mammals and phylogenetic reconstruction. *Lethaia*, 30, 353–366. https://doi.org/10.1111/j.1502-3931.1997.tb00481.x

Evans, A. R. (2013). Shape descriptors as ecometrics in dental ecology. *Hystrix, the Italian Journal of mammalogy*, 24, 133–140. https://doi.org/10.4404/hystrix-24.1-6363

Evans, A. R., & Jernvall, J. (2009). Patterns and constraints in carnivoran and rodent dental complexity and relative tooth size. *Journal of Vertebrate Paleontology*, 29, 92A. https://doi.org/10.1080/02724634.2009.10411818

Evans, A. R., Wilson, G. P., Fortelius, M., & Jernvall, J. (2006). High-level similarity of dentitions in carnivorans and rodents. *Nature*, 445, 78–81. https://doi.org/10.1038/nature05433

Fernandez, A., & Gomez, S. (2018). Package "mdendro": Variable-group methods for hierarchical clustering. R package version 1.0.1. https://cran.r-project.org/web/packages/mdendro.

Flynn, J. J., Finarelli, J. A., & Spaulding, M. (2010). Phylogeny of the Carnivora and Carnivoramorpha, and the use of the fossil record to enhance understanding of evolutionary transformations. In A. Goswami & A. Friscia (Eds.), *Carnivoran evolution: New views on phylogeny, form, and function* (pp. 25–63). Cambridge University Press. https://doi.org/10.1017/CBO9781139193436.003

Flynn, J. J., & Wesley-Hunt, G. D. (2005). Carnivora. In K. D. Rose & D. Archibald (Eds.), *Origin, timing, and relationships of the major clades of extant placental mammals* (pp. 175–198). Johns Hopkins University Press.

Friscia, A. R., & Van Valkenburgh, B. (2010). Ecomorphology of north American Eocene carnivores: Evidence for competition between carnivorans and creodonts. In A. Goswami & A. Friscia (Eds.), *Carnivoran evolution: New views on phylogeny, form, and function* (pp. 311–341). Cambridge University Press. https://doi.org/10.1017/CBO9781139193436.012

Fulwood, E. L. (2020). Ecometric modelling of tooth shape and precipitation gradients among lemurs on Madagascar. *Biological Journal of the Linnean Society*, 129, 26–40. https://doi.org/10.1093/biolinnean/blz158

Gheebrant, E., Iarochene, M., Amaghzaz, M., & Bouya, B. (2006). Early African hyaenodontid mammals and their bearing on the origin of the Creodonta. *Geological Magazine*, 143, 475–489. https://doi.org/10.1017/S0016756806002032

Gillespie, A. K., Archer, M., & Hand, S. J. (2019). A new oligo-Miocene marsupial lion from Australia and revision of the family Thylacoleonidae. *Journal of Systematic Palaeontology*, 17, 59–89. https://doi.org/10.1080/14772019.2017.1391885

Gingerich, P. D. (1980). *Tytthaena parrisi*, oldest known oxyaenid (Mammalia, Creodonta) from the late Paleocene of western America. *Journal of Paleontology*, 54, 570–576.

Goin, F. J., Woodburne, M. O., Zimicz, A. N., Martin, G. M., & Chornogubsky, L. (2016). Paleobiology and adaptations of Paleogene Metatherians. In *A brief history of south American Metatherians*. Springer Earth System Sciences. https://doi.org/10.1007/978-94-017-7420-8_6

Gregory, W. K., & Hellmann, M. (1939). On the evolution and major classification of the civets (Viverridae) and allied fossil and recent Carnivora: A phylogenetic study of the skull and dentition. *Proceedings of the American Philosophical Society*, 81, 309–392.

Harper, T., Parras, A., & Rougier, G. W. (2019). *Reigitherium* (Meridiolestida, Mesungulatoidea), an enigmatic late cretaceous mammal from Patagonia, Argentina: Morphology, affinities, and dental evolution. *Journal of Mammalian Evolution*, 26, 447–478. https://doi.org/10.1007/s10914-018-9437-x

Holliday, J. A. (2010). Evolution in Carnivora: Identifying a morphological bias. In A. Goswami & A. Friscia (Eds.), *Carnivoran evolution: New views on phylogeny, form, and function* (pp. 189–224). Cambridge University Press. https://doi.org/10.1017/CBO9781139193436.008

Holliday, J. A., & Steppan, S. J. (2004). Evolution of hypercarnivory: The effect of specialization on morphological and taxonomic diversity. *Paleobiology*, 30, 108–128. https://doi.org/10.1666/0094-8373(2004)030<0108:EOHTEO>2.0.CO;2

Hu, Y., Meng, J., Wang, Y., & Li, C. (2005). Large Mesozoic mammals fed on young dinosaurs. *Nature*, 433, 149–152. https://doi.org/10.1038/nature03102

Hutchins, M., Thoney, D. A., & Schlager, N. (2003). *Grzimek's animal life encyclopedia volumes 12–16, mammals I–V* (2nd ed.). Gale Group.

Jones, M. E., & Stoddart, D. M. (1998). Reconstruction of the predatory behaviour of the extinct marsupial thylacine (*Thylacinus cynocephalus*). *Journal of Zoology*, 246, 239–256. https://doi.org/10.1111/j.1469-7998.1998.tb00152.x

Kumar, S., Stecher, G., Suleski, M., & Hedges, S. B. (2017). TimeTree: A resource for timelines, timetrees, and divergence times. *Molecular Biology and Evolution*, 37, 1812–1819. https://doi.org/10.1093/molbev/msx116

Li, P., Morse, P. E., & Kay, R. F. (2020). Dental topographic change with macrowear and dietary inference in *Homunculus patagonicus*. *Journal of Human Evolution*, 144, 102786. https://doi.org/10.1016/j.jhevol.2020.102786

López-Torres, S., Selig, K. R., Prufrock, K. A., Lin, D., & Silcox, M. T. (2017). Dental topographic analysis of paromomyid (Plesiadapiformes, primates) cheek teeth: More than 15 million years of changing surfaces and shifting ecologies. *Historical Biology*, 30, 76–88. https://doi.org/10.1080/08912963.2017.1289378

Martín-Serra, A., Figueirido, B., & Palmqvist, P. (2014). A three-dimensional analysis of the morphological evolution and locomotor behaviour of the carnivoran hind limb. *BMC Evolutionary Biology*, 14, 129. https://doi.org/10.1186/1471-2148-14-129

Matthew, W. D. (1909). The Carnivora and Insectivora of the Bridger Basin, middle Eocene. *Memoirs of the American Museum of Natural History*, 9, 291–567.

Meloro, C., & Raia, P. (2010). Cats and dogs down the tree: The tempo and mode of evolution in the lower carnassial of fossil and living Carnivora. *Evolutionary Biology*, 37, 177–186. https://doi.org/10.1007/s11692-010-9094-3

Meng, J., Zhai, R., & Wyss, A. R. (1998). The late Paleocene Bayan Ulan Fauna of inner Mongolia, China. *Bulletin of Carnegie Museum of Natural History*, 34, 148–185.

Morlo, M. (1999). Niche structure and evolution in creodont (Mammalia) faunas of the European and north American Eocene. *Geobios*, 32, 297–305. https://doi.org/10.1016/S0016-6995(99)80043-6

O'Leary, M. A., Bloch, J. I., Flynn, J. J., Gaudin, T. J., Giallombardo, A., Giannini, N. P., Goldberg, S. L., Kraatz, B. P., Luo, Z. X., Meng, J., & Ni, X. (2013). The placental mammal ancestor and the post-K-Pg radiation of placentals. *Science*, *339*, 662–667. https://doi.org/10.1126/science.1229237

Osborn, H. F. (1907). *Evolution of mammalian teeth to and from the triangular type*. The Macmillian Company.

Pampush, J. D., Spradley, J. P., Morse, P. E., Griffith, D., Gladman, J. T., Gonzales, L. A., & Kay, R. F. (2018). Adaptive wear-based changes in dental topography associated with atelid (Mammalia: Primates) diets. *Biological Journal of the Linnean Society*, *124*, 587–606. https://doi.org/10.1093/biolinnean/bly069

Pampush, J. D., Winchester, J. M., Morse, P. E., Vining, A. Q., Boyer, D. M., & Kay, R. F. (2016). Introducing molaR: A new R package for quantitative topographic analysis of teeth (and other topographic surfaces). *Journal of Mammalian Evolution*, *23*, 397–412. https://doi.org/10.13140/RG.2.1.3284.9687

Pineda-Munoz, S., Lazagabaster, I. A., Alroy, J., & Evans, A. (2017). Inferring diet from dental morphology in terrestrial mammals. *Methods in Ecology and Evolution*, *8*, 481–491. https://doi.org/10.1111/2041-210X.12691

Pires, A. M., Silvestro, D., & Quental, T. B. (2015). Continental faunal exchange and the asymmetrical radiation of carnivores. *Proceedings of the Royal Society B*, *282*, 20151952. https://doi.org/10.13140/RG.2.1.3284.9687doi.org/10.1098/rspb.2015.1952

Prevosti, F. J., & Forasiepi, A. M. (2018). *Evolution of south American mammalian predators during the Cenozoic: Paleobiogeographic and paleoenvironmental contingencies*. Springer International Publishing. https://doi.org/10.1007/978-3-319-03701-1_3

Prevosti, F. J., Turazzini, G. F., Ercoli, M. D., & Hingst-Zaher, E. (2012). Mandible shape in marsupial and placental carnivorous mammals: A morphological comparative study using geometric morphometrics. *Zoological Journal of the Linnean Society*, *164*, 836–855. https://doi.org/10.1111/j.1096-3642.2011.00785.x

Prufrock, K. A., Boyer, D. M., & Silcox, M. T. (2016). The first major primate extinction: An evaluation of paleoecological dynamics of north American stem primates using a homology free measure of tooth shape. *American Journal of Physical Anthropology*, *159*, 683–697. https://doi.org/10.1002/ajpa.22927

R Core Team. (2020). *R: A language and environment for statistical computing*. R Foundation for Statistical Computing. http://R-project.org/

Rannikko, J., Adhikari, A., Karme, A., Žliobaitė, I., & Fortelius, M. (2020). The case of the grass-eating suids in the Plio-Pleistocene Turkana Basin: 3D dental topography in relation to diet in extant and fossil pigs. *Journal of Morphology*, *281*, 348–364. https://doi.org/10.1002/jmor.21103

Ravinsky, D. S., Evans, A. R., & Adams, J. W. (2019). The pre-Pleistocene fossil thylacinids (Dasyuromorphia: Thylacinidae) and the evolutionary context of the modern thylacine. *PeerJ*, *7*, e7457. https://doi.org/10.7717/peerj.7457

Renaud, S., & Ledevin, R. (2017). Impact of wear and diet on molar row geometry and topography in the house mouse. *Archives of Oral Biology*, *81*, 31–40. https://doi.org/10.1016/j.archoralbio.2017.04.028

Revell, L. J. (2020). Package "phytools": Phylogenetic tools for comparative biology (and other things). R package version 0.7-70. Retrieved from https://cran.r-project.org/web/packages/phytools.

Schlager, S., Jefferis, G., & Dryden, I. (2020). Package "Morpho": Calculations and visualisations related to geometric morphometrics. R package version 2.8. Retrieved from https://cran.r-project.org/web/packages/Morpho.

Selig, K. R., López-Torres, S., Sargis, E. J., & Silcox, M. T. (2018). First 3D dental topographic analysis of the enamel-dentine junction in nonprimate euarchontans: Contribution of the enamel-dentine junction to molar morphology. *Journal of Mammalian Evolution*, *26*, 587–598. https://doi.org/10.1007/s10914-018-9440-2

Selig, K. R., López-Torres, S., Sargis, E. J., & Silcox, M. T. (2019). First 3D dental topographic analysis of the enamel–dentine junction in nonprimate euarchontans: Contribution of the enamel-dentine junction to molar morphology. *Journal of Mammalian Evolution*, *26*, 587–598. https://doi.org/10.1007/s10914-018-9440-2

Selig, K. R., Sargis, E. J., Chester, S. G. B., & Silcox, M. T. (2020). Using three-dimensional geometric morphometric and dental topographic analyses to infer the systematics and paleoecology of fossil treeshrews (Mammalia, Scandentia). *Journal of Paleontology*, *94*, 1202–1212. https://doi.org/10.1017/jpa.2020.36

Selig, K. R., Sargis, E. J., & Silcox, M. T. (2019). The frugivorous insectivores? Functional morphological analysis of molar topography for inferring diet in extant treeshrews (Scandentia). *Journal of Mammalogy*, *100*, 1901–1917. https://doi.org/10.1093/jmammal/gyz151

Shan, S., Kovalsky, S. Z., Winchester, J. M., Boyer, D. M., & Daubechies, I. (2019). ariaDNE: A robustly implemented algorithm for Dirichlet energy of the normal. *Methods in Ecology and Evolution*, *10*, 541–552. https://doi.org/10.1111/2041-210X.13148

Simpson, G. G. (1959). The nature and origin of supraspecific taxa. *Cold Spring Harbor Symposia on Quantitative Biology*, *24*, 255–271. https://doi.org/10.1101/SQB.1959.024.01.025

Smits, P. D., & Evans, A. (2012). Functional constraints on tooth morphology in carnivorous mammals. *BMC Evolutionary Biology*, *12*, 146. https://doi.org/10.1186/1471-2148-12-146

Solé, F., & Ladevèze, S. (2017). Evolution of the hypercarnivorous dentition in mammals (Metatheria, Eutheria) and its bearing on the development of tribosphenic molars. *Evolution & Development*, *19*, 56–68. https://doi.org/10.1111/ede.12219

Solé, F., & Mennecart, B. (2019). A large hyaenodont from the Lutetian of Switzerland expands the body mass range of the European mammalian predators during the Eocene. *Acta Palaeontologica Polonica*, *64*, 275–290. https://doi.org/10.4202/app.00581.2018

Solé, F., Morgane, D., Le Verger, K., & Mennecart, B. (2018). Niche partitioning of the European carnivorous mammals during the Paleogene. *PALAIOS*, *33*, 514–523. https://doi.org/10.2110/palo.2018.022

Szalay, F. S., & Gould, S. J. (1966). Asiatic Mesonychidae (Mammalia, Condylarthra). *Bulletin of the American Museum of Natural History*, *132*, 127–174.

Tarquini, S. D., Chemisquy, M. A., & Prevosti, F. J. (2020). Evolution of the carnassial in living mammalian carnivores (Carnivora, Didelphimorphia, Dasyuromorphia): Diet, phylogeny, and allometry. *Journal of Mammalian Evolution*, *27*, 95–109. https://doi.org/10.1007/s10914-018-9448-7

Tomiya, S. (2011). A new basal caniform (Mammalia: Carnivora) from the middle Eocene of North America and remarks on the phylogeny of early carnivorans. *PLoS One*, *6*(9), e24146. https://doi.org/10.1371/journal.pone.0024146

Ungar, P. S. (2018). Tooth surface topography. In R. L. Anemone & G. C. Conroy (Eds.), *New geospatial approaches to the anthropological sciences* (pp. 101–120). University of New Mexico Press.

Van Valkenburgh, B. (1988). Trophic diversity in past and present guilds of large predatory mammals. *Paleobiology*, *14*, 155–173. https://doi.org/10.1017/S0094837300011891

Van Valkenburgh, B. (1989). Carnivore dental adaptations and diet: A study of trophic diversity within guilds. In J. L. Gitleman (Ed.), *Carnivore behavior, ecology, and evolution* (pp. 410–436). Springer. https://doi.org/10.1007/978-1-4757-4716-4_16

Van Valkenburgh, B. (1999). Major patterns in the history of carnivorous mammals. *Annual Review of Earth and Planetary Sciences*, *27*, 463–493. https://doi.org/10.1146/annurev.earth.27.1.463

Van Valkenburgh, B. (2007). Déjà vu: The evolution of feeding morphologies in the Carnivora. *Integrative and Comparative Biology*, *47*, 147–163. https://doi.org/10.1093/icb/icm016

Van Valkenburgh, B., Wang, X., & Damuth, J. (2004). Cope's rule, hypercarnivory, and extinction in north American canids. *Science*, *306*, 101–104. https://doi.org/10.1126/science.1102417

Voss, R. S., Gardner, A. L., & Jansa, S. A. (2004). On the relationships of 'Marmosa' Formosa Shamel, 1930 (Marsupialia: Didelphidae), a phylogenetic puzzle from the Chaco of northern Argentina. _American Museum Novitates_, _3442_, 1–18. https://doi.org/10.1206/0003-0082(2004)442%3C0001:OTROMF%3E2.0.CO;2

Voss, R. S., & Jansa, S. A. (2003). Phylogenetic studies on didelphid marsupials II. Nonmolecular data and new IRBP sequences: Separate and combined analyses of didelphine relationships with denser taxon sampling. _Bulletin of the American Museum of Natural History_, _276_, 1–82. https://doi.org/10.1206/0003-0090(2003)276%3C0001:PSODMI%3E2.0.CO;2

Wang, X., Qiu, Z., & Wang, B. (2005). Hyaenodonts and carnivorans from the early Oligocene to early Miocene of Xianshuihe formation, Lanzhou Basin, Gansu Province, China. _Palaeontologica Electronica_, _8_(1), 6A.

Werdelin, L. (1986). Comparison of skull shape in marsupial and placental carnivores. _Australian Journal of Zoology_, _34_, 109–117. https://doi.org/10.1071/ZO9860109

Werdelin, L. (1987). Jaw geometry and molar morphology in marsupial carnivores: Analysis of a constraint and its macroevolutionary consequences. _Paleobiology_, _13_, 342–350. https://doi.org/10.1017/S0094837300008915

Wesley-Hunt, G. D. (2005). The morphological diversification of carnivores in North America. _Paleobiology_, _31_, 35–55. https://doi.org/10.1666/0094-8373(2005)031%3C0035:TMDOCI%3E2.0.CO;2

Wesley-Hunt, G. D., & Flynn, J. J. (2005). Phylogeny of the Carnivora: Basal relationships among the carnivoramorphans, and assessment of the position of 'Miacoidea' relative to Carnivora. _Journal of Systematic Palaeontology_, _3_, 1–28. https://doi.org/10.1017/S1477201904001518

Winchester, J. M. (2016). MorphoTester: An open source application for morphological topographic analysis. _PLoS One_, _11_(2), e0147649. https://doi.org/10.1371/journal.pone.0147649

Winchester, J. M., Boyer, D. M., St Clair, E. M., Gosselin-Ildari, A. D., Cooke, S. B., & Ledogar, J. A. (2014). Dental topography of platyrrhines and prosimians: Convergence and contrasts. _American Journal of Physical Anthropology_, _153_, 29–44. https://doi.org/10.1002/ajpa.223

SUPPORTING INFORMATION

Additional supporting information may be found in the online version of the article at the publisher's website.